Université Catholique de Louvain (UCLouvain)

Institute of NeuroScience (IoNS)

Aging and Dementia Unit (AGAD)

The Nose as a Neurological Frontline: Unraveling Tauopathy through the Olfactory Gateway

Marion Dourte

Supervisor: Prof. Pascal Kienlen-Campard (UCLouvain)

Co-Supervisor: Prof. Patricia Renard (UNamur)

Thesis submitted for the degree of

Doctor of Biomedical and Pharmaceutical Sciences

Secteur des sciences de la santé

2025

Composition of the Jury

Supervisor:

Prof. Pascal Kienlen-Campard
(*UCLouvain, Institute of Neuroscience, CEMO, AGAD*)

Co-supervisor:

Prof. Patricia Renard
(*UNamur, Namur Research Institute for Life Sciences, URBC*)

President:

Prof. Bernard Hanseeuw
(*UCLouvain, Institute of Neuroscience, NEUR, LAB*)

Internal members:

Prof. Philippe Gailly
(*UCLouvain, Institute of Neuroscience, FYCL*)

Prof. Anabelle Decottignies
(*UCLouvain, de Duve Institute, GEPI*)

External members:

Prof. Charles Nicaise
(*UNamur, Namur Research Institute for Life Sciences, URPhyM, LNR*)

Prof. Luc Buée
(*ULille, U1172 – Lille Neuroscience et Cognition*)

Acknowledgments

Je voudrais commencer par remercier **Pascal**, mon promoteur de thèse, d'avoir cru en mes capacités à une époque où même moi je n'aurais pas misé sur moi. Merci d'avoir toujours répondu présent pendant ces 4 années de thèse, d'avoir toujours su me conseiller, me réorienter, afin d'arriver là où j'en suis aujourd'hui. Quand je vois l'équipe de grands stressés qu'est la AGAD team, je pense qu'on peut s'estimer chanceux d'avoir un « boss » qui reste toujours zen et qui nous permet de dédramatiser les petits soucis du quotidien. Je ne serai jamais aussi zen que toi, mais tu m'auras permis d'apprendre à relativiser. Merci également pour toutes ces discussions sur le sport, sur l'actualité, pour tous tes conseils en course à pied, merci de te rendre accessible et de nous avoir montré qu'un labo c'est n'est pas simplement une hiérarchie mais bien des personnes passionnées qui travaillent ensemble pour essayer de faire avancer la recherche.

Ensuite je voudrais remercier **Patsy**, merci d'avoir accepté de rejoindre le train en cours de route. Ton expertise en protéomique fut d'une grande aide, mais merci également d'avoir toujours écouter mes présentations avec intérêt, et d'avoir pris le temps de me conseiller au mieux. De la même façon que Pascal tu as su te rendre accessible et ta franchise est une qualité que j'ai toujours énormément appréciée.

Merci à tous les membres de l'ARC ; Caroline, Bernard, Anabelle, Pascal, et Florence d'avoir défendu et d'avoir cru en ce projet avant même que je ne commence mon doctorat, rien de tout cela n'aurait été possible sans votre implication personnelle.

Merci à tous les membres du jury, Bernard en tant que président vous avez su me guider au mieux dans cette épreuve de longue endurance qu'est la thèse. Merci également à Philippe, Anabelle, et Patsy d'avoir été présents pendant mes comités d'accompagnement, vos retours sur mon projet m'ont toujours permis de me remettre en question et d'améliorer mon travail. Finalement merci aux professeurs Charles Nicaise et Luc Buée d'avoir accepté d'être les membres externes de ce jury, je sais déjà que nos échanges seront enrichissants.

Sur une note un peu plus personnelle, merci **Emilien** d'avoir été le meilleur encadrant dont on puisse rêver. Tout a commencé par un rendez-vous sur le parking du Quick pour se rejoindre pour mon premier jour de stage, j'ai eu la chance de te suivre pendant 4 mois, d'assister à tes quelques gaffes mais surtout de découvrir quelqu'un de passionné, qui ne s'énerve jamais et qui m'a permis de faire mes premiers pas dans l'équipe AGAD (même si au début c'étaient plutôt des têtes à têtes pendant le lunch, merci le COVID). Je garde en mémoire toutes nos sorties running, mes premiers 20km de Bruxelles en ta compagnie, les recherches d'appart, les brunchs, les soirées, mais surtout les ragots, à toutes ces pauses clopes sans fumer où on pouvait papoter sur tout et n'importe quoi. Je suis tellement contente d'avoir pu partager 3 années de ma thèse avec toi, et je peux t'assurer que tu es une des raisons qui m'ont poussée à me lancer dans cette aventure.

Nuria, I would like to thank you for being the kindest and most patient person I have ever met. I have never seen you say no to anyone, you are always the first to offer help. Thank you for inspiring me every day by being

such an amazing researcher. The research world truly needs more people like you. I am so glad we were able to share one last congress together this year. I know I can leave the lab with peace of mind, knowing you will be there to guide the newcomers.

Ma **Loulou**, tu es probablement une des meilleures choses qui me soit arrivée pendant cette thèse. Je ne sais pas ce qui va le plus me manquer entre ta maladresse, ta bienveillance, tes blagues nulles ou bien tout simplement tous ces moments passés ensembles, que ce soit au labo autour d'un café ou bien en dehors pendant nos petits verres en terrasse, nos séances au Basic-Fit (oui j'ai quand même mis au pluriel). J'ai toujours admiré ta motivation et la passion que tu mets dans ton projet, je confonds toujours le nom de tes deux mutations mais ça ne m'empêche pas d'apprécier tout ton travail au quotidien, je sais que tu iras loin et j'espère que tu ne douteras plus de toi car tu es une personne exceptionnelle, et ne crois pas que la fin de ma thèse signe la fin de nos commérages, tu vas énormément me manquer, en plus je vais être obligée d'être aigrie avec mes prochains collègues parce qu'il est hors de question que quelqu'un prenne ta place de collègue préférée. Merci d'avoir toujours été la plus grande fan de mon travail.

Shirine, avec Emilien tu auras été là pendant pratiquement toute ma thèse (malgré ton petit séjour en Norvège). Je n'oublierai pas toutes nos discussions fashion (même si on n'est pas toujours d'accord), le partage des bonnes adresses, les potins café, … On peut dire que le labo sera sans doute un peu plus calme sans moi, mais je sais que tu seras là pour animer les

discussions (puisque tmtc on est connues pour parler FORT, n'en déplaise à certains). Merci également pour tes conseils de scientifique (les stats, les graphs, tout ça tout ça), je te souhaite de vivre une dernière année de thèse aussi chouette que la mienne (peut-être le stress en moins).

Debora, we started our thesis almost at the same time and went through it all together. I think we can agree it was not easy, but sometimes a good brunch or a spinning class helped make it easier. Thank you for always giving good advice, you are a great researcher, and I hope you will gain even more confidence in yourself and your work. I was happy to share this experience with you because it is always better to have someone next to you (to the left, exactly) who truly understands what you are going through. I am already looking forward to coming back in a few months to see your final work.

Merci à toi **Axelle** d'être une des personnes les plus gentilles que j'ai pu rencontrer (parfois un peu trop). Je ne sais pas si tu as conscience de l'impact de toutes ces actions au quotidien, toujours un petit mot gentil, un cookie, un petit cadeau. J'ai eu l'impression de pouvoir célébrer chaque étape de ma fin de thèse grâce à toi, et oui tu auras presque réussi à me faire pleurer. Avec loulou vous gagnez la première place des meufs beaucoup trop bien pour cette planète. Je voudrais également souligner tes qualités en tant que chercheuse, en tant que lab planner (comme les wedding planner tu as capté), que bio-informaticienne, autant de cordes à ton arc qui m'assure que tu marqueras le monde de la recherche. Essaye de ne pas nous oublier quand tu seras une PI super famous. Merci d'être toi, et je suis ravie d'avoir vu la petite Axelle s'endurcir pour défendre ses opinions. J'espère que mes super

blagues ne te manqueront pas trop, et que tu prendras bien soin de mon bureau.

Esther, par où commencer, de la même manière que certains pianistes font des morceaux à quatre mains, nous on faisait des traitements sur les souris à quatre mains. Pendant ces 4 années (ça fait beaucoup de 4), je n'ose pas compter le nombre d'heures passées en dissection, à injecter des gouttes dans des narines de souris, tout ça rendu beaucoup plus léger par nos discussions. Pendant ma première année tu as été une sorte de guide spirituel mais version labo, une vraie bible, toujours prête à m'aider à chercher des protocoles, on se souviendra de cette décalcification qui nous aura donné du fil à retordre. Et par la suite tu auras toujours répondu présente pour m'aider dans mes expériences, sans toi aucun de mes résultats n'auraient pu voir le jour. Merci d'avoir été là du début à la fin, d'avoir été mon binôme de choc pour les souris, mais également merci pour tout ton travail au quotidien dans le labo, car on sait tous que quand Esther est en vacances, c'est la panique. Je suis honorée d'avoir pu participer à l'enrichissement de ton vocabulaire de djeuns, même si tu étais parfois outrée par toutes les bêtises qu'on pouvait débiter. Et vivement le prochain barbecue à Nivelles !!

Marine, tu fais partie de ces personnes de l'ombre qui travaille sans te plaindre et qui contribue à l'équilibre du labo, merci pour tous ces moments que l'on a partagés, que ce soient les discussions plus ou moins sérieuses, les excursions, les temps de midi, je te souhaite le meilleur.

Je voulais également remercier toutes les personnes de l'équipe AGAD qui sont passées et restées plus ou moins longtemps pendant ma thèse ; Jithu, mais également les étudiants ; Joana, Mongia, avec une pensée particulière pour Claire, merci pour ton humour au quotidien, je n'ai aucun doute sur ta future brillante réussite.

Un merci particulier à **Anh** qui m'aurait vu évoluer depuis le début de ma thèse, depuis notre rencontre dans la salle culture jusqu'à nos dernières discussions. Côtoyer des gens comme toi au quotidien donne envie de venir au labo, toujours le sourire, toujours une bonne adresse food à partager, je ne saurais pas compter le nombre de temps de midi que nous avons partagés (en fait pas loin de 1000 j'ai compté) mais ce que je sais c'est que si je connais un peu mieux Bruxelles aujourd'hui c'est en grande partie grâce à toi. J'espère que tu n'oublieras jamais la belle brochette 😉.

Je voulais également remercier toute l'équipe de Namur sans qui ce projet n'aurait pas pu être mené à bien, merci **Marc** pour tout le temps que tu as passé à faire les analyses et ensuite à nous débriefer les résultats. Merci **Ayeh** d'avoir réalisés toutes les analyses transcriptomiques et protéomiques, et d'avoir mis ton expertise à notre disposition. Je pense que nous pouvons être fières du résultat de notre collaboration. Merci également à **Malika**, arrivée récemment dans l'équipe, ton enthousiasme pour le projet et pour la recherche en général m'a vraiment marquée, je te souhaite le meilleur pour la suite de ton parcours.

Merci à tout l'équipe admin de l'institut (Cathy, Sonia) de nous permettre de mener à bien nos projets et plus particulièrement merci à toi **Sara**, d'avoir

gérer d'une main de maître les comptes du labo, mais surtout merci d'avoir été une oreille attentive, merci pour toutes ces discussions ou je passais juste déposer un papier mais qui se prolongeaient souvent sur des sujets divers. Je suis certaine qu'on se reverra, si ce n'est pas au labo ce sera sans doute pour faire nos ongles avec Kelly ou bien chez Amaya. On sous-estime souvent tout le travail que vous faites pour nous accompagner durant nos thèses, merci d'avoir toujours été là pour répondre à mes questions.

Romélia, merci d'avoir pris soin de mes petites souris pendant plusieurs années, d'abord au Linné puis dans l'animalerie du +5, c'était toujours un plaisir de discuter avec toi, même si tu disais toujours que tu ne faisais que râler, je sais qu'au fond je pouvais te faire une confiance aveugle. Merci pour tes petits cocktails qui nous redonnaient du baume au cœur quand la motivation n'était plus là, une fois de plus tu fais partie de ces travailleurs de l'ombre sans qui rien de notre travail ne serait possible, alors merci pour tout. Merci également à **Jean-François** qui a su reprendre le flambeau et gérer l'animalerie parfaitement. Les prochains sont chanceux d'être entourés d'une si bonne équipe.

Je voulais également remercier plusieurs personnes qui ont contribué de près ou de loin à ce projet, merci à **Marc** de Bournonville d'avoir été un des premiers à m'aider quand je désespérais avec mes blocs de paraffine, merci également à son successeur **Olivier** Van Kerk d'avoir continué sur sa lancée avec toujours des conseils avisés que ce soit en termes de coupe ou de coloration. Merci à **Olivier** Schakman d'avoir réalisé toute l'étude comportementale de mes souris, j'imagine que ça doit être un peu long de

regarder les images de plusieurs dizaines de souris qui cherchent une croquette enfouie. Merci à **Yasmine** d'avoir toujours gérer les dissections. Merci à l'équipe de **Karelle Leroy**, plus particulièrement à **Emilie**, de m'avoir formée pendant plusieurs semaines en histologie et d'avoir toujours été de bons conseils.

Je voudrais remercier d'autres personnes qui ne font pas partie du monde de la recherche mais qui sont tout autant importants pour toi. Premièrement, mes parents (**MP** et **JL** pour les intimes), merci d'avoir toujours cru en moi, de m'avoir laissé faire ce que je voulais comme études en me soutenant tout au long de ce long parcours, même si c'est toujours compliqué d'expliquer ce que l'on fait, j'ai toujours pu voir la fierté dans vos yeux, et les allers-retours à Nollevaux m'ont permis de garder les pieds sur terre, de me ressourcer à la campagne, et de profiter de bons petits plats avec les légumes du jardin. Merci également à mes deux petits frères **Simon** et **Brieuc** d'avoir toujours été présents, on n'a pas l'habitude d'être démonstratifs mais en tant que grande sœur, sentir que ses petits frères sont fiers de nous, c'est un des plus beaux sentiments.

Merci également à tous mes amis présents depuis toutes ces années, vous m'avez accompagné dans les moments de doute mais vous étiez également présents pour fêter les réussites de mon parcours. Une pensée particulière à toutes mes copines qui font également un doctorat, **Christel, Romane, Camille, Mathilde, Pauline**[2], … se sentir entourée c'est bien mais quand ce sont des personnes qui vivent la même chose que vous c'est encore mieux.

Merci à tous mes copains de la salle, en particulier **Kenny** et **Diego**, vous m'avez permis de déconnecter et de me passionner pour autre chose que la science. Ces soirées au Basic-Fit m'auront permis de tenir le coup et de ne pas devenir complètement folle pendant les périodes de stress (qui n'ont pas manquées).

Finalement je voudrais remercier mon acolyte du quotidien, **Thomas**. Merci pour ton soutien indéfectible du début de ma thèse jusqu'à l'élaboration de la couverture de cette dernière. Merci pour toutes les corrections de mes travaux même si tu n'allais jamais assez vite à mon goût, merci d'avoir subi des dizaines de présentations ou point ou tu connais sans doute mon sujet mieux que moi, merci de m'avoir soutenue pendant les grosses périodes de stress, merci de toujours me suivre dans mes idées farfelues, merci pour tout simplement.

Table of Contents

Composition of the Jury 2
Acknowledgments 3
Abstract 15
List of Abbreviations 17
INTRODUCTION 19
I. Olfaction and Olfactory System 19
II. The Mouse Olfactory System and Associated Regions 21
III. Olfactory Dysfunction 34
IV. The Olfactory System and Its Vulnerability in Neurodegenerative Diseases (NDs) 39
V. Alzheimer's Disease (AD) 47
VI. The Tau Protein and its Normal Function in Neurons 53
VII. The Pathological Tau Protein 56
VIII. Tau-targeting Therapies 71
IX. The Olfactory System as a Promising Therapeutic Target and Diagnosis Tool 73
X. Tauopathy Mouse Models 79
OBJECTIVES 82
RESULTS – Chapter I 85
Tau Pathology in the Olfactory System and Associated CNS Regions in PS19 mice 88
Olfactory Function Assessment in PS19 mice 105
Pathological pTau Protein in the Human Olfactory System 110
RESULTS – Chapter II 118
Modulation of Tau Pathology in the CNS via Intranasal Interventions 119
RESULTS – Chapter III 127

Transcriptomic Profiling Reveals Age- and Region-Specific Gene Expression in PS19 mice 130

Functional Enrichment Analysis Highlights Temporal Progression of Tauopathy 133

Spatiotemporal Overlap of Differentially Expressed Genes Reveals Region- and Age-Specific Responses to Tau Pathology 140

Transcriptomic Signatures in the OE of PS19 mice as Early Biomarkers of Tau Pathology 144

GENERAL DISCUSSION 154

I. The Olfactory Epithelium as a Key Contributor to Tauopathy Progression 154

II. The Olfactory Epithelium as a Therapeutic Tool 165

III. The Olfactory Epithelium as a Diagnosis Tool 168

GENERAL CONCLUSION 174

METHODS 177

Animals 177

Tissue Harvesting 177

Sample Preparation for Immunostaining 177

Immunostaining 178

Behavioral Tests 181

Intranasal $ZnSO_4$ Irrigation 182

NFT-like Tau Accumulations Quantification 182

Intranasal hTau-P301S AAVs Irrigation 183

AT8 Signal Quantification 183

Postmortem Human Tissues 184

Protein Extraction 184

Western Blotting 185

Masson's Trichrome Stain 185

RNA Extraction (for qRT-PCR and RNAsequencing) 186
qRT-PCR 187
Statistical Analyses 188
Sample Preparation for RNA Sequencing 188
RNA-sequencing Data Processing and Analysis 189
Functional Annotation and Enrichment 189
qRT-PCR Validation of Candidate Biomarkers 189
Protein Sample Preparation 190
Protein Digestion 190
DIA-MS Protein Data Processing and Analysis 191
Data Available Statements 193
Appendices 213
Supplementary Information: An Early Olfactory Transcriptomic Signature of Tauopathy: Gbp2b Emerges as a Candidate Biomarker of Tau-Driven Neuroinflammation 213
Academic *Curriculum Vitae* 215

Abstract

Olfactory impairment is a well-recognized early indicator of neurodegenerative diseases (NDs), such as Alzheimer's disease (AD). Intracellular aggregates of hyperphosphorylated tau protein, referred to as neurofibrillary tangles (NFTs), are a hallmark of AD. NFTs are found in the olfactory bulb (OB) and entorhinal cortex (EC), both crucial for processing olfactory information.

The aim of our project was to document the possible progression of tau pathology along the olfactory system as an early event of AD pathogenesis. We investigated whether and how tau pathology initiates in the olfactory system and spreads to deeper brain regions, and whether this process could be targeted therapeutically. Using PS19 transgenic mice, which express human tau (1N4R isoform with the P301S mutation) and recapitulate key AD features, we mapped tau pathology across olfactory regions–including the olfactory epithelium (OE), OB, and piriform cortex (PC)–as well as downstream regions such as the hippocampus and EC. Notably, despite detectable tau lesions in olfactory regions, PS19 mice showed no significant olfactory performance deficits.

We found that hyperphosphorylated tau (pTau) accumulates early in the OE and appears to spread centrally along defined neuroanatomical pathways. This finding was supported by observations in human tissue from Braak stage I/II AD patients.

To establish a causal link between tau pathology in the OE and its progression in the CNS, we applied targeted interventions ($ZnSO_4$ and AAV-based vectors) directly at the OE level. These modulated tau pathology in the CNS, supporting the hypothesis that the OE is both an entry point and a potential therapeutic target in tauopathies.

To further investigate molecular mechanisms, we performed transcriptomic analyses of the OE, OB, and hippocampus from PS19 mice. We identified early, region-specific molecular disruptions–especially pronounced in the OE–starting at 3 months of age. These included markers of inflammation, stress responses, and olfactory dysfunction, which later evolved into broader impairments in neuronal signaling and metabolism by 9 months.

Among the differentially expressed genes, *Gbp2b* emerged as a promising biomarker due to its consistent upregulation, functional relevance to neuroinflammation, and detectability. Given the accessibility of the OE, we propose nasal brushing as a minimally invasive method for early biomarker detection.

In summary, we evidenced that tau pathology initiates early in the OE and propagates via defined anatomical routes to the CNS. It highlights the OE as both a therapeutic window and a diagnostic site, offering novel opportunities for early intervention and biomarker-based detection in tauopathies such as AD.

List of Abbreviations

AAVs: Adeno-associated viruses

ABs: Axon bundles

ALS: Amyotrophic lateral sclerosis

AD: Alzheimer's disease

AON: Anterior olfactory nucleus

BBB: Blood-brain barrier

CNS: Central nervous system

DEGs: Differentially expressed genes

DG: Dentate Gyrus

EC: Entorhinal cortex

EPL: External plexiform layer

FTD: Frontotemporal dementia

FTLD: Frontotemporal lobal degeneration

GCL: Granular cell layer

HD: Huntington's disease

IPL: Internal plexiform layer

MAPT: Microtubule associated protein tau

MCI: Mild cognitive impairment

MCL: Mitral cell layer

NDs: Neurodegenerative diseases

NFTs: Neurofibrillary tangles

OB: Olfactory bulb

OC: Olfactory cortex

OE: Olfactory epithelium

OMP: Olfactory marker protein

ONL: Olfactory nerve layer

OSNs: Olfactory sensory neurons

PC: Piriform cortex

PD: Parkinson's disease

PHFs: Paired helical filaments

PNS: Peripheral nervous system

WT: Wild-type

Introduction

INTRODUCTION

I. Olfaction and Olfactory System

Olfaction, the sense through which odors are perceived, is the most ancient of our senses apart from touch [1]. The olfactory system plays a central role in the sense of smell; it is responsible for detecting and interpreting odor signals. Sensory processing of odors, triggered by various chemical stimuli, is essential to maintain physiological and emotional balance. Indeed, odors play a crucial role in various aspects of life, including food perception, nutrition, and the detection of environmental hazards such as fires, gas leaks, and volatile chemicals. Beyond its sensory function, smell is deeply linked to semantic memory and contributes to reproductive behaviors and neuroendocrine regulation [2].

The sense of smell is typically defined by multiple abilities, including olfactory threshold detection, identification, discrimination, and olfactory memory, each playing a key role in how odors are perceived and processed (Fig. 1)[2]. Odor **sensitivity or threshold** can be defined as the ability to detect an odor at a given concentration, where the lowest concentration detected is considered the threshold. Odor **discrimination** is the ability to distinguish between two or more odors, relying on the hippocampus, piriform cortex (PC), orbitofrontal cortex, and thalamus. An odor must be known to be discriminated. This ability is known to decline with age [1]. Finally, odor **identification** in humans is the ability to detect, recall and name a scent that we associate with an experience. The regions involved are the PC, entorhinal cortex (EC), and hippocampus [3]. Odor identification is

directly associated with olfactory **memory**, defined as the ability to recall a previously encountered odor [3], mediated by the limbic system and relying on the structural integrity of the hippocampus [1].

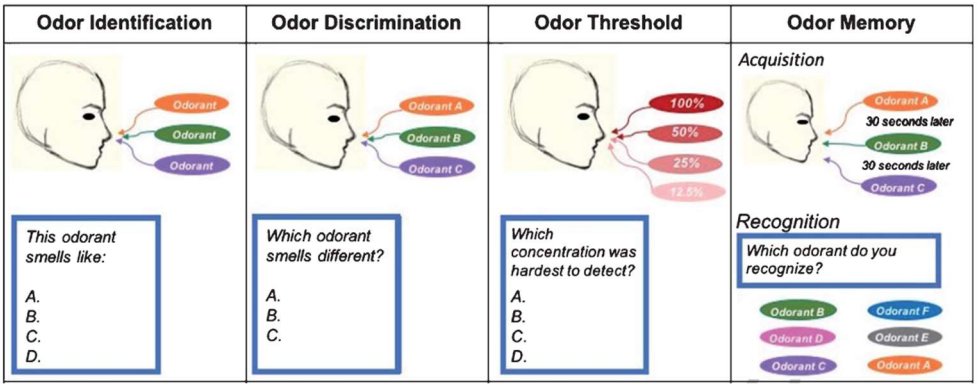

Fig. 1 Olfactory Functioning: Assessed by measuring four odor-related tasks: identification, discrimination, threshold, and memory [4].

Olfactory perception starts in the nasal olfactory structures and then reaches the olfactory bulb (OB), the primary central hub for olfactory processing [2].

1. <u>The Olfactory Pathway</u>

The transmission of the olfactory signals within the main olfactory system is a step-by-step process. First, the volatile odorants reach the olfactory epithelium (OE) via the nasal cavity, where the odor molecules are trapped in the mucus [5]. Then, there is a conversion from chemical signals to neuro-electrical signals by the olfactory sensory neurons (OSNs), bipolar neurons containing olfactory G-protein-associated receptors [2, 5]. These odorant molecules bind to a specific G-protein-coupled receptor. Then, the complex odorant receptor-odorants activates a cAMP-second messenger pathway

and a specific olfactive G-protein, and activates downstream adenylyl cyclase III, increasing cAMP levels in the cilia processes [2].

Increasing cAMP triggers the Ca^{2+} influx, opening the Cl-channel, and inducing the depolarization of the neuronal receptor axons [2]. The axons of the primary OSNs from the olfactory nerve cross the cribriform lamina to reach the OB [6, 7]. In the first instance, the projections innervate the olfactory glomeruli on the surface of the OB [5]. The neurons present in these glomeruli transduce the signal to mitral cells and tufted cells that will finally reach the olfactory areas in the central nervous system (CNS) [6, 5].

II. The Mouse Olfactory System and Associated Regions

The olfactory system of the mouse can be subdivided into two systems : the main olfactory system and the vomeronasal system [7]. The main olfactory system is composed of different primary or secondary areas. The primary olfactory areas include the nasal cavity containing the OE and OB while the secondary olfactory areas are the regions receiving projections from the OB [5]. The secondary olfactory areas are also known as the primary olfactory cortex, located in the inferior part of the temporal lobe of the brain. Similarly in humans and mice, it involves the anterior olfactory nucleus (AON), the PC, the olfactory tubercle, part of the amygdala, part of the EC and the periamygdaloid cortex [1, 5].

The vomeronasal pathway in rodents, in which the vomeronasal organ is present as the peripheral receptive system, runs in parallel to the main olfactory pathway (Fig. 2) and mediates responses to different classes of

chemosensory stimuli [8]. It is located on either side of the nasal septum and, by contrast to the main OB system, projects to the accessory olfactory bulb (AOB) [7]. Signals are then relayed to regions of the amygdala and hypothalamus implicated in behavioral and physiological effect of pheromones [8].

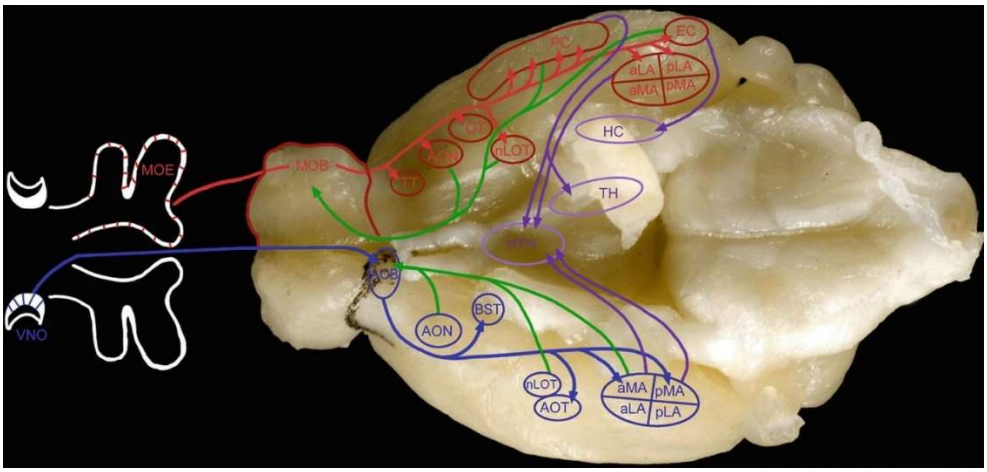

Fig. 2 Schematic view of the connectivity of the mouse olfactory system. Upper half (red): main olfactory system; Lower half (blue): vomeronasal system. Abbreviations: main olfactory epithelium (MOE), main olfactory bulb (MOB), taenia tecta (TT), olfactory tubercle (OT), lateral olfactory tract (LOT), piriform cortex (PC), the anterior (aLA) and posterior (pLA) lateral and the anterior (aMA) and posterior medial amygdala (pMA), hippocampus (HC), thalamus (TH), hypothalamus (HTH), vomeronasal organ (VNO), the accessory olfactory bulb (AOB), anterior olfactory nucleus (AON), bed nucleus of the stria terminalis (BST) [7].

Several structures of the main olfactory system will be described in the next sections.

1. The Olfactory Epithelium (OE)

The olfactory mucosa lines the roof of the nasal cavity, acting as the primary interface for detecting odorants as they enter the airway. This mucus-secreting tissue is composed of two key structures: the OE, which contains OSNs responsible for odor detection, and the lamina propria, a connective tissue which provides structural support and houses essential cellular components [2]. The mucus that lines the nasal cavity is produced by Bowman's glands, located in the lamina propria [2]. That mucus contains proteins that metabolize xenobiotics and help to maintain the integrity of the OE [9]. The olfactory mucosa is defined as a layered structure (Fig. 3). Starting from the nasal cavity lumen there is : the mucus layer (1), the cilia layer (2), the OE (3), and the lamina propria with the olfactory nerve fibers (4) [7].

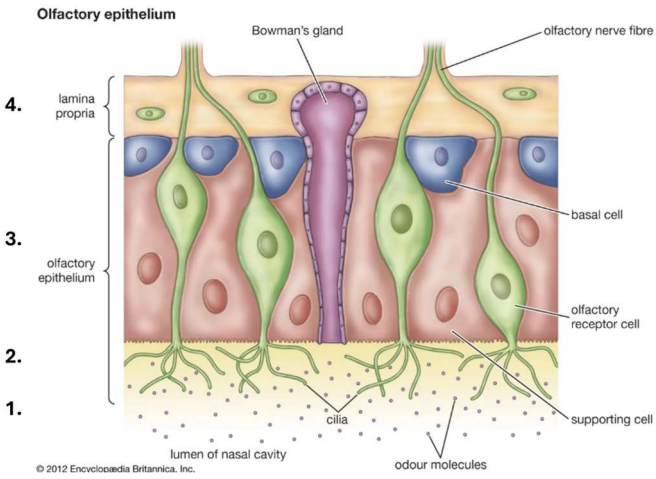

Fig. 3 Schematic illustration of the olfactory epithelium. The OE comprises olfactory receptors cells harboring cilia (OSNs)(green), basal cells (blue) and supporting cells (red). This epithelial layer rests upon the lamina propria, which contains Bowman's glands (purple) and olfactory nerve fibers [10].

The OE is the main olfactory receptor structure defined as a pseudo-stratified epithelium formed of three different cell types: OSNs, supporting cells and basal stem cells [11, 12, 7]. The OSNs are bipolar neurons bearing dendritic filaments with protruding cilia projected into the mucosal cavity [2]. The somas of the OSNs are located at an intermediate depth within the OE, while their unmyelinated axons converge to form the axon bundles (ABs) in the basal part. Olfactory ensheathing cells are present in the bundles to enwrap and support the axons of the OSNs in a similar way to which Schwann cells ensheathe unmyelinated peripheral neurons. These cells play a pivotal role in guiding axons during both development and regeneration [13]. Axons bundles cross the cribriform plate and constitute the olfactory nerve that reaches the outer layer of the OB [14]. OSNs have a lifespan of 30 to 60 days and are continuously replaced through replication from underlying stem cells located in the basal cell layer [12, 15]. The second cell type are supporting or sustentacular cells which are columnar epithelial cells with glial-like properties that provide mechanical support to the OSNs in the mammalian OE [16, 15]. Their apical process contains microvilli that project into the nasal cavity, and their basal process extends to the lamina propria [15]. The third type of cell present in the OE are the stem cells divided into globose basal cells (GBCs), which serve as active progenitors for OSN regeneration throughout life [11, 14, 17], and horizontal basal cells (HBCs), which function as multipotent reserve stem cells [11, 7].

2. The Olfactory Bulb (OB)

The OB is the convergence of the peripheral olfactory system and the central system that interconnect the olfactory sensory neuronal axons and the

mitral cell dendrites [18]. In mammals, the OB structure is characterized by six cell layers, arranged from the periphery to the center: the olfactory nerve layer I (ONL), the glomerular layer II (GL), the external plexiform layer III (EPL), the mitral cell layer IV (MCL), the internal plexiform layer V (IPL) and the granular cell layer VI (GCL) (Fig. 4)[19]. The ONL contains the projections of OSNs, which form synapses with glomerular cells (mitral cells, tufted cells and periglomerular cells) in the GL. The mitral and tufted cells, which are the main output neurons of the OB, are involved in the transmission of olfactory information via afferent inputs to other regions of the CNS including the PC [19]. Projections of the OB reach the amygdala via the PC or directly to specific amygdala subregions via monosynaptic projections [20]. Other projections from the OB also reach the EC which is involved in both olfactory learning and memory [5]. Both PC and EC regions are part of the olfactory cortex [7].

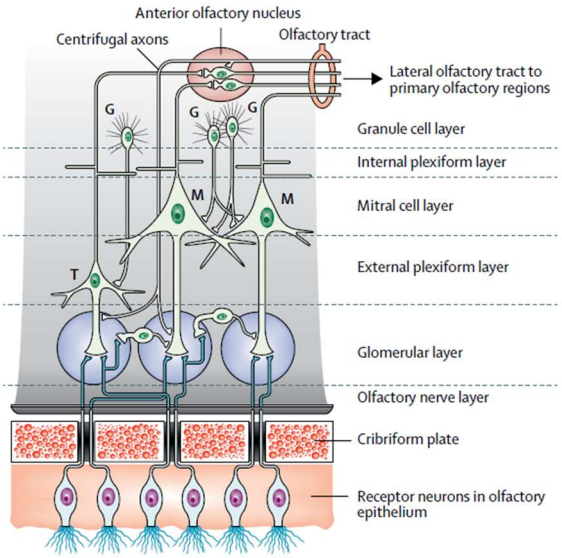

Fig. 4 Diagram of the main cell types and layers of the olfactory bulb, the first relay station of the olfactory system. The OB is located at the base of the brain immediately over the cribriform plate and receives axons from the olfactory receptor cells. These axons synapse with dendrites of the main output neurons, the mitral and tufted cells, within glomeruli [9].

The primary olfactory cortex refers to brain regions one synapse away from the OB, including the PC, AON, anterior cortical nucleus of the amygdala, and lateral EC (Fig. 5)[21].

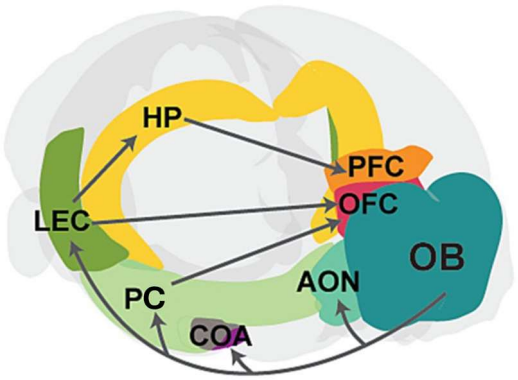

Fig. 5 Main connectivity between the olfactory bulb and higher-order brain regions. The OB connects to primary cortical regions, including the anterior olfactory nucleus (AON), cortical amygdaloid nucleus (COA), piriform cortex (PC), and lateral entorhinal cortex (LEC). Additionally, the PC and LEC extend projections to higher-order cognitive areas such as the hippocampus (HP), prefrontal cortex (PFC), and orbitofrontal cortex (OFC). Axonal projections are represented by gray arrows, with distinct regions highlighted in different colors [22].

3. The Olfactory Tract

The olfactory tract is a bundle of axons that carries output from the OB to higher regions of the brain involved in odor processing. Rather than bifurcating at a single point, such as the olfactory tubercle, the tract sends parallel projections to several primary olfactory areas. These include the olfactory tubercle, PC, EC, and amygdala—structures involved in odor perception, memory, and emotional responses [16, 7].

4. The Piriform Cortex (PC)

The PC is part of the olfactory cortex and is known to play a critical role for odor encoding and memory [23, 5]. It is divided into the anterior and posterior PC [5], and located at the ventrolateral side of the telencephalon central of the rhinal fissure [7].

Histologically, the structure can be divided into three layers (Fig. 6)[7]. The most superficial layer of the PC, Layer I, is a highly organized plexiform layer divided into two sublayers. Layer Ia, the outermost part, contains axons from mitral and tufted cells originating in the OB. Layer Ib, the deeper portion, consists of associative axons from neurons in the PC, other ipsilateral cortical structures such as the AON, and commissural axons from contralateral olfactory cortical neurons [21].

Beneath this, Layer II forms a densely packed cell body layer, housing most of the principal neurons of the PC. It is further divided into Layer IIa, which contains a specialized group of pyramidal-like neurons lacking basal dendrites, known as semilunar cells, and Layer IIb, which consists of superficial pyramidal cells along with small multipolar neurons [21].

The deepest layer, Layer III, contains deep pyramidal cells, two distinct types of multipolar neurons, and a dense network of associational fibers, which integrate signals both within the PC and from other brain regions, playing a crucial role in olfactory processing [21].

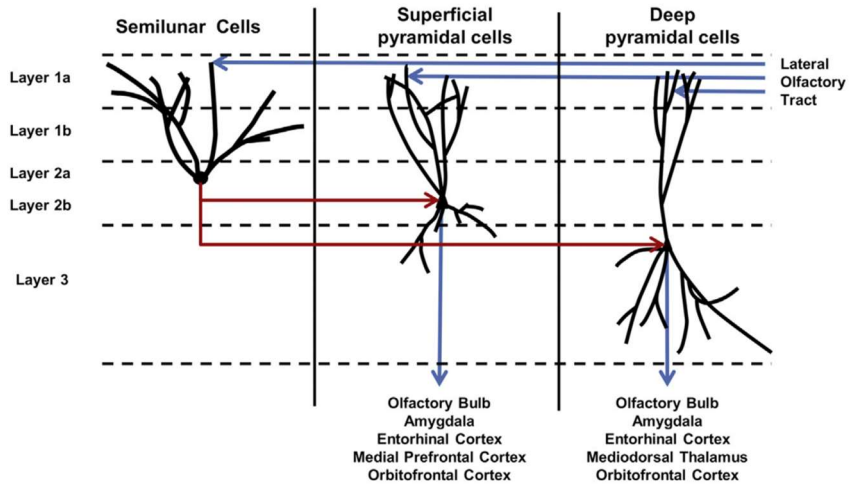

Fig. 6 Organization of Projection Neurons in the Piriform Cortex. The nuclei of semilunar cells are located in layer IIa of the PC, those of superficial pyramidal cells reside in layer IIb, and deep pyramidal cells are found in layer III [24].

The PC projects to a widespread and diverse set of forebrain structures. These structures include the OB, AON, lateral amygdala nucleus, EC, orbitofrontal cortex, and mediodorsal nucleus of the thalamus [21].

5. The Olfactory Tubercule

The olfactory tubercle is part of the primary olfactory cortex and monosynaptic olfactory input from both the OB and the PC [25]. Positioned at the crossroads of olfactory and reward circuits, it integrates odor information with motivational and emotional signals, contributing to behaviors like odor-guided decision-making [16, 7].

6. The Anterior Olfactory Nucleus (AON)

The AON is a complex brain area that is heavily interconnected and exchanges information with numerous olfactory centers. As a result, this region plays a role in many processes, such as odor processing, social

communication, odor memory, bilateral communication – by sending projections to both OB, and sensory gating [26].

The AON is a prominent structure located within the olfactory peduncle, positioned caudal to the OB and rostral to the PC, with which it merges at its caudal end. The AON has a laminar organization similar to that of the PC. It receives direct projection from the mitral and tufted cells located in the superficial plexiform layer (Layer I) of the OB. These projections synapse onto the apical dendrites of glutamatergic pyramidal cells, which form the principal cell population of the AON. The cell bodies of these pyramidal cells are located in layer II, and beneath it lies a poorly differentiated layer consisting of neuromodulatory and corticofugal inputs to the AON. GABAergic cells and terminals are scattered throughout the AON, indicating that it performs internal processing of olfactory information. The pyramidal cells of the AON primarily target three regions: the OB, the contralateral AON, and the PC [21].

7. The Amygdala

The amygdala has been studied extensively as a region critical for emotional processing, emotional learning, and threat detection. Its role in olfactory processing is less understood, despite the fact that several of its subregions are considered part of primary olfactory cortex [23]. In rodents, the OB sends projections to several amygdalar subregions, including the posterolateral cortical amygdala, the anterior cortical amygdala, the medial nucleus of the amygdala, the periamygdaloid cortex and the nucleus of the lateral olfactory tract [23].

8. The Entorhinal Cortex (EC)

The EC is known to be involved in both olfactory learning and memory [5]. In the rodent olfactory system, the EC is involved in processing earlier than in other sensory systems, as it receives direct input from the OB [23]. The EC is uniquely positioned as an interface between the neocortex and the hippocampal formation, located dorsal of the rhinal fissure in the medial temporal lobe while, rostrally and medially, it borders the PC [27].

This region can be subdivided into the lateral and the medial EC both projecting to the hippocampus [28]. These two subregions might have distinct functions. While the medial EC is critical for spatial navigation, the lateral EC processes non-spatial stimulus features, including olfactory information, and is essential for olfactory memory, discrimination, and associative learning [23].

The EC can also be subdivided into six distinct layers, with subdivisions (a, b) in layers I and VI [7]. The layers I-III are mostly involved in hippocampal input and processing while layers IV-VI contribute to cortical output and feedback connections [29]. The layers I and IV are relatively free of neurons [27]. All remaining layers do contain a variety of neuronal subtypes that have been characterized on the basis of their anatomical and/or electrophysiological properties [27].

Olfactory fibers are known to mainly distribute to molecular layer I, where they make synaptic contact with dendrites of neurons in layers II and III [28]. These Neurons in external granular layer II are the main source of the entorhinal projections to the dentate gyrus (DG) and fields CA2 and CA3 of

the hippocampus while neurons in external pyramidal layer III give rise to the entorhinal projections to CA1 and subiculum [28]. The lamina dissecans layer IV separates superficial (I-III) from deep (V-VI) layers [28]. The internal pyramidal layer V contains large pyramidal neurons that project to subcortical structures and back to the neocortex [28]. Finally, the multiform layer VI containing heterogeneous cell types is involved in output to the thalamus and other regions [28].

9. The Hippocampus

The hippocampus is a complex brain structure embedded deep into the temporal lobe. It has a major role in learning and memory [30]. At the histological level, the mouse and human hippocampal formation look quite similar [7]. The hippocampus is divided into two parts: the Cornu ammonis (CA) et the DG. There are four sub-divisions of the Cornu ammonis, from CA1 to CA4 [30, 7]. Four different layers can be found in the CA: the pyramidal layer (Stratum pyramidale), the oriens layer (Stratum oriens), the radiatum layer (Stratum radiatum) and finally the lacunosum-moleculare layer (Stratum lacunosum-moleculare) [7]. The main output of the hippocampus is the pyramidal layer that contains pyramidal neurons [7].

The DG consists of three layers: molecular, granular, and polymorphic. Neurons within the DG are notable for being one of two regions of the nervous system capable of neurogenesis, with newborn neurons contributing to the continuous growth, development, and regeneration of neural tissue [7].

10. The Perforant Pathway

The EC is connected to different brain regions, such as the hippocampus, amygdala, OB, and PC [5]. The perforant path is one of these routes from the EC connecting to all fields of the hippocampal formation [31, 32]. This pathway arises from EC layers II and III. Neurons in layer II (and possibly layer VI) project to the DG and CA3 while neurons in layer III (and possible V) project to CA1 and to the subiculum [31, 32]. The DG also synapses on pyramidal cells in CA3 via mossy fibers. CA3 then fires to CA1 via Schaffer collaterals. CA1 then projects to the subiculum, whose outputs are transmitted through the fornix of the brain. Together, the DG, CA1, and CA3 of the hippocampus compose a trisynaptic loop (Fig. 7)[31, 32].

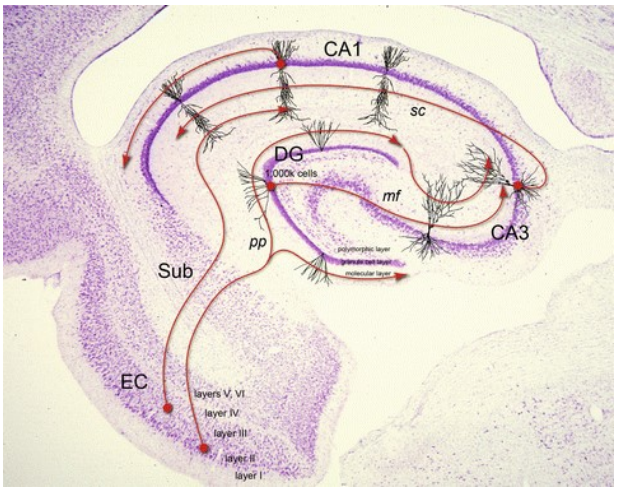

Fig. 7 The internal circuit of the hippocampus. The EC provides the primary cortical input to the hippocampus through the perforant path. Neurons in EC layer II project to the DG and CA3, while layer III neurons project to CA1 and the subiculum. Within the hippocampus, granule cells of the DG send mossy fiber projections to the pyramidal neurons of CA3. In turn, CA3 pyramidal cells project to CA1 pyramidal neurons via Schaffer collaterals**.** *EC:* entorhinal cortex, *DG:* dentate gyrus, *Sub:* subiculum, *pp:* perforant path, *mf:* mossy fibers, *sc:* Schaffer collateral [33]

11. Mouse versus Human Olfactory System

Mouse models constitute a model of choice for brain research, they have proven to be extremely useful for understanding diverse features of the brain, from its molecular neurobiological properties to its large-scale network properties. In fact, there are several key similarities between the human and mouse brain and olfactory systems, particularly in terms of structure, function, and organization. Despite difference in size and complexity, the basic architecture and pathways are evolutionarily conserved [34].

Both species share a similar olfactory pathway, which includes the OSNs in the nasal epithelium that detect odorants and transmit signal to the OB, and then to the olfactory cortex. The regions involved in olfactory processing (OB, PC and EC) are highly conserved across species (Fig. 8)[23, 35, 5]. One notable structural difference is that human adults lack an accessory olfactory bulb (AOB), and the vomeronasal organ is vestigial and non-functional [3].

In addition, the olfactory system is much larger relative to brain size and more developed in mice, given their reliance on smell for survival. The OB is particularly prominent compared to humans. In general, olfaction is less critical for daily functioning in humans than in mice. While the mouse olfactory system is more developed in terms of receptor gene diversity and sensitivity, the fundamental architecture – from sensory neuron function to cortical processing – is highly conserved between mice and humans [23, 35, 5]. This makes the mouse an excellent model for studying olfactory processing, neurodegeneration and investigating how impairment of the

olfactory system could relate to typical features of human neurodegenerative diseases (NDs).

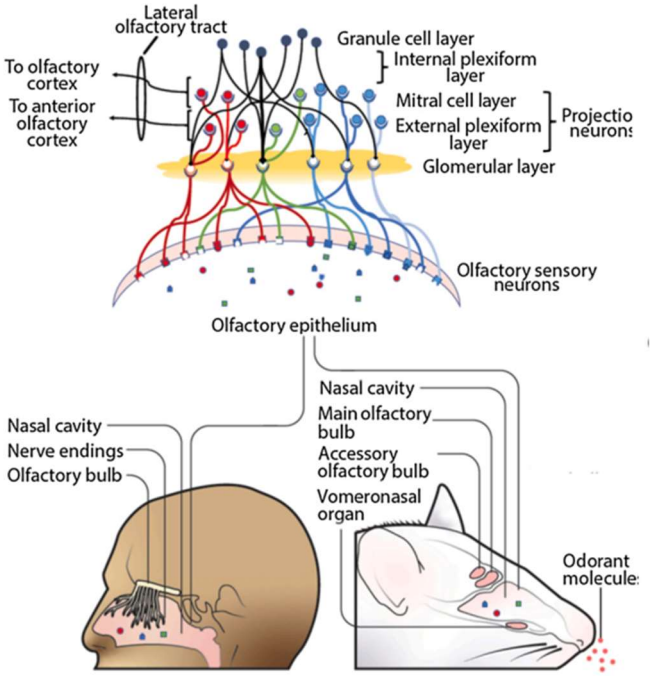

Fig. 8 The olfactory circuits in different organisms. Olfactory system in humans and mice. OSNs detect odorant molecules from OE, and project their signals to neurons in the glomerular layer, where axons then synapse with neurons in the mitral cell and external plexiform layers. Mitral cell axons transmit to the entire olfactory cortex, while axons of the external plexiform layers are confined to the anterior olfactory cortex. Mice have an AOB and vomeronasal system [3].

III. Olfactory Dysfunction

As mentioned before, a proper sense of smell is crucial for the recognition of danger, perception of the flavors of food and drink, and social interaction [2]. Olfactory dysfunction can therefore impact the quality of life and even lead to depressive symptoms [36]. This is particularly noteworthy

considering that 20% of the general adult population experiences olfactory dysfunction, increasing to 40% over the age of 65 and to 62,5% of people over 80 [37, 38].

1. Classification of Olfactory Dysfunction

Normal function of the sense of smell is termed **normosmia**. A quantitative decreased ability to smell is classified as **hyposmia** that can progress to a complete loss of ability named **anosmia**. Olfactory dysfunction can also be qualitative with **parosmia** that refers to a distorted perception of odors from an existing source, whereas **phantosmia** describes the sensation of smelling odors in the absence of any actual source. In most cases, quantitative and qualitative changes will coexist. Finally, a quantitatively increased ability to smell odors to abnormal level termed **hyperosmia** can also be observed in very few people. Hyposmia, anosmia, parosmia, phantosmia and hyperosmia fall under the broader category of olfactory dysfunction [36-38].

2. Causes of Olfactory Dysfunction

The primary cause of olfactory dysfunction is aging. Over time, the OE—which resides in the nasal cavities and houses OSNs—is gradually replaced by respiratory epithelium leading to a decreased regenerative capacity [14, 39]. In addition, as we age, the cribriform plate foramina, the openings in this plate, tend to decrease in size. This progressive closure of the foramina can impair the passage of olfactory nerve fibers, potentially leading to a decline in the sense of smell [16, 2].

Olfactory performance peaks at 40 years, after it gradually drops with aging [2]. Beyond the age of 80, two-thirds of this population experience reduced olfactory abilities [36].

In addition to age-related decline, olfactory dysfunction can arise from various other causes. It may develop following an upper respiratory tract infection, such as COVID-19 (postinfectious); after head trauma (post-traumatic); due to underlying sinonasal conditions like chronic rhinosinusitis with or without nasal polyps; in association with neurological or NDs; as a side effect of medications or exposure to toxic substances; after radiotherapy or surgery; or due to a tumor in the frontobasal region. Additionally, olfactory dysfunction can be congenital or classified as idiopathic when no known cause is identified [36].

Depending on the anatomical location of the lesion, the olfactory dysfunction might be classified in subcategories. The first one is **conductive** dysfunction that results from a blockage of odor transmission to the OE. A damage or loss at the level of the OE itself is referred to as **sensorineural** dysfunction. If damage occurs in the olfactory processing pathways of the CNS, it will be defined as **central** dysfunction [37].

3. Olfactory Function Assessment

Olfactory performance can be quantitatively assessed through subjective evaluations, psychophysical tests, or electrophysiological methods. Additionally, structural and functional imaging techniques are employed to evaluate olfactory function [36, 37].

Subjective assessment is the quickest and easiest method for evaluating olfactory function and, like medical history, plays a crucial role. However, due to individual differences in perceived impairment and self-awareness, these evaluations tend to be imprecise and often do not align with objective olfactory ability [36].

Psychophysical tests evaluate key aspects of olfactory function: odor threshold, discrimination, identification, and memory. Threshold testing determines the lowest concentration of an odor that can be detected. Odor discrimination measures the ability to distinguish between different scents, while odor identification assesses the ability to recognize and correctly name familiar odors, requiring previous exposure to odor stimulus [36, 37]. The olfactory threshold relies on the integrity of the periphery of the olfactory system such as the OE, while odor identification and discrimination mirror the central nervous processing of odors [37]. Among these tests, several are available for assessment of olfaction such as the Brief Smell Identification Test (B-SIT), the Alcohol Sniff Test, the Four-Minute Odor Identification Test, The Quick Smell Test, the Short Olfactory Screening Test, etc. [36]. More comprehensive tests are also available such as the Connecticut Chemosensory Clinical Research Center (CCCRG) Test, the University of Pennsylvania Smell Identification Test (UPSIT), The T&T Olfactometer, the Sniffin' Sticks Test, etc. [36].

Similarly, behavioral tests can be performed in mice to assess their olfactory capacities [22]. The olfactory behavioral tests in mice are classified in three categories: odor recognition, odor discrimination, and odor memory tests

[3, 5]. The odor recognition tests, used to evaluate the odor threshold in mice, are the most popular with the food-seeking test where mice are trained to look for buried food. There is also the odor sensitivity test where neutral odorants are diluted to various concentrations and presented in increasing order of odor concentration [5]. The second category includes olfactory discrimination tests, which comprise odor preference test, neutral odor discrimination test, odor cross-habituation test, and fine odor discrimination test [5]. Finally, the odor memory tests including episodic odor memory tests, context-independent odor memory test, and odor-emotion memory tests [5].

Olfactory testing differs significantly between humans and mice due to anatomical, cognitive, and methodological factors. In humans, olfactory function is typically assessed through psychophysical tests that measure conscious odor detection, discrimination, identification, and memory using standardized tools like the Sniffin' Sticks or UPSIT [40]. These rely on verbal responses and are influenced by factors such as attention, language, and cultural background. In contrast, mouse olfactory tests are behavioral and objective, often based on instinctive or learned responses to odor cues. Common paradigms include the buried food test or food-seeking test, habituation/dishabituation, and odor discrimination tasks, which assess odor sensitivity and memory through measurable behaviors like sniffing time or digging latency [5]. Unlike humans, mice are not consciously reporting perceptions, so motivation, stress, and task learning must be carefully controlled to avoid confounding results [41].

4. Current Approaches to Treating Olfactory Dysfunction

Currently, therapeutic options for olfactory disorders are limited, primarily focusing on treating the underlying conditions. Although several treatments have been tested in clinical trials, only olfactory training—deliberately inhaling a variety of odors multiple times a day—has demonstrated proven therapeutic efficacy [37]. To be efficient, olfactory training should be performed diligently and regularly, involving the inhalation of four different odors for 30 seconds each, twice daily, for a duration of 4–6 months or longer [36]. Olfactory stimulation might even be used in dementia care [42].

IV. The Olfactory System and Its Vulnerability in Neurodegenerative Diseases (NDs)

NDs are primarily characterized by the progressive degeneration of neurons and affect millions of people worldwide. The most common forms include Alzheimer's and Parkinson's disease, but the category also encompasses Amyotrophic Lateral Sclerosis (ALS), Huntington's disease (HD), Spinal Muscular Atrophy, and Friedreich's ataxia [43]. These diseases are particularly devastating because neurons are present throughout the body and, as post-mitotic cells, they cannot regenerate. As a result, their loss is irreversible [43].

Olfactory dysfunction, manifesting as hyposmia or anosmia, is present in 90% of Alzheimer's disease (AD) patients and individuals with idiopathic Parkinson's disease (IPD), especially in the early stage of the pathologies [44, 45]. Olfactory dysfunction is even defined as a prodromal symptom of AD/IPD, as it can emerge more than a decade before the cognitive

impairment or motor symptoms (Fig. 9)[36, 46-48]. Olfactory dysfunction is also an early marker for ALS, HD, Frontotemporal dementia (FTD), or schizophrenia [45, 49-51].

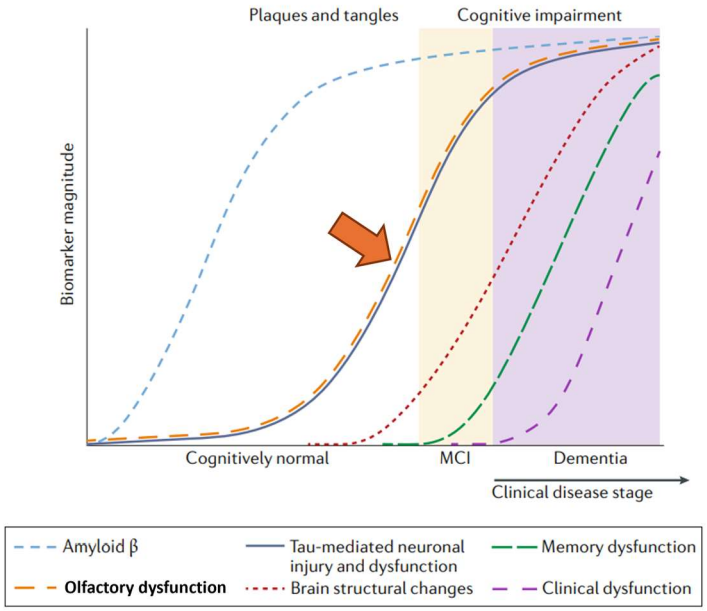

Fig. 9 Proposed emergence of olfactory functional impairment in Alzheimer disease pathological progression. This figure illustrates the emergence of olfactory impairment within the context of the emergence of other indicators of the pathological cascade described by Jack *et al.* (2010). MCI: Mild cognitive impairment [47].

The term "olfactory deficits/dysfunction/impairment" encompasses several functions, such as a decline in odor threshold (or sensitivity), odor identification, odor discrimination, and odor memory (or habituation) that cannot be measured by the same tests [16]. These various aspects of olfactory processing can be associated with the integrity of several brain regions (Fig. 10)[3].

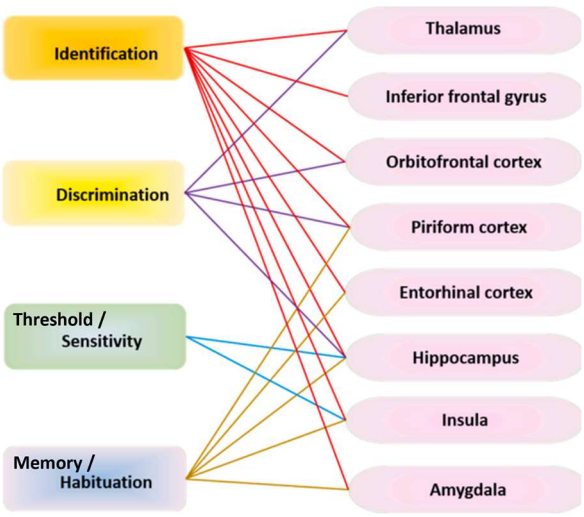

Fig. 10 The interconnection between different olfaction aspects and brain regions in human and mammalian animal models [3].

In addition, differentiating olfactory deficits caused by physiological aging from those associated with NDs presents a challenge [2]. During normal aging, the OE, which contains OSNs, is gradually replaced by respiratory epithelium. This is accompanied by ossification and closure of the foramina in the cribriform plate. Together, these changes can disrupt the transduction of olfactory information from the OE to the OB and the olfactory cortex [16, 18]. This can lead to an increase in odor threshold, which relies solely on the integrity of the OE and OSN transduction and therefore considered as a conductive dysfunction [16, 39]. In contrast, olfactory memory relies on hippocampal integrity, whereas odor identification/discrimination relies on the integrity of central olfactory structures [2, 52].

As noted earlier, NDs encompass a variety of disorders, including AD, PD, ALS, and HD, as well as pathological conditions such as frontotemporal lobar degeneration (FTLD). FTLD includes Pick's disease (PiD), progressive supranuclear palsy (PSP), corticobasal degeneration (CBD), and FTLD-17—a

familial form linked to MAPT mutations [53]. As we will see, the manifestation of olfactory deficits varies depending on the specific pathology involved.

1. Olfactory Dysfunction in AD

In AD patients, it has been shown that odor **identification** is particularly impaired (Fig. 11B) [16, 54, 18, 55]. This impairment reflects a cognitive deficit rather than a direct impairment of olfactory perception [49, 52, 54], since higher cognitive skills, such as verbal and semantic skills, are required for this odor identification ability [2]. Some odor tests, such as the "Odorant Item Specific Olfactory Identification test" have already been proposed, in which certain odors can differentiate AD patients from individuals with normal aging [18, 56].

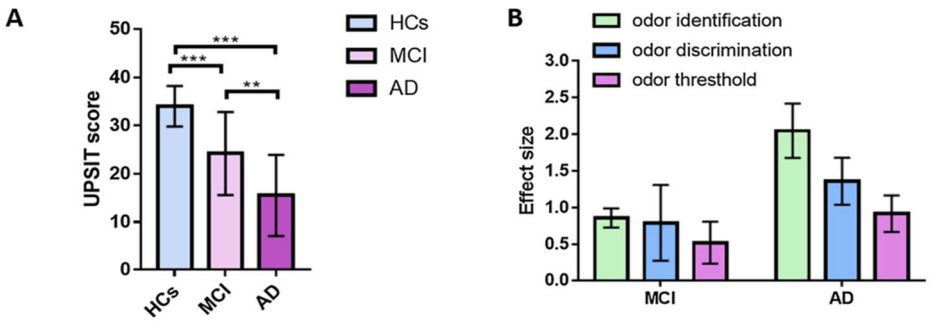

Fig. 11 Olfactory dysfunction in AD. Comparison of odor identification ability among HCs (healthy controls), MCI, and AD patients. Graph plotted based on Vasavada et al. (Vasavada et al., 2017). HCs (n = 27): 69.5 ± 10.4, MCI (n = 21): 73.2 ± 9.0, AD (n = 15): 71.9 ± 11.9. Mean ± SD. ** P < 0.01, *** P < 0.001 (a). Effect sizes for different olfactory domain deficits in prodromal MCI and AD (error bars indicate 95% confidence interval). Prior convention has classified effect sizes as small (d = 0.2), medium (d = 0.5) or large (d≥0.8). Graph plotted based on 2 meta-analyses (b)(Rahayel et al., 2012; Roalf et al., 2017) [3].

From a histopathological point of view, hyperphosphorylated tau has been observed both in the OB of AD patients and tauopathy mouse model [46].

In addition, *postmortem* analysis of olfactory regions in AD patients showed the presence of tau pathology in the OB, but also in the AON, and PC [35, 48]. pTau immunoreactivity has also been reported in the OE of AD patients [57, 58, 18].

Olfactory dysfunction and the accumulation of tau pathology in the OB progressively worsen with the severity of AD and directly correlates with Braak stage progression [59, 44, 60]. Importantly, tau pathology is observed in the olfactory system in all definite AD cases – diagnosis confirmed by neuropathological evidence – and in more than 1/3 of elderly individuals with or without MCI associated with Braak stage II [61]. Moreover, the OB is often considered as an access point for external insults and so, as the starting point for the spread of prion-like pathogens in the brain [46].

Some studies showed that olfactory impairment (especially odor identification deficit) is associated with both progression from normal cognition to mild cognitive impairment (MCI) and conversion from MCI to AD dementia [62, 55]. Alone, olfactory impairment correlates with baseline cerebral spinal fluid (CSF) biomarkers such as total tau and p-tau$_{181}$ and predicts future cognitive decline [63]. When combined with CSF markers, olfactory testing improves early detection of individuals at risk of MCI [1].

Moreover, plasma biomarkers—notably phosphorylated tau and neurofilament light chain (NfL)—also exhibit correlations with sensory deficits: anosmia is associated with elevated plasma levels of total tau and NfL. Studies show that combining olfactory dysfunction with plasma

biomarkers yields strong predictive value for conversion from MCI to AD over 2–3 years follow-up [1].

In individuals with smell impairment, plasma p-tau$_{181}$ and NfL are significantly higher compared to those with normal olfaction, suggesting that sensory decline may reflect early neuronal injury rather than amyloid burden [1, 63].

2. Olfactory Dysfunction in PD

Similarly to AD, up to 90% of PD patients have some degree of olfactory impairment. Olfactory dysfunction can appear 5-10 years before the motor symptoms, making it a potential early biomarker for PD. In these patients, odor identification is typically the most impaired, but odor discrimination and threshold can also be impacted [64].

The sensory dysfunction could result from early α-synuclein pathology in the OB, AON, and related cortical areas. The degeneration of dopaminergic and cholinergic pathways may also contribute to olfactory deficits [65].

While olfactory dysfunction is nearly universal in AD and PD, it is more variable in other NDs.

3. Olfactory Dysfunction in ALS

UPSIT-based studies have reported that 43.6% of ALS patients exhibit olfactory dysfunction, including 33.3% with hyposmia and 10.3% with anosmia [51]. The underlying mechanisms of olfactory dysfunction in ALS are not yet fully elucidated. However, it is hypothesized that the involvement of

the frontotemporal cortex, which is implicated in both olfactory processing and cognitive functions, may contribute to these deficits [66, 51].

4. Olfactory Dysfunction in HD

Olfactory deficits are present in both premanifest and manifest HD patients, with a progressive decline observed over time. Individuals with HD experience difficulties in detecting, identifying, discriminating, and recognizing odors, with significant impairments noted in odor memory compared to healthy controls [67]. These deficits are associated with worse motor and cognitive symptoms, suggesting that olfactory changes may serve as indicators of disease progression [68]. Finally, huntingtin aggregates have been identified in the OB individuals with HD, indicating that the olfactory system is among the early sites affected by the disease [69].

5. Olfactory Dysfunction in FTD/FTLD

As a reminder, the clinical syndrome of FTD is generally underpinned by FTLD [70]. In contrast to AD and PD, olfactory dysfunction in FTLD, including the familial FTLD-17 form caused by mutations in the MAPT gene, appears more variable, partly due to the limited comprehensive clinical data on olfactory function in such patients. While some studies report impaired odor identification and detection in FTLD-17 patients, the severity and pattern often differ from those observed in AD [71-73]. FTLD-related olfactory deficits are thought to reflect selective degeneration of frontal and anterior temporal regions rather than primary olfactory structures. However, tau accumulation in olfactory pathways can occur depending on the specific mutation [71]. Importantly, the relative preservation of medial temporal

structures in early FTLD may explain why olfactory impairment is less pronounced or manifests differently in FTLD-related pathologies such as PSP, CBD, and PiD compared to AD [73].

The frequency and early onset of olfactory impairments in AD patients highlight their potential as clinical markers. To understand the origin of these deficits, it is important to revisit the fundamental aspects of AD, the primary pathological framework in which these alterations occur.

V. Alzheimer's Disease (AD)

1. Background

AD is the most common type of dementia (60-80%), clinically characterized by a decline in cognitive function, that includes memory loss and difficulties with thinking, language and problem-solving skills [74]. Aging is considered as the most important risk factor in AD and because of the overall ageing of the population, the number of people suffering from dementia worldwide is likely to triple by 2050 [75, 74]. Healthcare systems in Europe currently lack the capacity to detect, diagnose, and effectively treat AD [75, 74].

The majority (more than 95%) of AD dementia cases are sporadic and influenced by both genetic and environmental factors [76]. In contrast, less than 5% are familial forms, among which the inherited autosomal dominant AD cases (ADAD) that arise from mutations in three major genes: the amyloid precursor protein (APP) gene, presenilin 1 and presenilin 2 genes and represent less than 1% of the cases. These familial forms tend to develop earlier and are thus over-represented in Early Onset AD (EOAD) [77, 76].

AD is a progressive and incurable ND that can be characterized neuropathologically by abnormal accumulation of protein aggregates including amyloid beta plaques and neurofibrillary tangles (NFTs). Amyloid

or senile plaques are composed of misfolded amyloid-β (Aβ) proteins and are first found in the basal temporal cortex and orbitofrontal cortex, then progress to the neocortex, basal ganglia, hippocampal formation, and the amygdala as AD progresses. Aβ plaque pathology is observed to accumulate outside neurons, where plaques interfere with their ability to communicate [78]. In contrast, NFTs made of hyperphosphorylated tau inclusions appear in the locus coeruleus and EC, then spread to the neocortex and hippocampal formation throughout the brain [75, 18]. Hyperphosphorylated tau accumulates within neurons through a series of maturity levels with a gradual deposition of aggregates within specific areas is instrumental to AD pathology [79, 80, 78]. During this maturation process, NFTs form inside the affected neuron resulting in axonal instability that impairs transport of nutrients and cell signal communication [78].

The distribution pattern of tau lesions progresses according to a sequence known as Braak staging [81, 79]. In Braak stages I/II, NFTs are confined mainly to the (trans-)entorhinal region in the temporal lobe. Stages III/IV involve limbic regions such as the hippocampal formation and parahippocampal areas, and extensive neocortical involvement is observed in later stages V-VI [81, 79].

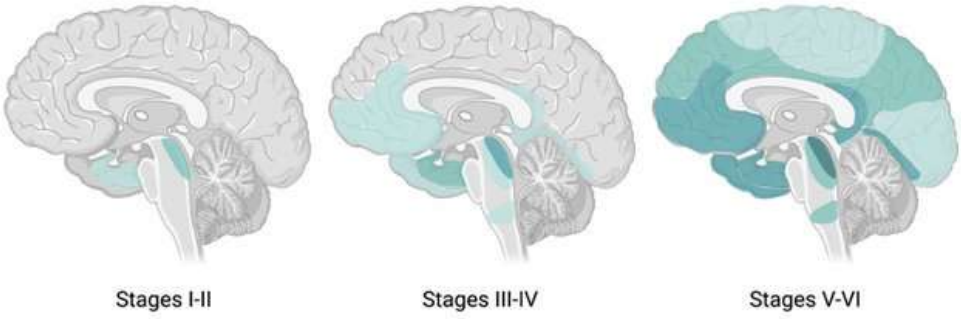

Fig. 12 Tau spreading pattern in each Braak stage. Spreading pattern of tau throughout the brain from Braak stage I-II to stage III-IV (limbic regions) and stage V-VI (isocortical areas) [82].

Braak stages are considered as the neuropathological gold standard used in *postmortem* examinations to confirm AD [79, 83]. Braak staging is also used to classify the clinical diagnosis of AD because it reflects the temporal and spatial spread of tau pathology that seem to be strongly correlated with cognitive decline [83]. Indeed, global tau-PET is a better predictor of future cognitive decline than global amyloid-PET and an advanced Braak-stage is associated with faster cognitive decline [84].

Studies show that these pathological hallmarks appear two decades before the clinical onset of AD symptoms leading to a typical course of AD in three phases (Fig. 13)[85]. First, preclinical AD where abnormal AD biomarkers can be measured without clinical symptoms [86]. This can progress to MCI where individuals are mildly symptomatic but do not have dementia [87]. When people finally develop dementia, they show a progressive loss of cognitive function and of their ability to live independently [88].

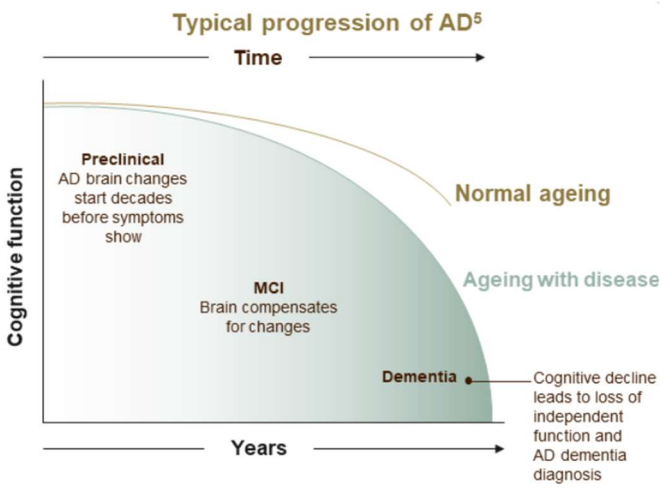

Fig. 13 Typical progression of AD. Preclinical, MCI and AD dementia phases [88].

2. AD Diagnosis

AD affects approximately 7 million people in Europe alone, with diagnosis typically occurring at a late stage in the disease's progression [89].

The diagnosis of AD in Europe relies on a multidisciplinary approach that integrates several methods (Fig. 14). It begins with a clinical and cognitive assessment, where tests such as the Mini-Mental State Examination (MMSE) or the Montreal Cognitive Assessment (MoCA) evaluate memory, attention, and executive functions [90].

Medical imaging plays a crucial role, with brain MRI used to detect hippocampal atrophy, while PET scans assess cerebral metabolism. Additionally, amyloid PET imaging provides a direct visualization of amyloid plaques, a hallmark of the disease [89, 90].

These imaging techniques are complemented by cerebrospinal fluid (CSF) analysis, obtained through a lumbar puncture. Key biomarkers include a

reduced level of β-amyloid protein and an elevated presence of tau and phosphorylated tau proteins, which indicate neurodegeneration [90].

More recently, blood biomarkers have started to be incorporated, offering a less invasive alternative for early detection and monitoring [91, 92].

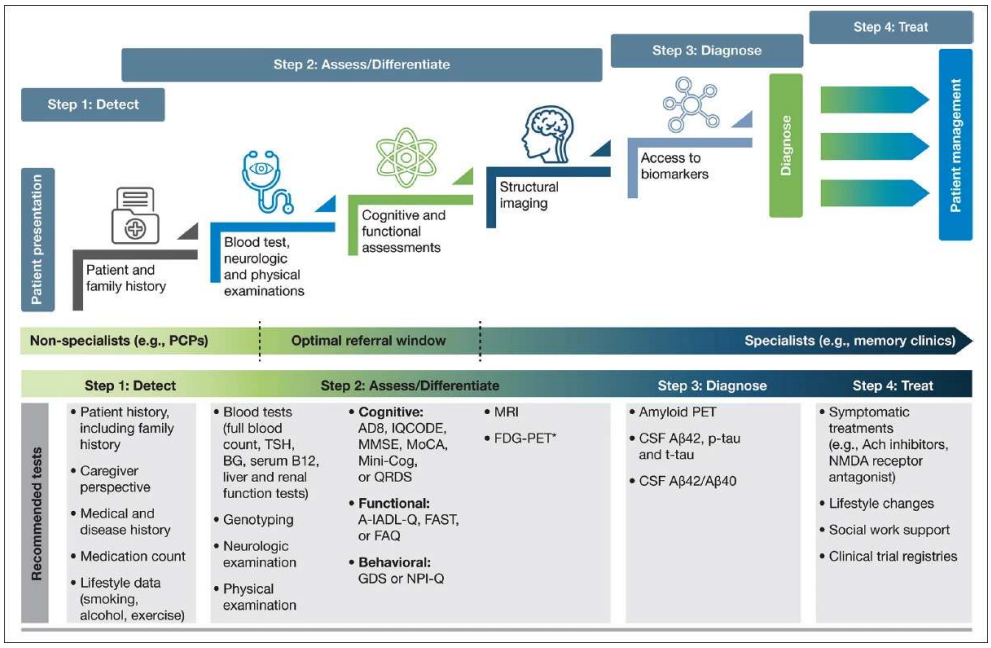

Fig. 14 A stepwise infographic to highlight key stages within the diagnostic process, along with the recommended tests to support each step [90]. The first step involves detection through patient anamnesis and family history. This is followed by a comprehensive assessment, including blood tests, neurological and physical examinations, as well as cognitive and functional evaluations. Structural imaging is then performed to support and refine the diagnostic process. The final step encompasses treatment planning and long-term patient management.

Nowadays, under-detection and late diagnosis of AD remain major challenges, underscoring the need for improved tools that enable earlier detection and more effective management of patients and support their families.

3. AD Treatment

The quest of safer and more effective AD drugs is still ongoing even if in 2025, treatments for AD are seeing significant advancements.

Currently, most of available drug treatments have only symptomatic effects such as inhibitors to cholinesterase enzyme and antagonists to *N*-methyl d-aspartate (NMDA) but do not cure or prevent the disease [75]. The main challenge is that drug delivery to the CNS remains a complex process and represents a challenge for developing therapeutic and preventive strategies [93].

More recently, therapies targeting the underlying mechanisms of AD have been developed to slow its progression. Among them, lecanemab, a monoclonal antibody designed to target beta-amyloid protofibrils, has garnered significant attention for its ability to reduce amyloid plaques in the brain [94].

After an initially unfavorable assessment in July 2024, the European Medicines Agency (EMA) granted approval for lecanemab in November 2024 under the brand name Leqembi, for patients in the early stages of AD. The treatment had previously received FDA approval in January 2023 [94].

Regardless of these advancements, the high cost of these therapies, along with potential risks, underscores the need for continued research to develop safer and more effective treatment options [94].

Despite extensive efforts to understand and target Aβ pathology as the initial trigger of AD, the disappointing outcomes of numerous clinical trials—

marked by limited efficacy and weak correlation between amyloid burden and clinical symptoms—have prompted a critical reassessment of therapeutic priorities. These shortcomings have shifted attention toward alternative pathological markers, with tau protein emerging as a key candidate. While the molecular mechanisms underlying AD are complex and multifactorial, growing evidence implicates tau as a central driver of neurodegeneration. Consequently, this project will focus exclusively on tau, exploring its structure, pathological transformations, and role in disease progression.

VI. The Tau Protein and its Normal Function in Neurons

The tau protein - discovered in 1975 - is defined as a microtubule-associated protein (MAP) [95]. Structurally, tau is a natively unfolded protein, is highly soluble and shows little tendency for aggregation [96]. It is encoded by the *MAPT* gene [97, 98]. This gene is found on chromosome 17q21 in humans and contains 16 different exons [98, 99]. Alternative splicing of exons 2,3, 4A, 6, 8 and 10 can lead to the expression of six different isoforms in the human brain ranging from 352 to 441 amino acids (Fig. 15)[97, 98, 100].

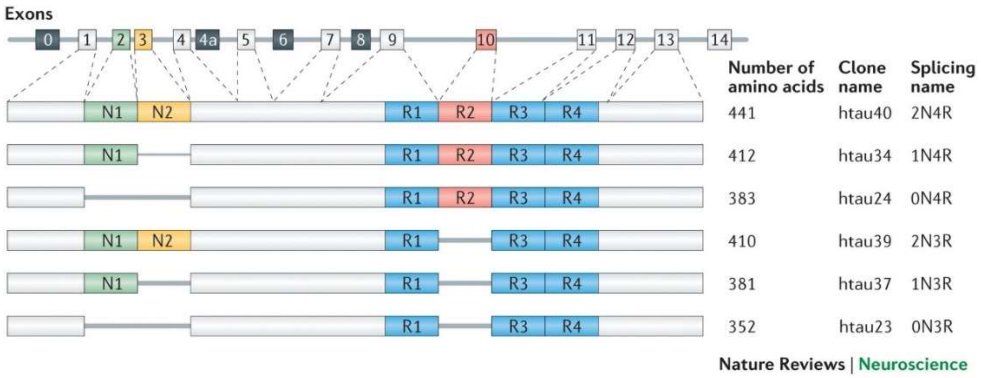

Fig. 15 Human brain Tau isoforms. *MAPT* and the six Tau isoforms expressed in adult human brain. *MAPT* consists of 16 exons (E). Alternative mRNA splicing of E2 (green), E3 (yellow), and E10 (red) gives rise to six Tau isoforms (352–441 amino acids). The constitutively spliced exons (E1, E4, E5, E7, E9, E11, E12, and E13) are shown in grey. E0, which is part of the promoter, and E14 are non-coding (white). E6 and E8 are almost always spliced out and therefore do not appear in tau mRNA in the human brain. E4a is only expressed in the PNS. The repeats (R1–R4) are shown, with three isoforms having four repeats each (4R) and three isoforms having three repeats each (3R) [96] .

The tau protein contains: N-terminal projection domains that play an important role in regulating distance among microtubules, a proline-rich domain helps in cell signaling and interaction with protein kinases and contains abundant phosphorylation sites, a microtubule-biding region and a C terminal domain involved in microtubules polymerization [100, 99]. The tau isoform can contain 0, 1 or 2 inserts of 29 amino acids (0N, 1N, 2N) in the N-terminal end (alternative splicing of exons 2 and 3) and can also be 3R or 4R (number of microtubule-binding repeats domains) depending on the splicing of exon 10 [100]. This leads to the six possible tau isoforms: 3R0N, 3R1N, 3R2N, 4R0N, 4R1N, and 4R2N [99]. 4R tau will then have more repeats and show an increased binding affinity for microtubules [100]. In human healthy adults the ratio 3R:4R is around 1 but in AD patients, an excess in 4R forms is found [97]. Actually, most of tau mutations leading to dementia

have an impact on protein splicing and increase 4R forms expression [97]. Besides the six major tau isoforms in the adult human brain, big tau is a high-molecular-weight isoform that includes exon 4a. This isoform is predominantly expressed in the peripheral nervous system (PNS) and has an extended projection domain of approximately 250 amino acids, resulting in a protein of 110kDa [101]. Unlike humans, adult mice do not express the 3R tau isoforms, although they do express big tau [102].

Tau is predominantly found in neuronal axons associated with microtubules. The microtubule-biding domain contain 18 positively-charged lysine residues, driving tau biding to the microtubule, a negatively-charged polymer [103]. It is known to play a crucial role in microtubule stabilization and dynamic to preserve integrity of the cell's cytoskeleton, preserving axonal structure and function [98, 103]. Recent studies have revealed additional physiological functions of tau as a synaptic protein, highlighting its role in promoting spine formation, dendritic growth, and synaptic plasticity [103].

As a matter of fact, regulation of tau function is predominantly achieved through post-translational modifications (PTMs) including phosphorylation, acetylation, ubiquitination, glycation, glycosylation, SUMOylation, methylation, oxidation, truncation and nitration [104]. These PTMs have been recognized as affecting protein function and being the proteinaceous hallmark of tauopathies [104, 99]. For instance, tau phosphorylation on specific sites is known to decrease its microtubules-binding affinity [97].

The phosphorylation extent of tau is the result of an equilibrium in the activity of protein kinases – adding a phosphate group and phosphatases – removing a phosphate group [105]. Tau contains 85 potential phosphorylation sites, which occur at serine (45), threonine (35), and tyrosine (5) [99].

There are three families of kinases involved in tau phosphorylation. The "proline-directed" protein kinases tend to phosphorylate serine and threonine motifs outside the microtubule-binding domains, the "non-proline directed" protein kinases and the protein kinases specific for tyrosines [99]. In pathological conditions, the kinase-phosphatase balance is shifted, creating hyperphosphorylated species of the tau protein [97]. This equilibrium disruption has been assumed to be at the origin of tau hyperphosphorylation and the subsequent toxicity and progress of the disease [105].

VII. The Pathological Tau Protein

1. Tauopathies

Tauopathies are a class of NDs where abnormal filamentous and hyperphosphorylated tau is found [106, 78]. They can be defined as primary or secondary. In primary tauopathies, tau pathology is the main feature and drives the disease. In secondary tauopathies, another protein is necessary to drive the neurodegeneration, like Aβ in AD [106]. Despite the fact that tau aggregation is present in every tauopathy, there are variabilities in the predominant tau isoforms, the affected brain regions, and the clinical symptoms [106].

Tauopathies are commonly categorized based on the predominant tau protein isoform in the aggregates (3R/4R) that accumulate in the brain. These include 3R tauopathies, such as PiD; 4R tauopathies, which include PSP, CBD, argyrophilic grain disease (AGD), and globular glial tauopathy (GGT); and mixed 3R/4R tauopathies, such as AD, chronic traumatic encephalopathy (CTE), and primary age-related tauopathy (PART) [107].

2. NFTs Formation

Under pathological conditions, the highly soluble tau monomers can undergo hyperphosphorylation, which increases their tendency to aggregate, leading to the formation of tau oligomers. The charge balance between tau and microtubules becomes disrupted. Consequently, hyperphosphorylated tau dissociates from microtubules and accumulates in the cytosol [103]. These tau oligomers act as intermediate structures that can induce conformational changes in the structure of tau, resulting in the formation of stacked β-sheet strands and forming insoluble paired helical filaments (PHFs) [108, 99]. These PHFs accumulate within the neuralperikaryal cytoplasm, axons and dendrites and finally cause a loss of cytoskeletal microtubules and tubulin-associated proteins. The PHFs and straight filaments accumulate inside neurons, forming NFTs, composed primarily of insoluble, aggregated tau, resistant to degradation [108, 99].

In the cytoplasm, mislocalized tau undergoes multiple post-translational modifications, including acetylation, sumoylation, ubiquitination, glycosylation, methylation, nitration, truncation, and the formation of intermolecular bonds. Acetylation of tau inhibits the degradation of

phosphorylated tau. Additionally, the formation of disulfide bonds between tau molecules stabilizes tau oligomers, which are crucial for tau aggregation and propagation [103].

With a better understanding of tau's various forms, from hyperphosphorylation to NFTs, we now turn to the tools used to study these pathologies. Tau-specific antibodies play a key role in both diagnosing and targeting tau-related abnormalities and will be discussed in the following section (Fig. 16).

3. Tau Antibodies

Tau can be detected independently of its phosphorylation status using total tau antibodies, such as Tau-5 or HT7 [109]. In contrast, other antibodies specifically recognize tau when it is phosphorylated. Among these, AT8 is one of the most widely used antibodies for detecting phosphorylated tau, particularly in AD. It targets phosphorylation at the Ser202/Thr205 epitopes and was instrumental in defining the Braak staging system of tau pathology [81, 110].

Several antibodies, such as AT180 (Thr231) and AT270 (Thr181), are associated with early phosphorylation events in the progression of tau pathology [111, 112]. Alz-50 is a conformational antibody that detects early pathology tau [113]. Others, including AT100 (Thr212/Ser214) and PHF-1 (Ser396/Ser404), are typically linked to more mature forms of pathological tau [114]. However, evidence suggests that these latter antibodies may also detect early stages of tau pathology [115].

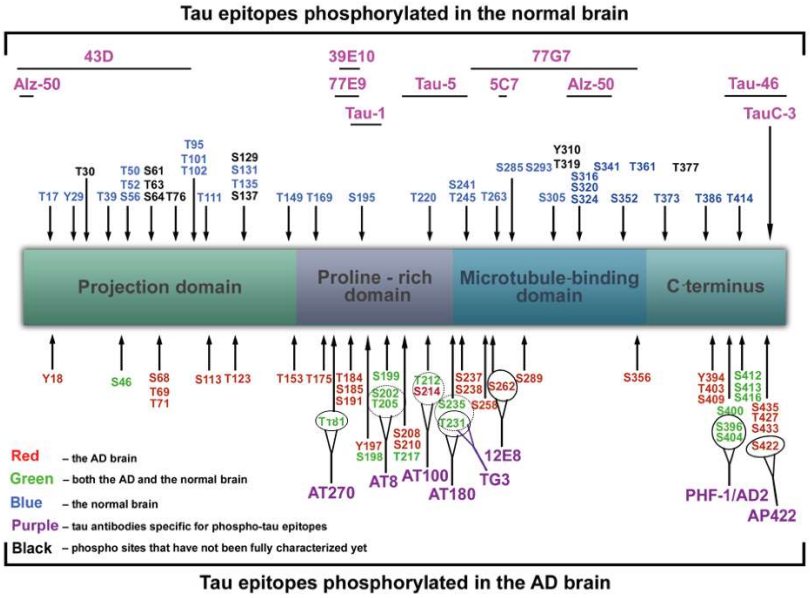

Fig. 16 Putative phosphorylation sites on tau protein and epitopes specific to major tau antibodies. Red color denotes amino acids phosphorylated in AD brain, green in both AD and normal brain, blue in normal brain, while black color means that those phosphorylation sites have not been fully characterized yet. Tau antibodies specific for phospho-tau epitopes are cited in purple, while pink denotes antibodies specific for non-phosphorylated tau epitopes [116].

4. NFT Maturity

The hyperphosphorylated tau protein is the major constituent of NFTs in the brains of AD patients, and its evolution can reflect NFT morphological stages. The first stage is the pre-tangle phase or NFT-like tau accumulations (I) defined by morphologically normal neurons with a healthy nucleus where phosphorylated tau proteins are accumulated in the somatodendritic compartment without the formation of PHF. The second phase is called the mature NFTs (II), gallyas-positive and characterized by filament aggregation of tau protein with the displacement of the nucleus to the periphery part of the soma. Finally, the ghost tangles (III) present in the extracellular

compartment result from a neuronal loss with partial resistance to proteolysis (Fig. 17)[117, 75, 78].

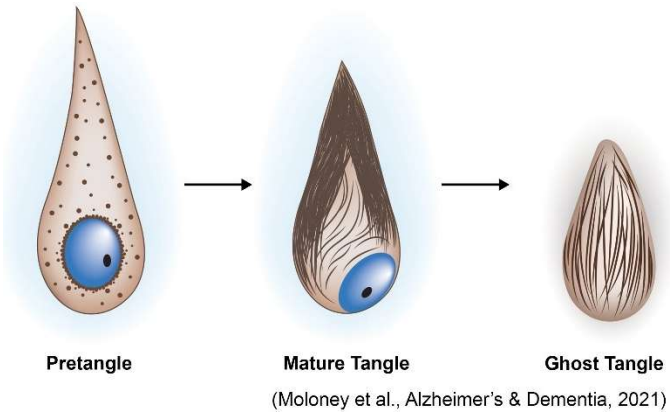

Fig. 17 Neurofibrillary tangle (NFT) maturity level in the CA1 subsector of the hippocampus. Pretangles have perinuclear accumulation of tau, in addition to a diffuse or granular staining pattern. Mature tangles assume the shape of the neuron in which they reside (e.g., "flame-shaped") and are composed of tightly packed bundles of fibers. The neuron has a dislocated and/or shrunken nucleus. Ghost tangles are loosely arranged bundles of fibers with no associated nucleus as they are the remnants of mature tangles once the neuron has died. AT8 was used for pretangle, PHF-1 was used for mature tangles. Ab39 was used for ghost tangles. It is important to note that these antibodies recognize a range of the NFT maturity levels. Immunohistochemistry was counterstained with hematoxylin. Arrows point to the labeled pathology. Bracket includes the entire neuritic plaque structure. Scale bar measures 25 μm [78].

5. Neuritic Pathology

In addition to intracellular NFTs, neuritic pathologies are also consistently observed in AD brains. It includes neuropil threads, neuritic plaques and tangle associated neuritic clusters (TANCs). Neuropil threads were described as thread-like structures outside of cells bodies, identified in dendrites of tangle-bearing neurons in AD brains. Neuropil threads can be observed in proximity to pretangles, mature tangles, and ghost tangles. These structures are revealed by antibodies that recognize hyperphosphorylated tau [78]. Neuritic plaques are larger than a neuron and are principally composed of extracellular Aβ deposits and thread-like dystrophic neurites. They can be stained with a variety of tau antibodies [78]. Finally, TANCs are composed of neurites surrounding a ghost tangle. They are identified by silver staining and multiple tau antibodies, like AT8 and Alz-50 (Fig. 18)[78].

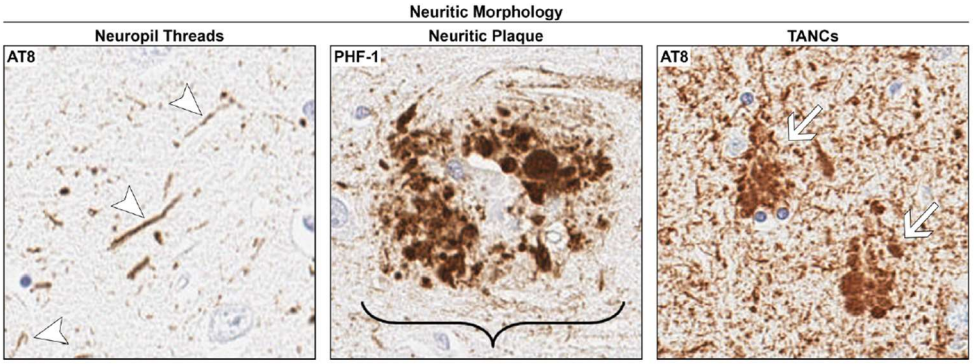

Fig. 18 Neuritic morphologies in the CA1 subsector of the hippocampus. Neuropil threads are the thread-like staining pattern outside of the soma. Neuritic plaques are the accumulation of dystrophic neurites and are larger than a neuron. Tangle associated neuritic clusters (TANCs) are the accumulation of neurites around a ghost tangle and are around the same size as a neuron. AT8 was used for neuropil threads, and TANCs. PHF-1 was used for neuritic plaques. Immunohistochemistry was counterstained with hematoxylin. Arrows point to the labeled pathology. Bracket includes the entire neuritic plaque structure. The scale bar measures 25 μm [78].

6. Tau Clearance Mechanisms

The recognition and removal of misfolded, damaged, or potentially toxic proteins is essential for maintaining healthy and functional neurons. Tau plays an important role in modulating physiological processes, and the accumulation of toxic tau proteins is deleterious to cells. It is therefore essential to maintain effective clearance mechanisms, the disruption of these mechanisms being a significant contributor to NDs [103].

There are two major systems that regulate tau clearance: the proteasome system and the autophagy-lysosome pathway [103, 118].

6.1. The Proteasome System

The catalytic core particle of the proteasome or 20S proteasome is a barrel-shaped 700 kD multimeric cellular structure that has three proteolytic activities: chymotryptic-like, tryptic-like, and caspase-like. The 20S proteasome can be uncapped, singly capped or doubly capped with the 19S regulatory particle (RP) (or in some cases the 11S RP) to form the 26S proteasome [118].

The 20S proteasome can directly degrade natively unfolded proteins or intrinsically disordered proteins through an ATP- and ubiquitin-independent process. The 26S proteasome primarily degrades proteins that have been polyubiquitylated with a ubiquitin chain of at least four molecules. The process of ubiquitylation is ATP dependent and requires the action of three enzymes (E1, E2, and E3)[118].

Tau is considered as one of the largest intrinsically disordered proteins and is therefore degraded by the 20S proteasome. Indeed, ubiquitylation is not required for **physiological** tau degradation by the proteasome. However, when tau undergoes **pathological** modifications such as phosphorylation in AD, the induced structural changes decrease the efficiency of the degradation by the 20S proteasome. Aggregated tau can also be ubiquitylated but is not effectively degraded by the 26S proteasome, impairing its function [118].

6.2. The Autophagy-Lysosome Pathway

Autophagy is a process that involves degradation of substrates by the lysosome. It involves the formation and elongation of a double membrane structure called phagophore, which closes around cargos to form autophagosomes which subsequently fuses with lysosomes. This fusion results in the formation of an autolysosome. Alternatively, the autophagosome can fuse with an endosome to form an amphisome which also then fuses with the lysosome. Evidence showed that autophagy is a significant contributor in the degradation of tau and that attenuation of autophagy may potentially be a contributing risk factor for the onset of age-related NDs including AD [118].

Tau is likely degraded through different autophagic routes. Cytosolic, as well as extracellular tau, can also be incorporated into endosomes which then can go on to fuse directly with lysosomes forming endolysosomes or the endosome can fuse with an autophagosome to form an amphisome prior to fusing with lysosomes [118]. In contrast to the proteasome, degradation by

autophagy is crucial for the degradation of large tau aggregates, including NFTs [118].

Finally, extracellular tau can also be recognized and degraded by brain immune cells such as microglia or astrocytes via phagocytosis. However, chronic neuroinflammation can also impair this process [119, 103].

7. Tau Pathobiology

The pathogenesis of tau-mediated neurodegeneration in tauopathies remains unclear. Even though, loss of function, toxic gain of function and mislocalization have each been implicated in tau-mediated neurodegeneration.

Tau is required for normal neuronal and brain function. Therefore, neurotoxicity owing to loss of tau function can occur in tauopathies. Loss of tau function is generally induced by the protein aggregation or its hyperphosphorylation. The hyperphosphorylation of tau within the repeat domain weakens its ability to bind microtubules, potentially causing microtubule disassembly and leading to disruptions in axonal transport. Additionally, the aggregation of tau reduces the availability of soluble, functional tau, further contributing to microtubule destabilization. Beyond its structural role, tau is involved in various critical functions, including iron transport, neurogenesis, long-term depression, and neuronal DNA protection. The loss of these functions due to tau dysfunction may further drive neurodegeneration by impairing these essential cellular processes [96].

In addition to its classical cytoskeletal role, tau also localizes to the nucleus, where it contributes to genome stability. Nuclear tau binds DNA and chromatin components, protecting neurons from oxidative stress–induced DNA damage [120]. Dysregulation of this function, as seen in tauopathies, may lead to impaired DNA damage response pathways, increased genomic instability, and neuronal vulnerability [121]. Interestingly, given its involvement in genome protection, aberrant tau expression or localization has also been observed in several cancers, suggesting potential mechanistic links between tau dysfunction, DNA repair alterations, and oncogenic processes [122].

The accumulation of NFTs was initially recognized as a major trigger of neuroinflammation, resulting in neuronal damage [99]. It seems that the neurotoxic gain of pathological tau function relies on the hyperphosphorylated soluble tau oligomers instead [96].

In healthy neurons, only a small proportion of tau localize in the dendritic compartment. In tauopathies, the increase in dendritic tau levels, due to the mislocalization of tau induced by its hyperphosphorylation, mutation and overexpression, results in synaptic dysfunction [96]. Neurotoxic tau protein can also disrupt the structural and functional integrity of mitochondria including impaired mitochondrial biogenesis, abnormal mitochondrial fusion, fission, trafficking, and distribution, impaired mitochondrial biogenesis, and damaged mitophagy [123].

As mentioned before, tau degradation occurs through two main pathways: the ubiquitin-proteasome system (UPS) and the autophagy-lysosome

pathway. The UPS serves as the primary mechanism for clearing pathological hyperphosphorylated tau, whereas the autophagy-lysosome pathway becomes more active in the later stages of NFT formation. Overall, when these clearance mechanisms fail or become overwhelmed, tau accumulates, leading to aggregation and the formation of NFTs—hallmarks of tauopathies such as AD [99].

8. Pathological Tau Propagation and the Prion-Like Hypothesis

As originally proposed by the findings of Heiko and Eva Braak [79], the development of tau pathology in AD occurs in a hierarchical pattern of accumulation starting from the layer II of EC and spreading toward cortical regions. Growing evidence indicates that in many ND, aggregates of misfolded and pathological proteins propagate through neuroanatomically connected regions of the brain, mimicking the spread of pathological prion proteins (PrP) [124]. When tau protein becomes hyperphosphorylated, it gains the ability to convert normal tau proteins into pathological forms. This process is similar to that of prions; infectious agents composed of misfolded proteins that propagate disease by inducing the misfolding of healthy proteins (Fig. 19).

Consequently, hyperphosphorylated tau can trigger the conversion of healthy neighboring proteins into misfolded forms, driving the progression of tauopathies [124]. Indeed, tau can act as a central hub for its own aggregation and as a template for inducing further misfolding in a process known as templated misfolding. Once aggregated, these pathological tau seeds can spread from one cell to another, propagating the pathology from

affected to healthy cells and to previously unaffected regions of the brain. In a groundbreaking study in 2009, researchers showed that tau extracted from tau transgenic mice - which harbor a mutation (P301S) linked to frontotemporal dementia and develop tau inclusions - when injected into healthy mice that do not typically develop tau inclusions, led to the onset of tau pathology [124, 125].

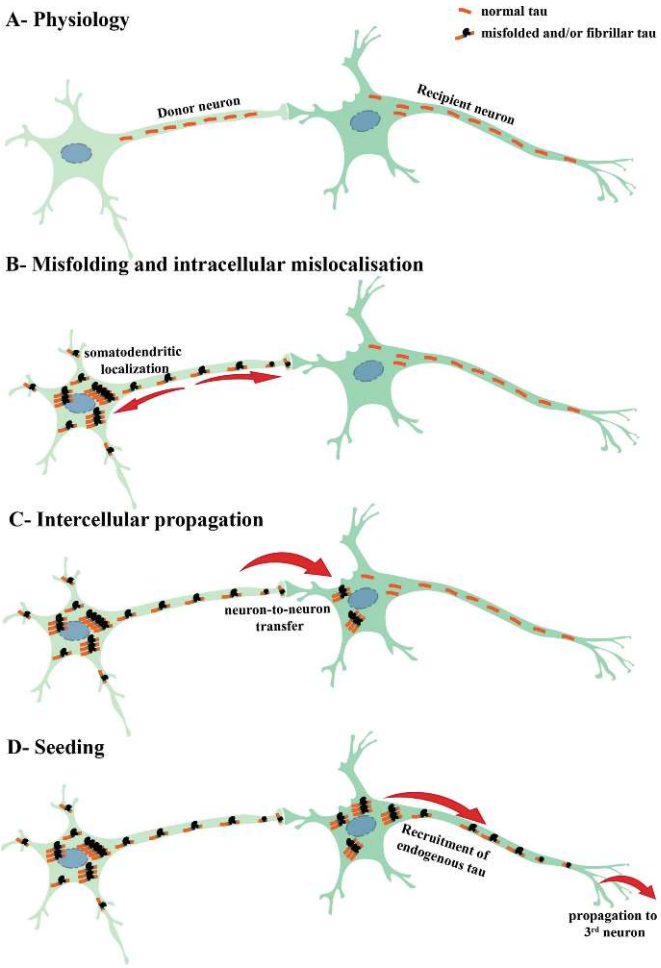

Fig. 19 Tau prion-like propagation model. In physiology normal tau proteins (orange) are predominantly located in the axonal part of neurons (a). Tau propagation starts with an early misfolded event that spreads through a neuron and many tau proteins accumulate into the somatodendritic as well as the synaptic terminals of the neurons (b). Misfolded tau proteins are transferred from neuron-to-neuron through the synapses (c) and in the recipient neuron, recruit endogenous tau, transmit their misfolding properties in a seeding mechanism and spread the pathology (d). Not to scale [126].

Although tau is primarily an intracellular protein, recent studies have revealed that, in addition to being released by dying neurons, tau can also be actively secreted into the extracellular space both *in vitro* and *in vivo*

[127]. Many aspects of tau secretion remain to be elucidated, but it appears that tau can exit cells through various pathways. Consequently, it can be found and measured in the CSF, with elevated levels in AD patients [124].

The first mechanism of cell-to-cell transfer of pathological tau protein described is direct secretion across the plasma membrane involving clustering of tau protein at the plasma membrane, interaction with specific lipids, penetration across the plasma membrane and release facilitated by heparan sulfate proteoglycans on the cell surface. Tau can also be secreted into exosomes, formed by inward budding of multivesicular bodies and later released upon fusion of these multivesicular bodies with the plasma membrane. Similarly, tau can be secreted in ectosomes shed from the plasma membrane. These microvesicles, larger than exosomes, can fuse with or be endocytosed by other cells. Finally, tau seeds can pass through tunneling nanotubes that directly connect the cytosols of two neighboring cells (Fig. 20)[127].

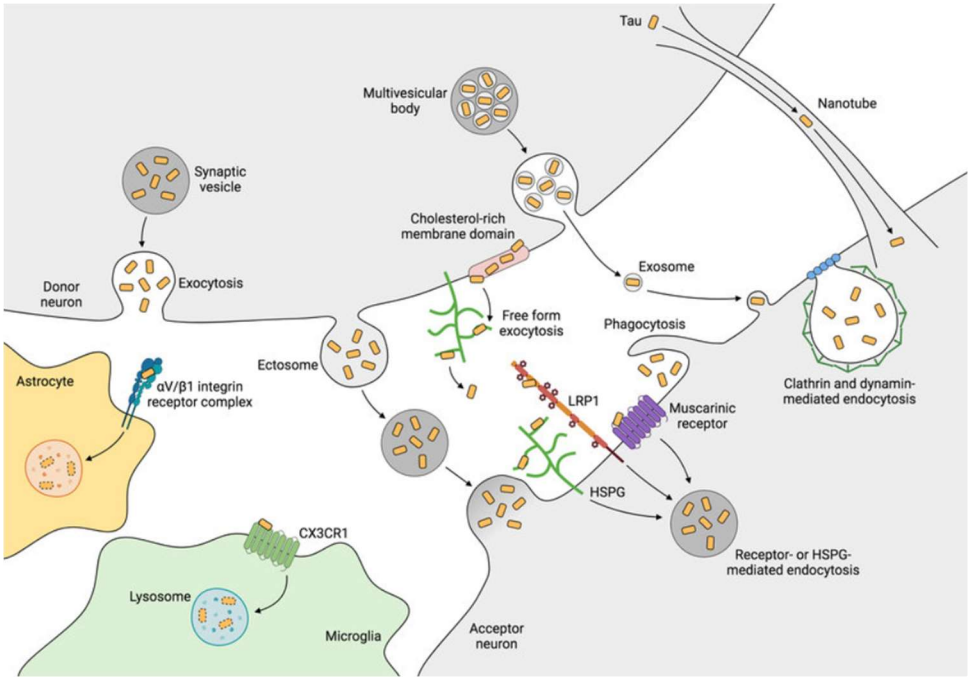

Fig. 20 Tau transmission mechanisms. The processes depicted above occur commonly at synapses, where tau can be released to the extracellular space through synaptic vesicles or by direct translocation. Tau is then internalized through receptor- or heparan sulfate proteoglycan (HSPG)-mediated endocytosis, clathrin- and dynamin-mediated endocytosis, and phagocytosis. In addition, tau can be spread through extracellular vesicles (ectosomes and exosomes) that fuse to the membrane of the recipient cell. Moreover, nanotubes establish intercellular communication that serves as a bridge for tau propagation [128].

VIII. Tau-targeting Therapies

Tau-directed therapeutics aim to alleviate the neurotoxic gain of tau function or the loss of tau function [96]. Different strategies have been explored: tau reduction, inhibition of tau phosphorylation and aggregation, microtubule stabilizers, enhancing quality control of tau protein and, immunotherapy (Fig. 21)[107, 96].

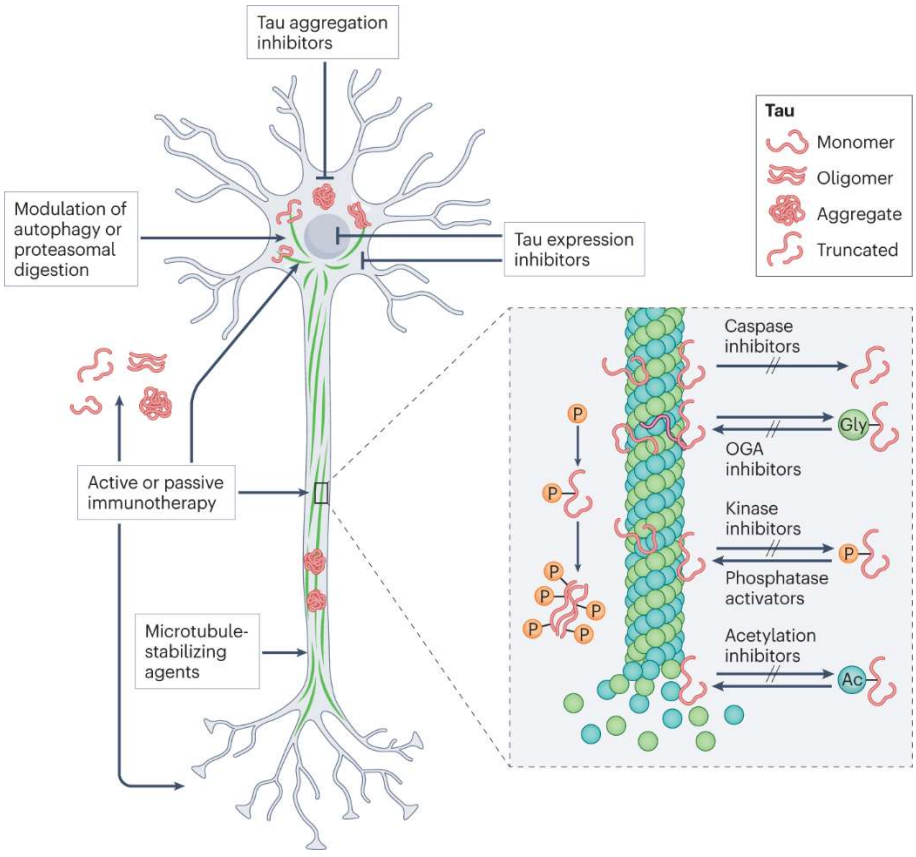

Fig. 21 Tau-related therapeutic strategies. These strategies target various aspects of tau pathology, including tau aggregation inhibitors, modulation of autophagy or proteasomal digestion, tau expression inhibitors, active or passive immunotherapy, and microtubule-stabilizing agents. Each approach is designed to act on different forms of tau, such as monomers, oligomers, aggregates, or truncated species [129].

These therapeutic approaches have been developed to target tau expression, modification, aggregation, and clearance [129]. One strategy focuses on reducing tau expression itself, using antisense oligonucleotides, microRNAs, small interfering RNAs (siRNAs), or inhibitors of transcription factors to lower tau levels and mitigate its pathological effects [129, 96].

Since post-translational modifications, particularly hyperphosphorylation, play a crucial role in tau aggregation, another approach aims to restore tau homeostasis by inhibiting kinases or stimulating phosphatases to prevent excessive phosphorylation [96].

Additionally, therapies directly targeting tau aggregation have been explored to prevent the formation of toxic oligomers and NFTs. Since pathological tau loses its ability to stabilize microtubules, microtubule-stabilizing agents have also been investigated, with some studies showing promising results in transgenic mouse models [96].

With aging, protein degradation systems become less efficient, leading to the accumulation of misfolded tau. Strategies to enhance tau clearance include the inhibition of heat shock proteins (HSP70 and HSP90), redirecting tau towards proteasomal degradation rather than refolding. Furthermore, stimulating autophagy, for instance with rapamycin, has emerged as another potential approach to enhance tau clearance and prevent its pathological accumulation [96, 123].

Finally, immunotherapy represents a promising strategy. The use of tau-specific antibodies has been shown to reduce tau pathology and improve

cognitive performance in transgenic mice [123]. These antibodies can target both intracellular tau, preventing its aggregation, and extracellular tau, inhibiting its spread and trans-cellular propagation [129, 96].

Overall, these diverse therapeutic strategies offer hope for the development of effective treatments for tauopathies, though further research is needed to refine their efficacy and safety in human patients [96].

IX. The Olfactory System as a Promising Therapeutic Target and Diagnosis Tool

As previously mentioned, the olfactory system is particularly vulnerable to NDs. However, due to its unique position at the interface between the external environment and the CNS, it holds great potential as a key element in brain research.

1. Nose-to-Brain Delivery System as Therapeutic Strategy

The nose-brain axis (NBA) supports a bidirectional communication pathway between the nose (PNS) and the brain (CNS). As mentioned before, the OSNs send projections towards the OB, providing direct CNS access by bypassing the protection of the blood-brain barrier (BBB) [130]. The OB serves as a critical node in this NBA and achieves this bidirectional communication [131].

The highly effective protection of the BBB continues to be a real struggle for the management of NDs [43]. As a selective barrier, it regulates the passage of substances from the bloodstream into the brain. It is formed by the interaction of various cell types, including brain microvascular endothelial

cells, tight junctions, neurons, astrocytes, and basal membranes [43]. The BBB blocks 98% of small molecules and an even greater percentage of large molecules from reaching the brain. Indeed, the ability of compounds to cross the BBB depends on their physicochemical properties, such as size, molecular weight, surface activity, lipid solubility, and charge. While only small, lipophilic molecules can pass through via passive diffusion, larger or hydrophilic molecules require receptor-mediated transport mechanisms. Additionally, specialized drug carriers, such as nanoparticles, can enhance the delivery of therapeutic agents across the BBB [43].

This limitation could be addressed by using the nose-brain axis [132]. Intranasal drug delivery is an alternative to systemic drug administration where the drug is delivered into the nasal cavity, which houses OSNs and their projections. Chemicals traveling through or alongside these fibers, bypass the BBB, and take advantage of the special physiological and structural connection between the nasal cavity and the CNS [133]. There are two major pathways. On one side, when a drug is delivered to the olfactory region, where olfactory nerves are present, it can migrate along these nerves to the OB and subsequently reach the brain, known as the olfactory pathway. On the other side, the respiratory pathway, where the drug can also access the brain through the trigeminal nerves, which are situated deep within the nasal cavity (Fig. 22)[133].

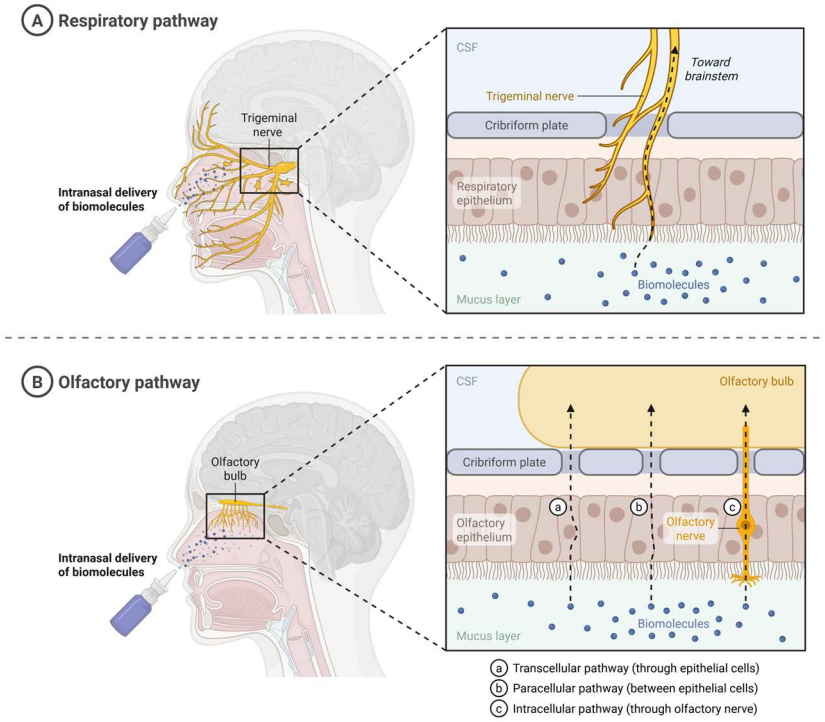

Fig. 22 Direct Pathways of Nose-To-Brain Biomolecule Delivery. In the respiratory pathway, the biomolecules can directly access the trigeminal nerve, whereas in the olfactory pathway, the biomolecules reach the OB via the transcellular, paracellular, or intracellular pathways. Adapted from *BioRender.com*.

These delivery methods offer a higher bioavailability compared to oral medications; they can achieve more rapid and efficient therapeutic effects. The nasal mucosa is highly permeable and richly supplied with blood vessels and has a large surface area, which facilitates rapid absorption of drugs. This allows for faster onset of action. Considered as non-invasive, this delivery option is also more comfortable and convenient for patients, removing the need for injections [134]. This route of administration is already widely used for the local treatment of rhinitis or nasal polyposis [134]

New findings highlight the potential of intranasal drug delivery to target NDs via the olfactory pathway, offering a way to reduce the side effects associated with systemic administration [130]. Research in mouse models has demonstrated that nasal tau immunotherapy can clear intracellular tau pathology and improve cognitive function in aged tauopathy mice [135]. In another study, they used nasal spray to target microglia and astrocytes, thereby reducing neuroinflammation, known to be deleterious in the context of NDs [136]. In humans, the intranasal route has also been explored in multiple studies as a promising therapeutic strategy for various NDs [132, 133, 137]. One example is the use of rivastigmine nasal spray to alleviate AD symptoms [133].

2. Nasal Brushing for Biomarkers Analysis

In addition to its therapeutic potential, the olfactory system also represents an accessible source of potential biomarkers in ND. If we take the example of AD - the most common ND - several biomarkers have been developed and studied in recent years [138]. A biomarker can be defined by various characteristics but the World Health Organization (WHO) has defined a biomarker as “any substance, structure, or process that can be measured in the body or its products and influence or predict the incidence of outcome or disease” [139]. It can also highlight the effects of treatments, interventions, and even unintended environmental exposure [139].

To date, fluid biomarkers have advanced AD diagnosis, with new ones being studied for early detection in CSF and blood [140]. Some of these biomarkers are collected through invasive techniques, especially CSF from lumbar

puncture [141]. Blood-based biomarkers (BBMs) were also proposed to diagnose AD, however these BBMs are not yet accurate enough to replace CSF and PET testing [142]. In recent years, nasal brushing has garnered significant interest as a minimally invasive and straightforward technique for assessing OE-derived biomarkers in NDs [143-145].

Nasal brushing or exfoliation consists of introducing a small brush into the nasal cavity at the level of the middle turbinate, and with circular movements, allows to recover OE cells such as OSNs and olfactory neurons precursors (ONP) for biomarker analysis [146, 145]. The OE is considered as the only source of neuronal cells than can be obtained from a living human being as well as one of the few regions where neuronal regeneration exists continuously throughout human adult life [147]. As mentioned, this technique is noninvasive, does not require anesthesia and the collected cells show a well-preserved morphology [146, 143, 145].

Few studies have investigated the OE in the context of AD. The first study, conducted by Arnold *et al.* in 2010, reported higher expression of amyloid-β and PHFs in the OE of AD patients [148]. Other findings have shown increased levels of total tau and phosphorylated Tau (pTau) in the ONP of AD patients using this nasal brushing method [149]. However, subsequent studies have yielded conflicting results, likely due to cellular and molecular changes occurring during the *postmortem* delay, emphasizing the importance of studying antemortem samples [145].

One promising approach to overcoming the challenge of early diagnosis could be the nasal brushing technique, which allows for the collection of

viable samples before death. This sampling method presents a promising approach for analyzing biomarkers in the OE. It may enable the identification of biomarkers that distinguish between control individuals and early-onset AD patients.

To explore the link between tau pathology and olfactory dysfunction in AD, and to experimentally investigate mechanisms that cannot be directly assessed in humans, appropriate animal models are required. Tauopathy mouse models that could replicate key aspects of tau accumulation in olfactory regions provide a valuable tool for studying early pathological changes and testing diagnostic or therapeutic strategies. The last section presents tauopathy mouse models as well as the specific one used in this thesis, selected for its relevance to olfactory system involvement in neurodegeneration.

X. Tauopathy Mouse Models

There are more than 100 different genetically engineered mouse lines reported to capture some aspects of NDs, and especially tauopathies [150].

Although it is not possible to discuss all available models here, the PS19 mice is among the most widely studied and used to model "tau transmission" [151, 152]. It is also a good model to test manipulations expected to either ameliorate or accelerate pathology thanks to the mid-life onset of the pathology [150]. On the contrary, rTg4510 mice–another tauopathy mouse model–develop aggressive tau pathology making them unsuitable for studying virus-induced models designed to explore the pathways of tau propagation [150]. Similarly, hTau mice, which express the six isoforms of human tau, exhibit a progression that is too mild to be suitable for studying such interventions [150].

1. PS19 Mice

PS19 mice, also known as tau P301S mice, were firstly described as a transgenic tauopathy mouse model by Yoshiyama *et al.* in 2007 [153]. These transgenic mice express mutant human MAPT under the control of the mouse prion protein promoter (Prnp). The transgene encodes the disease-associated P301S mutation and includes four microtubule-binding domains and one N-terminal insert (4R1N)[153]. The transgene insertion results in a deletion that does not interfere with any other gene expression. The human tau expression in this model has been reported as fivefold higher than the endogenous mouse protein [153].

NFTs can be observed in the neocortex, amygdala, hippocampus, brain stem and spinal cord at 6 months of age with progressive accumulation. However, these mice will not develop amyloid plaques. Neurodegeneration starts around 9 months [153]. A sexual dimorphism has been reported in this model with an earlier pathology in males [154, 155]. Behavioral abnormalities recapitulating the neurological deficits observed in human tauopathies with dementia were measured in these mice using numerous tests, including the open field test, elevated plus maze test, hot plate test, Y-maze test, Barnes maze test, Morris water maze test, contextual fear conditioning test and novel object recognition test [154, 156, 155, 157]. In the Barnes maze test evaluating spatial memory, PS19 mice showed a progressive memory impairment starting at 3-4 months and persisted through 5-6 months [156]. In the novel object recognition test, a short-term memory task, a similar memory decline was found [156].

There is comparatively less literature characterizing pathology in the olfactory system in this model. Even though, previous studies highlighted an excessive pTau expression in the OB of PS19 mice, particularly in the mitral cells. The mice also exhibited progressive neuronal cell loss in the OB and PC, along with increased latency in finding buried food [5].

Objectives

OBJECTIVES

Our project will aim to characterize the early progression of tau pathology in the olfactory system as an initial event in AD pathogenesis. We will investigate how tau pathology initiates, spreads to deeper brain regions, and whether this process can be targeted therapeutically. To achieve this, we will use the PS19 mouse model, which exhibits a moderate rate of disease progression suitable for monitoring early stages and testing interventions that may mitigate or exacerbate pathology. This thesis project will be structured around several key objectives:

- The first objective will be to validate the selected tauopathy model and characterize the progression of tau pathology over time. We will study pathology in both olfactory system regions (such as the OE and OB) and CNS regions, including the PC, EC, and hippocampus. Additionally, we will examine tau pathology in the OE and OB of human patients at early Braak stages (I/II) to assess the translatability of our findings (Chapter I).
- The second objective, based on our initial findings and the nose-to-brain axis hypothesis, will be to target the OE in PS19 mice with localized treatments to assess their impact on CNS pathology progression. As a first approach, we will selectively strip OSNs in the nasal cavity using intranasal zinc sulfate irrigations to evaluate whether this intervention could reduce pathology in the CNS. Conversely, we will perform intranasal irrigations with adeno-associated viruses (AAVs) carrying a mutated human tau sequence

to determine whether this could exacerbate tau pathology in the CNS (Chapter II).

- Finally, we will focus on collecting samples from these regions at critical time points (3, 6, and 9 months) for transcriptomic analyses in collaboration with the university of Namur (Patsy Renard, Ayeh Bouloki, Marc Dieu, Malika Magomadov). These analyses will allow us to identify the cellular pathways involved in tauopathy development in PS19 mice, as well as to detect differentially expressed genes, providing a set of potential biomarkers. The goal will be to validate some of these biomarkers for further investigation (Chapter III).

Our findings should help clarify the role of the OE in the spread of pathological tau and evaluate its potential as both therapeutic target and diagnostic tool in NDs.

Results - Chapter I

The Olfactory Epithelium: A Critical Gateway for Pathological Tau Propagation

RESULTS – Chapter I

In this first chapter, we characterized the pathological expression pattern of hyperphosphorylated tau (pTau) in regions of the olfactory and central nervous systems. The regions investigated were the OE, OB, PC, EC, and hippocampus, with the common feature that they all share neuronal connections. All the results presented in the first two chapters can be found in a research paper published in *Acta Neuropathologica*. For this study, I collected all samples, performed most of the experiments, analyzed the data, and prepared the initial draft of the manuscript. The collaborators listed below provided additional contributions.

› Acta Neuropathol. 2025 Jun 19;149(1):64. doi: 10.1007/s00401-025-02902-6.

The olfactory epithelium: a critical gateway for pathological tau propagation and a target for mitigating tauopathy in the central nervous system

Marion Dourte [1], Esther Paître [1], Mongia Bouchoucha [1], Emilien Boyer [1], Sandra O Tomé [2], Emilie Doeraene [3], Caroline Huart [4 5], Karelle Leroy [3], Dietmar Rudolf Thal [2 6], Anabelle Decottignies [7], Bernard Hanseeuw [8 9], Nuria Suelves [1], Pascal Kienlen-Campard [10]

Affiliations + expand

PMID: 40536690 PMCID: PMC12179005 DOI: 10.1007/s00401-025-02902-6

Abstract: Olfactory impairment is a recognized early indicator of neurodegenerative diseases (NDs), such as Alzheimer's disease (AD). Intracellular aggregates of hyperphosphorylated tau protein, referred to as neurofibrillary tangles (NFTs), are a hallmark of AD. NFTs are found in the olfactory bulb (OB) and entorhinal cortex (EC), both crucial for processing olfactory information. We explored the hypothesis that typical tau lesions could appear early and progress along olfactory regions to reach connected

areas critically affected in AD (e.g., EC and hippocampal formation). To that end, we used transgenic PS19 mice expressing mutated human tau protein (1N4R isoform, P301S mutation). They recapitulate major phenotypes of AD, such as accumulation of NFTs, synaptic dysfunction, cognitive impairment, and neuronal loss. The presence of pathological hyperphosphorylated human tau protein (pTau) was monitored in olfactory regions: olfactory epithelium (OE), OB, piriform cortex (PC), and in connected regions of the hippocampal formation (hippocampus and EC). pTau was detected in the OE's middle stratum and in the OB's olfactory nerve layer (ONL) at 1.5 months. At 6 months of age, tau accumulations were found in the PC and EC, along with the CA3 region and dentate gyrus of the hippocampus. We found that olfactory function remained unaffected in PS19 mice, despite the presence of tau pathology in key regions of the olfactory system. Targeted treatments ($ZnSO_4$ and AAVs) were applied at the OE level to assess the impact on tau pathology in the CNS. Complete stripping of the OE by intranasal administration of $ZnSO_4$ led to a significant reduction in pretangle-like tau pathology within the PC, amygdala, and EC of 6-month-old PS19 mice. Finally, we observed in human *postmortem* samples that pTau signal was present in the olfactory regions (OE and OB) of patients at early Braak stages (I/II). Based on these observations, we propose that pTau could appear, due to aging or environmental agents, in the OE and subsequently spread in a prion-like manner to the hippocampal formation along neuroanatomical connections. These findings also indicate the interest of the OE as a target for intervention aimed at mitigating the progression of tauopathy in the CNS.

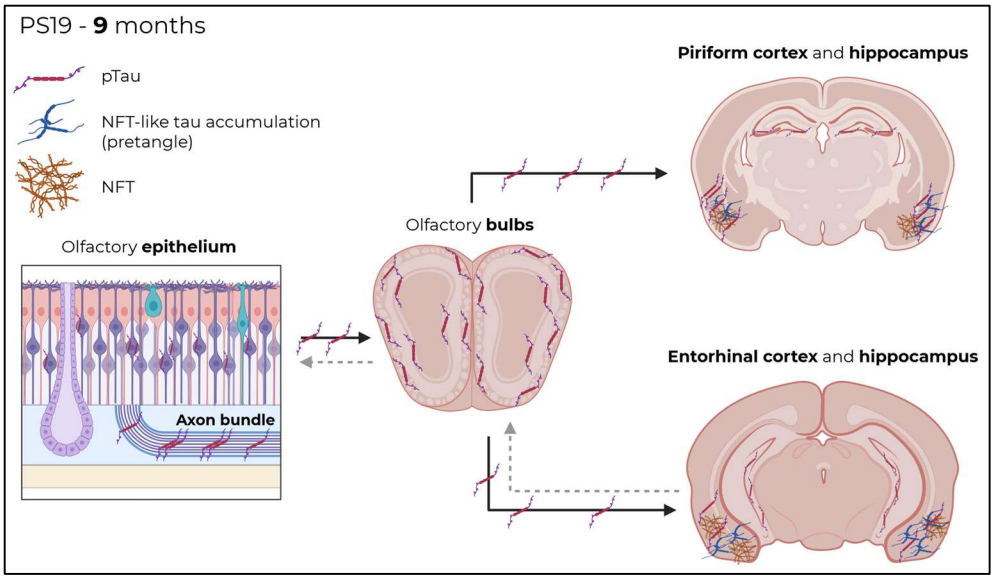

Graphical abstract – Chapter I, Created in BioRender. Kienlen-Campard, P. (2025) https://BioRender.com/sxk4wcj

Tau Pathology in the Olfactory System and Associated CNS Regions in PS19 mice

1. Tau Pathology in the Olfactory Epithelium of PS19 mice

The presence of hyperphosphorylated tau protein (pTau) was first evidenced in this region using the PHF-1 antibody. This antibody is generated against PHFs isolated from the brains of AD patients, that recognizes tau phosphorylated at Ser396 and Ser404. It binds to tau filaments and is a recognized standard to evidence the pathological conformations found in NFTs [158, 114].

pTau detected at around 60kDa using this antibody is present only in PS19 mice, at 3,6 and 9 months of age, both in males and females. No signal around 60kDa is observed in the WT mice regardless of ageing stage (Fig. I.1).

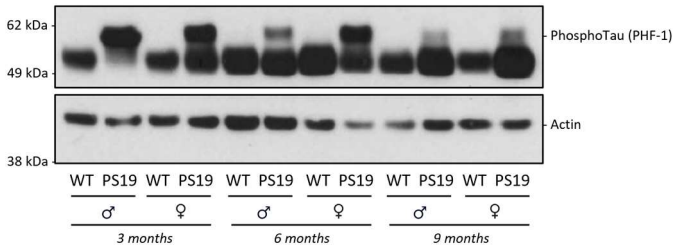

Fig. I.1 pTau expression in the OE of PS19 mice. pTau (**PHF-1** (Ser396, Ser404)) is detected in the OE of PS19 or WT males and females at 3, 6 and 9 months. pTau detected at around 60kDa using this antibody is present only in PS19 mice, as soon as 3 months of age, both in males and females. No signal around 60kDa is observed in the WT mice regardless of ageing stage.

The presence of pTau was then evidenced using the AT8 antibody (pTau (Ser202, Thr205)) in coronal sections of the OE from WT and PS19 mice. To that end, a specific protocol of decalcification has been set up to soften the

nasal bone, allowing *in situ* sectioning of the OE while preserving its structural organization. AT8 immunoreactivity was observed only in PS19 mice and was localized to the OE middle stratum and to the axon bundles (ABs), located in the lamina propria underlying the OE (Fig. I.2a-d). The AT8 signal in the OE was assessed and compared at different ages: 1.5, 3, 6 and 9 months (Fig. I.2a-d). AT8 immunoreactivity was detected as soon as 1.5 months (Fig. I.2a, a'), increased progressively up to 6 months (Fig. I.2c, c'), and decreased at 9 months, especially in the middle stratum (Fig. I.2d, d'). Based on morphology, no NFT-like tau accumulations were observed in this region for up to 9 months. A closer examination of the nasal cavity showed no pTau signal in the respiratory epithelium of PS19 mice (Fig. I.2e). Similarly, no pTau signal was detected in the OE or ABs of 6-month-old WT mice (Fig. I.2f), indicating that the AT8 signal is specific to PS19 mice and related to the expression of pathological human tau.

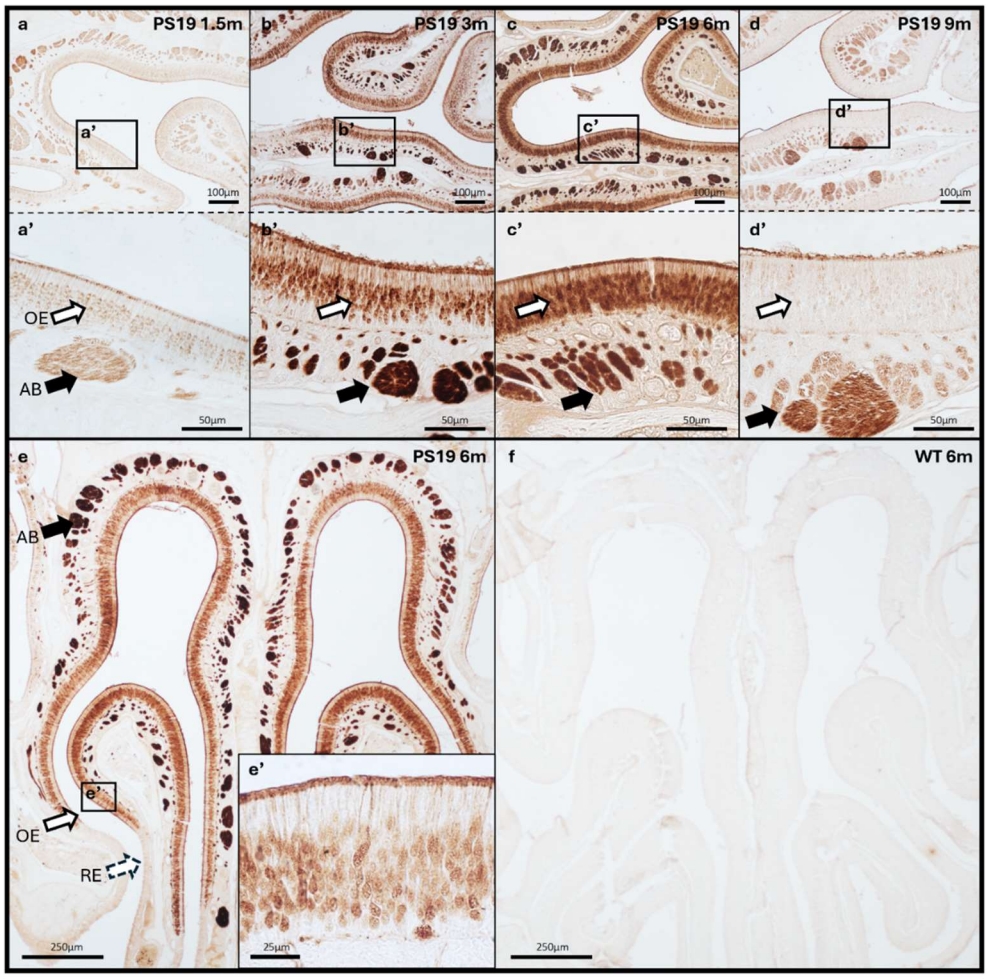

Fig. I.2 pTau expression in the OE of PS19 mice. The OE from 1.5-month (a, a'), 3-month (b, b'), 6-month (c, c', e), 9-month-old PS19 mice (d, d'), and 6-month-old WT mice (f) were fixed and stained with the **AT8** antibody (pTau (Ser202,Thr205)). pTau recognized by the **AT8** antibody is found in the middle stratum of the OE (white arrows) and in the ABs (black arrows) as soon as 1.5 months in PS19 mice (a, a'). The signal increases up to 6 months (c, c', e) and appears to decrease at 9 months (d, d'). No signal is detected in WT mice (f). All the mice used were **males**. The immunostainings shown are representative of n=4 mice/time point. High magnification of the OE (white arrows) is shown in the inset (e'). ABs: axon bundles, OE: olfactory epithelium, RE: respiratory epithelium.

Additional stainings with other widely used tau antibodies were included to expand characterization in this region. The presence of pTau was evidenced

using the PHF-1 antibody in the middle stratum of the OE as well as in the ABs in PS19 mice, similarly to AT8 (Fig. I.3a). Using this antibody, a faded signal appeared in the apical region of the OE in WT mice (Fig. I.3e). The TTau antibody detecting both endogenous murine tau protein and human tau protein, evidenced all layers of the OE in addition to ABs in PS19 mice (Fig. I.3c). Some signals appeared in the basal and apical regions of the OE in WT mice (Fig. I.3g). The hTau antibody (Tau-13) specific to human tau gave similar results to the AT8 antibody with no signal in WT mice (Fig. I.3d, h).

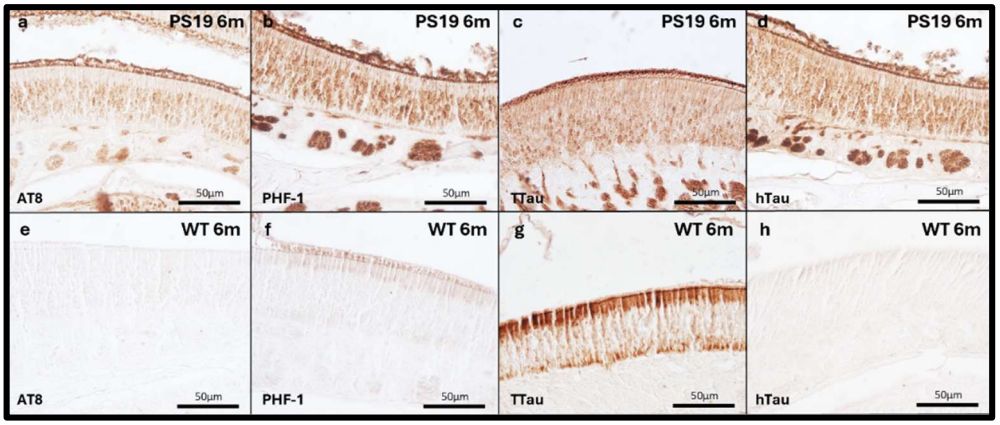

Fig. I.3 Tau protein expression in the OE of PS19 and WT mice. The OE from 6-month-old PS19 and WT mice were immunohistochemically stained with **AT8** (a, e), **PHF-1** (b, f), **TTau** (c, g) and **hTau** (d, h). pTau (**AT8**) is observed in the middle stratum and ABs of the OE of PS19 mice (a), while no **AT8** signal is detected in the OE of WT mice (e). **PHF-1** staining reveals pTau in the middle stratum and ABs of the OE of PS19 mice (b), with some signal also detected in the apical region of the OE of WT mice (f). Total tau (**TTau**) is detected throughout all strata of the OE in PS19 mice (c), whereas in WT mice, **TTau** staining is restricted to the basal and apical regions of the OE (g). Like the **AT8** signal, **hTau** immunoreactivity is observed in the middle stratum and ABs of the OE of PS19 mice (d), while no **hTau** signal is detected in the OE of WT mice (h). All mice used for immunostaining were **males.**

Together, these observations indicate (i) that tau is endogenously expressed in the mouse OE, (ii) that the specific AT8-positive signal observed in the OE of PS19 mice is not an artifact simply related to ectopic expression of the human tau transgene in in OE of PS19 mice.

Then, colocalization analyses were carried out via immunofluorescence to confirm the cellular localization of the pTau signal in the OE of PS19 mice. The following antibodies were used: total tau antibody (TTau), olfactory marker protein (OMP) antibody (specific to mature OSNs and their neurites), and AT8 antibody (Fig. I.4a-c). Colocalization was observed between the OMP signal and both TTau and AT8 signals in the cellular bodies and neurites of the OSNs, as well as in the ABs of the PS19 mice at 3 months (Fig. I.4d, e). OMP and AT8 were also specifically colocalized in the dendritic knobs of OSNs (Fig. I.4e). This result confirmed that pTau is found not only in mature OSNs of the OE but also in ABs within the lamina propria (Fig. I.4e).

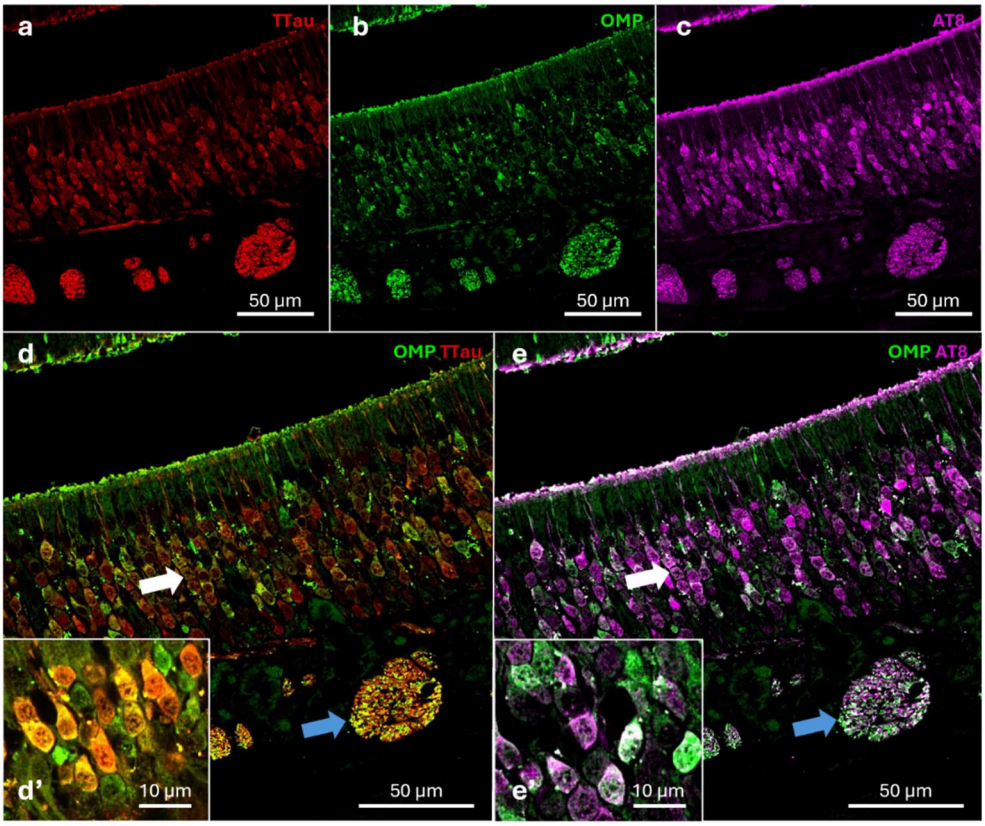

Fig. I.4 pTau expression in the OSNs and ABs of PS19 mice. Paraffin sections immunostained for total tau (**TTau**, red) (a, d), olfactory marker protein (**OMP,** green) (b, d, e) and pTau (**AT8,** purple) (c, e) show colocalization between **TTau-OMP** (yellow)(d) and **AT8-OMP** (white)(e) indicating tau hyperphosphorylation in the OSNs (white arrows) and in the ABs (blue arrows) of PS19 mice at 3 months. High magnifications (white arrows) are shown in the insets (d', e').

2. Tau Pathology in the Olfactory Bulbs of PS19 mice

Since OSN axons extend through the cribriform plate of the ethmoid bone to reach the OB, where they form its outermost layer (ONL) [14], we next investigated the AT8 profile in the OB of PS19 mice. Accumulation of hyperphosphorylated tau in the OB of PS19 mice was confirmed by Western

blotting of soluble protein extracts using the AT8 antibody (around 60kDa)(Fig. I.5).

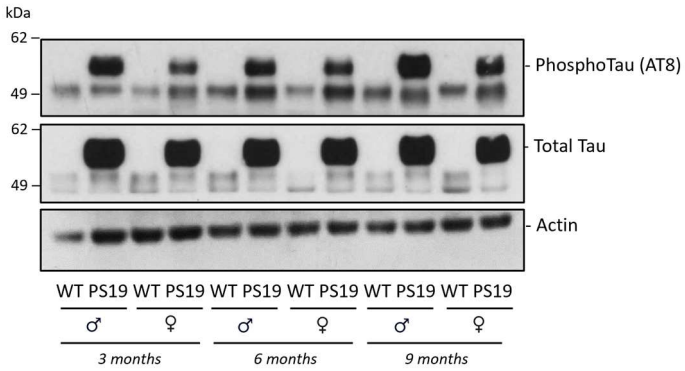

Fig. I.5 pTau expression in the OB of PS19 mice. pTau (**AT8**) and **Total Tau** are detected around 60kDa in the OB of PS19 males and females at 3, 6 and 9 months. This upper band is not present in the WT mice regardless of ageing stage. Actin was used as loading control.

The experiments were repeated and quantified using the PHF-1 antibody (Fig. I.6). A band around 60kDa was observed exclusively in PS19 mice, both in males and females, as early as 3 months of age. No positive signal for PHF-1 or AT8 was observed in WT mice at any age (Fig. I.6a-c). Western blot quantification revealed no significant differences in pTau expression between males and females in the OB at 3, 6 and 9 months (Fig. I.6a-c). Finally, the PHF-1 signal was quite stable over time in PS19 males, suggesting that pTau, although already present at 3 months, did not further accumulate in the OB (Fig. I.6d).

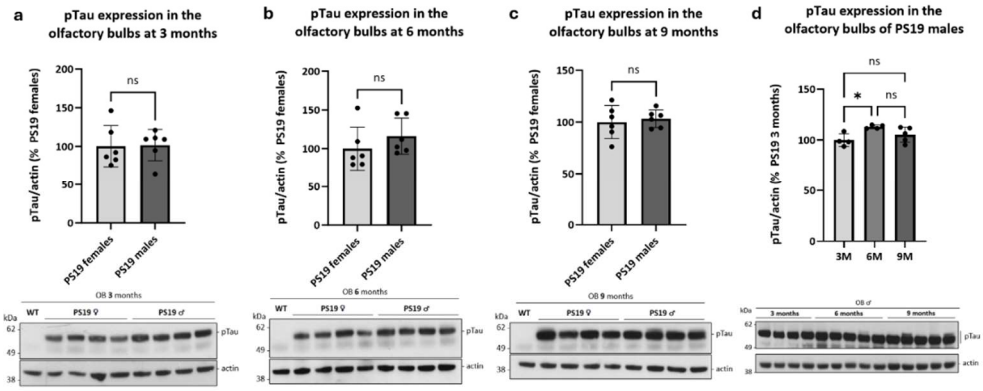

Fig. I.6 pTau expression in the OB of PS19 mice. Western blot analyses showing pTau (**PHF-1**) relative protein levels in the OB of PS19 mice at 3, 6 and 9 months (a-d). Actin was used as loading control, and the levels in the females' group (a-c) or at 3 months (d) were set as 100%. It shows no significant difference in pTau expression between males and females (a-c) (One-way ANOVA with Tukey's post-hoc analysis, n = 6 mice/group). pTau expression is shown as stable between 3 and 9 months in the OB (d). *P < 0.05 (One-way ANOVA with Tukey's post-hoc analysis, n = 4-5 mice/group).

The AT8 staining profile was then investigated in coronal sections of the OB in PS19 mice. The AT8 signal was specifically present in the olfactory nerve layer (ONL) of the OB as early as 1.5 months in PS19 mice (Fig. I.7a-d). In addition, AT8 immunoreactivity was also detected in the mitral cell layer (MCL). In some 9-month-old mice, a stronger pTau signal appeared in the central region (e.g., granular cell layer) of the OB (Fig. I.7d). Here also, no AT8 signal was observed in the OB of WT mice (Fig. I.7f).

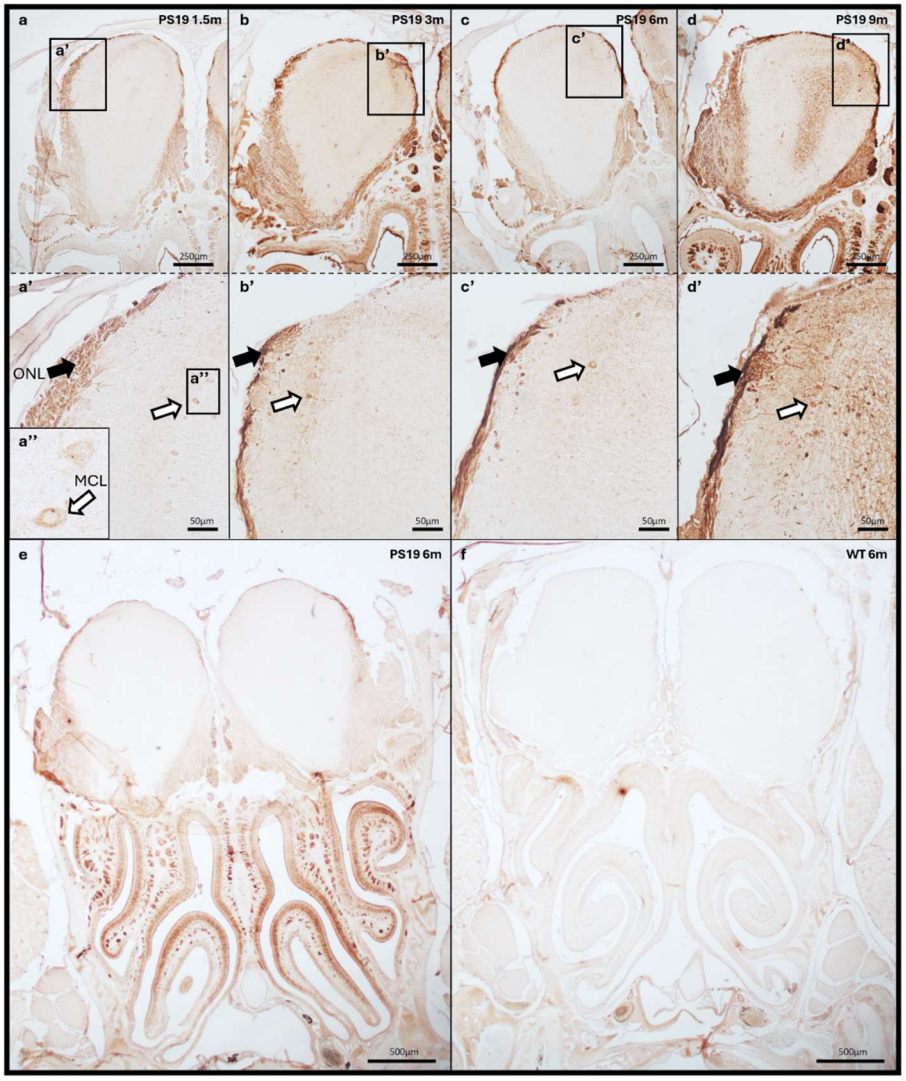

Fig. I.7 pTau expression in the OB of PS19 mice. The OB from 1.5-month (a, a'), 3-month (b, b'), 6-month (c, c', e), 9-month-old PS19 mice (d, d') and 6-month-old WT mice (f) were immunohistochemically stained with **AT8** (a-d, a'-d'). pTau recognized by the **AT8** antibody is found in the external layer of the OB (black arrows) and in the MCL (white arrows) from 1.5 months (a-d, a'-d'). The pTau signal seems stable over time (a'-d'). No signal is detected in WT mice (f). All the mice used for immunostainings were **males**. The immunostainings shown are representative of n=4 mice/time point. High magnification of the MCL (white arrows) is shown in the inset (a''). ONL: olfactory nerve layer, MCL: mitral cells layer.

The characterization was strengthened using the PHF-1, TTau and hTau antibodies in the OB from 6-month-old PS19 and WT mice. As previously described, AT8 signal is present in the ONL and MCL of the OB in PS19 mice and no signal is detected in the OB in WT mice (Fig. I.8a, e). PHF-1 staining is present in the ONL and MCL of both PS19 and WT mice (Fig. I.8b, f). TTau staining is observed in the ONL and MCL of PS19 mice but is limited to the MCL in WT mice (Fig. I.8c, g). Similarly to AT8, staining is present in the ONL and MCL of PS19 mice but is absent in WT mice (Fig. I.8d, h).

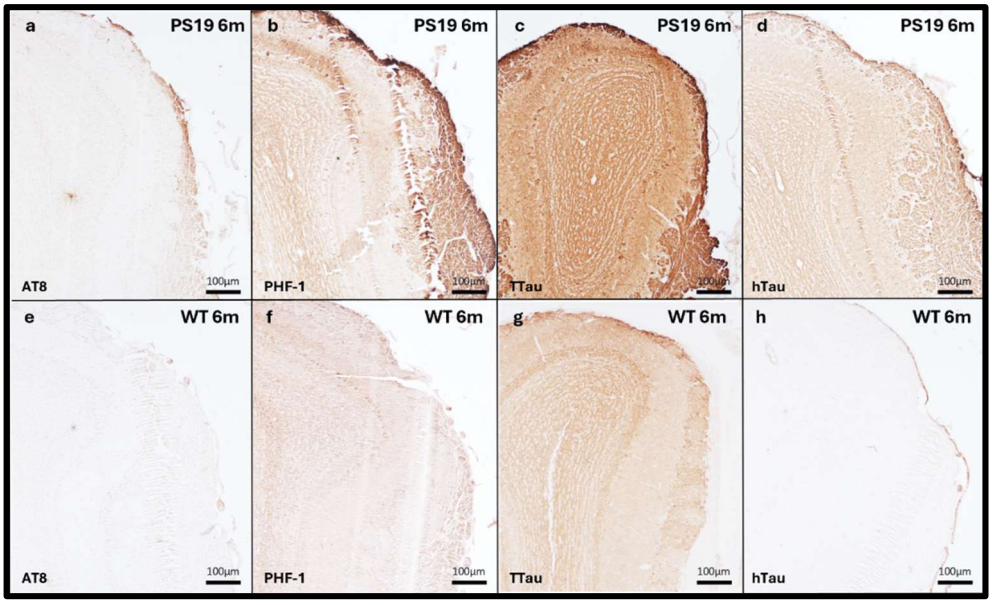

Fig. I.8 Tau protein expression in the OB of PS19 and WT mice. The OB from 6-month-old PS19 and WT mice were immunohistochemically stained with **AT8** (a, e), **PHF-1** (b, f), **TTau** (c, g) and **hTau** (d, h). In the OB, **AT8** staining is present in the ONL and MCL of PS19 mice (a), whereas no AT8 signal is observed in WT mice (e). **PHF-1** staining is present in the ONL and MCL of both PS19 (b) and WT (f) mice. **TTau** staining is observed in the ONL and MCL of PS19 mice (c) but is limited to the MCL in WT mice (g). Like the **AT8** signal, **hTau** staining is present in the ONL and MCL of PS19 mice (d) but is absent in WT mice (h). All mice used for immunostaining were **males.**

Immunofluorescence analyses of the OB in 3-month-old PS19 mice (Fig. I.9a-c) revealed colocalization between TTau and OMP, indicating tau protein expression in both the ONL and the GL (Fig. I.9d). Additionally, strong colocalization between OMP and AT8 was observed in the ONL, providing evidence of pTau accumulation in the outermost layer of the OB in PS19 mice (Fig. I.9e). Some AT8 signal, which did not colocalize with OMP, was also observed in the inner layers of the OB (Fig. I.9c).

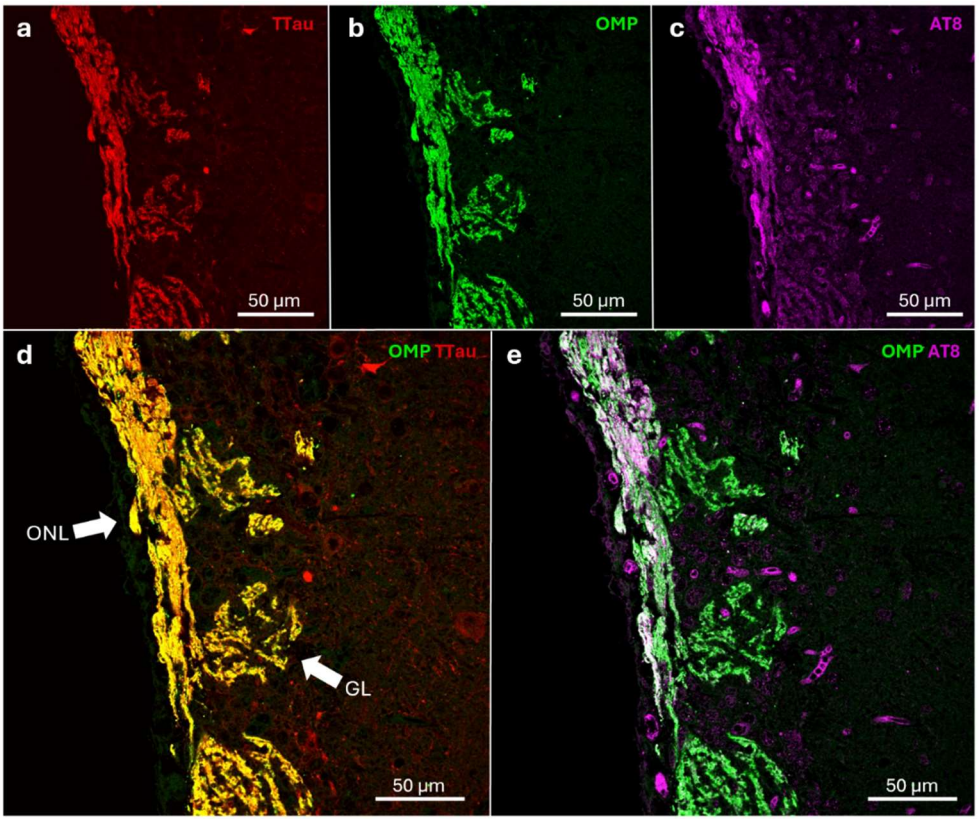

Fig. I.9 pTau expression in the ONL of PS19 mice. Paraffin sections immunostained for total tau (a, d) (**TTau**, red), **OMP** (b, d, e) (green) and **AT8** (c, e) (purple) show colocalization between **TTau-OMP** (yellow)(d) and **AT8-OMP** (white)(e) indicating tau protein expression both in ONL and GL as well as pTau expression in the ONL and inner layers of the OB from 3-month-old PS19 mice. ONL: olfactory nerve layer, GL: glomerular layer.

3. Tau Pathology in the Piriform and Entorhinal Cortex of PS19 mice

Next, we explored tau pathology in CNS regions of PS19 mice that are connected to the OB and involved in the processing of olfactory information along with olfactory memory: the PC, the EC, and the hippocampus. All these CNS regions are connected by neuroanatomical pathways [159]. Efferent projections from the OB reach both the PC and EC, and the perforant path wires the EC to hippocampal subregions [160]. In the PC, faint pTau immunoreactivity (AT8), indicative of the first step of abnormal tau modification [115], appeared in the neuronal cell bodies at 3 months (Fig. I.10b, b'). By 6 months, the first perikaryal NFT-like tau accumulations were observed, with an accumulation of pTau in both the cell bodies and neurites of neurons within the PC pyramidal layer (Fig. I.10c, c'). These tau accumulations progressively increased up to 9 months and eventually spread throughout the entire PC (Fig. I.10d, d'). 9-month-old WT mice showed no AT8-positive accumulations in the PC (Fig. I.10e). In the EC, AT8 immunoreactivity appeared in the neuronal cell bodies as early as 1.5 months and increased over time (Fig. I.10f-i). Perikaryal NFT-like tau accumulations were detectable at 6 months, with signal present in both the cell bodies and neurites in the lateral part of the EC (Fig. I.10h, h'). Tau lesions gradually accumulated up to 9 months and spread to the whole EC (Fig. I.10i, i'). The accumulation pattern of tau pathology was similar to that observed in the PC, although with an earlier onset. In WT mice, AT8 signal was not detected until 9 months of age (Fig. I.10j).

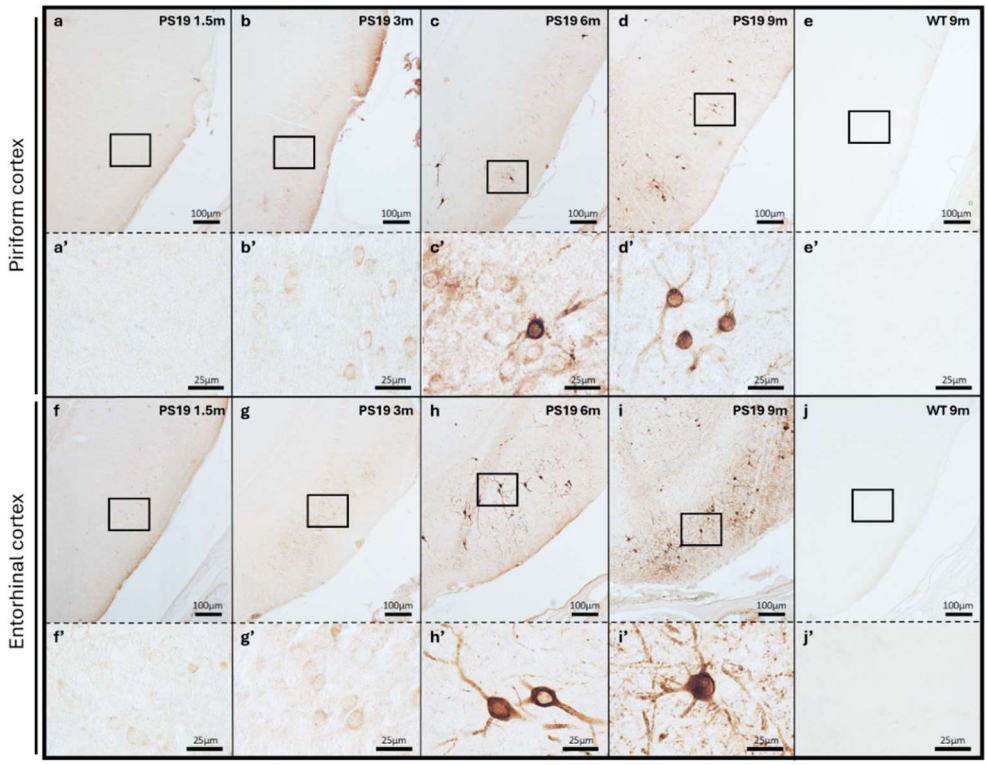

Fig. I.10 pTau expression in the PC and EC of PS19 mice. The PC from 1.5-month (a, a'), 3-month (b, b'), 6-month (c, c'), 9-month-old PS19 mice (d, d') and 9-month-old WT mice (e, e') were immunohistochemically stained with **AT8** (a-e). pTau recognized by the **AT8** antibody is found in the PC as soon as 3 months (b, b') with an accumulation up to 9 months (b-d, b'-d'). The first NFT-like tau accumulations appear at 6 months (c, c'). There is no **AT8** signal in the PC of WT mice (e, e'). The EC from 1.5-month (f, f'), 3-month (g, g'), 6-month (h, h'), 9-month-old PS19 mice (i, i') and 9-month-old WT mice (j, j') were immunohistochemically stained with **AT8** (f-j). pTau recognized by the **AT8** antibody is found in the EC as soon as 1.5 months (f, f') with an accumulation up to 9 months (f-i, f'-i'). PS19 mice develop NFT-like tau accumulations in this region at 6 months (h, h'). No **AT8** signal is detected in the EC of WT mice (j, j'). All the mice used were **males**. The immunostainings shown are representative of n=4 mice/time point. Insets were taken from the PC area (a'-e') and in the lateral EC (f'-j').

4. <u>Tau Pathology in the Hippocampus of PS19 mice</u>

pTau expression in soluble hippocampal extracts was confirmed by Western blotting with the AT8 antibody (around 60kDa)(Fig. I.11).

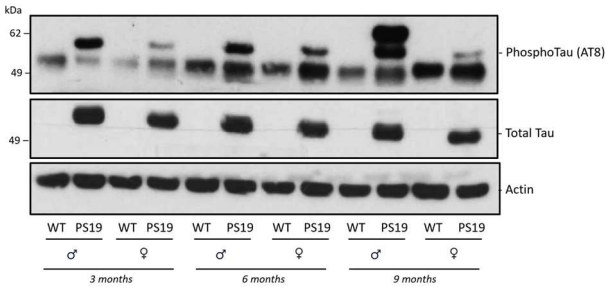

Figure I.11 pTau expression in the hippocampus of PS19 mice. pTau (**AT8**) and **Total Tau** are detected around 60kDa in the OB of PS19 males and females at 3, 6 and 9 months. This upper band is not present in the WT mice regardless of ageing stage. Actin was used as loading control.

Equivalent results were obtained and quantified using the PHF-1 antibody. pTau was detected as a band around 60kDa and was present only in PS19 mice, as soon as 3 months of age in both males and females. No positive signal for PHF-1 or AT8 was observed in the WT mice regardless of the aging stage (Fig. I.12a-c). At the same age, the average pTau levels were significantly greater in males than in females. Although the difference was already significant at 3 months, it was more pronounced at 9 months (Fig. I.12a-c). Western blot analysis finally revealed a significant increase in the pTau signal between 3 and 9 months in PS19 males, consistent with the staining results, suggesting that pTau accumulation in the hippocampus occurs in a time-dependent manner (Fig. I.12d).

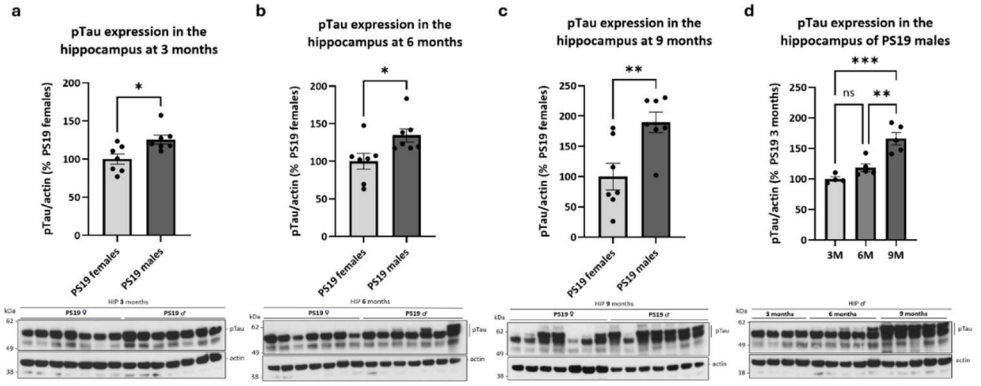

Fig. I.12 pTau expression in the hippocampus of PS19 mice. Western blot analyses showing pTau (**PHF-1**) relative protein levels in the hippocampus of PS19 mice at 3, 6 and 9 months (a-d). Actin was used as loading control, and the levels in the females' group (a-c) or at 3 months (d) were set as 100%. It shows a significant increase in pTau expression in males compare to females at 3, 6 and 9 months (a-c). *P < 0.05, **P < 0.01 (One-way ANOVA with Tukey's post-hoc analysis, n = 7 mice/group). pTau expression increases significantly with age in PS19 males (d). **P < 0.01, ***P < 0.001 (One-way ANOVA with Tukey's post-hoc analysis, n = 4-5 mice/group).

In the hippocampus, AT8 immunoreactivity was faintly detected in the CA3 subregion at 3 months (Fig. I.13b). By 6 months, pTau (AT8) was clearly present in the CA3 region and in the DG (Fig. I.13c), with an increased signal at 9 months (Fig. I.13d). In the CA3 region, pTau was found in the CA3 mossy fibers and in the stratum pyramidale (Sp). In the DG, pTau was located primarily in the granular cell layer (Fig. I.13e). No AT8 signal was detected in the hippocampus of WT mice (Fig. I.13f).

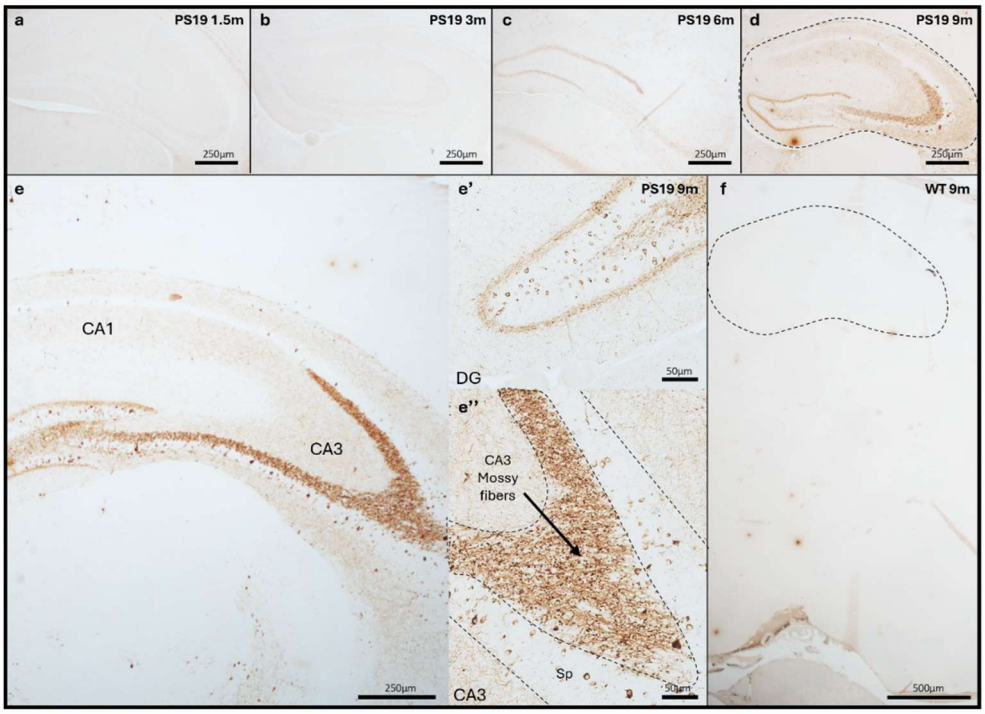

Fig. I.13 pTau expression in the hippocampus of PS19 mice. The hippocampus from 1.5-month (a), 3-month (b), 6-month (c), 9-month-old PS19 mice (d, e) and 9-month-old WT mice (f) were immunohistochemically stained with **AT8** (a-f). pTau recognized by the **AT8** antibody is found in specific hippocampal subregions like the CA3 (e'') and DG (e') as soon as 6 months with an increased signal at 9 months (c-e). No **AT8** signal is found in the hippocampus of WT mice (f). All the mice used for immunostainings were **males**. The immunostainings shown are representative of n=4 mice/time point. DG: dentate gyrus, CA: Cornu Ammonis, Sp: Stratum pyramidale.

To distinguish AT8-positive NFT-like tau accumulations from mature filamentous tau aggregates referred to as mature NFTs, Gallyas silver staining was performed in all previously studied regions and time points. No NFTs were observed in the OE (Fig. I.14a-d) and OB (Fig. I.14f-i) of PS19 mice. In the PC and EC, Gallyas-positive NFTs were detected only at 9 months of age in PS19 mice (Fig. I.14n, s) and were very sparse compared to the AT8 signal observed previously (Fig. I.10). In the hippocampus of PS19 mice, no

NFTs were observed at any age (Fig. I.14u-x). As a control, no NFTs were detected by silver staining in WT mice (Fig. I.14e, j, o, t, y).

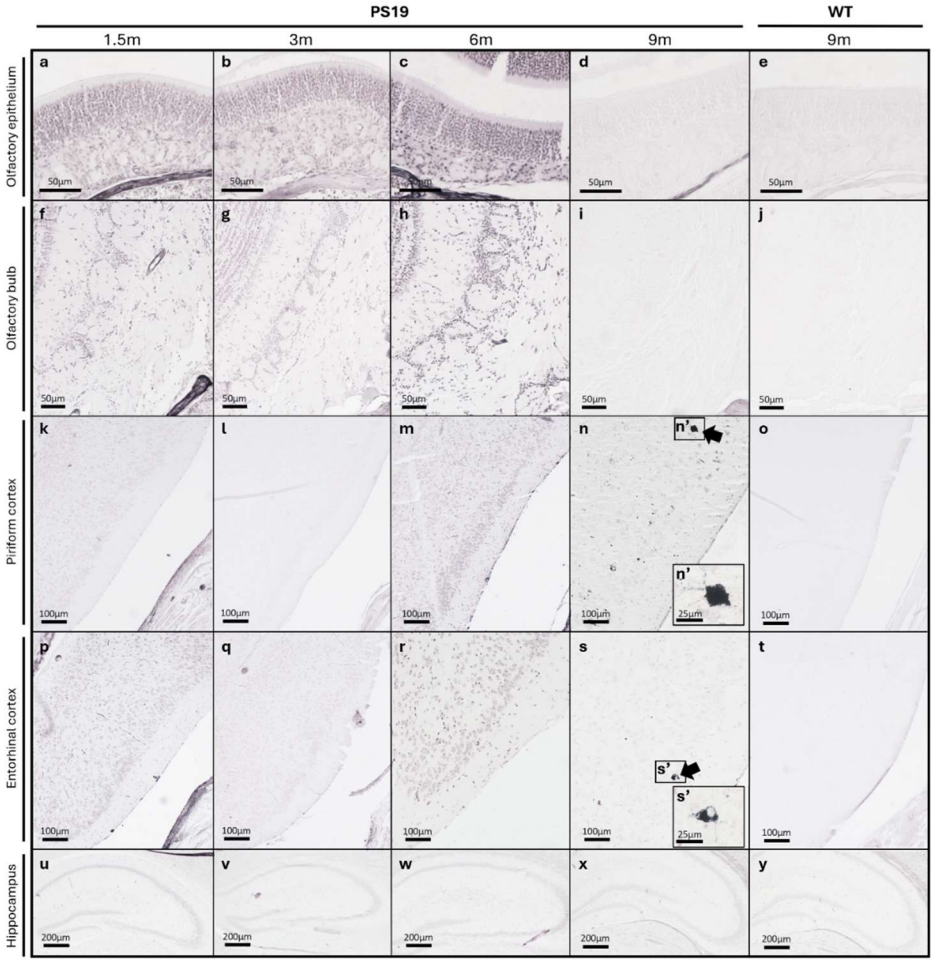

Fig. I.14 Gallyas staining in the OE, OB, PC, EC, and hippocampus of PS19 mice. The OE (a-e), OB (f-j), PC (k-o), EC (p-t) and hippocampus (u-y) of PS19 mice at 1.5, 3, 6, and 9 months, as well as 9-month-old WT mice were stained with Gallyas silver staining to highlight NFT inclusions. Few Gallyas-positive inclusions (black arrows) are only observed in the PC (n) and EC (s) from 9 months PS19 mice. No NFTs are detected in the OE, OB, or hippocampus at any time point, nor in the PC or EC before 9 months. No signal is detected in WT mice (e, j, o, t, y). High magnifications of the Gallyas-positive aggregates (black arrows) are shown in the inset (n') and (s'). All the mice used for Gallyas silver staining were **males.** The Gallyas stainings shown are representative of n=3 mice/time point.

These results clarify some aspects of the temporal and spatial staging of tau pathology in PS19 mice by distinguishing pTau (i.e., recognized by AT8 or PHF-1 antibodies), perikaryal NFT-like tau accumulations or pretangles (AT8-positive) and mature NFTs evidenced by Gallyas staining. Strikingly, pathological pTau accumulated very early (from 1.5 months of age) in the OE without the formation of typical NFTs, as shown by the Gallyas staining. A similar profile (pTau staining without NFTs) was observed in the OB. pTau immunoreactivity was found in the EC and OE from 1.5 months on and in the hippocampus from 6 months. NFT-like tau accumulations appeared later, from 6 months in the PC and EC, and at 9 months in the hippocampus (Sp). While only a few NFTs (Gallyas-positive) were present in the PC and EC at 9 months. Overall, our extensive analysis of the accumulation of pTau in connected olfactory regions gives a solid support to the hypothesis that tau pathology progresses along the olfactory system to reach regions of the temporal lobe that are particularly vulnerable in AD (e.g., EC, hippocampus).

Olfactory Function Assessment in PS19 mice

The impact of tau lesions in the olfactory system on olfactory function was assessed in PS19 mice using two specific olfactory tests: the olfactory discrimination test and the food-seeking test. The first test evaluated odor discrimination, whereas the food-seeking test measured odor threshold in mice. As a proof of concept, control and $ZnSO_4$-treated mice were first evaluated since intranasal irrigation with $ZnSO_4$ induces OE stripping and transient anosmia [161].

In the olfactory discrimination test, the curve for the number of sniffing events in non-treated (control mice) showed two peaks at 6 and 12 minutes (Fig. I15a). The first peak corresponded to the presentation of the geraniol odor, which induced a greater number of head movements toward the cotton swab in the control mice. Following this peak, the mice exhibited fewer head movements as they became accustomed to the odor. A second peak was observed after 12 minutes, when the second odor, lime, was presented. As expected, both peaks were absent in the mice that received intranasal $ZnSO_4$ administration (Fig.S9a). Similarly, during the food-seeking test, none of the $ZnSO_4$-treated mice were able to locate buried food before the end of the test (300 seconds)(Fig. I15a').

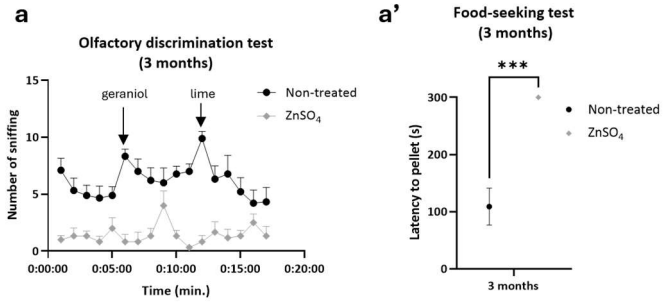

Fig. I.15 Olfactory function assessment in $ZnSO_4$-treated mice. The olfactory discrimination (a) and food-seeking tests (a') show a significant effect (***p<0,001) of $ZnSO_4$ treatment on olfactory function. For $ZnSO_4$ mice; n=6 (3 months) or non-treated controls; n=9 (3 months). Data were analyzed using two-way ANOVA with Šídák's multiple comparisons test (olfactory discrimination test) or using independent t-test (food-seeking test).

The same tests were conducted in WT and PS19 mice at 3, 6 and 9 months (Fig. I.16a-f) to evaluate the impact of tau pathology in the OE and associated CNS regions on olfactory function. In the olfactory discrimination test, both WT and PS19 mice showed two peaks corresponding to the introduction of

each new odor. Each peak was followed by reduced reactions due to habituation to the odor (Fig. I16a-f). All mice appeared to react more strongly, with a greater number of head movements, when presented with the second odor of lime. The superposition of curves indicates that all the mice, independently of their genotype and age, have similar olfactory discrimination capacities and that PS19 mice do not perform worse as they age. Statistical analyses revealed a significant impact of time as the mice responded to odor changes. However, no significant effect of genotype on olfactory capacities was observed at 3, 6 and 9 months in both males and females (Fig. I.16a-f). The results from the olfactory discrimination test suggested that the odor discrimination abilities of PS19 mice are not impaired by the presence of tau pathology in the OE.

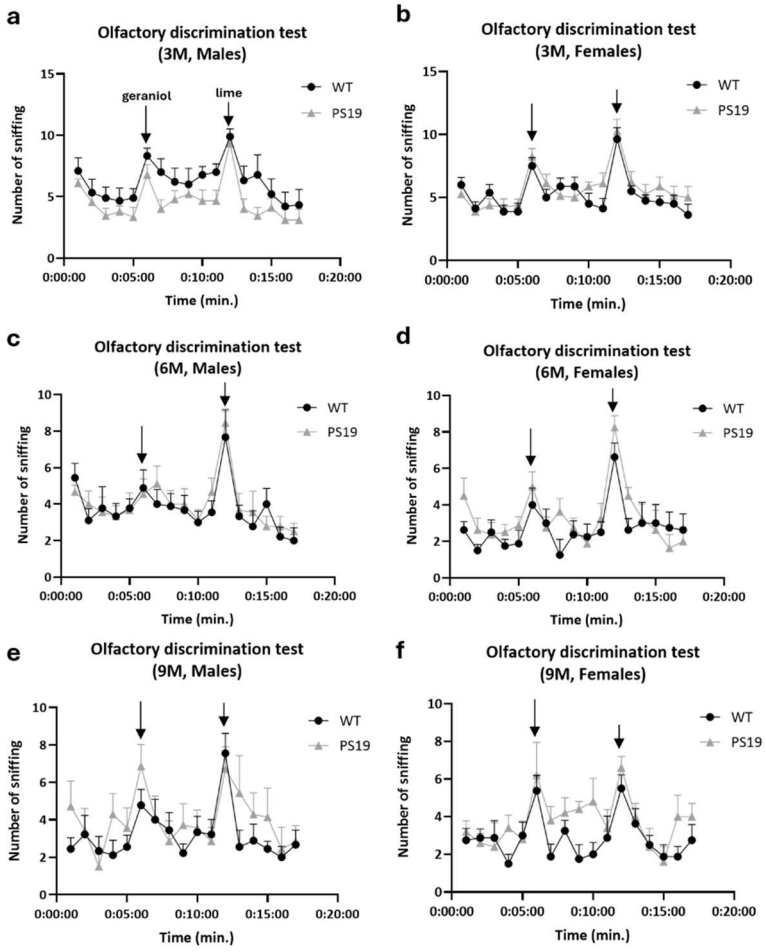

Fig. I.16 Olfactory function assessment in PS19 mice. The olfactory discrimination test (a-f) shows no significant effect of genotype (PS19) on olfaction at either 3, 6 or 9 months, both in males and females (a-f). For PS19 males; n=9 (3 months), n=9 (6 months) and n=7 (9 months). For WT males; n=9 (3 months), n=9 (6 months) and n=9 (9 months). For PS19 females; n=8 (3 months), n=8 (6 months) and n=5 (9 months). For WT females; n=8 (3 months), n=8 (6 months) and n=8 (9 months). Data were analyzed using two-way ANOVA with Šídák's multiple comparisons test.

In the food-seeking test, there was no significant difference between WT and PS19 mice in the latency to find the pellet (Fig. I.17a-c). This observation was consistent at 3, 6 and 9 months in both males and females (Fig. I.17a-c). No

significant difference in performance was observed between male and female mice of the same genotype (Fig. I.17a-c).

Together, these data indicate that despite progression of tau pathology along the olfactory regions with age, PS19 mice did not show a significant impairment in odor discrimination or detection threshold (sensitivity). Of note, another parameter (odor identification) difficult to address in mice was not evaluated here.

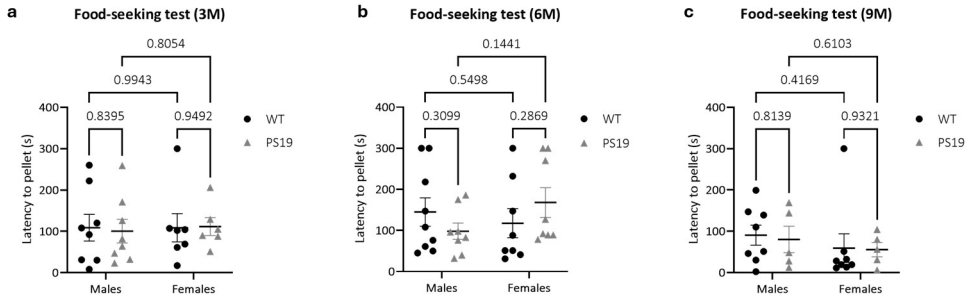

Fig. I.17 Olfactory function assessment in PS19 mice. The food-seeking test shows no significant effect of genotype (PS19) on olfaction at either 3, 6 or 9 months, both in males and females (a-c).For PS19 males; n=9 (3 months), n=9 (6 months) and n=7 (9 months). For WT males; n=9 (3 months), n=9 (6 months) and n=9 (9 months). For PS19 females; n=8 (3 months), n=8 (6 months) and n=5 (9 months). For WT females; n=8 (3 months), n=8 (6 months) and n=8 (9 months). Data were analyzed using Two-Way ANOVA.

Pathological pTau Protein in the Human Olfactory System

Finally, we investigated whether a similar pattern of tau pathology was observed in OE and OB collected from patients at early Braak stages I and II (patients 1-4, Table M2). In the OE collected from patient 4 (Braak stage II), pTau immunoreactivity (PHF-1 (Ser396, Ser404)) was detected and colocalizing with the OMP signal, indicating the presence of pTau in OSNs (Fig. I.18b). PHF-1 signal was also detected in the ABs present within the OE structure and revealed by the OMP antibody (Fig. I.18c-e). Still, PHF-1 and OMP signals are not fully overlapping. PHF-1 signal is mostly around the nuclei while the OMP stains all the axonal fibers present in the ABs (Fig. I.18f'). Interestingly, while colocalization was observed between OMP and PHF-1 within the ABs (Fig. I.18f), AT8 signal was detected neither in the ABs (Fig. I.18g) nor in the OSNs.

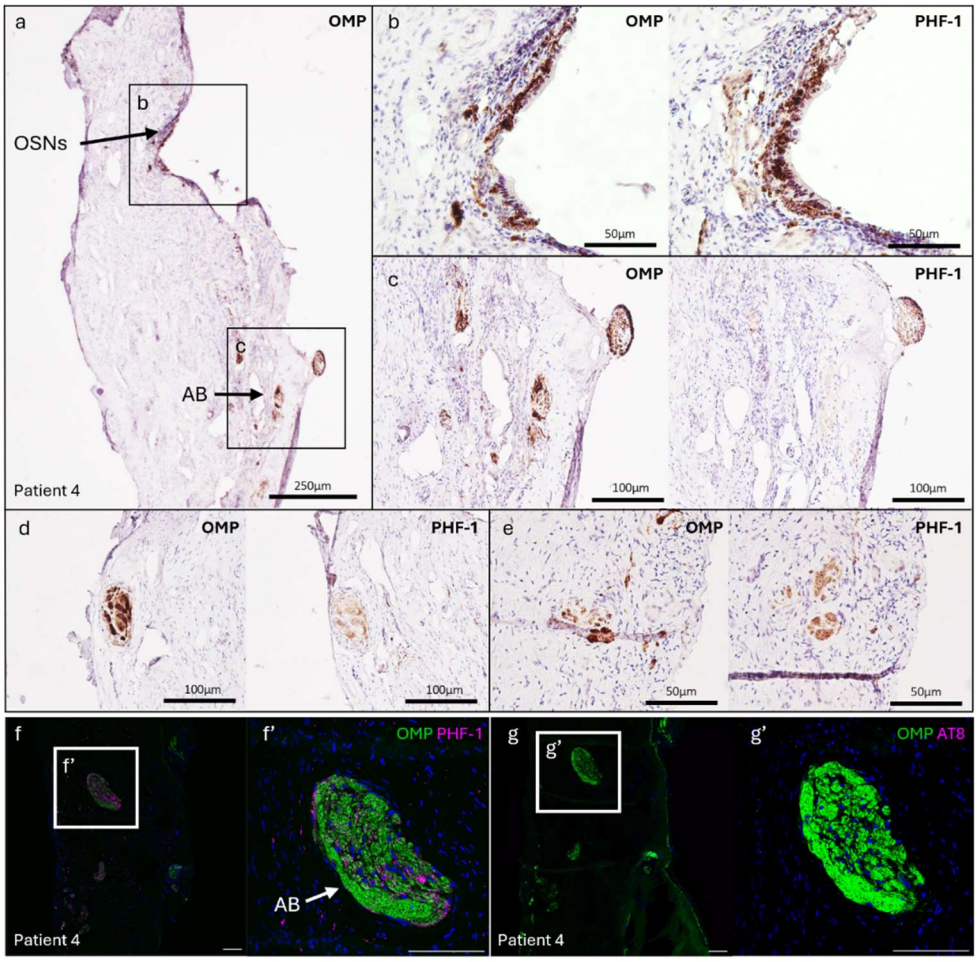

Fig. I.18 pTau expression in human OE. The OE was obtained from a Braak stage II patient (patient 4). The sections were immunohistochemically stained with **PHF-1** or with **OMP** (a-e). **PHF-1** signal is observed in the **OMP**-positive OSNs (b) and ABs (c-e) of the OE. Paraffin sections immunostained for **OMP** (green) and **PHF-1** (purple) show colocalization between **OMP-PHF-1** (white) in the AB (f, f'). PHF-1 signal is also observed inside the tissue (f). Paraffin sections immunostained for **OMP** (green) and **AT8** (purple) show no colocalization between **OMP-AT8** (g, g'). No signal is detected in the negative controls without primary antibodies. Scale bar: 100µm.

In the OB of Braak stage I/II patients, PHF-1 and OMP colocalization was consistently detected in the ONL, and to a lesser extent, in the GL (Fig. I.19a-d, d'). Some PHF-1 pTau signal was additionally found in the inner layers of the OB (Fig. I.19a-d, d"). No colocalization was observed between OMP and AT8 in the ONL (Fig. I.19e-h, h') but similarly to PHF-1, neuropil threads highlighted by the AT8 antibody were observed in the inner layers of the OB from Braak stage I and II patients (Fig. I.19e-h, h").

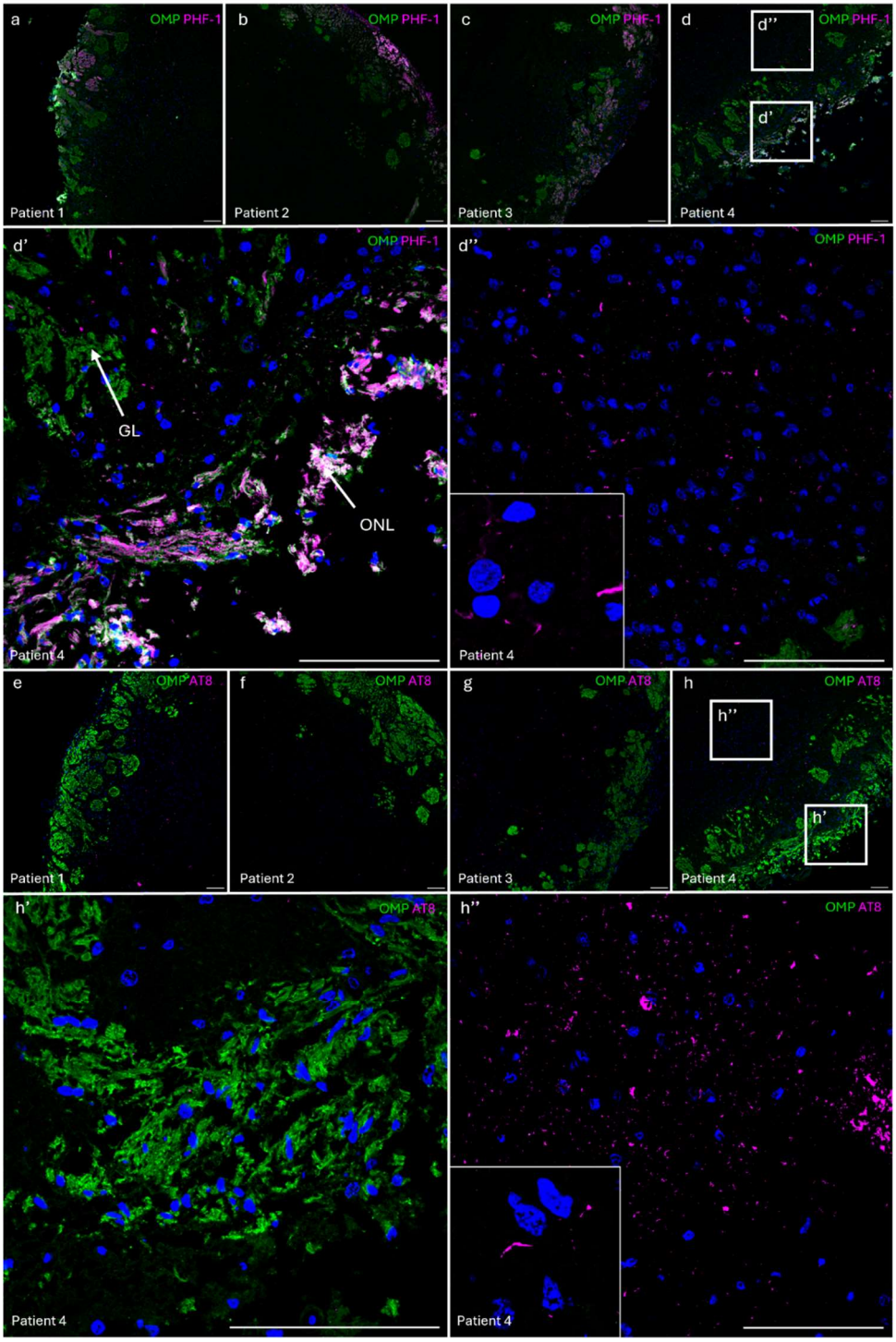
a
OMP PHF-1
Patient 1
b
OMP PHF-1
Patient 2
c
OMP PHF-1
Patient 3
d
d''
d'
OMP PHF-1
Patient 4
d'
OMP PHF-1
GL
ONL
Patient 4
d''
OMP PHF-1
Patient 4
e
OMP AT8
Patient 1
f
OMP AT8
Patient 2
g
OMP AT8
Patient 3
h
h''
h'
OMP AT8
Patient 4
h'
OMP AT8
Patient 4
h''
OMP AT8
Patient 4

Fig. I.19 pTau expression in human OB. The OB were obtained either from patients 1 and 2 (Braak stage I)(a, b, e, f) or from patients 3 and 4 (Braak stage II)(c, d, g, h). Paraffin sections immunostained for **OMP** (green) and **PHF-1** (purple) show colocalization between **OMP-PHF-1** (white) in the ONL of all patients (a-d, d'). **PHF-1** signal is also found in the inner layers of the OB (a-d, d''). Paraffin sections immunostained for **OMP** (green) and **AT8** (purple) show no colocalization between **OMP-AT8** (e-h, h'). AT8 signal is only found in the inner layers of the OB, similarly to **PHF-1** (e-h, h''). No signal is detected in the negative controls without primary antibodies. Scale bar: 100µm. ONL: olfactory nerve layer, GL: glomerular layer.

All OB included in the study were Gallyas-negative, highlighting the absence of mature NFTs at this stage (Braak stage I/II) of the pathology (Fig. I.20). These results underscore the early appearance of pathological tau markers in the sensory regions of the human olfactory system in agreement with observations in the PS19 mouse model.

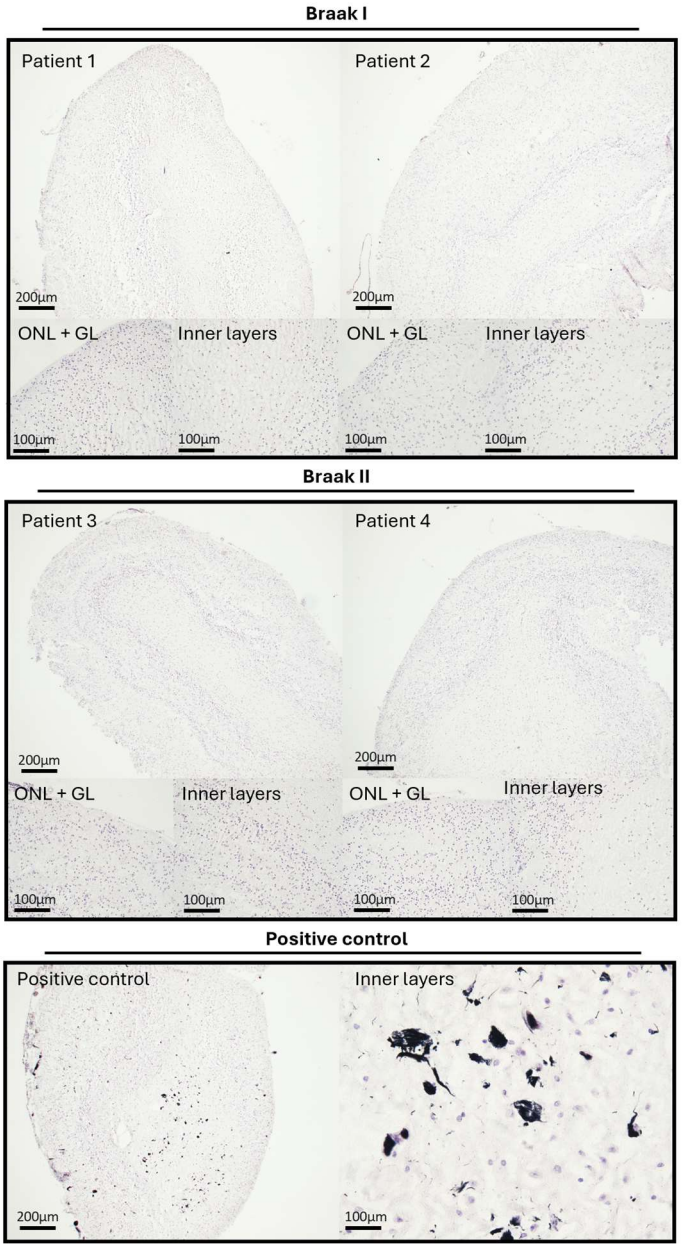

Fig. I.20 Gallyas staining in human OB. The paraffin sections of OB were obtained either from patients 1 and 2 (Braak stage I) or from patients 3 and 4 (Braak stage II). All OB are Gallyas-negative, highlighting the absence of mature NFTs at this early stage of the tau pathology in the olfactory nerve, glomerular, or inner layers.

In summary, this chapter highlights that pTau appears early in the OE of PS19 mice and subsequently spreads to the CNS following neuroanatomical pathways, like the olfactory and perforant pathways. Despite the presence of tau lesions in regions of the olfactory system, the olfactory threshold of PS19 mice was not significantly impaired. We additionally confirmed the appearance of pTau signal in the olfactory regions of Braak stage I/II patients. Overall, our findings support the spread of tau pathology according to anatomical neuronal connectivity, highlight the therapeutic potential of the OE region in tauopathies, and suggest its likely contribution to the progression of pathology in the CNS.

Results - Chapter II

The Olfactory Epithelium: A Target for Mitigating Tauopathy in the Central Nervous System

RESULTS – Chapter II

The interventions described in this second chapter were developed in response to the observation of an early onset of tau pathology in the OE. To explore a potential causal link between the emergence of pathology in the OE and its progression into the CNS, we employed two distinct strategies that directly targeted the OSNs in the OE, with the aim of modulating the existing pathological processes.

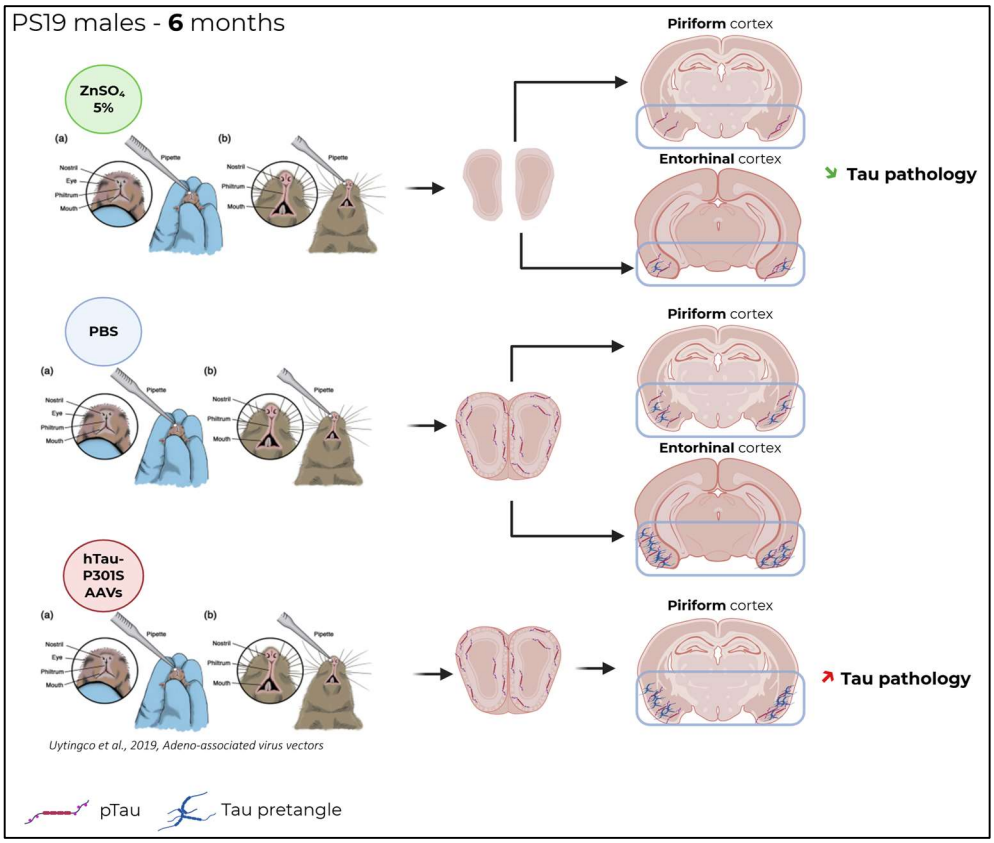

Graphical abstract – Chapter II, Created in BioRender. Kienlen-Campard, P. (2025) https://BioRender.com/m7r7nyt

Modulation of Tau Pathology in the CNS via Intranasal Interventions

Given the staged progression of tauopathy in olfactory regions and its early manifestation in the OE, we administered localized treatments to the OE to either mitigate tau pathology or exacerbate its spread to the CNS.

First, we examined the impact of targeted removal of the source of pathological tau present in the OE on tau pathology progression in the CNS. Our approach was designed to specifically remove the pTau accumulation in the OE using $ZnSO_4$ nasal irrigation, known to strip the OE and cause transient anosmia [162], both of which subsequently recover over time. Indeed, we were able to validate the effects of this treatment, which induces stripping of the OE and of the ONL at the level of the bulb (Fig. II.1a-d, a'-d'). We observed no morphological alterations at the cortical level indicating that $ZnSO_4$ treatment of the OE did not result in loss of density of the connected olfactory regions (Fig. II.1e-j).

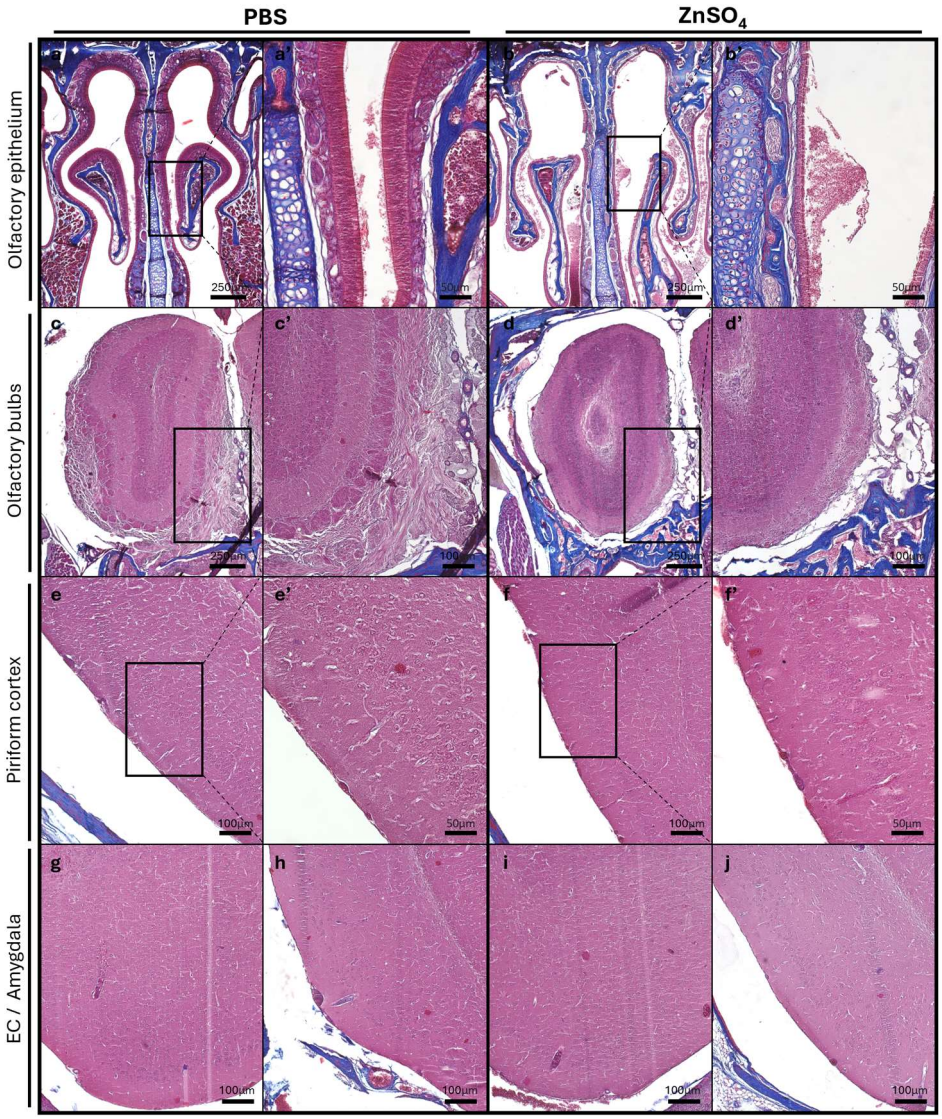

Fig. II.1 The OE, OB, PC amygdala, and EC stained with Masson's trichrome blue following PBS or $ZnSO_4$ nasal irrigation. The staining shows that $ZnSO_4$ nasal irrigation induces the stripping of the OE (b, b') and of the ONL in the OB (d, d') but no morphology alterations are observed in the PC (f, f'), amygdala (i) and EC (j) of 6-month-old PS19 males.

Next, the impact of intranasal $ZnSO_4$ treatment on the progression of tauopathy in the OB, PC, EC, and amygdala (a connected region in the limbic

system) was assessed. PS19 mice were intranasally administered with either $ZnSO_4$ or PBS (control). To ensure that the accumulation of tau in the OE was prevented for a sufficiently long period, nasal irrigation with $ZnSO_4$ was performed repeatedly at 1.5, 2.5, and 4 months, prior to analysis of tauopathy at 6 months.

In vehicle-treated PS19 mice, the structure of the OE remained intact, with strong AT8-positive tau immunoreactivity in OSNs and ABs. However, following intranasal $ZnSO_4$ administration, the OE was completely stripped, and the AT8 signal was almost absent at 6 months (Fig. II.2). In the OB of PBS-treated mice, all six layers were present and structurally preserved, with AT8-positive signal characteristic of PS19 mice. After $ZnSO_4$ treatment, the AT8 signal in the ONL was no longer detectable (Fig. II.2). Tau pathology was next examined in regions receiving direct inputs from the OB, such as the PC, EC, and amygdala. At 6 months, vehicle-treated PS19 mice exhibited NFT-like tau accumulations in these regions. However, following $ZnSO_4$ treatment of PS19 mice, no NFT-like tau accumulations were detectable in the PC, and only a few remained in the EC and amygdala at 6 months compared to control PS19 mice (Fig. II.2).

Fig. II.2 pTau expression in 6-month-old PS19 males after PBS or $ZnSO_4$ intranasal administration. Sections of the OE, OB, PC, EC, and amygdala from 6-month-old PS19 males were fixed and stained with the AT8 antibody. After intranasal $ZnSO_4$ irrigation, the OE and ONL of the OB are stripped, no more pTau signal is found in these areas (n=3 mice/group).

Quantification of the number of NFT-like tau accumulations per mm^2 in the PC, EC, and amygdala (Fig. S11), further confirmed a massive reduction of pTau signal associated to tau pathology in the PC, EC and amygdala following intranasal $ZnSO_4$ administration (Fig. II.3b). In other terms, removing the source of pTau present in the OE sharply reduces tau pathology in the connected regions of the temporal lobe and limbic system.

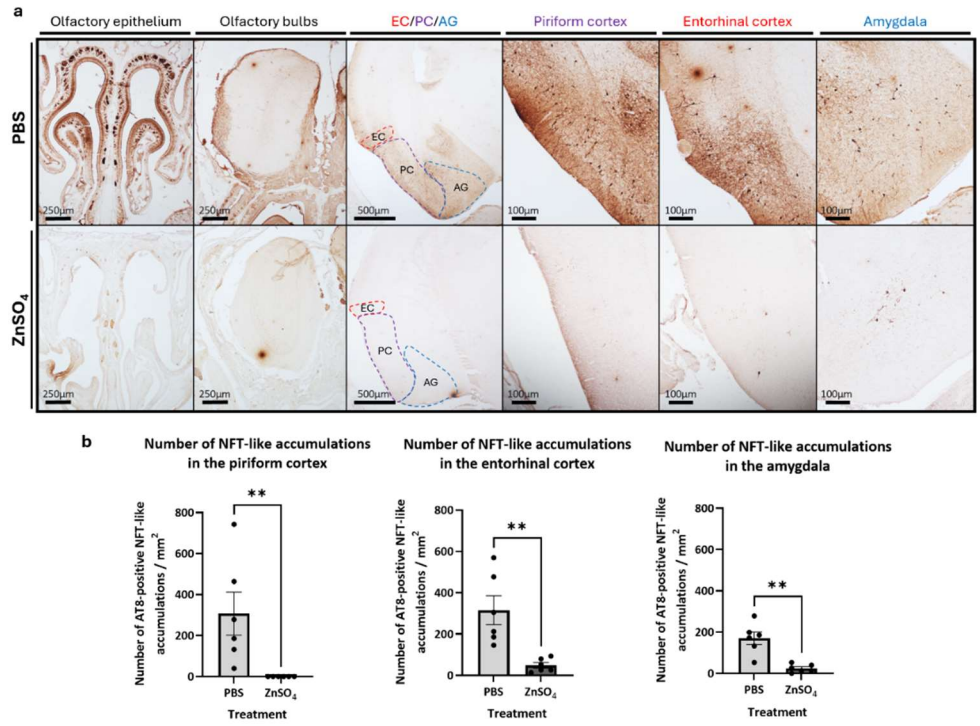

Fig. II.3 Modulation of tau pathology in the CNS via intranasal $ZnSO_4$ irrigation. Sections of the OE, OB, PC, EC, and amygdala from 6-month-old PS19 males were fixed and stained with the AT8 antibody. After intranasal $ZnSO_4$ irrigation, the OE and ONL of the OB are stripped, no more pTau signal is found in these regions (a). Quantification of the number of NFT-like tau accumulations/mm^2 was performed in the PC, EC, and amygdala. In the PC, there are no NFT-like tau accumulations compared to the PBS-treated mice. In the EC and amygdala there is a significant decrease in NFT-like accumulations compared to the control condition. **P < 0.01 (Mann Whitney test, n=6 mice/group)(b).

To further validate the hypothesis that tau pathology spreads from olfactory regions, we aimed to determine whether increasing pathology at the OE level could accelerate the progression of tau pathology in the CNS. To this end, we performed intranasal administrations of AAVs encoding the P301S-mutated human tau protein (referred to as hTau-P301S AAVs). The efficacy of AAV infection was first validated by the presence of GFP, which is co-expressed from the same vector. One week after the infection, a GFP-positive (green) signal was detected exclusively in the OE of AAV-treated mice, but not in PBS-treated controls (Fig. II.4), confirming successful viral transduction.

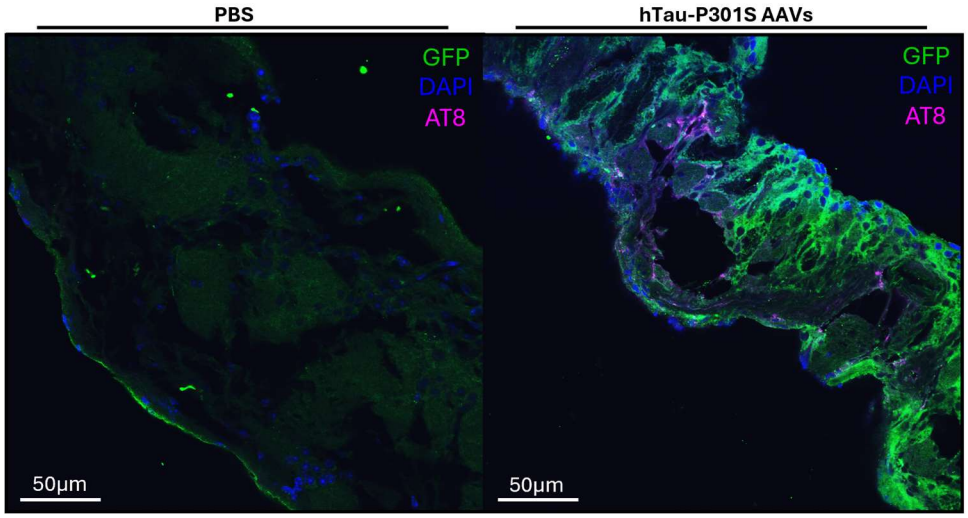

Fig. II.4 AAV transduction in the olfactory epithelium. OE sections immunostained for **GFP** (green), **AT8** (purple) and DAPI (blue) show efficient transduction following intranasal administration of hTau-P301S AAVs.

Subsequently, we assessed tau pathology using the AT8 antibody. We focused our analysis on the PC; a region directly connected to the OB and one of the first affected areas in tauopathies. At the end of the treatment,

when the mice were 4 months old, we observed that the intranasal delivery of hTau-P301S AAVs increased AT8 immunoreactivity in the PC of AAV-treated mice compared to controls (Fig. II.5) though the difference did not reach statistical significance — likely due to variability in AAV transduction efficiency — the pattern was consistent: all control mice displayed similar baseline levels of pathology, whereas all AAV-treated mice exhibited more advanced tau pathology in the PC (Fig. II.5).

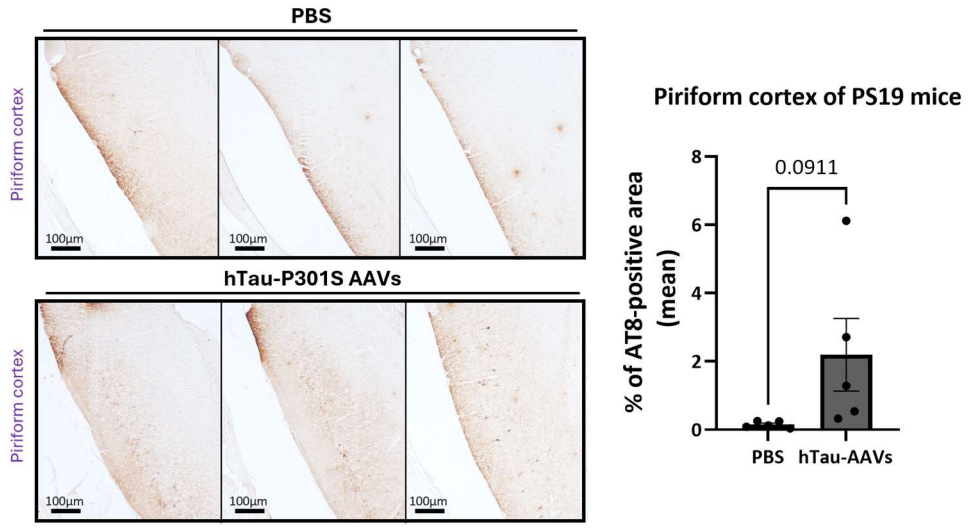

Fig. II.5 Modulation of tau pathology in the CNS via intranasal administration of hTau-P301S AAVs. PC sections are immunostained for AT8. In the PC, AT8 immunoreactivity appears increased in AAV-treated mice compared to PBS controls. Quantification of the AT8-positive area in the PC shows a trend toward increased pTau signal following nasal delivery of hTau-P301S AAVs (Mann Whitney, n=5 mice/group).

Overall, our data indicates that early accumulation of pTau in the OE can be instrumental to the progression of tau pathology that eventually reaches the EC and the hippocampal formation.

Results - Chapter III

Transcriptomic Profiling of the Olfactory Epithelium, Olfactory Bulb, and Hippocampus in PS19 mice: Identifying Biomarkers of Early Tauopathy

RESULTS – Chapter III

The results obtained and discussed in the first chapters have enabled us to highlight the pivotal role played by the olfactory system in the progression of tau pathology in PS19 mice, with results that are partly transferable to humans.

In this last chapter, we tried to gain deeper insight into the underlying mechanisms and cellular pathways active in these regions as well as molecular alterations underlying tau pathology. We performed transcriptomic and proteomic analyses with the final aim of identifying potential biomarkers in this model. All results presented in this chapter result from a collaboration with the University of Namur (Patricia Renard's team). For this research paper, I collected and prepared all the samples for the RNA sequencing while Dr. Ayeh Bouloki analyzed the data. Following this, I conducted results validation. The proteomic data were generated and analyzed by Marc Dieu and Malika Magomadov from Patricia Renard's team. With the help of Dr. Ayeh Bouloki, we wrote the initial manuscript draft. This research paper is under review in Alzheimer's & Dementia and available in BioRXiv.

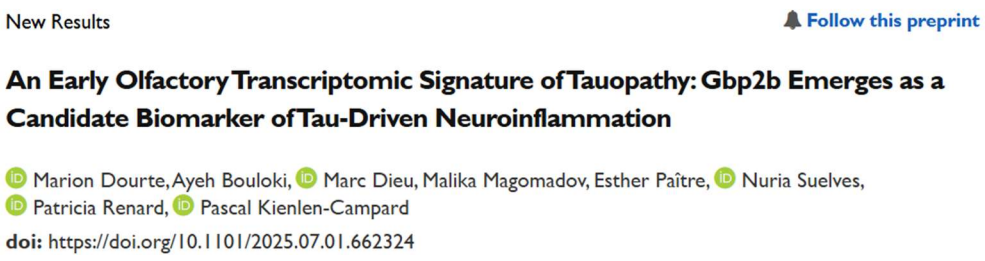
New Results

Follow this preprint

An Early Olfactory Transcriptomic Signature of Tauopathy: Gbp2b Emerges as a Candidate Biomarker of Tau-Driven Neuroinflammation

Marion Dourte, Ayeh Bouloki, Marc Dieu, Malika Magomadov, Esther Paître, Nuria Suelves, Patricia Renard, Pascal Kienlen-Campard

doi: https://doi.org/10.1101/2025.07.01.662324

Abstract : Olfactory dysfunction is increasingly recognized as an early feature of neurodegenerative diseases such as Alzheimer's disease. PS19 mice, a well-established tauopathy model, exhibit hallmarks of tau pathology—including hyperphosphorylated tau and pretangle formations—in various regions of the olfactory system. Notably, very recent data demonstrated that aberrantly hyperphosphorylated tau (pTau) was detected as early as 1.5 months of age in the olfactory epithelium (OE). This region contains olfactory sensory neurons projecting to the olfactory bulb (OB), where similar pTau pattern was also observed at this early stage. By 6 months, tau pretangles were evidenced in higher olfactory areas such as the piriform and entorhinal cortices. Given the early involvement of the OE and OB in tau pathology, we performed transcriptomic analyses at 3, 6, and 9 months to investigate the molecular pathways underlying tau pathology in these olfactory regions. Due to the OE's peripheral location and anatomical accessibility, we also aimed in that respect to identify potential early biomarkers of tauopathy. The hippocampus, a key brain region affected in Alzheimer's disease and related disorders, was included in the analysis as a comparative reference due to its known vulnerability and clinical relevance. Our analyses revealed region- and age-specific gene expression changes in PS19 mice. Functional enrichment analyses indicated a temporal progression of molecular alterations associated with tau pathology. We identified a subset of genes differentially expressed across different time points and/or regions. Among these, Gbp2b emerged as a particularly promising early biomarker candidate for tauopathy in the OE, showing consistent upregulation across tau pathological stages and brain regions.

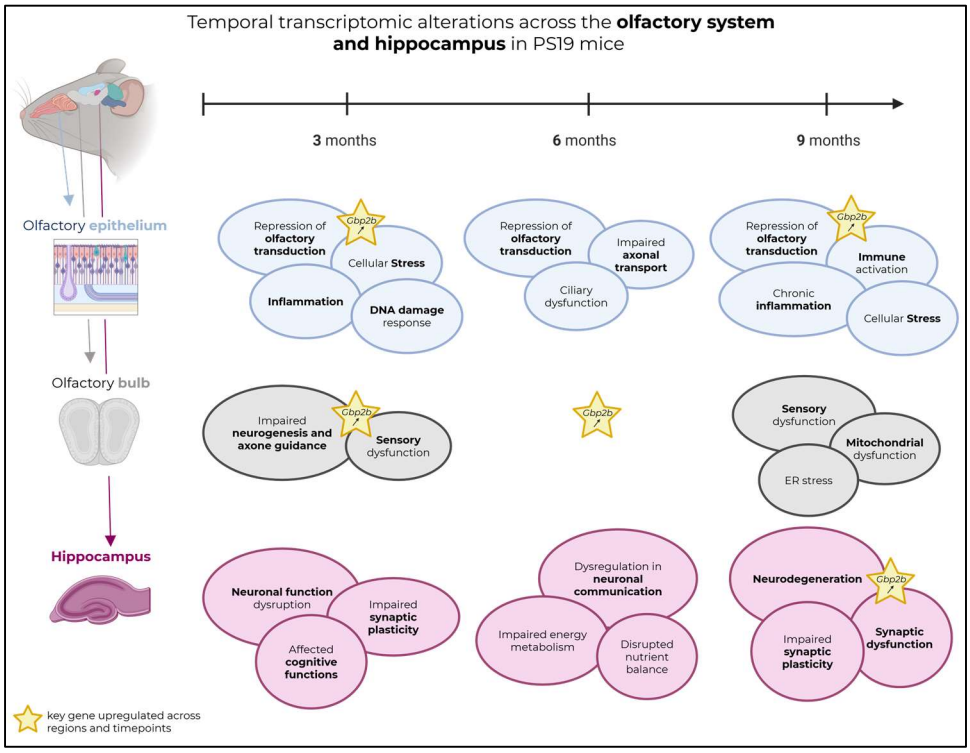

Graphical abstract – Chapter III, Created in BioRender. Kienlen-Campard, P. (2025) https://BioRender.com/k7xoypd

Transcriptomic Profiling Reveals Age- and Region-Specific Gene Expression in PS19 mice

To characterize tauopathy progression, RNA sequencing was performed on the hippocampus, OB, and OE of PS19 and WT mice at 3, 6, and 9 months. Heatmaps and PCA analyses confirmed robust separation by genotype and age across all regions (Fig. III.1, Fig. S1).

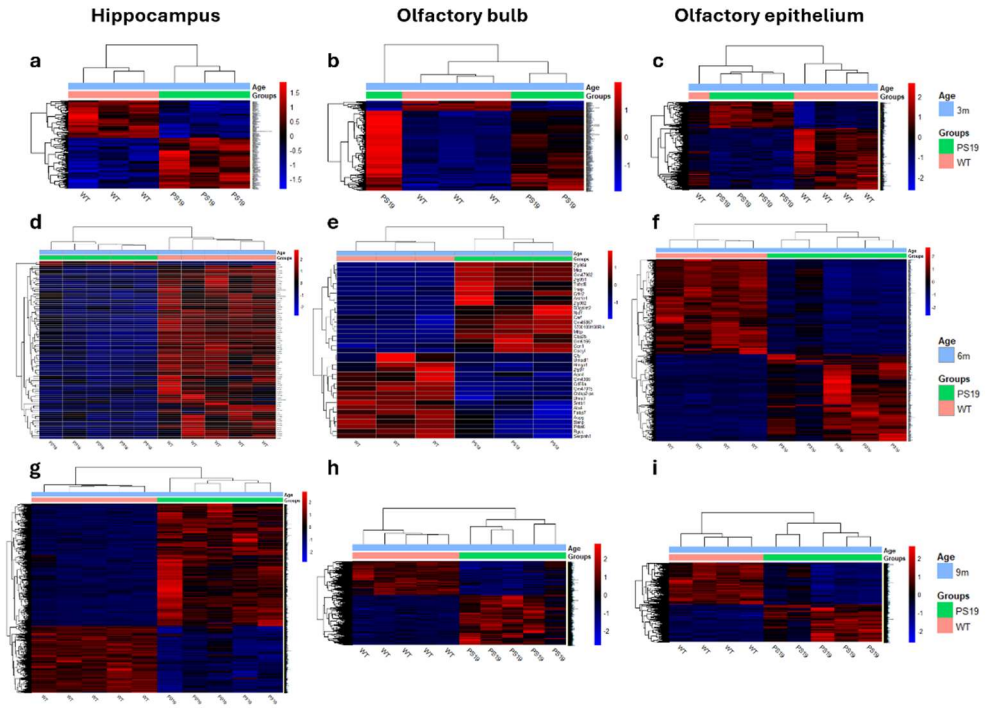

Fig. III.1 Hierarchical clustering heatmaps of normalized gene expression levels across multiple brain and olfactory regions in PS19 and WT mice at 3, 6, and 9 months. Heatmaps are shown for the hippocampus (a, d, g), OB (b, e, h), and OE (c, f, i). Gene expression was assessed over time at 3 months (a–c), 6 months (d–f), and 9 months (g–i). Rows represent differentially expressed genes, and columns correspond to individual samples (PS19 in green; WT in pink). Color scale indicates relative expression levels, with blue representing low expression and red representing high expression. n=3-5 mice/group.

At 3 months, the OE exhibited the most transcriptomic disruption (hippocampus: 160, OB: 239, OE: 1023 DEGs). DEG numbers decreased in the hippocampus and OB by 6 months but remained high in the OE (1031), suggesting sustained dysfunction in the olfactory system. At 9 months, DEGs sharply increased across all regions (Hippocampus: 4599, OB: 2896, OE: 3665), aligning with disease progression. The top 10 DEGs per anatomical region and time point are listed in **Table 1.**

Table 1. Top 10 DEGs ranked by the absolute logFC values across three regions (hippocampus, OB, and OE) at three time points (3, 6, and 9 months) in PS19 mice.

GeneSymbol	LogFC	GeneSymbol	LogFC	GeneSymbol	LogFC
HP-3 months		**HP-6months**		**HP-9 months**	
Lamr1-ps1	9.17	*Ttr*	-8.57	*Slc10a6*	9.32
Bglap3	1.42	*Prr32*	-7.11	*Gbp2b*	8.56
Hif3a	-1.34	*Gm36901*	-6.63	*Ctse*	8.55
Plin4	-1.31	*Kcnj13*	-6.59	*Lamr1-ps1*	8.35
Cdkn1a	-1.28	*Slc16a8*	-6.38	*Atp6v0d2*	8.29
Mlph	-1.26	*Cdh3*	-6.22	*Ifi204*	8.26
Prnp	1.16	*Tmprss11a*	-6.09	*Gm50008*	7.60
Nostrin	-1.16	*Wdr72*	-6.03	*Cxcl9*	7.40
Exph5	1.10	*F5*	-5.87	*Ccl4*	7.33
Gm45426	1.02	*Clic6*	-5.73	*Stra6l*	7.16
OB-3 months		**OB-6 months**		**OB-9 months**	
Gbp2b	7.98	*Gbp2b*	7.03	*Slc10a6*	7.99
Prdm8	4.34	*Zfp991*	5.59	*Tigit*	7.29
Igfn1	3.65	*Zfp982*	5.49	*Lamr1-ps1*	6.98
Satb2	3.61	*Gm6166*	4.14	*Scnn1g*	6.64
Npy2r	3.46	*Zfp984*	3.91	*Or2h2*	6.51
Alox12b	2.86	*Tnfrsf8*	3.79	*6820402A03Rik*	6.51
Tnnc1	2.86	*Ctdsp2-ps*	-2.79	*Gm16410*	6.28
Grp	2.83	*Gm47015*	-2.36	*Gm50015*	6.17
Mal2	2.76	*Zfp97*	-2.13	*Iqcf6*	6.08
Scn4b	2.54	*Gm4366*	-2.09	*Or2y8*	6.03
OE-3 months		**OE-6 months**		**OE-9 months**	
Mrgprg	-8.82	*Scgb2b27*	-8.04	*Gbp2b*	8.15
Mup5	-8.36	*AA388235*	-5.88	*Mcpt1*	7.64
Gm3896	-8.31	*Obp1a*	5.09	*Zfp990*	6.56
Gbp2b	7.56	*Obp1b*	4.43	*Elfn2*	6.56
BC051076	-6.30	*Scgb1b27*	-4.32	*Gm12961*	6.11
5430402E10Rik	-6.24	*Or14j10*	-4.20	*Mcpt2*	5.70
Gm14744	-5.75	*Krt4*	-3.86	*Gm11738*	5.62
Lcn11	-5.70	*Il13*	-3.79	*A230103L15Rik*	5.60
Obp1a	-5.65	*Igkv14-126*	3.26	*Ppp1r1c*	5.59
Chil4	-4.97	*Klk1b22*	3.16	*Eno1b*	5.31

Functional Enrichment Analysis Highlights Temporal Progression of Tauopathy

GO and KEGG pathway analysis of DEGs showed age- and region-specific enrichment. In the hippocampus, early changes (3 months) involved processes related to cognition, extracellular matrix organization, and cAMP signaling (Fig. III.2a). At 6 months, signaling and metabolic disruptions emerged (Fig. III.2b), while by 9 months, enrichment shifted toward neurodegeneration, synaptic dysfunction, and circadian regulation (Fig. III.2c).

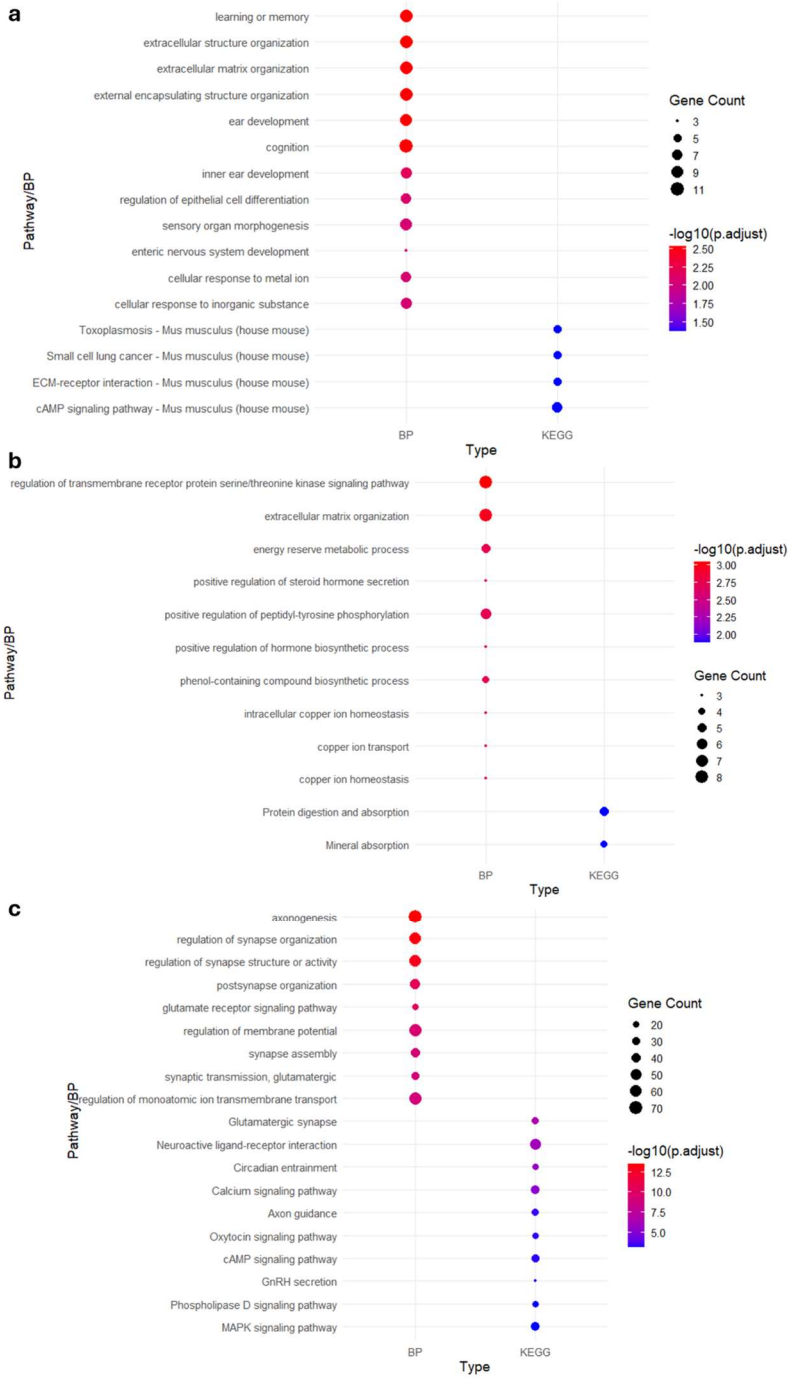

Fig. III.2 Enrichment analysis of DEGs in the hippocampus at 3 (a), 6 (b), and 9 (c) months. Dot plot showing significantly enriched terms among DEGs in these conditions. The y-axis

lists enriched terms from GO Biological Processes (BP) and KEGG pathways, as indicated on the x-axis. Dot size represents the number of DEGs associated with each term (Gene Count), while dot color reflects statistical significance, shown as $-\log_{10}$(adjusted p-value).

In the OB, early DEGs were linked to axon guidance and neuroactive signaling (Fig. III.3a). At 6 months, enrichment was minimal, suggesting transient stabilization. By 9 months, DEGs in the OB showed strong enrichment in olfactory signaling, endoplasmic reticulum stress, and synaptic targeting (Fig. III.3b).

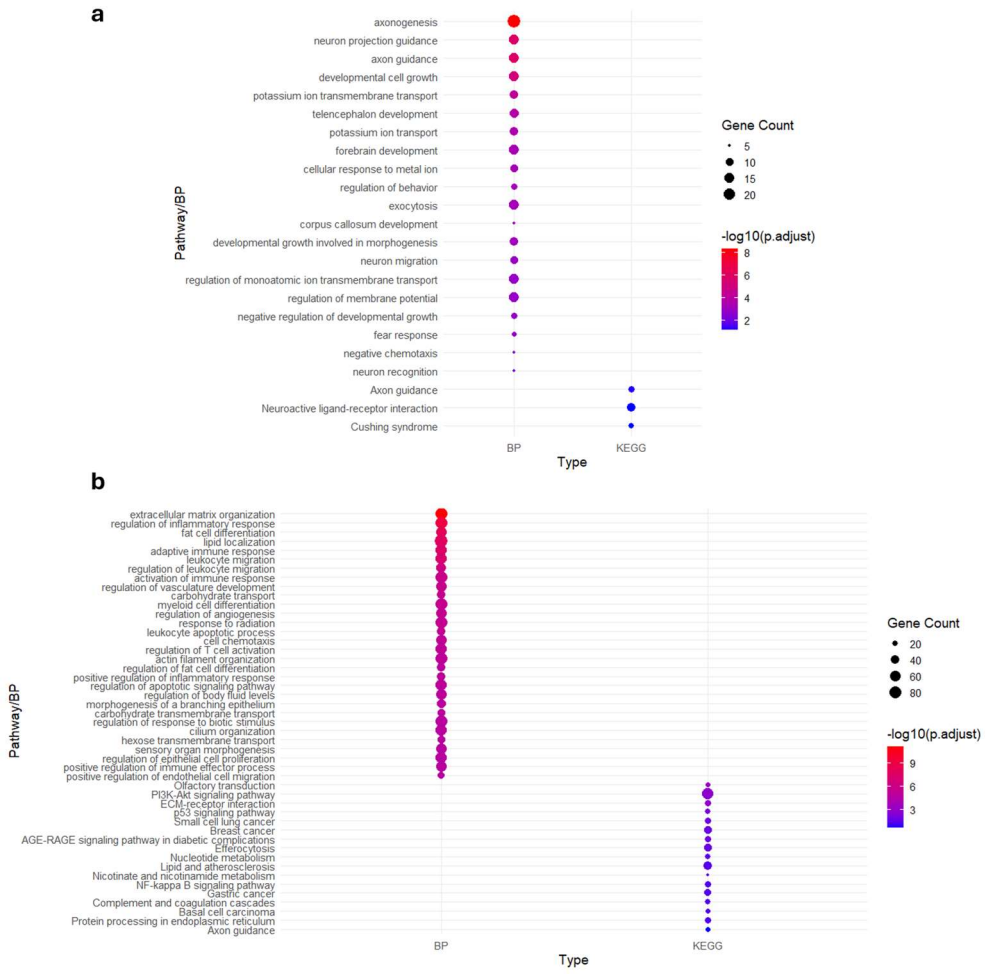

Fig. III.3 Enrichment analysis of DEGs in the OB at 3 (a) and 9 (b) months. No significantly enriched pathways in the OB at 6 months. Dot plot showing significantly enriched terms among DEGs in these conditions. The y-axis lists enriched terms from GO Biological Processes (BP) and KEGG pathways, as indicated on the x-axis. Dot size represents the

number of DEGs associated with each term (Gene Count), while dot color reflects statistical significance, shown as $-\log_{10}$(adjusted p-value).

The OE exhibited early signs of stress and immune activation at 3 months, with enrichments in sensory perception, DNA damage response, and p53 signaling (Fig. III.4a). By 6 and 9 months, structural (cilium organization), inflammatory (TNF, NF-κB), and metabolic pathways (HIF-1) were increasingly dysregulated (Fig. III.4b, c). Repression of olfactory transduction pathways was consistent with declining olfactory function.

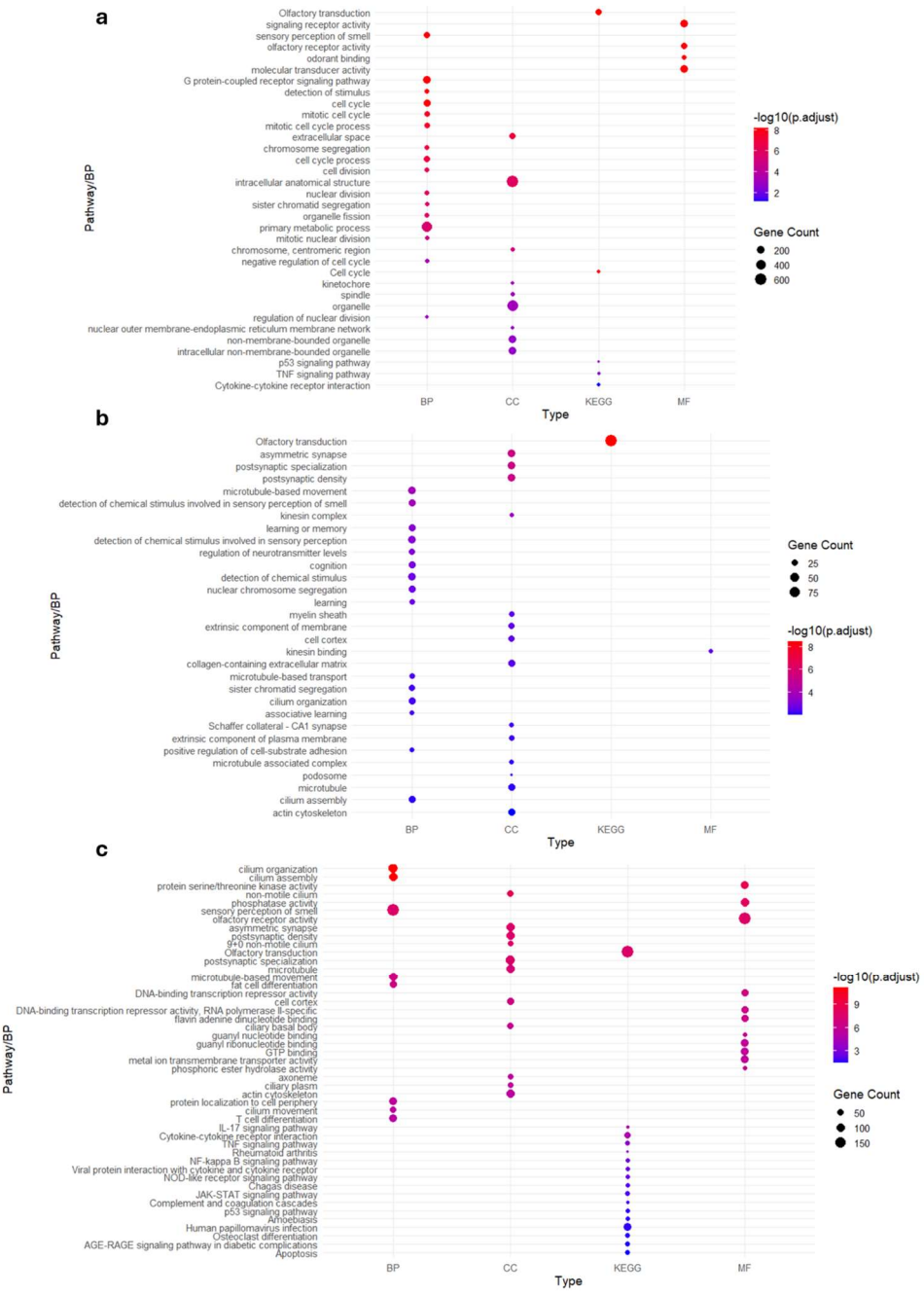

Fig. III.4 Enrichment analysis of DEGs in the OE at 3 (a), 6 (b), and 9 (c) months. Dot plot showing significantly enriched terms among DEGs in these conditions. The y-axis lists enriched terms from GO Biological Processes (BP), Cellular Component (CC), KEGG

pathways, and Molecular Function (MF), as indicated on the x-axis. Dot size represents the number of DEGs associated with each term (Gene Count), while dot color reflects statistical significance, shown as $-\log_{10}$(adjusted p-value).

These findings highlight the progressive features of tauopathy and suggest that cellular stress, inflammation, and disrupted synaptic and neuronal functions play a key role in tau-related neurodegeneration across the studied regions. The olfactory system appears to be an early and vulnerable target of tau accumulation, with significant implications for sensory and cognitive functions in tauopathies.

Spatiotemporal Overlap of Differentially Expressed Genes Reveals Region- and Age-Specific Responses to Tau Pathology

To investigate the spatiotemporal dynamics of gene expression in tauopathy, we examined the overlap of DEGs across the hippocampus, OB, and OE in PS19 mice at 3, 6, and 9 months of age. Venn diagrams and DEG comparisons were used to identify common and region-specific transcriptional responses during pathology progression (Fig. III.5).

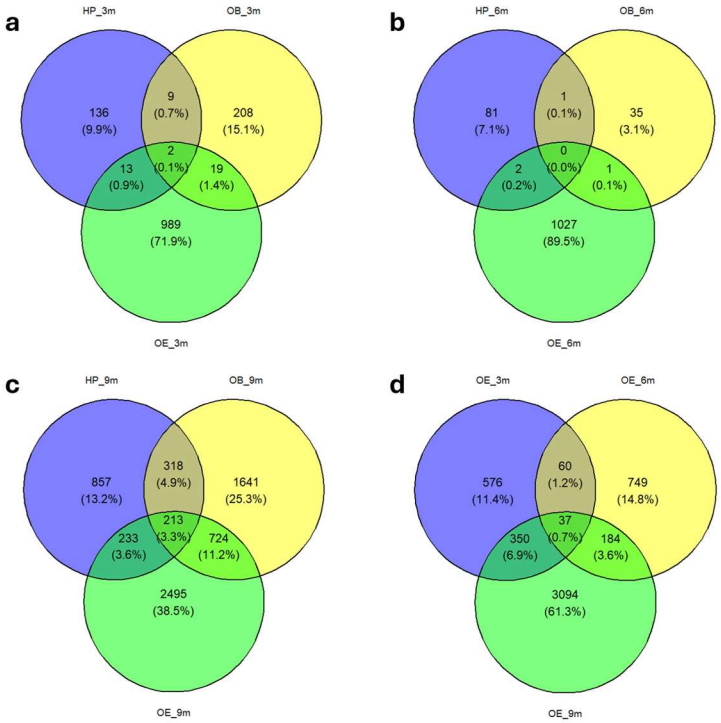

Fig. III.5 Venn diagrams showing the overlap of DEGs across regions and time points in PS19 mice. Overlap of DEGs among the hippocampus, OB, and OE at 3 months (a), 6 months (b), and 9 months (c). The majority of DEGs are specific to the OE, with limited overlap across regions at early time points and greater overlap observed at 9 months. Comparison of DEGs in the OE across 3, 6 and 9 months (d), showing progressive change over time. Percentages within the diagrams represent the proportion of total genes in each category.

At 3 months, overlap analysis revealed two DEGs—*Wnt9a and Prnp*—shared across all three regions (Fig. III.5a). *Prnp* was consistently upregulated in all studied regions and may represent a neuronal stress response linked to tau accumulation. *Wnt9a* showed region-specific regulation, being upregulated in the hippocampus and OB but downregulated in OE. Given Wnt signaling's role in neurogenesis and plasticity [163], this pattern may reflect compensatory responses in hippocampus/OB and impaired regenerative capacity in OE, potentially contributing to early olfactory dysfunction—a hallmark of Alzheimer's and Parkinson's disease [3, 50]. Further overlap between OB and OE identified 19 shared DEGs. Genes such as *Fosl2* and *Nr4a3* were downregulated in both regions, while others (e.g., *Gramd2a, Cgref1*) displayed opposing expression, indicating region-specific metabolic or stress responses. Immune-related genes, including *Gbp2b*, and Wnt pathway regulators *Dkk3* and *Wnt4*, were upregulated in both regions, suggesting activation of inflammatory and neurogenic pathways. Shared DEGs between hippocampus and OE (n = 13) included genes with both uniform and opposing expression patterns. For instance, *Ldlr* and *Mansc1* were upregulated in hippocampus but downregulated in OE, suggesting differential vulnerability to lipid dysregulation and stress. Uniformly downregulated genes—*Tsc22d3, Recql4, and Nkd2*, among others—highlighted common impairments in DNA repair, stress resilience, and synaptic function. Upregulated genes such as *Gm56721* further underscore overlapping responses to tau burden.

At 6 months, the number of shared DEGs decreased, indicating increased regional specificity with aging (Fig. III.5b). Only *Sulf1* and *Crb2* were common

to hippocampus and OE, and *Gfy* to OB and OE. Notably, *Sulf1* and *Crb2* were upregulated in OE but downregulated in hippocampus, potentially reflecting continued regenerative activity in OE versus degenerative changes in hippocampus. *Gfy* upregulation in OB and downregulation in OE may indicate disrupted olfactory neurogenesis and connectivity.

At 9 months, DEG overlap increased substantially, with 213 genes shared across all three regions (3.3% of total DEGs), indicating a convergence of disease-associated molecular alterations (Fig. III.5c). In hippocampus and OE, overlapping DEGs were enriched in synapse-related functions and ciliary components associated with long-term potentiation and calcium signaling—critical pathways for cognitive and sensory function. A large set of 724 overlapping DEGs (11.2%) between OB and OE included genes involved in DNA replication, cytokine signaling, apoptosis, and synapse pruning, emphasizing shared neurodegenerative mechanisms in olfactory regions.

Across all ages, multiple guanylate-binding proteins (GBPs) were consistently upregulated in OB and OE. These proteins are involved in immune responses, particularly in regulating inflammation, antiviral defense, and immune signaling, suggesting a sustained neuroinflammatory response in olfactory regions—a process increasingly linked to tauopathy progression [164].

Lastly, 37 genes in OE were differentially expressed across all time points in PS19 mice (Fig. III.5d). 16 of these genes, including *Depdc1a, Sox4, and Hmgb2*, shifted from downregulation at 3 months to upregulation at 6 and 9 months. Many of these genes are involved in cell cycle regulation, signal

transduction, and neurogenesis, which are key processes for maintaining the structural integrity of OSNs. This temporal pattern suggests an age-dependent compensatory response aimed at restoring homeostasis, particularly in pathways involving cell cycle regulation, neurogenesis, and DNA repair. In contrast, 21 genes were found to be upregulated at 3 months but downregulated at 6 and 9 months. Many of these genes encode olfactory receptors (ORs) such as *Or10g7*, *Or8b51*, or *Or5d39* suggesting an early overactivation of olfactory signaling, followed by a decline as disease progresses. This shift likely reflects impaired olfactory transduction and OSNs loss, aligning with the known early olfactory deficits in NDs like AD and Parkinson's disease [3, 50].

Collectively, these findings reveal early and progressive transcriptomic changes in response to tau accumulation, with distinct and shared regional signatures. The OE, with its neurogenic capacity, displays dynamic regulatory shifts that are likely to contribute to early sensory impairments observed in tauopathies.

Transcriptomic Signatures in the OE of PS19 mice as Early Biomarkers of Tau Pathology

A secondary objective of this study was to uncover early phenotypic alterations that may act as potential biomarkers for the early detection of tau-related NDs. The OE, due to its anatomical accessibility, serves as a valuable diagnostic tool compared to CNS regions like the OB or hippocampus, which are challenging to access in living organisms. While these regions are crucial for understanding the mechanisms driving tau pathology, our focus was on identifying potential biomarkers by analyzing DEGs in the OE. The 3-month time point was particularly relevant for early diagnosis, as these molecular changes emerge even before pathology develops in regions such as the hippocampus. We established a panel of candidate biomarkers (Table 2), from which a subset was selected for validation by qRT-PCR.

Table 2. Biomarker panel in the OE at 3 months. Selection based on the DEGs in the OE at 3 months, and the overlapping genes analyses. The candidates validated by qRT-PCR are highlighted in pink.

OE – 3 months							
GeneSymbol	LogFC	GeneSymbol	LogFC	GeneSymbol	LogFC	GeneSymbol	LogFC
Gbp2b	7.56	*Or2w6*	1.03	*Fosl2*	-0.71	*Trim29*	-1.23
Or8a1	2.55	*Wdr17*	0.93	*Lama5*	-0.72	*Wnt4*	-1.23
Sfmbt2	2.37	*Asphd2*	0.90	*Ldlr*	-0.73	*Nr4a3*	-1.24
Cyp2c23	2.20	*D430041D05Rik*	0.88	*Wnt9a*	-0.74	*Gramd2a*	-1.25
Or10n7-ps1	1.84	*Gng13*	0.80	*Mgp*	-0.81	*Map3k6*	-1.25
Or9q2	1.81	*Cabp1*	0.73	*Plk3*	-0.83	*Mxd3*	-1.26
Tmem236	1.68	*Kcnk10*	0.69	*Zgrf1*	-0.85	*Spag5*	-1.30
Or1ad8	1.65	*Ltk*	0.67	*Ccdc3*	-0.85	*Ascl1*	-1.42
Or10d5j	1.63	*Fam131b*	0.67	*Slc47a1*	-0.86	*Depdc1a*	-1.76
Or8c14-ps1	1.63	*Rarg*	0.62	*Arl4d*	-0.86	*Tns4*	-2.02
Prnp	1.60	*Plpp7*	0.61	*Nkd2*	-0.87	*Pigr*	-2.45
S100a3	1.48	*Kcnt1*	0.59	*Tsc22d3*	-0.88	*Or8b12*	-2.73
Or2at1	1.42	*Ppp1r1a*	0.57	*Ier3*	-0.88	*Cxcl2*	-4.60
Or10d4	1.35	*Lipe*	-0.51	*Btg2*	-0.88	*Chil4*	-4.97
Or5p4	1.34	*Anxa2*	-0.54	*Ckap2l*	-0.93	*Obp1a*	-5.65
Or5ak25	1.32	*Osmr*	-0.54	*Tnfrsf25*	-0.98	*Lcn11*	-5.70
Or51f23b	1.32	*Mansc1*	-0.56	*Six3*	-0.99	*Gm14744*	-5.75
Or5d39	1.30	*Klf5*	-0.58	*Gtse1*	-1.01	*5430402E10Rik*	-6.24
Or8b51	1.26	*Fam20a*	-0.63	*Zfp52*	-1.02	*BC051076*	-6.30
Or10g7	1.22	*Smim3*	-0.64	*Recql4*	-1.02	*Gm3896*	-8.31
Ifit1	1.17	*Sox4*	-0.65	*Sult5a1*	-1.02	*Mup5*	-8.36
Gm56721	1.07	*Dkk3*	-0.66	*Cgref1*	-1.03	*Mrgprg*	-8.82
Taar7f	1.03	*Hmgb2*	-0.68	*Trpm6*	-1.23		

We chose to perform the validation in a male cohort, consistent with the RNA-sequencing analysis, and additionally included a female cohort to assess potential sex-related differences in gene expression. We first validated *Prnp* increased expression in the OE and OB, since it was one of the two candidates upregulated across all three regions. The increase was significant from 6 months in the OE (Fig. III.6a) and from 3 months in the OB (Fig. III.6b).

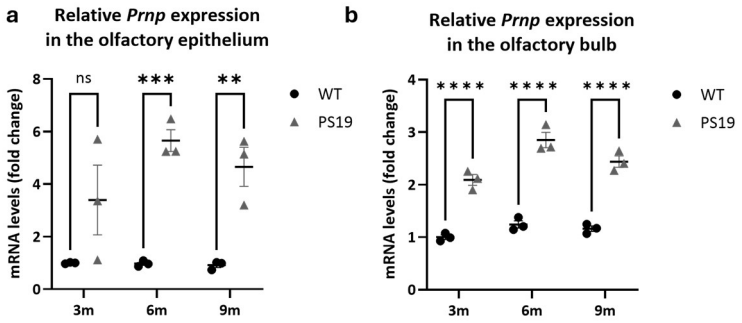

Fig. III.6 *Prnp* expression in the OE and OB of WT and PS19 mice. mRNA levels of *Prnp* expression were measured by RT-qPCR in OE and OB extracts from WT and PS19 mice at 3, 6, and 9 months. *Prnp* is significantly increased in the OE of 6- and 9-month-old PS19 mice (a). **P < 0.01, ***P < 0.001. (Two-way ANOVA, n=3 mice/group). *Prnp* is significantly increased in the OB of 3-, 6-, and 9-month-old PS19 mice (b). ****P < 0.0001. (Two-way ANOVA, n=3 mice/group).

Then we focused on several candidates that might be of interest for further validation among the top 10 DEGs in the OE at 3 months (*Mrgprg, Mup5, Gm3896, Gbp2b, BC051019, 5430402E10Rik, Gm14744, Lcn11, Obp1a, Chil4*)(Table 1). We further investigated other candidates that showed an almost perfect segregation in the box plots, with the formation of two clearly distinct groups (WT and PS19), such as *Mup5, Pon1,* and *Tsc22d1* (Fig. S2). Finally, we also checked for *Wnt9a* expression since it showed region-

specific regulation: upregulated in hippocampus and OB but downregulated in OE.

qRT-PCR analysis confirmed the trend of reduced expression of *Mup5, 5430402E10Rik, Gm14744,* and *Obp1a* both in males and females, consistent with RNA-sequencing data (Fig. III.7b-e). However, these differences did not reach statistical significance in all conditions, likely due to high inter-individual variability or low baseline expression. *Pon1* and *Tsc22d1* showed more distinct clustering patterns, but their expression trends appeared to diverge between sexes – showing opposite directions in males and females. Furthermore, the overall differences were modest and did not reach statistical significance in both sexes (Fig. III.7g, h). For *Chil4* and *Wnt9a*, a trend toward decreased expression was seen in males but not in females. (Fig. III.7f, i). Taken together, the combination of sex-dependent variability and the absence of significant differences in both sexes suggest that these genes are unlikely to be strong biomarker candidates.

a

GeneSymbol	logFc
Mup5	-8.36
5430402E10Rik	-6.24
Gm14744	-5.75
Obp1a	-5.65
Chil4	-4.97
Wnt9a	-0.74
Pon1	0.36
Tsc22d1	0.35

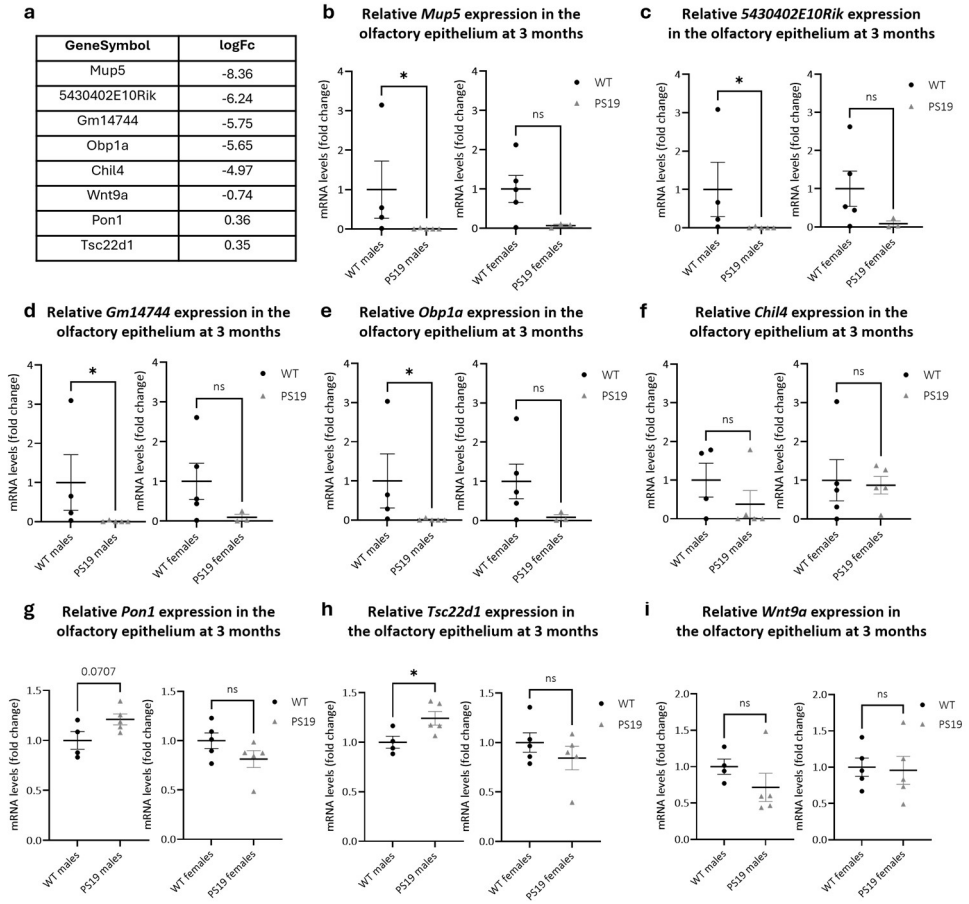

Fig. III.7 Biomarkers panel validation in the OE of 3-month-old PS19 and WT mice. Log fold-change (logFC) values were derived from RNA-sequencing analysis comparing PS19 mice to WT controls. Negative logFC values indicate downregulation, while positive values indicate upregulation in PS19 mice (a). mRNA expression levels of *Mup5, 5430402E10Rik, Gm14744, Obp1a, Chil4, Pon1, Tsc22d1*, and *Wnt9a* were analyzed by RT-qPCR in the OE of WT and PS19 mice at 3 months of age (b-i). The results in males showed expression trends consistent with those observed in the RNA-sequencing data, although the differences did not always reach statistical significance (Unpaired t-tests, n=3–5 mice/group).

Next, we focused on *Gbp2b*, the only gene among the top 10 DEGs upregulated in the OE of 3-month-old PS19 males (Table 1, Fig. III.8a). *Gbp2b* also ranked among the top 10 DEGs in the OE at 9 months, in the OB at 3 and 6 months, and in the hippocampus at 9 months (Table 1). Notably, we observed a highly significant increase in *Gbp2b* expression in the OE of both male and female PS19 mice at 3 months (Fig. III.8b). In the OB, expression of *Gbp2b* was elevated as early as 3 months in both sexes and remained high at 9 months (Fig. III.8c, d). In the hippocampus, we confirmed increased expression at 3 months in males and females, with the upregulation persisting at 9 months (Fig. III.8e, f). So far, these findings suggest that this candidate represents the most promising early biomarker of tau pathology in the olfactory system of PS19 mice.

a

GeneSymbol	logFc
Mrgprg	-8.82
Mup5	-8.36
Gm3896	-8.31
Gbp2b	7.56
BC051076	-6.30

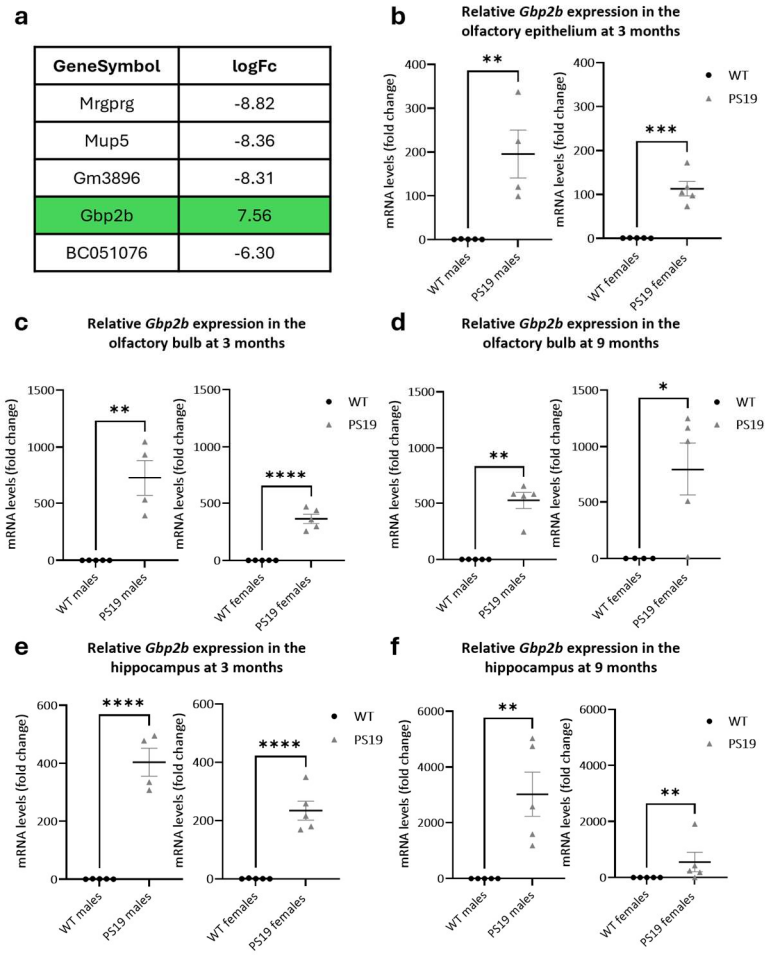

Fig. III.8 *Gbp2b* expression in the OE, OB, and hippocampus of PS19 and WT mice. mRNA levels of *Gbp2b* expression were measured by RT-qPCR in OE, OB, and hippocampal extracts from WT and PS19 mice at 3 months (for OE) and 9 months (for OB and hippocampus)(a-f). Top 5 DEGs in the OE of PS19 mice at 3 months with logFC values (a). *Gbp2b* expression is significantly increased in the OE of 3-month-old PS19 mice (b). **P < 0.01, ****P < 0.0001 (Unpaired t-tests, n=4-5 mice/group). *Gbp2b* expression is significantly increased in the OB of 3-month-old PS19 mice (c). *P < 0.05, **P < 0.01 (Unpaired t-tests, n=4-5 mice/group). *Gbp2b* expression is significantly increased in the OB of 3-month-old PS19 mice (d). *P < 0.05, **P < 0.01 (Unpaired t-tests, n=4-5 mice/group). *Gbp2b* expression is significantly increased in the hippocampus of 3-month-old PS19 mice (e). ****P < 0.0001 (Unpaired t-tests n=4-5 mice/group). *Gbp2b* expression is significantly increased in the hippocampus of 9-month-old PS19 mice (f). **P < 0.01 (Unpaired t-tests, n=4-5 mice/group).

To further validate these transcript-level findings at the protein level, we employed a data-independent acquisition (DIA) proteomic approach, which, unlike data-dependent acquisition (DDA), systematically fragments all ions, resulting in higher sensitivity for low-abundance peptides, improved specificity, and enhanced reproducibility in complex samples [165].

Using DIA, we detected the mouse Gbp2b protein in all OE samples from PS19 mice, while it was absent in all OE samples from WT mice (Fig. III.9a). Similarly, Gbp2b was detected in 9 out of 10 OB samples from PS19 mice and in none of the OB samples from WT mice (Fig. III.9b). In the hippocampus, Gbp2b was only detected in 3 samples out of 10 from PS19 mice and absent in all WT mice samples (*data not shown*). These findings support the exclusive expression of Gbp2b under PS19 condition and confirm that its upregulation is not limited to the transcriptomic level but is also reflected at the proteomic level.

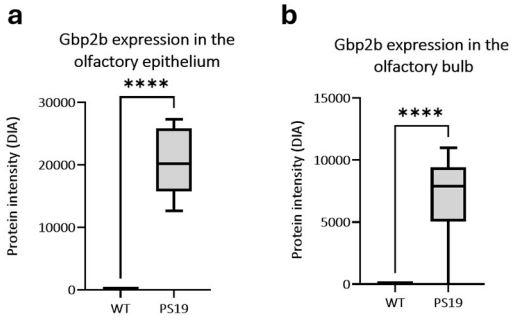

Fig. III.9 *G*bp2b expression in the OE, and OB of PS19 and WT mice. Box plot showing Gbp2b protein intensity (log_2-transformed DIA signal) in the OE (a) and OB (b) of PS19 and WT mice. Protein levels were quantified using data-independent acquisition (DIA) mass spectrometry. Gbp2b was detected in all PS19 OE samples but was absent from WT samples (a). Gbp2b was detected in 9 out of 10 PS19 OB samples but was absent from WT samples (b). Boxes represent the interquartile range (IQR), horizontal lines indicate medians, and whiskers extend to 1.5× IQR. Statistical significance was assessed using an unpaired t-test (****P < 0.0001)(n=10 mice/group).

Naturally, this targeted study evaluated only a limited subset of candidates. Additional potential biomarkers from the panel (Table 2) may warrant validation in future research.

In conclusion, our integrated transcriptomic profiling reveals that tau overexpression and aberrant phosphorylation in PS19 mice leads to early, region-specific molecular changes—particularly in the OE. These changes begin with olfactory dysfunction, inflammation, and cellular stress at 3 months, and progress to broader disruptions in neuronal signaling and metabolism by 9 months. We identified several potential biomarkers, with *Gbp2b* standing out due to its consistent upregulation, ease of detection, and established relevance in inflammation and neurodegeneration. Importantly, *Gbp2b* expression was validated in both sexes and across multiple time points and brain regions. These findings underscore the diagnostic potential of OE-derived biomarkers and highlight nasal brushing as a promising and viable method for early detection. Ultimately, this approach may accelerate the development of predictive diagnostics and targeted interventions for tau-related NDs.

General Discussion & Perspectives

GENERAL DISCUSSION

I. The Olfactory Epithelium as a Key Contributor to Tauopathy Progression

The OE forms a direct appendix of the CNS. In fact, OSNs are the only neurons connected to the CNS being in direct contact with the external environment [18], lacking the protection of the BBB [16]. These unique anatomical characteristics make the OE highly vulnerable to harming environmental conditions and a possible starting point for the spread of pathologies through its connections to various regions of the olfactory and central nervous systems [2, 18].

In the context of tauopathies, the presence of pTau immunoreactivity in the OE of AD patients has been reported [57, 58, 18, 35]. NFTs are also present in the OB of AD patient early in AD progression [166, 167] and are correlated to bulb size reduction [168]. Tau pathology could thus appear early in the sensory part of the olfactory system (OE), due to neurotoxic compounds present in the environment or to the gradual loss of its ability to regenerate. Considering that tau spreading along neuronal connections is now well documented [169], one can imagine that pathological forms cross the cribriform plate to penetrate the CNS and spread through the olfactory tract to regions known to be affected in AD (EC, amygdala, hippocampus).

The Olfactory Epithelium as an Early Site of Tau Pathology and Propagation

Here, we provide the first evidence of the staging of tau pathology across the olfactory system. In PS19 mice, pTau accumulation was detected in OSNs of the OE as early as 1.5 months. The signal increased up to 6 months, and decreased at 9 months, which could be explained by the reduction in the number of OSNs with aging [2]. Neurogenesis occurs in the OE throughout life but aging and exposure to pathogens contribute to a reduction in this regenerative capacity [3, 4]. pTau immunoreactivity was also detected in ABs suggesting that the signal appears early in OSNs and spreads following their axonal projections to accumulate within ABs. These nerve fibers then reach the OB following efferent projections and constitute its most external layer, the ONL. Immunohistochemical analyses showed strong pTau signal in the ONL but also in the MCL. Mitral cells in the MCL are neurons that receive afferences from OSNs within the olfactory glomeruli and project to various regions in the brain, notably the PC or EC. These two brain areas are part of the olfactory cortex that allows the integration of olfactory information [16, 19]. pTau was also detected in these two cortical regions: as early as 3 months in the PC – which receives direct inputs from the OB – and 1.5 months in the lateral EC – receiving direct inputs from the PC [170]. Finally, pTau pathology was found in hippocampal subregions (CA3 and DG), which receive direct projections from EC neurons in layers II and III [32]. Together, these findings demonstrate a temporally ordered progression of tau pathology from the OE through the OB and olfactory cortex to the hippocampus, consistent with known neuroanatomical connections and previous CNS observations in PS19 mice [169].

Prion-like Spreading of Tauopathy within the Olfactory System

This pattern supports the hypothesis of prion-like propagation of tau. Misfolded tau can seed aggregation in neighboring neurons and spread trans-synaptically, a mechanism demonstrated by transmission of pathology following injection of PS19 brain extracts into transgenic tau mice [125]. Such neuron-to-neuron progression is shared across several proteinopathies [126]. Our results suggest that in PS19 mice, tau pathology originates in OSNs and propagates along olfactory pathways without forming mature NFTs in early regions, as confirmed by the absence of Gallyas-positive inclusions in the OE and OB. NFTs emerged only later (9 months) and selectively in PC and EC, indicating that NFTs are a late manifestation of tau pathology that do not appear in all brain regions where pathological tau (e.g. AT8-positive) is available. This crucial point should be further investigated to define what pathological forms of tau are responsible for its transsynaptic spreading. Additionally, it is imperative to elucidate how pTau contributes to the formation of typical paired helicoidal filaments (PHFs) in more specific subregions.

Given the anatomical proximity between the OB and limbic regions, and considering the olfactory deficits in AD patients, it has previously been suggested that tau pathology spreads from olfactory circuits to limbic structures including the amygdala, as well as the piriform and entorhinal cortices [107]. This route of propagation may exacerbate an already existing tauopathy within the CNS, making the OE a promising target region for early treatment intervention.

Tau Pathology in Human Olfactory System

The expression pattern of tau pathology observed in the olfactory system of PS19 mice might resemble that found in AD patients where tau-immunoreactive fibers have been reported in the ONL [52], and tau-containing neurites were present in the OE [57, 52]. The anterior olfactory nucleus (AON) is also one of the early-affected region by neurofibrillary tau pathology together with the central olfactory areas, as reflected by the Braak staging [52]. These regions receive direct input from the OB such as: the PC, olfactory tubercle, AON, amygdala, and EC [171].

We showed here pTau staining (PHF-1) in the ONL – formed by the axons of OSNs –from Braak stage I/II patients, as well as in OSNs and ABs within the OE. PHF-1 has been reported to detect phosphorylated tau in axons and the neuropil, preceding pretangle formation, while AT8 stains pretangles and is considered an early marker of tau pathology [115]. In our observations, PHF-1 staining was detected in the OE and in the ONL of the OB but also evidenced neuropil threads in the inner layers of the OB, whereas AT8 staining was restricted to these inner layers of the bulbs. This suggests that hyperphosphorylated tau may be present in the OE at early Braak stages without converting over time to aggregate, possibly due regenerative capacity of the OE that continuously produces newborn OSNs. Still, these pTau forms detected by PHF-1 in the OSNs could be heading for the ONL, which is formed by the axons of the OSNs. Consistent with our data, hyperphosphorylated tau then accumulates within the inner layers of the OB to form pretangles evidenced by both AT8 and PHF-1 staining. These results

and the underlying scenario of pTau progression are consistent with other studies showing phosphorylated tau evidenced by AT8 or PHF-1 staining in the OB of AD patients [172, 58]. This study did not include a characterization of human tau pathology in the central olfactory regions, as we prioritized more accessible areas such as the OE. However, expanding this analysis may provide valuable insights for future research.

Our results strongly suggest that tau pathology may develop early in these olfactory regions. These findings extend beyond the transgenic mouse model, indicating the relevance of our observations to human pathology. While there is an ongoing debate regarding whether tau pathology in the olfactory system arises earlier, simultaneously, or subsequently than in the EC, our results suggest that the olfactory system may be a site of early tau pathology development in NDs [52, 173]. Importantly, the direction of the progression of tau pathology in the olfactory system is matter of different hypothesis. On one hand, different studies postulate that the olfactory system serves as an entry point for pathogens or as an access point for environmental aggressions, which can trigger pathological changes that would then spread throughout the brain via anterograde olfactory pathways [3, 9, 174, 18]. Our data illustrate this hypothesis but are not at odds with the one supporting tau pathology appears early in the brain, particularly in the EC, and then spreads to the olfactory system using the retrograde olfactory circuit [175].

Given the presence of tau pathology in olfactory regions early in the disease process, it is not surprising that olfactory dysfunction often emerges as one of the earliest clinical signs of dementia [16].

Olfactory Dysfunction: A Prodromal Sign of Dementia

Olfactory deficits have been observed and associated with NDs, including AD, since 1974 [175, 55]. Olfactory dysfunction is present not only in the early stages of AD but also in MCI patients [18] and is now recognized as a prodromal sign of dementia [16] and as a tool to predict MCI-to-AD conversion [54].

Since then, behavioral studies aimed at evaluating olfactory function have been conducted in mouse models of these pathologies. In our study, the results of the food-seeking and olfactory discrimination tests did not show any significant difference between the PS19 and age-matched control mice. PS19 mice did not take longer to find the buried food and reacted in the same way as the control mice did when presented with two different odors, contrary to what had been previously demonstrated [46]. These results could be explained by the fact that the term "olfactory deficits/dysfunction/impairment" encompasses several functions, such as a decline in odor threshold, identification, discrimination, and memory that cannot be measured by the same tests [16].

In addition, differentiating olfactory deficits caused by physiological aging from those associated with NDs presents a challenge [3, 2]. During normal aging, the OE, which contains OSNs, is gradually replaced by respiratory

epithelium. This is accompanied by ossification and eventual closure of the cribriform plate foramina. Together, these changes can disrupt the transduction of olfactory information from the OE to the OB and the olfactory cortex, referred to as conductive dysfunction [16, 36, 37, 18]. This led to an increase in odor threshold, which relies solely on the integrity of the OE and OSN transduction [16, 39]. In contrast, olfactory memory relies on hippocampal integrity, whereas odor identification/discrimination relies on the integrity of central olfactory structures [2, 52]. In AD patients, it has been shown that odor identification is particularly impaired [16, 54, 18, 55]. This impairment reflects a cognitive deficit rather than a direct impairment of olfactory perception [49, 52, 54], since higher cognitive skills, such as verbal and semantic skills, are required for odor identification [2].

Our findings show that following intranasal $ZnSO_4$ irrigation, which disrupts the peripheral olfactory system [176], mice are no longer able to find buried food, suggesting an increased odor threshold. Additionally, they are no longer able to differentiate between odors, indicating that their discrimination abilities could be impaired. The effectiveness of the tests conducted cannot, therefore, be questioned. These tests primarily evaluate peripheral damage at the level of the OE and conductive dysfunction (odor threshold). It is thus possible that PS19 mice do not present strong peripheral impairment despite the presence of tau pathology in the OE. They might retain their ability to smell odors because of the lack of fibrillar tau (NFTs) in this region. However, the presence of lesions in the primary olfactory cortex (OB, PC, EC) might compromise olfactory discrimination and identification [16], two functions that are truly challenging to evaluate in

mice. Consistent with our hypothesis, in Tg2576 mice – an amyloid mouse model – odor memory is impaired while odor perception is spared, suggesting that the underlying mechanisms might be different [16].

In parallel, it is known that, compared with mice, humans have a poorly developed sense of smell [177]. In rodents, the OE covers 50% of the nasal cavities, while it covers only 3 to 5% of these cavities in humans. Consequently, olfactory neuronal loss has a greater impact on odor perception in humans than in rodents [12]. Mice rely heavily on their olfactory function for survival, and given their significant olfactory capabilities, we hypothesize that the pTau pathological pattern detected in the olfactory regions might not be sufficient to induce olfactory dysfunction detectable by the two tests conducted.

While olfactory dysfunction is a well-documented early symptom of dementia, its underlying causes remain incompletely understood [44, 47]. Emerging evidence suggests that tau pathology may not act alone but rather trigger a cascade of neuroinflammatory responses that contribute to early olfactory system impairment and broader neurodegeneration [178, 179]. The next section explores the role of tau-driven neuroinflammation in the context of disease progression.

Tau-driven Neuroinflammation

Neuroinflammation in AD is widely recognized as a crucial driver of tau pathology and cognitive deterioration [180]. Chronic CNS inflammation—primarily driven by sustained microglial activation and the release of

cytotoxic mediators—perpetuates neuronal dysfunction and degeneration [181, 178].

Microglia, the brain's resident immune cells, maintain surveillance in a ramified "resting" state, but shift to an activated phenotype upon encountering misfolded proteins (e.g., hyperphosphorylated tau). This activation triggers the NLRP3 inflammasome, IL 1β release, and elevated tau phosphorylation and aggregation in neurons [180, 182].

In our study of PS19 mice, *Gbp2b* expression was strongly induced at 3 months in the OE, OB, and hippocampus—regions where *Gbp2b* was hardly detectable in WT controls. As an interferon-γ-inducible guanylate-binding protein (GBP), *Gbp2b* is known to activate inflammasomes and amplify inflammatory cell signaling [183, 184]

Early *Gbp2b* upregulation in olfactory–hippocampal regions may serve as an inflammatory seed in NDs. Supporting this, GBP2 homologues in microglia are implicated in early immune responses and local neuroinflammatory regulation [164]. Notably, inflammasome-driven microglial activation has been causally linked to tau hyperphosphorylation and neurotoxicity in tauopathy models where blocking NLRP3 attenuates tau tangle formation and cognitive deficits [182, 185].

Our findings suggest a potential mechanistic link between tau pathology, microglial activation, and *Gbp2b*-mediated neuroinflammation. Hyperphosphorylated tau accumulation in the OE, OB, and hippocampus may drive the transition of microglia from a resting to an activated state,

resulting in the production of interferon-γ/-β. These interferons could induce early overexpression of *Gbp2b* across these brain regions, consistent with a role for this protein in initiating inflammatory signaling [184].

Elevated *Gbp2b* may activate the NLRP3 inflammasome, promoting the release of pro-inflammatory cytokines interleukin-1β and interleukin-18 [186]. Both cytokines are known to exacerbate tau hyperphosphorylation and facilitate its propagation [180], outlining a self-amplifying cycle in which tau pathology and neuroinflammation reinforce each other. This cycle may ultimately contribute to chronic inflammation and progressive neurodegeneration.

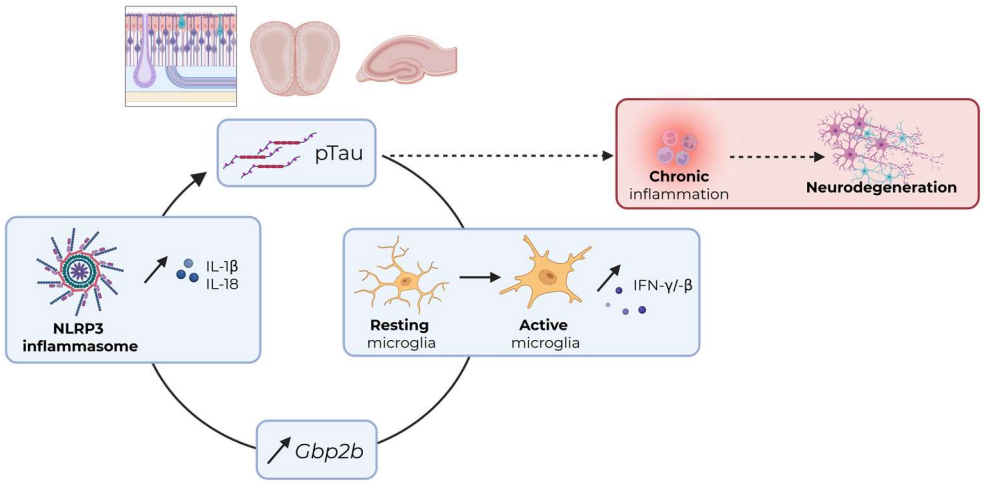

***Gbp2b* and neuroinflammation hypothesis.** Hyperphosphorylated tau present in the OE, OB, and hippocampus may trigger the transition of microglia from a resting to an activated state, characterized by the production of interferon-γ and interferon-β. These cytokines could in turn induce the early overexpression of *Gbp2b* in all three regions. Elevated Gbp2b levels may activate the NLRP3 inflammasome, leading to the release of interleukin-1β and interleukin-18, which can further promote tau hyperphosphorylation and propagation. This self-amplifying cycle of neuroinflammation may ultimately drive chronic inflammation and neurodegeneration. Created with *BioRender.com*.

These results align with previous studies implicating interferon signaling and inflammasome activation in early-stage tauopathies and highlight *Gbp2b* as a potential mediator linking innate immune responses to the progression of tau pathology.

II. The Olfactory Epithelium as a Therapeutic Tool

Targeting the OE Modulates Tau Pathology in the CNS

To establish a causal link demonstrating that the OE serves as a gateway for pathology and worsens pre-existing conditions in the CNS of PS19 mice, we directly targeted the OE and assessed its impact on the tau pathology progression in the CNS. Intranasal $ZnSO_4$ irrigation was used to specifically strip the OSNs in the OE and ONL in the OB [176, 187], providing a model to study the downstream effects on the CNS. Repeated intranasal irrigation with $ZnSO_4$ in PS19 mice resulted in near-complete stripping of the OE and ONL. Additionally, NFT-like tau accumulations were absent in the PC and only a few residual lesions were present in the EC and amygdala, compared to vehicle-treated controls. This suggests that modulating tau pathology in the olfactory system delays its progression in interconnected CNS regions. Given that all these regions receive input from the OB, our findings reinforce the hypothesis that the olfactory pathway – particularly the OE – serves as an early site for pathology development and as a potential entry point for the spread of pathology to the PC and EC. Our "prion-like" propagation hypothesis was further strengthened by the results obtained following intranasal administration of AAVs encoding the P301S-mutated human tau protein, which lead to increased tau pathology in the PC of PS19 mice.

These findings highlight the potential of intranasal drug delivery to target NDs via the olfactory pathway, offering a way to reduce the side effects associated with systemic administration [52]. Research in mouse models has demonstrated that nasal tau immunotherapy can clear intracellular tau

pathology and improve cognitive function in aged tauopathy mice [135]. In humans, the intranasal route has also been explored in multiple studies as a promising therapeutic strategy for various NDs [132, 133, 137].

In this study, we focused on the histopathological characterization following intranasal treatment with either $ZnSO_4$ or hTau-P301S AAVs. However, it would be valuable to repeat the experiments using AAVs to assess their impact on other brain regions and to strengthen the overall characterization. Evaluating the long-term effects of these treatments through longitudinal studies would also provide important insights. Given that zinc sulfate appears to delay pathology, it is plausible that this treatment could prolong survival and preserve cognitive function in PS19 mice. Notably, these mice typically exhibit cognitive impairments at a relatively late stage (around 6 months of age)[188]. Therefore, it would be of interest to determine whether, unlike zinc sulfate, intranasal administration of AAVs accelerates cognitive decline and reduces survival. Additionally, investigating how peripheral disease exacerbation affects olfactory function could yield further understanding of early pathological changes.

Targeting Tau-driven Neuroinflammation via Gbp2b in the Olfactory Epithelium

Therapeutic strategies that modulate neuroinflammation rather than targeting tau directly are rapidly gaining ground. While over 50 inflammation-related agents have entered clinical trials for AD, about 22 of them focus on modulating microglial functions, inflammatory signaling pathways, or cytokine release to slow neurodegeneration [180].

Based on our findings, we propose *Gbp2b* as a novel therapeutic target: its early, exclusive, and high expression in the OE, OB, and hippocampus of PS19 mice—even before any detectable tau accumulation—suggests a potential role as an inflammatory initiator. As mentioned before, Gbp2b, an IFN-γ–inducible guanylate-binding protein, can activate inflammasomes and elevate inflammatory signaling in immune cells [183, 184].

Crucially, silencing *GBP2* (a close homolog active in microglia) via shRNA shifts cells to an anti-inflammatory phenotype, reduces pro-inflammatory cytokines, suppresses the NF-κB pathway, and diminishes neuronal damage in vitro [164].

Therefore, targeting *Gbp2b* expression in the OE—via localized gene silencing or pharmacological blockade—and evaluating subsequent effects on microglial activation and behavioral or tauopathy endpoints, could provide a proof-of-concept for anti-*Gbp2b* therapy in tauopathies.

III. The Olfactory Epithelium as a Diagnosis Tool

Fifty million people worldwide currently suffer from NDs such as AD, and this number is expected to rise as life expectancy increases [28]. Despite extensive efforts to understand the underlying mechanisms and develop effective treatments, reliable early biomarkers for detecting these diseases before irreversible damage occurs remain elusive. Therefore, one of the goal of this study was to identify molecular signatures and biomarkers associated with tau pathology accumulation in the olfactory system, a uniquely accessible region with strong potential for monitoring CNS diseases [55].

The cerebral transcriptome of PS19 mice was previously established in the hippocampus [6] and cortex [15, 23] but data were still missing in regions of the olfactory system. Here, we used an integrated transcriptomic approach to map tau-driven molecular alterations in the OE, OB, and hippocampus at 3, 6, and 9 months of age.

Region-Specific Molecular Changes Mirror Tau Pathology Progression in a Spatiotemporal Transcriptomic Analysis

Our results highlight a region-specific progression of tau pathology in PS19 mice, with distinct temporal and molecular signatures in the OE, OB, and hippocampus. In the OE, tau pathology is detectable as early as 3 months, persists at 6 months, and declines by 9 months, likely due to OSNs loss [11]. This trajectory corresponds with early transcriptomic changes involving stress responses, immune activation, and repression of olfactory transduction that persists over time. By 9 months, chronic inflammation,

disrupted cilium organization, and metabolic disturbances dominate, suggesting that the OE's regenerative capacity is overwhelmed by ongoing pathology [7]. Notably, chronic inflammation in this region may also arise as a downstream response to neuronal loss. These findings are consistent with transcriptomic profiles from human AD brains, which show downregulation of synaptic and neurotransmission-related genes alongside upregulation of immune responses and cell death pathways [24, 38].

In the OB, early changes affect sensory processing and neurogenesis, consistent with findings from transgenic AD models [39]. Although no major pathway enrichment is observed at 6 months, the 9-month time point reveals mitochondrial dysfunction, ER stress, and emerging sensory deficits. Pathologically, the OB remains relatively stable with a stall in pathological progression where tau remains in a hyperphosphorylated state without aggregating further. This limited progression may explain the delayed but modest transcriptional response, despite early evidence of synaptic dysfunction. It is even more striking knowing that soluble forms of pathological tau rather than aggregated tau are suggested to induce synaptic dysfunction [8, 40].

In contrast, the hippocampus shows a more classic, gradual accumulation of tau pathology from 3 to 9 months, reflected in a steady increase in DEGs. Early disruptions in synaptic plasticity and neuronal function evolve into widespread neurodegeneration and impaired neurotransmission by late stages, aligning with established role of the hippocampus in cognitive decline and with previous observations in PS19 mice [6].

Early and Region-Specific Gene Expression Changes in PS19 Mice Highlight Potential Biomarkers for Tauopathies

Overlap analysis of DEGs across regions and time points revealed both shared and region-specific responses. The earliest and most distinct molecular changes were observed in the OE—the first region to show tau pathology. We focused on this region at 3 months of age and identified several DEGs, including *Gbp2b, Prnp, Wnt9a, Mup5, Chil4*, and *Obp1a* (Table 1). Some, like *Wnt9a* and *Prnp*, have been previously associated with AD or reported in other tauopathy models [1, 6]. *Wnt9a*, part of the Wnt signaling pathway critical for synaptic plasticity [25], was upregulated in the hippocampus and OB but downregulated in the OE. Similar enrichment of synaptic, mitochondrial, and calcium-related genes in the hippocampus parallels prior findings in the hippocampus and cortex of PS19 mice [1]. In the cerebral cortex of PS19 mice, overexpression of aggregation-prone tau alone has been reported to trigger early neuroinflammatory responses—including upregulation of immune-related genes like *Aqp1, Lbp, Prnp*, and *Hsb1*—as early as 3 months [15]. We observed similar changes, alongside upregulation of apoptotic and mitochondrial genes, reinforcing the idea that tau pathology initiates broad, system-wide immune and metabolic responses.

Among these DEGs in the OE, *Gbp2b* emerged as a particularly compelling biomarker due to its consistent transcript-protein match, temporal persistence, and cross-region upregulation. This is supported by earlier reports showing elevated GBP2 – belonging to the GBP family – expression

in the cortex, hippocampus, and OB of 5xFAD mice and its involvement in microglial activation and neuronal apoptosis after brain injury [21, 23]. As an interferon-induced gene, GBP2 is known to be activated early in the inflammatory response and has been proposed as a biomarker and therapeutic target in AD models [43]. The early vulnerability of olfactory regions to tau pathology may explain the strong and consistent upregulation of *Gbp2b* observed in these areas. This candidate is particularly striking given that mouse *Gbp2b* and human GBP1/GBP2 proteins are true orthologs, sharing a high degree of sequence similarity, approximately 70%, which underscores their likely functional conservation.

While *Gbp2b* was found to be significantly upregulated, several other genes displayed the opposite expression pattern. We found that some of the genes downregulated in the OE at 3 months (e.g., *Mup5, Obp1a, 5430402E10Rik*, and *Gm14744*) are linked to odorant binding and chemical communication — processes critical for olfactory function. We also observed reduced expression of Chil4, which is involved in OE regeneration via inflammatory pathways [37]. Impairments in these biological processes may contribute to the progressive olfactory deficits often observed in AD patients [2, 3, 45] and supports a link between tau pathology and olfactory dysfunction. Internal validation of these candidates confirmed a decrease expression in the OE at 3 months in both PS19 males and females.

Nasal Brushing as a Minimally Invasive Strategy for Early Detection of Tauopathy Biomarkers

To date, biomarkers are collected through invasive techniques, especially CSF obtained through lumbar puncture [26]. Blood-based biomarkers were also proposed for diagnosing AD, but they are not yet accurate enough to replace CSF and PET testing [5]. In recent years, nasal brushing has garnered significant interest as a minimally invasive and straightforward technique for assessing OE-derived biomarkers in NDs [12, 17, 30]. In the search for reliable biomarkers, those that are upregulated under pathological conditions — such as *Gbp2b* — are generally preferred. Indeed, elevated expression levels are easier to detect and interpret, offering greater analytical sensitivity [35]. In contrast, biomarkers with decreased expression can be more challenging to measure accurately, increasing the risk of false negatives due to low signal levels [14, 36].

A promising avenue is to validate the biomarkers identified in our tauopathy mouse model by determining whether these markers can be detected in human nasal brushing samples. This approach is particularly valuable for assessing their ability to reliably distinguish between control subjects and early-stage AD patients, despite the greater heterogeneity typically observed in human samples.

Given that the OE is one of the first regions affected by AD pathology and maintains a direct connection to the CNS [32, 34], OE-derived biomarkers may offer earlier and more reliable diagnosis of NDs.

Conclusion

GENERAL CONCLUSION

In this thesis, we presented a comprehensive temporal characterization of tau pathology progression within the olfactory system of PS19 mice, a well-established model of tauopathy. We highlighted that pTau appears early in the OE of PS19 mice and subsequently spreads to the CNS following neuroanatomical pathways, like the olfactory and perforant pathways. Despite the presence of tau lesions in regions of the olfactory system, the olfactory threshold of PS19 mice was not significantly impaired. We additionally confirmed the appearance of pTau signal in the olfactory regions of Braak stage I/II patients.

We also applied intranasal treatments to modulate tau pathology in the CNS of PS19 mice. We observed that, by specifically targeting OSNs in the OE, we were able to either mitigate or increase tau pathology in CNS regions that share direct connections with the OB.

Our integrated transcriptomic profiling reveals that tau overexpression and aberrant phosphorylation in PS19 mice leads to early, region-specific molecular changes—particularly in the OE. These changes begin with olfactory dysfunction, inflammation, and cellular stress at 3 months, and progress to broader disruptions in neuronal signaling and metabolism by 9 months. We identified several potential biomarkers, with *Gbp2b* standing out due to its consistent upregulation, ease of detection, and established relevance in neuroinflammation and neurodegeneration. Importantly, *Gbp2b* expression was validated in both sexes and across multiple time points and brain regions.

Conclusion

Overall, our findings support the notion that tau pathology spreads in accordance with anatomical neuronal connectivity, underscore the therapeutic relevance of the OE in tauopathies, and suggest its likely contribution in driving the progression of pathology within the CNS. Additionally, we emphasize the diagnostic potential of OE-derived biomarkers and propose nasal brushing as a promising, non-invasive method for early detection. Ultimately, this approach could accelerate the development of predictive diagnostic tools and targeted therapies for tau-related NDs, including AD.

Methods

METHODS

Animals

PS19 mice were obtained from the Jackson Laboratory (B6; C3-Tg(Prnp-MAPT*P301S)PS19Vle/J; Strain #008169) and maintained on a C57BL/6 genetic background. Wild-type (WT) and heterozygous PS19 mice were crossed to obtain WT and heterozygous PS19 mice at 1.5, 3, 6 and 9 months of age. The genotype was determined by PCR analysis of ear/tail DNA. The animals were housed in ventilated cages, maintained on a 12-hour light/dark cycle, and provided *ad libitum* access to food and water. All the mice were individually identified by ear tagging and their general health was closely monitored. All experiments involving mice were conducted with prior approval from the ethical committee at UCLouvain (2021/UCL/MD/018).

Tissue Harvesting

All the mice were sacrificed by cervical dislocation. The cranium was opened, and the brain was cut sagittally in half. Next, the two OBs and the two hippocampi were collected. The mouse snout was then recovered and cut along the midsagittal plane between the two nasal cavities. The OE was recovered from these cavities, distinguishable by its characteristic yellow color. The harvested tissues were snap-frozen by immersion in isopentane maintained at freezing temperature and then stored at –80°C until use.

Sample Preparation for Immunostaining

Decalcification

For immunostaining experiments, decalcification was needed to preserve the OE structure because of its localization within the nasal cavity. The skin, eyes, and lower jaw were removed from the mouse head. The head was directly rinsed in phosphate-buffered saline (PBS) and subsequently fixed with modified Davidson's fixative (mDF) (37% formalin, ethanol, glacial acetic acid, water) for four days under agitation at room temperature (RT). The heads were rinsed for 24 hours in PBS and transferred to OsteoRAL R (RAL Diagnostics,

#320715-2500), a commercial decalcifier, for five days under agitation at RT. After decalcification, the mouse heads were embedded in paraffin.

Paraffin sections

Paraffin-embedded sections were obtained via a microtome. Coronal sections of 5 µm and 10 µm thickness were placed on Superfrost slides for IF and IHC, respectively. The coronal brain sections were collected according to standard stereotaxic coordinates relative to Bregma, as defined in the *Mouse Brain Atlas* by Paxinos and Franklin. Sections ranging from approximately Bregma -1.82 to -2.18mm were used to analyze the hippocampal formation, Bregma -1.94mm to analyze the PC and Bregma 3.08mm for the EC.

Immunostaining

For immunohistochemistry, paraffin-embedded sections of 10 µm were immersed in different solutions as follows: 2x5 minutes in toluene, 2x2 minutes in absolute isopropanol, and 30 minutes in 0,3% H_2O_2 in methanol. The slides were finally placed in distilled water. Then, 1X Tris-buffered saline (TBS) was placed on each paraffin section for 10 minutes. This washing step was repeated two times.

Then, the sections were blocked with 10% normal goat serum (NGS) diluted in TBS for one hour at room temperature. Primary antibodies of interest were prepared in 1% NGS (supplementary table M1), placed on each section, and left overnight at RT. The negative control was incubated with 1% NGS only.

The next day, the sections were rinsed three times for 10 minutes with TBS 1X. The secondary antibodies were diluted with TBS 1X and put on the corresponding sections for 30 minutes at room temperature. This step was followed by 3 TBS rinses. Stabilized Elite ABC reagent (Vector Laboratories, #PK-7100) was added to each section for 30 minutes. After another washing step, ImmPACT® DAB EqV Substrate (Vector Laboratories, #VEC.SK-4103-100) was prepared. Equivalent amounts of reagent 1 and reagent 2 were mixed and incubated on each section. The reaction was stopped after three minutes by transferring the slides into distilled water. The sections were dehydrated by immersion in different

solutions as follows: 2 minutes in 70% isopropanol, 2 minutes in 90% isopropanol, 2x2 minutes in absolute isopropanol and 3x2 minutes in toluene. The sections were mounted with DPX mounting medium (Sigma-Aldrich, #1.00579.0500) and left to dry overnight at room temperature. The images were captured via an Axioskop 40 microscope (Zeiss).

Paraffin-embedded sections of 10 µm were stained with the Gallyas silver-staining method to identify NFTs (Alzheimer and Other Tauopathies Research Group, ULB Neuroscience, Karelle Leroy)[189]. The images were captured via an Axioskop 40 microscope (Zeiss).

For immunofluorescence, 5 µm paraffin sections were dewaxed by immersion in different solutions as described below: 3x5 minutes in toluene, 3 minutes in absolute isopropanol, 3 minutes in 100% ethanol, 3 minutes in 90% ethanol, 3 minutes in 70% ethanol, 2 minutes in distilled water and a final rinse in 1X PBS. Heat-induced antigen retrieval was performed using 10 mM sodium citrate buffer at pH 6.0. The sections were placed in a tank filled with antigen retrieval solution and heated for 3x5 minutes in a microwave, maintaining the temperature around 96°C. The solution was left to cool for 20 minutes, followed by rinsing with PBS.

For the permeabilization step, the sections were immersed in 0.3% Triton X-100 in PBS for 30 minutes at room temperature. The blocking solution was prepared with PBS-Triton, normal goat serum (NGS) and bovine serum albumin (BSA) to reach 0.3% PBS-Triton, 3% NGS and 5% BSA. This solution was added to each section for one hour at room temperature. The primary antibodies were prepared in blocking solution (Antibodies table M1), added to the corresponding sections, and left overnight at 4°C.

The next day, 3x5 minutes rinses with PBS-Triton 0.1% were performed, followed by one-hour incubation at room temperature with the secondary antibodies prepared in in 0.1% Triton X-100 in PBS (Antibodies table M1). The sections were rinsed twice in 0.1% Triton X-100 in PBS for 5 minutes, followed by a final rinse in 1X PBS. The sections were mounted with Mowiol (Merck, #475904-100GM-M) and left to dry overnight. The images were acquired via an EVOS™ FL Auto fluorescence or confocal microscope.

All immunostainings were performed in PS19 males, as sexual dimorphism has been described in this model, with males exhibiting an earlier onset of the pathology [155].

Table M1. Antibodies table.

Primary antibodies			
Antibody	**Species**	**Dilution**	**Company (Catalog#)**
AT8 (Phospho-Tau (Ser202, Thr205))	Monoclonal IgG1 Mouse	1/250	ThermoFisher (#MN1020)
Tau Total (D1M9X)	Monoclonal Rabbit	1/1000	Cell Signaling Technology (#46687)
PHF-1 conditioned medium (Phospho-Tau (Ser396, Ser404))	Monoclonal IgG1 Mouse	1/100-200	Kindly provided by Peter Davies' Team
Tau-13	Monoclonal IgG1 Mouse	1/1000	Biolegend (#835201)
OMP	Monoclonal Mouse	1/50	Santa cruz biotechnology (#sc-365818)
OMP	Polyclonal Goat	1/50	Novus biotechnology (#NB110-74751)
Secondary antibodies			
Anti-mouse biotin-labeled	IgG Goat	1/200	PerkinElmer, (#NEF823001)
Anti-Rabbit biotin-labeled	IgG Goat	1/100	Thermofisher (#65-6140)
Goat anti-Mouse IgG1 Cross Adsorbed Alexa Fluor™ 647	Goat	1/500	InVitrogen (#A21240)
Goat anti-Mouse IgG2a Cross Adsorbed Alexa Fluor™ 488	Goat	1/500	InVitrogen (#A21131)
Goat anti-Rabbit IgG (H+L) Highly Cross-Adsorbed Alexa Fluor™ 568	Goat	1/500	InVitrogen (#A11036)
Goat anti-Mouse IgG (H+L) Highly Cross-Adsorbed Alexa Fluor™ 488	Goat	1/500	InVitrogen (A11029)
Chicken anti-Goat IgG (H+L) Cross-adsorbed Alexa Fluor™ 488	Chicken	1/500	InVitrogen (#A21467)

Behavioral Tests

All behavioral tests were approved beforehand by the ethical committee (2021/UCL/MD/018) and conducted in collaboration with the behavioral analysis platform (BEAP, UCLouvain) following validated protocols. A dedicated cohort of mice (males and females) was used to perform olfactory function measurements at 3, 6 and 9 months. One week before the required time point, the mice were acclimatized on the behavioral analysis platform. Each mouse performed the olfactory discrimination test followed by the buried food test at each time point. Between the analyses, the mice were kept in quarantine and monitored closely. At 9 months, after the last test, the mice were sacrificed by cervical dislocation, and the tissues of interest were harvested.

Olfactory discrimination test

Test animals were placed in a clean plastic cage with a fresh layer of bedding covered by a removable Plexiglas lid with a 1.25 cm central hole for odorant exposure. After a five-minute adaptation period, a dry disposable applicator with a cotton tip was placed at a depth of 2.5 cm through the hole in the cage lid. After each minute, the applicator was removed and immediately replaced with a new applicator. After the sixth minute, an applicator with a cotton tip saturated with an odorant solution was positioned through the hole and again replaced every minute by a fresh applicator containing the same odor. After the 12th minute, an applicator with a tip saturated with a different odorant was inserted and replaced six times at one-minute intervals (see timeline below). The two odors used were geraniol and lime. The number of times the animal headed toward each applicator introduced into the cage was recorded via a camera throughout the experiment and was counted by an experimenter blinded to the experimental conditions.

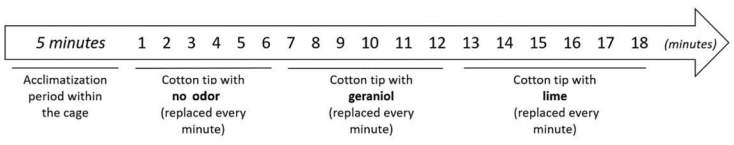

Food-seeking test

The mice were deprived of food for 16 hours with access to water *ad libitum*. The test mice were introduced into a clean cage covered with a 3 cm thick layer of bedding, under which a 1.0-gram food pellet had been buried. The time elapsed between the animal's introduction into the cage and the moment it retrieved the food with its front paws was measured in seconds, with a maximum of 300 seconds. From then on, a result equivalent to 300 seconds indicates that the mouse did not find the food.

Intranasal $ZnSO_4$ Irrigation

At 1.5 months, the mice received an intranasal application of either 0.17M (5%) zinc sulfate ($ZnSO_4$) or vehicle solution (PBS). Awake mice were held on their backs by one experimenter while a second experimenter administered 25 µL of either PBS or $ZnSO_4$ solution, dropwise to the right nostril with a few seconds between each drop. After an hour, to allow the mice to recover, the same procedure was repeated for the left nostril. The mice were then monitored for the next hour for any breathing discomfort. Since the OE regenerates over time [162], the mice were treated three times: at 1.5, 2.5 and 4 months. The mice were finally sacrificed at 6 months by cervical dislocation and samples were retrieved. For the evaluation of olfactory functions following $ZnSO_4$ treatment, the treatment was performed only once at 3 months, and olfactory tests were conducted 24 hours after the treatment.

NFT-like Tau Accumulations Quantification

For each region of interest, the numbers of NFT-like tau accumulations visualized with anti-pTau immunostaining were counted in an equivalent area corresponding to the sum of 5 delimited areas placed in that same region (Fig. M1). The number of NFT-like tau accumulations per mm^2 in the vehicle and $ZnSO_4$-treated conditions was compared and analyzed via statistical tests.

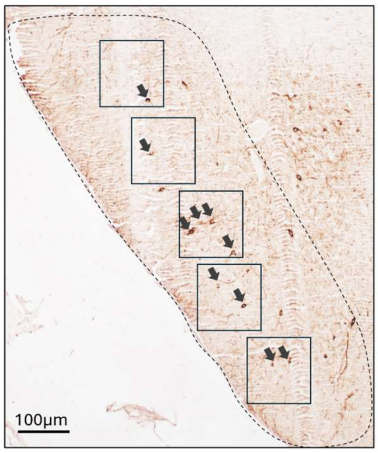

Fig. M1 DAB quantification of the NFT-like tau accumulations in the PC. For each region of interest, the numbers of NFT-like tau accumulations (indicated by black arrows) were counted in an equivalent area corresponding to the sum of 5 squares placed in that region. The number of NFT-like tau accumulations per mm^2 in the vehicle and $ZnSO_4$-treated conditions was compared and analyzed for each region using a Mann-Whitney test.

Intranasal hTau-P301S AAVs Irrigation

Adeno-associated viruses (AAVs) serotype 8 harboring the human tau sequence with the P301S mutation as well as an EGFP sequence (hereafter referred to as hTau-P301S AAVs) were designed and produced by VectorBuilder (Vector ID #VB240323-1105jux). At 1.5 months, the mice received an intranasal application of either hTau-P301S AAVs prepared in PBS or vehicle solution (PBS). The total dose for each AAV treatment was $1x10^{11}$ genome copies (GC), administered over two consecutive days. Awake mice were held on their backs by one experimenter while a second experimenter administered 20 µL of either PBS or AAV solution ($2.5x10^{10}$ GC/nostril/day), dropwise to the right nostril with a few seconds between each drop. After allowing the mice to recover for an hour, the same procedure was repeated for the left nostril. The mice were then monitored for the next hour for any breathing discomfort. Since the OE regenerates over time [162], the mice were treated twice: at 1.5 and 2.5 months. The mice were finally sacrificed at 4 months by cervical dislocation and samples were retrieved.

AT8 Signal Quantification

A consistent threshold was established to distinguish AT8-positive signal from background noise. This threshold was uniformly applied across a defined region equivalent in size to the sum of five delimited areas positioned within the same anatomical zone. The results

presented in Fig. II.5 represent the percentage of this total area that is positive for AT8 staining in the vehicle and AAVs-treated conditions. The results were compared and analyzed via statistical tests.

Postmortem Human Tissues

OBs were collected from 4 different Braak stage I or II patients and the OE was retrieved from 1 Braak stage II patient (Table M2). The autopsies were performed in UCLouvain (Belgium) in accordance with the applicable laws. Informed consent was obtained following local legislation. The recruitment protocols for the collection of human samples were approved by the ethical committees of UCLouvain (2020/02JUL/355). After collection, the tissues were immediately placed in 10% formalin for 48 hours. The tissues were subsequently embedded in paraffin and cut to obtain 5 and 10 µm paraffin sections. Neuropathological evaluation was conducted for each patient at KU Leuven (Leuven Brain Institute, Dietmar Thal), and the patients were classified based on the Braak stage (I or II in this study). Neuropathological analysis of these brains was approved by the UZ/KU-Leuven ethical committee (S-64363).

Table M2. Overview of the human cohort characteristics.

Case number	Age	Sex	Braak NFT stage	Aβ phase	Aβ MTL	CERAD
Patient 1 (UCL-14)	74	F	1	3	2	0
Patient 2 (UCL-17)	75	M	1	4	3	1
Patient 3 (UCL-15)	90	F	2	4	3	0
Patient 4 (UCL-16)	80	M	2	/	2	0

Protein Extraction

Proteins were isolated from snap-frozen samples of OE, OB, and hippocampus. Lysis buffer (LB) containing 50 mM Tris base (pH 7.5), 150 mM NaCl, 2 mM EDTA, 1% NP-40, % glycerol was prepared with an adjusted pH of 8.0. Before each experiment phosphatase inhibitor (Merck) and protease inhibitor cocktail (Roche) were added in the lysis buffer. A specific amount of ice-cold LB was added to each sample: 50 µL for the pooled right and left OE, 150 µL for a single OB and 200 µL for a single hippocampus.

Tissues were homogenized by sonication for 15 seconds, and then centrifuged at 16.100 g for 15 minutes at 4°C. The supernatants containing protein extracts were collected and stored at -80°C. Protein concentration was quantified using Pierce™ BCA Protein assay kit (Invitrogen, Thermo Fisher Scientific). Each sample was diluted 20 times for dosage.

Western Blotting

A total of 20 µg of protein extracts were mixed in a final volume of 20 µL with NuPAGE™ LDS Sample Buffer (Invitrogen, Thermo Fisher Scientific) and 50 mM dithiothreitol (DTT). The samples were vortexed, spun down and heated at 70°C for 10 minutes. Samples were loaded into polyacrylamide gel (NuPAGETM 4-12% Bis Tris Gel, InvitrogenTM #NP0336BOX) using SeeBlue™ Plus2 pre-stained (Thermo Fisher Scientific) as standard. Electrophoresis was run for 3 hours at 110 volts. This step was followed by protein transfer onto a nitrocellulose membrane (Thermo Fisher Scientific) for 2 hours at 30 volts. Membranes were blocked with 5% non-fat powdered milk in PBS-Tween 0,1% (PBS-T) for one hour with agitation, then rinsed and incubated overnight at 4°C with the primary antibodies (supplementary table M1) of interest prepared in PBS-T.

The next day, membranes were rinsed twice in PBS-T for 10 minutes and incubated with horseradish peroxidase (HRP)-conjugated species-specific secondary antibodies (Sigma-Aldrich) for one hour at room temperature under agitation. After a final rinse, the signal was detected by incubating with chemiluminescence ECL substrate (1:1 reagent A and B) for 2 minutes. Membranes were then exposed to chemiluminescence film and developed. ImageJ software was used to quantify protein band intensity, normalized to actin intensity.

Masson's Trichrome Stain

Paraffin sections (10µm) were processed through a series of solutions for deparaffinization and staining. Sections were immersed sequentially: three times for 5 minutes in toluene, followed by 3x5 minutes in absolute isopropanol, 95% isopropanol, and 70% isopropanol. After a 10-minute rinse in running water and a 5-minute rinse in distilled water, the sections were incubated in Mayer's hemalum solution for 10 minutes. This was followed by identical rinsing steps. The sections were stained in ponceau fuchsine solution for 3 minutes, rinsed

in distilled water for 1 minute, and incubated in 1% phosphomolybdic acid for 5 minutes before a quick rinse in distilled water. A final staining step with 1% aniline blue for 3 minutes was performed, followed by two distilled water rinses.

The sections were dehydrated through a graded series of isopropanol (70%, absolute x2), followed by 2x5 minutes in toluene and 5 minutes in xylene. The sections were mounted using DPX mounting medium (Sigma-Aldrich, #1.00579.0500) and left to dry overnight at room temperature. Images were captured using a Zeiss Axioskop 40 microscope.

RNA Extraction (for qRT-PCR and RNAsequencing)

RNA was extracted from the olfactory epithelium, olfactory bulb, and hippocampus. 500uL (for the olfactory epithelium) or 1mL (other tissues) of TriPure Isolation Reagent (#11667165001, Roche Diagnostics GmbH) were added on each sample. The tissue was dissociated by several passages through 21G needles placed on 1mL syringes first, and then through 26G needles. 200uL of chloroform was added in each sample, followed by 15 seconds agitation before 15 minutes incubation at room temperature. The samples were then centrifuged for 15 minutes at 12.000xg, at 4°c. The supernatant, containing the RNA, was recovered for each sample and mixed with either 170uL (OE) or 340uL of isopropanol, and vortexed for 5 seconds. For the end of the extraction, the ReliaPrep™ RNA Tissue Miniprep System (#Z6111, Promega) was used. Each lysate was transferred to a mini-column from the kit placed on a collection tube. The lysate-containing columns were centrifuged for 1 minute at 13.000xg, at 20°c. The collection tubes were emptied and 500uL of RNA wash solution were added on each column, then centrifuged for 30 seconds at 13.000xg. The collection tubes were emptied. The DNAse mix was prepared according to manufacturer's instructions, 30uL from this mix were added directly on the column's membrane and left for 15 minutes. 200uL of column wash solution were then added to each column and centrifuged for 30 seconds at 13.000xg. 500uL of RNA wash solution were added and the columns were centrifuged again for 30 seconds at 13.000xg. The collection tubes were discarded and replaced by new ones. 300uL of RNA wash solution were added into the columns that were centrifuged at high speed for 2 minutes. The columns were finally placed on elution tubes and 20uL (OE) or 30uL of RNAse free water were added on

the columns, centrifuged during 1 minute at 13.000xg. The nucleic acid centration (RNA) in ng/µL as well as the OD260/280 and OD260/230 were measured using the BioSpec-nano analyzer.

qRT-PCR

The reverse transcription was performed using the iScript cDNA synthesis Kit (#1708891, BIO-RAD). For each reaction, 1uL of iScript RT enzyme, 4uL of reaction mix, the equivalent volume for 1ug RNA and the remaining volume of water to reach a final volume of 20uL were mixed. The RT Script program was used, consisting of 5 minutes at 25°c, 30 minutes at 42°c and 5 minutes at 85°c. At the end of the program, 80uL of RNAse free water was added to each sample to have a final volume of 100uL of cDNA at 10ng/µL then used for quantitative PCR.

The primers used for qRT-PCR were at 7.5µM concentration (Table M3). The standards were prepared taking 30uL for each cDNA stock at 10ng/µL and pooling them together. A serial dilution starting from standard A and with a dilution factor of 4 was carried out until standards A, B, C, D, E and F were obtained. Finally, the cDNA stock at 10ng/µL was diluted three times to work with cDNA at 3,3g/µL to fill the qPCR plate.

Table M3. qRT-PCR Primer sequences.

Gene	Forward Primer	Reverse Primer
Gapdh	5'-ACCCAGAAGACTGTGGATGG-3'	5'-ACACATTGGGGGTAGGAAC-3'
Prnp	5’-CCCGCGTTGTCGGATCA-3’	5’-AGAATGCTTCAGCTCGGTTG-3’
Mup5	5’-TCCAGTGTTGAGTGGAGACT-3’	5’-CTTGTCACCCCATGCTGTAT-3’
5430402E10Rik	5’-GCGCCCTTTTCTTTCACAAC-3’	5’-TTGCTCAGGGTCTCTCCTTT-3’
Gm14744	5’-CGCCCTTTTCTTTCACAACG-3’	5’-TGCTCAGGGTCTCTCCTTTT-3’
Obp1a	5’-AGCTGGAAACATCAGAGAAGTC-3’	5’-GTCAAGACCACATGATCATAATTC-3
Chil4	5’-GCCAAGCTCATTCTTGTCAC-3’	5’-ACACAGGCAGGGGTCAATA-3’
Pon1	5’-GGACTGGTGTTGGCACTTTA-3’	5’-CTGGCGTTACTTCACGGAAA-3’
Tsc22d1	5’-CTCTGGTGCAAGTGTGGTAG-3’	5’-CCCTCACCGCATACATCAAA-3’
Wnt9a	5’-GTGGACTTCCACAACAACCT-3’	5’-TGGCATTTGCAAGTGGTTTC-3’
Gbp2b	5’-AGACTCCTGGAAAGGGACTC-3’	5’-TGTGAGTGACTGGTCCATCT-3’

Following a pre-established template, either 10µL of standard in duplicate or 10µL of diluted cDNA in triplicate were added into the plate at the bottom of each well. The primer mix was prepared by mixing 12,5µL of GoTaq qPCR Master Mix (#A600A, Promega) and 1,25µM. 15µL of this mix were added on the wall of each well. The plate was sealed with a plastic film and launched in the CFX Connect Real-Time System (BIO-RAD).

Gene expression levels were normalized to housekeeping genes (e.g., Gapdh), and relative expression was calculated using the $2^{-\Delta\Delta Ct}$ method. Statistical comparisons between groups were made using Two-way ANOVA, with $p < 0.05$ considered significant.

Statistical Analyses

GraphPad Prism software version 10 (GraphPad Software, Inc., La Jolla, CA, USA) was used for statistical analysis. All the data were tested for normality using the Shapiro–Wilk test. Parametric Student's *t*-tests or nonparametric Mann-Whitney tests were used to evaluate the level of significance between two groups. When more than two groups were compared, parametric one-way or two-way ANOVA with the indicated post-hoc tests or nonparametric Kruskal–Wallis were used. The data are expressed as the mean +/- SEM. and P values <0.05 were considered significant (*P < 0.05, **P < 0.01, ***P < 0.001). The number of mice used in each group of experiment is indicated by “n=”.

Sample Preparation for RNA Sequencing

Tissues from the OE (pooled bilaterally), one OB, and one hippocampus were collected from PS19 and WT males at 3, 6, and 9 months (n=5 per tissue/genotype/time point; total n=90). RNA was extracted using TriPure™ Isolation Reagent (Roche) followed by chloroform phase separation. Further purification was performed with the ReliaPrep™ RNA Tissue Miniprep System (Promega), and RNA was resuspended in RNase-free water. RNA concentration and purity were assessed by measuring absorbance at 260 nm using a BioSpec-nano spectrophotometer. A260/A280 and A260/A230 ratios were used to evaluate sample purity (Shimadzu). RNA integrity was confirmed by RNA Quality Number (RQN) with a cutoff ≥8.0. Samples (800 ng RNA each) were sent to the GIGA Institute (Liège, Belgium) for RNA sequencing.

RNA-sequencing Data Processing and Analysis

Raw Illumina reads underwent quality control with Fastp (v0.24.0), FastQC (v0.12.1), and MultiQC (v1.25.2) for adapter trimming and filtering of low-quality bases (>5% Ns) . Clean reads were aligned to the GENCODE M36 (GRCm39) reference genome using STAR. Alignments were sorted with SAMtools (v1.21), and gene-level counts were generated with HTSeq (v2.0.5). Multidimensional scaling (MDS) plots using DESeq2-normalized counts assessed sample clustering. Differential expression analysis was conducted with DESeq2, applying thresholds of adjusted p-value <0.05 and |log2 fold-change| >0.58 to identify significantly DEGs.

Functional Annotation and Enrichment

Gene Ontology (GO) and KEGG pathway enrichment analyses were performed using ClusterProfiler and g:Profiler in R (v4.2.1). Enriched terms (adjusted $p < 0.05$) were categorized into biological process, molecular function, and cellular component domains, providing insight into the molecular pathways disrupted in tauopathy. Results were visualized via bar plots, dot plots, and network diagrams to facilitate interpretation.

qRT-PCR Validation of Candidate Biomarkers

To experimentally validate candidate biomarkers, we performed quantitative reverse transcription PCR (qRT-PCR) on OE samples. Tissue was collected from 3, 6, 9-month-old male and female PS19 transgenic mice and age-matched WT mice (n = 4 or 5/group).

Total RNA was extracted using TriPure™ Isolation Reagent (Roche) followed by chloroform phase separation. Further purification was performed with the ReliaPrep™ RNA Tissue Miniprep System (Promega), and RNA was resuspended in RNase-free water. Concentration and purity were assessed via absorbance at 260 nm using a BioSpec-nano spectrophotometer (Shimadzu). cDNA was synthesized using iScript cDNA synthesis Kit (Bio-Rad). qRT-PCR was performed using SYBR Green Master Mix on a Bio-Rad CFX96 real-time PCR system. Each reaction was run in technical triplicates. Gene expression levels were normalized to housekeeping gene (Table S6)(Gapdh), and relative expression was calculated

using the 2–ΔΔCt method. Data were first tested for normality using the Shapiro–Wilk test. When data followed a normal distribution, parametric statistical analysis was performed using a two-tailed unpaired Student's t-test. For data that did not meet normality assumptions, non-parametric analysis was conducted using the Mann–Whitney U test. A p-value < 0.05 was considered statistically significant. Candidate genes were selected for validation based on magnitude of differential expression, overlapping genes and OE-specificity.

Protein Sample Preparation

Samples preparation and analysis were performed in the Mass Spectrometry Facility from the University of Namur. At 6 months, OE (pooled), one OB, and one hippocampus were collected from PS19 and sex-matched WT controls mice (n=10 per group; total n=30). Tissue samples (~10 mg) were homogenized in 200 µL urea lysis buffer (8 M urea, 2% SDS, 1 mM EDTA, 50 mM Tris-HCl, pH 8.0) supplemented with protease and phosphatase inhibitors. Homogenization employed zirconium beads and a FastPrep-24 (MP Biomedicals) device (3 × 20 s cycles at 6.5 m/s with 2-min cooling intervals at 4°C). Samples were sonicated using a Bioruptor (Diagenode)(5 × 30 s bursts, 60 s intervals on ice), then centrifuged at 14,000 rpm for 5 min at 4°C. The clarified supernatant was collected, and protein concentration determined by Pierce 660 nm assay (ThermoFisher). Protein aliquots were stored at −80°C prior to proteomic analysis.

Protein Digestion

The samples were treated using Filter-aided sample preparation (FASP) using the following protocol. To first wash the filters, 100 µl of 1% formic acid was added to each Microcon 30 filter unit (Millipore), followed by centrifugation at 14500 rpm for 15 minutes. For each sample, 40 µg of protein was brought to a final volume of 150 µl using 8M urea buffer (urea 8 M in buffer Tris 0.1 M at pH 8,5) and was loaded into a column and centrifuged at 14500 rpm for 15 minutes. The filtrate was discarded and the columns were washed three times by adding 200 µl of urea buffer followed by a centrifugation at 14500 rpm for 15 minutes. For the reduction step, 100 µl of 8mM dithiothreitol (DTT) was added to the columns and

mixed for 1 minute at 400 rpm with a thermomixer before an incubation of 15 minutes at 24 °C. Samples were then centrifuged at 14500 rpm for 15 minutes, the filtrate was discarded and the filter was rinsed by adding 100 µl of urea buffer, followed by another centrifugation at 14500 rpm for 15 minutes. An alkylation step was performed by adding 100 µl of 50mM iodoacetamide (IAA), in urea buffer) to each column, followed by mixing at 400 rpm for 1 minute in the dark. The samples were then incubated for 20 minutes in the dark and centrifuged at 14500 rpm for 10 minutes. To remove the excess of IAA, 100 µl of urea buffer was added and the samples were centrifugated at 14500 rpm for 15 minutes. To quench residual IAA, 100 µl of DTT was placed on the column, mixed for 1 minute at 400 rpm and incubated for 15 minutes at 24 °C before centrifugation at 14500 rpm for 10 minutes. To remove the excess of DTT, 100 µl of urea buffer was added to the column and centrifuged at 14500 rpm for 15 minutes. The filtrate was discarded, and the column was washed three times by adding 100 µl of sodium bicarbonate buffer 50 mM (ABC) in ultrapure water, followed by a centrifugation at 14500 rpm for 10 minutes. The last 100 µl of buffer was left at the bottom of the filter unit to avoid any evaporation in the column. The protein digestion process was performed by adding 80 µl of mass spectrometry-grade trypsin (1/50 in ABC buffer) to the column, followed by mixing at 400 rpm for 1 minute before an incubation overnight at 24°C in a water saturated environment. The Microcon columns were placed into LoBind tubes of 1.5 ml and centrifuged at 14500 rpm for 10 minutes. 40 µl of ABC buffer was placed on the column before centrifugation at 14500 rpm for 10 minutes. 10 % Trifluoroacetic acid (TFA) in ultrapure water was added to the content of the LoBind Tube to obtain a final concentration of 0.2 % TFA. The samples were dried in a SpeedVac to a final volume of 20 µl and transferred into injection vials.

DIA-MS Protein Data Processing and Analysis

DIA-MS Protein Data Processing and Analysis was used as target validation. The protein digest was analyzed using nano-LC-ESI-MS/MS time TOF HT (Bruker, Billerica, MA, USA) coupled with an UHPLC nanoElute 2 (Bruker).

Peptides were separated using a nanoUHPLC system (nanoElute2, Bruker) equipped with a 150 µm inner diameter × 25 cm column packed with 1.5 µm C18 particles (PepSep, Bruker).

Methods

A CaptiveSpray emitter with a preassembled union was used to interface the column with the CaptiveSpray ion source (Bruker). The liquid chromatography mobile phases consisted of solvent A: water with 0.1% formic acid (v/v), and solvent B: acetonitrile (ACN) with 0.1% formic acid (v/v). Samples were loaded directly on the analytical column at a constant pressure of 800 bar. The digest (1 µl) was injected, and the organic content of the mobile phase was increased linearly from 5% to 27 % B in 56 minutes at a flow rate of 600 nl/min, from 27 % to 35% B in 7 minutes, from 35% to 95 % B in 1 minute. Data acquisition on the tims TOF HT was performed using Hystar 6.3. Mass-spectrometric analyses were carried out using the data-independent parallel accumulation serial fragmentation acquisition method (DIA-PASEF) [22]. The DIA-PASEF acquisition scheme was 1 MS1 ramp and 6 MS2 ramps with 18 windows. Mass range was restricted from 300 to 1200 m/z and ion mobility was set from 0.6 to 1.4 1/K0.

DIA-NN 2.0 [10] was used to process the raw data with an in silico spectral library of 54644 proteins and 22086 genes created from Mus Musculus proteome database (UNIPROT) and a contaminants database.

Trypsin/P was used with a maximum of 1 missed cleavage. Variable modifications on peptides were set to methionine oxidation, and fixed modification was set to carbamidomethylation on cysteine. The maximum number of variable modifications on a peptide was set to 3. The peptide length for the search ranged from 7 to 30 amino acids. m/z ranges were specified as 300 to 1400 for precursors and 100 to 1700 for fragment ions. Both MS1 and MS2 mass accuracy were set to 15ppm. Scoring was set to generic. Match-between-run (MBR) and protein inference options were checked. RT-dependent cross-run normalization and QuantUMS (high precision) options were selected for quantification. A 1% FDR cutoff was applied at the precursor level.

In order to perform the differential expression analysis, protein group matrix from DIA-NN was loaded to the web application DIA-Analyst from Monash University [44]. Adjusted p-value cutoff was set to 0.05 and log2 fold changed cutoff to 1. No imputation and t-statistics-based FDR correction were applied.

Data Available Statements

All datasets generated and analyzed during this study are included in this published article and its supplementary material. The raw RNA-seq data generated in this study have been deposited in the NCBI Sequence Read Archive (SRA) under accession number PRJNA1293667. The mass spectrometry proteomics data have been deposited to the ProteomeXchange Consortium via the PRIDE [27] partner repository with the dataset identifier PXD066157.

Bibliography

References

1. Liao W, Wang Y, Wang L, Li J, Huang D, Cheng W, and Luan P, *The current status and challenges of olfactory dysfunction study in Alzheimer's Disease.* Ageing Res Rev, 2024. **100**: p. 102453. https://doi.org/10.1016/j.arr.2024.102453
2. Fatuzzo I, Niccolini GF, Zoccali F, Cavalcanti L, Bellizzi MG, Riccardi G, de Vincentiis M, Fiore M, Petrella C, Minni A, and Barbato C, *Neurons, Nose, and Neurodegenerative Diseases: Olfactory Function and Cognitive Impairment.* Int J Mol Sci, 2023. **24**(3). https://doi.org/10.3390/ijms24032117
3. Dan X, Wechter N, Gray S, Mohanty JG, Croteau DL and Bohr VA, *Olfactory dysfunction in aging and neurodegenerative diseases.* Ageing Res Rev, 2021. **70**: p. 101416. https://doi.org/10.1016/j.arr.2021.101416
4. Parvand M and Rankin CH, *Is There a Shared Etiology of Olfactory Impairments in Normal Aging and Neurodegenerative Disease?* J Alzheimers Dis, 2020. **73**(1): p. 1-21. https://doi.org/10.3233/jad-190636
5. Zhang J, Zhao Z, Sun S, Li J, Wang Y, Dong J, Yang S, Lou Y, Yang J, Li W, and Li S, *Olfactory Evaluation in Alzheimer's Disease Model Mice.* Brain Sci, 2022. **12**(5). https://doi.org/10.3390/brainsci12050607
6. Nagayama S, Enerva A, Fletcher M, Masurkar A, Igarashi K, Mori K, and Chen W, *Differential Axonal Projection of Mitral and Tufted Cells in the Mouse Main Olfactory System.* Frontiers in Neural Circuits, 2010. **4**. https://doi.org/10.3389/fncir.2010.00120
7. Schröder H, Moser N and Huggenberger S, *Neuroanatomy of the Mouse*. 2020: Springer Cham. 350.
8. Boehm U, *The vomeronasal system in mice: from the nose to the hypothalamus- and back!* Semin Cell Dev Biol, 2006. **17**(4): p. 471-9. https://doi.org/10.1016/j.semcdb.2006.04.013
9. Doty RL, *Olfactory dysfunction in neurodegenerative diseases: is there a common pathological substrate?* Lancet Neurology, 2017. **16**(6): p. 478-488. https://doi.org/10.1016/S1474-4422(17)30123-0
10. Chapman R and Bernays E, *chemoreception.* Encyclopedia Britannica, 2024. https://doi.org/https://www.britannica.com/science/chemoreception
11. Barrios AW, Núñez G, Sánchez QP and Salazar I, *Anatomy, histochemistry, and immunohistochemistry of the olfactory subsystems in mice.* Frontiers in Neuroanatomy, 2014. **8**. https://doi.org/10.3389/fnana.2014.00063
12. Dorman DC, *13.15 - Olfactory System*, in *Comprehensive Toxicology (Second Edition)*, C.A. McQueen, Editor. 2010, Elsevier: Oxford. p. 263-276.
13. Jiang Y, Guo J, Tang X, Wang X, Hao D and Yang H, *The Immunological Roles of Olfactory Ensheathing Cells in the Treatment of Spinal Cord Injury.*

Frontiers in Immunology, 2022. **Volume 13 - 2022**. https://doi.org/10.3389/fimmu.2022.881162

14. Chen CR, Kachramanoglou C, Li D, Andrews P and Choi D, *Anatomy and cellular constituents of the human olfactory mucosa: a review.* J Neurol Surg B Skull Base, 2014. **75**(5): p. 293-300. https://doi.org/10.1055/s-0033-1361837
15. Wooten C, *Chapter 18 - Anatomy of the Olfactory Nerves*, in *Nerves and Nerve Injuries*, R.S. Tubbs, et al., Editors. 2015, Academic Press: San Diego. p. 273-276.
16. Bathini P, Brai E and Auber LA, *Olfactory dysfunction in the pathophysiological continuum of dementia.* Ageing Res Rev, 2019. **55**: p. 100956. https://doi.org/10.1016/j.arr.2019.100956
17. Talamo BR, Feng WH, Perez-Cruet M, Adelman L, Kosik K, Lee MY, Cork LC, and Kauer JS, *Pathologic changes in olfactory neurons in Alzheimer's disease.* Ann N Y Acad Sci, 1991. **640**: p. 1-7. https://doi.org/10.1111/j.1749-6632.1991.tb00182.x
18. Son G, Jahanshahi A, Yoo SJ, Boonstra JT, Hopkins DA, Steinbusch HWM, and Moon C, *Olfactory neuropathology in Alzheimer's disease: a sign of ongoing neurodegeneration.* BMB Rep, 2021. **54**(6): p. 295-304. https://doi.org/10.5483/BMBRep.2021.54.6.055
19. Smith TD and Bhatnagar KP, *Anatomy of the olfactory system.* Handb Clin Neurol, 2019. **164**: p. 17-28. https://doi.org/10.1016/b978-0-444-63855-7.00002-2
20. Noto T, Zhou G, Yang Q, Lane G and Zelano C, *Human Primary Olfactory Amygdala Subregions Form Distinct Functional Networks, Suggesting Distinct Olfactory Functions.* Frontiers in Systems Neuroscience, 2021. **15**. https://doi.org/10.3389/fnsys.2021.752320
21. Illig KR and Wilson DA, *Olfactory Cortex: Comparative Anatomy*, in *Reference Module in Biomedical Sciences*. 2014, Elsevier.
22. Chen YN and Kostka JK, *Beyond anosmia: olfactory dysfunction as a common denominator in neurodegenerative and neurodevelopmental disorders.* Front Neurosci, 2024. **18**: p. 1502779. https://doi.org/10.3389/fnins.2024.1502779
23. Lane G, Zhou G, Noto T and Zelano C, *Assessment of direct knowledge of the human olfactory system.* Experimental Neurology, 2020. **329**: p. 113304. https://doi.org/https://doi.org/10.1016/j.expneurol.2020.113304
24. Young JC, Vaughan DN, Nasser HM and Jackson GD, *Anatomical imaging of the piriform cortex in epilepsy.* Experimental Neurology, 2019. **320**: p. 113013. https://doi.org/https://doi.org/10.1016/j.expneurol.2019.113013
25. Wesson DW and Wilson DA, *Sniffing out the contributions of the olfactory tubercle to the sense of smell: Hedonics, sensory integration, and more?*

Neuroscience & Biobehavioral Reviews, 2011. **35**(3): p. 655-668. https://doi.org/https://doi.org/10.1016/j.neubiorev.2010.08.004

26. Brunert D, Medinaceli Quintela R and Rothermel M, *The anterior olfactory nucleus revisited – An emerging role for neuropathological conditions?* Progress in Neurobiology, 2023. **228**: p. 102486. https://doi.org/https://doi.org/10.1016/j.pneurobio.2023.102486
27. Witter MP, *Entorhinal Area (Cortex)*, in *Encyclopedia of Neuroscience*, M.D. Binder, N. Hirokawa, and U. Windhorst, Editors. 2009, Springer Berlin Heidelberg: Berlin, Heidelberg. p. 1126-1129.
28. Witter MP, Doan TP, Jacobsen B, Nilssen ES and Ohara S, *Architecture of the Entorhinal Cortex A Review of Entorhinal Anatomy in Rodents with Some Comparative Notes.* Frontiers in Systems Neuroscience, 2017. **Volume 11 - 2017**. https://doi.org/10.3389/fnsys.2017.00046
29. van Groen T, Miettinen P and Kadish I, *The entorhinal cortex of the mouse: Organization of the projection to the hippocampal formation.* Hippocampus, 2003. **13**(1): p. 133-149. https://doi.org/https://doi.org/10.1002/hipo.10037
30. Anand KS and Dhikav V, *Hippocampus in health and disease: An overview.* Ann Indian Acad Neurol, 2012. **15**(4): p. 239-46. https://doi.org/10.4103/0972-2327.104323
31. Witter MP, *The perforant path: projections from the entorhinal cortex to the dentate gyrus*, in *Progress in Brain Research*, H.E. Scharfman, Editor. 2007, Elsevier. p. 43-61.
32. Witter MP, Naber PA, van Haeften T, Machielsen WCM, Rombouts S, Barkhof F, Scheltens P, and Lopes da Silva FH, *Cortico-hippocampal communication by way of parallel parahippocampal-subicular pathways.* Hippocampus, 2000. **10**(4): p. 398-410. https://doi.org/10.1002/1098-1063(2000)10:4<398::AID-HIPO6>3.0.CO;2-K
33. Song D, Harway M, Marmarelis VZ, Hampson RE, Deadwyler SA and Berger TW, *Extraction and restoration of hippocampal spatial memories with non-linear dynamical modeling.* Frontiers in Systems Neuroscience, 2014. **8**. https://doi.org/10.3389/fnsys.2014.00097
34. Beauchamp A, Yee Y, Darwin BC, Raznahan A, Mars RB and Lerch JP, *Whole-brain comparison of rodent and human brains using spatial transcriptomics.* Elife, 2022. **11**. https://doi.org/10.7554/eLife.79418
35. Tzeng WY, Figarella K and Garaschuk O, *Olfactory impairment in men and mice related to aging and amyloid-induced pathology.* Pflügers Archiv - European Journal of Physiology, 2021. **473**(5): p. 805-821. https://doi.org/10.1007/s00424-021-02527-0

36. Hummel T, Liu DT, Müller CA, Stuck BA, Welge-Lüssen A and Hähner A, *Olfactory Dysfunction: Etiology, Diagnosis, and Treatment.* Dtsch Arztebl Int, 2023. **120**(9): p. 146-154. https://doi.org/10.3238/arztebl.m2022.0411
37. Hummel T, Whitcroft KL, Andrews P, Altundag A, Cinghi C, Costanzo RM, Damm M, Frasnelli J, Gudziol H, Gupta N, Haehna A, Holbrook E, Hong SC, Hornung D, Hüttenbrink KB, Kamel R, Kobayashi M, Konstantinidis I, Landis BN, Leopold DA, Macchi A, Miwa T, Moesges R, Mullol J, Mueller CA, Ottaviano G, Passali GC, Philpott C, Pinto JM, Ramakrishnan VJ, Rombaux P, Roth Y, Schlosser RA, Shu B, Soler G, Stjärne P, Stuck BA, Vodicka J, and Welge-Luessen A, *Position paper on olfactory dysfunction.* Rhinol Suppl, 2017. **54**(26): p. 1-30. https://doi.org/10.4193/Rhino16.248
38. Whitcroft KL and Hummel T, *Clinical Diagnosis and Current Management Strategies for Olfactory Dysfunction: A Review.* JAMA Otolaryngology–Head & Neck Surgery, 2019. **145**(9): p. 846-853. https://doi.org/10.1001/jamaoto.2019.1728
39. Kondo K, Kikuta S, Ueha R, Suzukawa K and Yamasoba T, *Age-Related Olfactory Dysfunction: Epidemiology, Pathophysiology, and Clinical Management.* Front Aging Neurosci, 2020. **12**: p. 208. https://doi.org/10.3389/fnagi.2020.00208
40. Doty RL, Shaman P and Dann M, *Development of the university of pennsylvania smell identification test: A standardized microencapsulated test of olfactory function.* Physiology & Behavior, 1984. **32**(3): p. 489-502. https://doi.org/https://doi.org/10.1016/0031-9384(84)90269-5
41. Witt RM, Galligan MM, Despinoy JR and Segal R, *Olfactory behavioral testing in the adult mouse.* J Vis Exp, 2009(23). https://doi.org/10.3791/949
42. D'Andrea F, Tischler V, Dening T and Churchill A, *Olfactory stimulation for people with dementia: A rapid review.* Dementia (London), 2022. **21**(5): p. 1800-1824. https://doi.org/10.1177/14713012221082377
43. Lamptey RNL, Chaulagain B, Trivedi R, Gothwal A, Layek B and Singh J, *A Review of the Common Neurodegenerative Disorders: Current Therapeutic Approaches and the Potential Role of Nanotherapeutics.* Int J Mol Sci, 2022. **23**(3). https://doi.org/10.3390/ijms23031851
44. Attems J, Walker L and Jellinger KA, *Olfactory bulb involvement in neurodegenerative diseases.* Acta Neuropathologica, 2014. **127**: p. 459-475. https://doi.org/10.1007/s00401-014-1261-7
45. De Cleene N, Schwarzová K, Labrecque S, Cerejo C, Djamshidian A, Seppi K, and Heim B, *Olfactory dysfunction as potential biomarker in neurodegenerative diseases: a narrative review.* Frontiers in Neuroscience, 2025. **Volume 18 - 2024**. https://doi.org/10.3389/fnins.2024.1505029
46. Li S, W. Li, Wu X, Li J, Yang J, Tu C, Ye X, and Ling S, *Olfactory deficit is associated with mitral cell dysfunction in the olfactory bulb of P301S tau*

transgenic mice. Brain Res Bull, 2019. **148**: p. 34-45. https://doi.org/10.1016/j.brainresbull.2019.03.006

47. Murphy C, *Olfactory and other sensory impairments in Alzheimer disease.* Nature Reviews Neurology, 2019. **15**(1): p. 11-24. https://doi.org/10.1038/s41582-018-0097-5
48. Yang S, Kuan WL and Spillantini MG, *Progressive tauopathy in P301S tau transgenic mice is associated with a functional deficit of the olfactory system.* Eur J Neurosci, 2016. **44**(6): p. 2396-403. https://doi.org/10.1111/ejn.13333
49. Franco R, Garrigós C and Lillo J, *The Olfactory Trail of Neurodegenerative Diseases.* Cells, 2024. **13**(7). https://doi.org/10.3390/cells13070615
50. Marin C, Vilas D, Langdon C, Alobid I, López-Chacón M, Haehner A, Hummel T, and Mullol J, *Olfactory Dysfunction in Neurodegenerative Diseases.* Curr Allergy Asthma Rep, 2018. **18**(8): p. 42. https://doi.org/10.1007/s11882-018-0796-4
51. Viguera C, Wang J, Mosmiller E, Cerezo A and Maragakis NJ, *Olfactory dysfunction in amyotrophic lateral sclerosis.* Annals of Clinical and Translational Neurology, 2018. **5**(8): p. 976-981. https://doi.org/https://doi.org/10.1002/acn3.594
52. Kovács T, *The olfactory system in Alzheimer's disease: Pathology, pathophysiology and pathway for therapy.* Translational Neuroscience, 2013. **4**(1): p. 34-45. https://doi.org/doi:10.2478/s13380-013-0108-3
53. Zhang X, Wang J, Zhang Z and Ye K, *Tau in neurodegenerative diseases: molecular mechanisms, biomarkers, and therapeutic strategies.* Translational Neurodegeneration, 2024. **13**(1): p. 40. https://doi.org/10.1186/s40035-024-00429-6
54. Lad M, Sedley W and Griffiths TD, *Sensory Loss and Risk of Dementia.* Neuroscientist, 2024. **30**(2): p. 247-259. https://doi.org/10.1177/10738584221126090
55. Yan Y, Aierken A, Wang C, Song D, Ni J, Wang Z, Quan Z, and Qing H, *A potential biomarker of preclinical Alzheimer's disease: The olfactory dysfunction and its pathogenesis-based neural circuitry impairments.* Neurosci Biobehav Rev, 2022. **132**: p. 857-869. https://doi.org/10.1016/j.neubiorev.2021.11.009
56. Woodward MR, Hafeez MU, Qi Q, Riaz A, Benedict RHB, Yan L, and Szigeti K, *Odorant Item Specific Olfactory Identification Deficit May Differentiate Alzheimer Disease From Aging.* Am J Geriatr Psychiatry, 2018. **26**(8): p. 835-846. https://doi.org/10.1016/j.jagp.2018.02.008
57. Arnold SE, Smutzer GS, Trojanowski JQ and Moberg PJ, *Cellular and molecular neuropathology of the olfactory epithelium and central olfactory*

pathways in Alzheimer's disease and schizophrenia. Ann N Y Acad Sci, 1998. **855**: p. 762-75. https://doi.org/10.1111/j.1749-6632.1998.tb10656.x

58. Shimizu S, Tojima I, Nakamura K, Kouzaki H, Kanesaka T, Ogawa N, Hashizume Y, Akatsu H, Hori A, Tooyama I, and Shimizu T, *A Histochemical Analysis of Neurofibrillary Tangles in Olfactory Epithelium, a Study Based on an Autopsy Case of Juvenile Alzheimer's Disease.* Acta Histochem Cytochem, 2022. **55**(3): p. 93-98. https://doi.org/10.1267/ahc.22-00048
59. Attems J, Lintner F and Jellinger KA, *Olfactory involvement in aging and Alzheimer's disease: an autopsy study.* J Alzheimers Dis, 2005. **7**(2): p. 149-57; discussion 173-80. https://doi.org/10.3233/jad-2005-7208
60. Tsuboi Y, Wszolek ZK, Graff-Radford NR, Cookson N and Dickson DW, *Tau pathology in the olfactory bulb correlates with Braak stage, Lewy body pathology and apolipoprotein epsilon4.* Neuropathol Appl Neurobiol, 2003. **29**(5): p. 503-10. https://doi.org/10.1046/j.1365-2990.2003.00453.x
61. Attems J and Jellinger KA, *Olfactory tau pathology in Alzheimer disease and mild cognitive impairment.* Clin Neuropathol, 2006. **25**(6): p. 265-71.
62. Jobin B, Zigrand C, Frasnelli J, Boller B and Albers MW, *Lower odor identification in subjective cognitive decline: a meta-analysis.* Alzheimer's & Dementia: Diagnosis, Assessment & Disease Monitoring, 2025. **17**(3): p. e70168. https://doi.org/https://doi.org/10.1002/dad2.70168
63. Reijs BLR, Ramakers I, Elias-Sonnenschein L, Teunissen CE, Koel-Simmelink M, Tsolaki M, Wahlund L.O, Waldemar G, Hausner L, Johannsen P, Vanderstichele H, Verhey F, Devanand DP, and Visser PJ, *Relation of Odor Identification with Alzheimer's Disease Markers in Cerebrospinal Fluid and Cognition.* J Alzheimers Dis, 2017. **60**(3): p. 1025-1034. https://doi.org/10.3233/jad-170564
64. Haehner A, Hummel T and Reichmann H, *Olfactory loss in Parkinson's disease.* Parkinsons Dis, 2011. **2011**: p. 450939. https://doi.org/10.4061/2011/450939
65. Doty RL, *Olfaction in Parkinson's disease and related disorders.* Neurobiol Dis, 2012. **46**(3): p. 527-52. https://doi.org/10.1016/j.nbd.2011.10.026
66. Huang X, Wu J, Zhang N, Teng J, Yang Q, Zhang Y, Yin T, Zhou W, Fan D, and Ye S, *Smell loss is associated with cognitive impairment in amyotrophic lateral sclerosis patients.* CNS Neurosci Ther, 2024. **30**(7): p. e14851. https://doi.org/10.1111/cns.14851
67. Patino J, Karagas NE, Chandra S, Thakur N and Stimming EF, *Olfactory Dysfunction in Huntington's Disease.* J Huntingtons Dis, 2021. **10**(4): p. 413-422. https://doi.org/10.3233/jhd-210497
68. Zadegan S, Feik M, Coco H, Liang A, Ramirez F, Murillas JP, Rocha NP, and Furr-Stimming E, *Olfactory Dysfunction as an Indicator of Cognitive and Motor Impairment Severity in Huntington's Disease (P6-3.006).* Neurology,

2024. **102**(7_supplement_1): p. 2447. https://doi.org/doi:10.1212/WNL.0000000000204544

69. Highet B, Dieriks BV, Murray HC, Faull RLM and Curtis MA, *Huntingtin Aggregates in the Olfactory Bulb in Huntington's Disease.* Frontiers in Aging Neuroscience, 2020. **Volume 12 - 2020**. https://doi.org/10.3389/fnagi.2020.00261
70. Bang J, Spina S and Miller BL, *Frontotemporal dementia.* The Lancet, 2015. **386**(10004): p. 1672-1682. https://doi.org/10.1016/S0140-6736(15)00461-4
71. Markopoulou K, Chase BA, Robowski P, Strongosky A, Narożańska E, Sitek EJ, Berdynski M, Barcikowska M, Baker MC, Rademakers R, Sławek J, Klein C, Hückelheim K, Kasten M, and Wszolek ZK, *Assessment of Olfactory Function in MAPT-Associated Neurodegenerative Disease Reveals Odor-Identification Irreproducibility as a Non-Disease-Specific, General Characteristic of Olfactory Dysfunction.* PLoS One, 2016. **11**(11): p. e0165112. https://doi.org/10.1371/journal.pone.0165112
72. Rami L, Loy CT, Hailstone J and Warren JD, *Odour identification in frontotemporal lobar degeneration.* Journal of Neurology, 2007. **254**(4): p. 431-435. https://doi.org/10.1007/s00415-006-0379-5
73. Tonacci A and Billeci L, *Olfactory Testing in Frontotemporal Dementia: A Literature Review.* Am J Alzheimers Dis Other Demen, 2018. **33**(6): p. 342-352. https://doi.org/10.1177/1533317518775037
74. Khan S, Barve KH and Kumar MS, *Recent Advancements in Pathogenesis, Diagnostics and Treatment of Alzheimer's Disease.* Curr Neuropharmacol, 2020. **18**(11): p. 1106-1125. https://doi.org/10.2174/1570159x18666200528142429
75. Breijyeh Z and Karaman R, *Comprehensive Review on Alzheimer's Disease: Causes and Treatment.* Molecules, 2020. **25**(24). https://doi.org/10.3390/molecules25245789
76. Piaceri I, Nacmias B and Sorbi S, *Genetics of familial and sporadic Alzheimer's disease.* Front Biosci (Elite Ed), 2013. **5**(1): p. 167-77. https://doi.org/10.2741/e605
77. Chakrabarti S, Khemka VK, Banerjee A, Chatterjee G, Ganguly A and Biswas A, *Metabolic Risk Factors of Sporadic Alzheimer's Disease: Implications in the Pathology, Pathogenesis and Treatment.* Aging Dis, 2015. **6**(4): p. 282-99. https://doi.org/10.14336/ad.2014.002
78. Moloney CM, Lowe VJ and Murray ME, *Visualization of neurofibrillary tangle maturity in Alzheimer's disease: A clinicopathologic perspective for biomarker research.* Alzheimer's & Dementia, 2021. **17**(9): p. 1554-1574. https://doi.org/https://doi.org/10.1002/alz.12321

79. Braak H and Braak E, *Neuropathological stageing of Alzheimer-related changes.* Acta Neuropathologica, 1991. **82**(4): p. 239-259. https://doi.org/10.1007/BF00308809
80. Braak H and Del Tredici K, *Neuroanatomy and Pathology of Sporadic Alzheimer's Disease*. Advances in Anatomy, Embryology and Cell Biology. 2014: Springer Cham.
81. Braak H, Alafuzoff I, Arzberger T, Kretzschmar H and Del Tredici K, *Staging of Alzheimer disease-associated neurofibrillary pathology using paraffin sections and immunocytochemistry.* Acta Neuropathol, 2006. **112**(4): p. 389-404. https://doi.org/10.1007/s00401-006-0127-z
82. van Oostveen WM and de Lange ECM, *Imaging Techniques in Alzheimer's Disease: A Review of Applications in Early Diagnosis and Longitudinal Monitoring.* International Journal of Molecular Sciences, 2021. **22**(4): p. 2110.
83. Nelson PT, Alafuzoff I, Bigio EH, Bouras C, Braak H, Cairns NJ, Castellani RJ, Crain BJ, Davies P, Del Tredici K, Duyckaerts C, Frosch MP, Haroutunian V, Hof PR, Hulette CM, Hyman BT, Iwatsubo T, Jellinger KA, Jicha GA, Kövari E, Kukull WA, Leverenz JB, Love S, Mackenzie IR, Mann DM, Masliah E, McKee AC, Montine TJ, Morris JC, Schneider JA, Sonnen JA, Thal DR, Trojanowski JQ, Troncoso JC, Wisniewski T, Woltjer RL, and Beach TG, *Correlation of Alzheimer disease neuropathologic changes with cognitive status: a review of the literature.* J Neuropathol Exp Neurol, 2012. **71**(5): p. 362-81. https://doi.org/10.1097/NEN.0b013e31825018f7
84. Biel D, Brendel M, Rubinski A, Buerger K, Janowitz D, Dichgans M, and Franzmeier N, *Tau-PET and in vivo Braak-staging as prognostic markers of future cognitive decline in cognitively normal to demented individuals.* Alzheimer's Research & Therapy, 2021. **13**(1): p. 137. https://doi.org/10.1186/s13195-021-00880-x
85. Jack CRJr, Knopman DS, Jagust WJ, Petersen RC, Weiner MW, Aisen PS, Shaw LM, Vemuri P, Wiste HJ, Weigand SD, Lesnick TG, Pankratz VS, Donohue MC, and Trojanowski JQ, *Tracking pathophysiological processes in Alzheimer's disease: an updated hypothetical model of dynamic biomarkers.* Lancet Neurol, 2013. **12**(2): p. 207-16. https://doi.org/10.1016/s1474-4422(12)70291-0
86. McDade E, Bednar MM, Brashear HR, Miller DS, Maruff P, Randolph C, Ismail Z, Carrillo MC, Weber CJ, Bain LJ, and Hake AM, *The pathway to secondary prevention of Alzheimer's disease.* Alzheimers Dement (N Y), 2020. **6**(1): p. e12069. https://doi.org/10.1002/trc2.12069
87. Albert MS, DeKosky ST, Dickson D, Dubois B, Feldman HH, Fox NC, Gamst A, Holtzman DM, Jagust WJ, Petersen RC, Snyder PJ, Carrillo MC, Thies B, and Phelps CH, *The diagnosis of mild cognitive impairment due to Alzheimer's*

disease: recommendations from the National Institute on Aging-Alzheimer's Association workgroups on diagnostic guidelines for Alzheimer's disease. Alzheimers Dement, 2011. **7**(3): p. 270-9. https://doi.org/10.1016/j.jalz.2011.03.008

88. Liss JL, Seleri Assunção S, Cummings J, Atri A, Geldmacher DS, Candela SF, Devanand DP, Fillit HM, Susman J, Mintzer J, Bittner T, Brunton SA, Kerwin DR, Jackson WC, Small GW, Grossberg GT, Clevenger CK, Cotter V, Stefanacci R, Wise-Brown A, and Sabbagh MN, *Practical recommendations for timely, accurate diagnosis of symptomatic Alzheimer's disease (MCI and dementia) in primary care: a review and synthesis.* J Intern Med, 2021. **290**(2): p. 310-334. https://doi.org/10.1111/joim.13244
89. Dumas A, Destrebecq F, Esposito G, Suchonova D and Steen Frederiksen K, *Rethinking the detection and diagnosis of Alzheimer's disease: Outcomes of a European Brain Council project.* Aging Brain, 2023. **4**: p. 100093. https://doi.org/10.1016/j.nbas.2023.100093
90. Porsteinsson AP, Isaacson RS, Knox S, Sabbagh MN and Rubino I, *Diagnosis of Early Alzheimer's Disease: Clinical Practice in 2021.* The Journal of Prevention of Alzheimer's Disease, 2021. **8**(3): p. 371-386. https://doi.org/10.14283/jpad.2021.23
91. Boyer E, Deltenre L, Dourte M, Colmant L, Paître E, Sleegers K, Suelves N, Hanseeuw B, and Kienlen-Campard P, *Comparison of plasma soluble and extracellular vesicles-associated biomarkers in Alzheimer's disease patients and cognitively normal individuals.* Alzheimers Res Ther, 2024. **16**(1): p. 141. https://doi.org/10.1186/s13195-024-01508-6
92. Grande G, Valletta M, Rizzuto D, Xia X, Qiu C, Orsini N, Dale M, Andersson S, Fredolini C, Winblad B, Laukka EJ, Fratiglioni L, and Vetrano DL, *Blood-based biomarkers of Alzheimer's disease and incident dementia in the community.* Nature Medicine, 2025. https://doi.org/10.1038/s41591-025-03605-x
93. Bhunia S, Kolishetti N, Vashist A, Yndart Arias A, Brooks D and Nair M, *Drug Delivery to the Brain: Recent Advances and Unmet Challenges.* Pharmaceutics, 2023. **15**(12). https://doi.org/10.3390/pharmaceutics15122658
94. Jönsson L, Wimo A, Handels R, Johansson G, Boada M, Engelborghs S, Frölich L, Jessen F, Kehoe PG, Kramberger M, de Mendonça A, Ousset PJ, Scarmeas N, Visser PJ, Waldemar G, and Winblad B, *The affordability of lecanemab, an amyloid-targeting therapy for Alzheimer's disease: an EADC-EC viewpoint.* Lancet Reg Health Eur, 2023. **29**: p. 100657. https://doi.org/10.1016/j.lanepe.2023.100657
95. Weingarten MD, Lockwood AH, Hwo SY and Kirschner MW, *A protein factor essential for microtubule assembly.* Proceedings of the National Academy

of Sciences, 1975. **72**(5): p. 1858-1862. https://doi.org/doi:10.1073/pnas.72.5.1858

96. Wang Y and Mandelkow E, *Tau in physiology and pathology.* Nature Reviews Neuroscience, 2016. **17**(1): p. 22-35. https://doi.org/10.1038/nrn.2015.1
97. Kopeikina KJ, Hyman BT and Spires-Jones TL, *Soluble forms of tau are toxic in Alzheimer's disease.* Transl Neurosci, 2012. **3**(3): p. 223-233. https://doi.org/10.2478/s13380-012-0032-y
98. Korde DS and Humpel C, *Spreading of P301S Aggregated Tau Investigated in Organotypic Mouse Brain Slice Cultures.* Biomolecules, 2022. **12**(9): p. 1164.
99. Rawat P, Sehar U, Bisht J, Selman A, Culberson J and Reddy PH, *Phosphorylated Tau in Alzheimer's Disease and Other Tauopathies.* Int J Mol Sci, 2022. **23**(21). https://doi.org/10.3390/ijms232112841
100. Park SA, Ahn SI and Gallo JM, *Tau mis-splicing in the pathogenesis of neurodegenerative disorders.* BMB Rep, 2016. **49**(8): p. 405-13. https://doi.org/10.5483/bmbrep.2016.49.8.084
101. Fischer I, *Big Tau: What We Know, and We Need to Know.* eNeuro, 2023. **10**(5). https://doi.org/10.1523/eneuro.0052-23.2023
102. Hernández F, Merchán-Rubira J, Vallés-Saiz L, Rodríguez-Matellán A and Avila J, *Differences Between Human and Murine Tau at the N-terminal End.* Frontiers in Aging Neuroscience, 2020. **Volume 12 - 2020**. https://doi.org/10.3389/fnagi.2020.00011
103. Seitkazina A, Kim KH, Fagan E, Sung Y, Kim YK and Lim S, *The Fate of Tau Aggregates Between Clearance and Transmission.* Front Aging Neurosci, 2022. **14**: p. 932541. https://doi.org/10.3389/fnagi.2022.932541
104. Alquezar C, Arya S and Kao AW, *Tau Post-translational Modifications: Dynamic Transformers of Tau Function, Degradation, and Aggregation.* Front Neurol, 2020. **11**: p. 595532. https://doi.org/10.3389/fneur.2020.595532
105. Benítez MJ, Cuadros R and Jiménez JS, *Phosphorylation and Dephosphorylation of Tau Protein by the Catalytic Subunit of PKA, as Probed by Electrophoretic Mobility Retard.* J Alzheimers Dis, 2021. **79**(3): p. 1143-1156. https://doi.org/10.3233/jad-201077
106. Gayatri D, *Handbook of Clinical Neurology, Chapter 12 - The tauopathies* Vol. 196. 2023.
107. Samudra N, Lane-Donovan C, VandeVrede L and Boxer AL, *Tau pathology in neurodegenerative disease: disease mechanisms and therapeutic avenues.* J Clin Invest, 2023. **133**(12). https://doi.org/10.1172/jci168553
108. Iqbal K, Liu F, Gong CX and Grundke-Iqbal I, *Tau in Alzheimer disease and related tauopathies.* Curr Alzheimer Res, 2010. **7**(8): p. 656-64. https://doi.org/10.2174/156720510793611592

109. Ellis MJ, Lekka C, Holden KL, Tulmin H, Seedat F, O'Brien DP, Dhayal S, Zeissler M, Knudsen JG, Kessler BM, Morgan NG, Todd JA, Richardson SJ, and Stefana MI, *Identification of high-performing antibodies for the reliable detection of Tau proteoforms by Western blotting and immunohistochemistry.* Acta Neuropathologica, 2024. **147**(1): p. 87. https://doi.org/10.1007/s00401-024-02729-7

110. Goedert M, Jakes R and Vanmechelen E, *Monoclonal antibody AT8 recognises tau protein phosphorylated at both serine 202 and threonine 205.* Neurosci Lett, 1995. **189**(3): p. 167-9. https://doi.org/10.1016/0304-3940(95)11484-e

111. Amniai L, Lippens G and Landrieu I, *Characterization of the AT180 epitope of phosphorylated Tau protein by a combined nuclear magnetic resonance and fluorescence spectroscopy approach.* Biochem Biophys Res Commun, 2011. **412**(4): p. 743-6. https://doi.org/10.1016/j.bbrc.2011.08.046

112. Goedert M, Jakes R, Crowther RA, Cohen P, Vanmechelen E, Vandermeeren M, and Cras P, *Epitope mapping of monoclonal antibodies to the paired helical filaments of Alzheimer's disease: identification of phosphorylation sites in tau protein.* Biochemical Journal, 1994. **301**(3): p. 871-877. https://doi.org/10.1042/bj3010871

113. Nukina N, Kosik KS and Selkoe DJ, *The monoclonal antibody, Alz 50, recognizes tau proteins in Alzheimer's disease brain.* Neurosci Lett, 1988. **87**(3): p. 240-6. https://doi.org/10.1016/0304-3940(88)90455-7

114. Otvos LJr, Feiner L, Lang E, Szendrei GI, Goedert M and Lee VM, *Monoclonal antibody PHF-1 recognizes tau protein phosphorylated at serine residues 396 and 404.* J Neurosci Res, 1994. **39**(6): p. 669-73. https://doi.org/10.1002/jnr.490390607

115. Aragão Gomes L, Uytterhoeven V, Lopez-Sanmartin D, Tomé SO, Tousseyn T, Vandenberghe R, Vandenbulcke M, von Arnim CAF, Verstreken P, and Thal DR, *Maturation of neuronal AD-tau pathology involves site-specific phosphorylation of cytoplasmic and synaptic tau preceding conformational change and fibril formation.* Acta Neuropathologica, 2021. **141**(2): p. 173-192. https://doi.org/10.1007/s00401-020-02251-6

116. Simic G, Babić Leko M, Wray S, Harrington C, Delalle I, Jovanov-Milošević N, Bažadona D, Buee L, Silva R, Di Giovanni G, Wischik C, and Hof P, *Tau Protein Hyperphosphorylation and Aggregation in Alzheimer's Disease and Other Tauopathies, and Possible Neuroprotective Strategies.* Biomolecules, 2016. **6**: p. 6. https://doi.org/10.3390/biom6010006

117. Bancher C, Brunner C, Lassmann H, Budka H, Jellinger K, Wiche G, Seitelberger F, Grundke-Iqbal I, Iqbal K, and Wisniewski HM, *Accumulation of abnormally phosphorylated tau precedes the formation of neurofibrillary*

tangles in Alzheimer's disease. Brain Res, 1989. **477**(1-2): p. 90-9. https://doi.org/10.1016/0006-8993(89)91396-6

118. Tang M, Harrison J, Deaton CA and Johnson GVW, *Tau Clearance Mechanisms*, in *Tau Biology*, A. Takashima, B. Wolozin, and L. Buee, Editors. 2019, Springer Singapore: Singapore. p. 57-68.
119. Majerova P, Zilkova M, Kazmerova Z, Kovac A, Paholikova K, Kovacech B, Zilka N, and Novak M, *Microglia display modest phagocytic capacity for extracellular tau oligomers.* J Neuroinflammation, 2014. **11**: p. 161. https://doi.org/10.1186/s12974-014-0161-z
120. Sultan A, Nesslany F, Violet M, Bégard S, Loyens A, Talahari S, Mansuroglu Z, Marzin D, Sergeant N, Humez S, Colin M, Bonnefoy E, Buée L, and Galas MC, *Nuclear Tau, a Key Player in Neuronal DNA Protection *.* Journal of Biological Chemistry, 2011. **286**(6): p. 4566-4575. https://doi.org/10.1074/jbc.M110.199976
121. Younas N, Saleem T, Younas A and Zerr I, *Nuclear face of Tau: an inside player in neurodegeneration.* Acta Neuropathologica Communications, 2023. **11**(1): p. 196. https://doi.org/10.1186/s40478-023-01702-x
122. Callari M, Sola M, Magrin C, Rinaldi A, Bolis M, Paganetti P, Colnaghi L, and Papin S, *Cancer-specific association between Tau (MAPT) and cellular pathways, clinical outcome, and drug response.* Scientific Data, 2023. **10**(1): p. 637. https://doi.org/10.1038/s41597-023-02543-y
123. Ye J, Wan H, Chen S and Liu G, *Targeting tau in Alzheimer's disease: from mechanisms to clinical therapy.* Neural Regeneration Research, 2024. **19**(7): p. 1489-1498. https://doi.org/10.4103/1673-5374.385847
124. Brunello CA, Merezhko M, Uronen RL and Huttunen HJ, *Mechanisms of secretion and spreading of pathological tau protein.* Cell Mol Life Sci, 2020. **77**(9): p. 1721-1744. https://doi.org/10.1007/s00018-019-03349-1
125. Clavaguera F, Bolmont T, Crowther RA, Abramowski D, Frank S, Probst A, Fraser G, Stalder AK, Beibel M, Staufenbiel M, Jucker M, Goedert M, and Tolnay M, *Transmission and spreading of tauopathy in transgenic mouse brain.* Nat Cell Biol, 2009. **11**(7): p. 909-13. https://doi.org/10.1038/ncb1901
126. Dujardin S and Hyman BT, *Tau Prion-Like Propagation: State of the Art and Current Challenges.* Adv Exp Med Biol, 2019. **1184**: p. 305-325. https://doi.org/10.1007/978-981-32-9358-8_23
127. Fuster-Matanzo A, Hernández F and Ávila J, *Tau Spreading Mechanisms; Implications for Dysfunctional Tauopathies.* Int J Mol Sci, 2018. **19**(3). https://doi.org/10.3390/ijms19030645
128. Perea JR, Bolós M and Avila J, *Microglia in Alzheimer's Disease in the Context of Tau Pathology.* Biomolecules, 2020. **10**(10): p. 1439.

129. Congdon EE, Ji C, Tetlow AM, Jiang Y and Sigurdsson EM, *Tau-targeting therapies for Alzheimer disease: current status and future directions.* Nature Reviews Neurology, 2023. **19**(12): p. 715-736. https://doi.org/10.1038/s41582-023-00883-2
130. Drath I, Richter F and Feja M, *Nose-to-brain drug delivery: from bench to bedside.* Translational Neurodegeneration, 2025. **14**(1): p. 23. https://doi.org/10.1186/s40035-025-00481-w
131. Mou Y, Song X, Wang H, Wang Y, Liu W, Yang T, M. Zhan, Hu Y, Ren C, and Song X, *Understanding the nose–brain axis and its role in related diseases: A conceptual review.* Neurobiology of Disease, 2024. **202**: p. 106690. https://doi.org/https://doi.org/10.1016/j.nbd.2024.106690
132. Djupesland PG, Messina JC and Mahmoud RA, *The Nasal Approach to Delivering Treatment for Brain Diseases: An Anatomic, Physiologic, and Delivery Technology Overview.* Therapeutic Delivery, 2014. **5**(6): p. 709-733. https://doi.org/10.4155/tde.14.41
133. Guo H, Wang G, Zhai Z, Huang J, Huang Z, Zhou Y, Xia X, Yao Z, Huang Y, Zhao Z, Wu C, and Zhang X, *Rivastigmine nasal spray for the treatment of Alzheimer's Disease: Olfactory deposition and brain delivery.* International Journal of Pharmaceutics, 2024. **652**: p. 123809. https://doi.org/https://doi.org/10.1016/j.ijpharm.2024.123809
134. Grassin-Delyle S, Buenestado A, Naline E, Faisy C, Blouquit-Laye S, Couderc LJ, Le Guen M, Fischler M, and Devillier P, *Intranasal drug delivery: an efficient and non-invasive route for systemic administration: focus on opioids.* Pharmacol Ther, 2012. **134**(3): p. 366-79. https://doi.org/10.1016/j.pharmthera.2012.03.003
135. Gaikwad S, Puangmalai N, Sonawane M, Montalbano M, Price R, Iyer MS, Ray A, Moreno S, and Kayed R, *Nasal tau immunotherapy clears intracellular tau pathology and improves cognitive functions in aged tauopathy mice.* Sci Transl Med, 2024. **16**(754): p. eadj5958. https://doi.org/10.1126/scitranslmed.adj5958
136. Madhu LN, Kodali M, Upadhya R, Rao S, Somayaji Y, Attaluri S, Shuai B, Kirmani M, Gupta S, Maness N, Rao X, Cai JJ, and Shetty AK, *Extracellular vesicles from human-induced pluripotent stem cell-derived neural stem cells alleviate proinflammatory cascades within disease-associated microglia in Alzheimer's disease.* Journal of Extracellular Vesicles, 2024. **13**(11): p. e12519. https://doi.org/https://doi.org/10.1002/jev2.12519
137. Lofts A, Abu-Hijleh F, Rigg N, Mishra RK and Hoare T, *Using the Intranasal Route to Administer Drugs to Treat Neurological and Psychiatric Illnesses: Rationale, Successes, and Future Needs.* CNS Drugs, 2022. **36**(7): p. 739-770. https://doi.org/10.1007/s40263-022-00930-4

138. Jack Jr. CR, Bennett DA, Blennow K, Carrillo MC, Dunn B, Haeberlein SB, Holtzman DM, Jagust W, Jessen F, Karlawish J, Liu E, Molinuevo JL, Montine T, Phelps C, Rankin KP, Rowe CC, Scheltens P, Siemers E, Snyder HM, and Sperling R, *NIA-AA Research Framework: Toward a biological definition of Alzheimer's disease.* Alzheimer's & Dementia, 2018. **14**(4): p. 535-562. https://doi.org/https://doi.org/10.1016/j.jalz.2018.02.018
139. Strimbu K and Tavel JA, *What are biomarkers?* Curr Opin HIV AIDS, 2010. **5**(6): p. 463-6. https://doi.org/10.1097/COH.0b013e32833ed177
140. Jamerlan AM, An SSA and Hulme JP, *Current status of fluid biomarkers for early Alzheimer's disease and FDA regulation implications.* Journal of the Neurological Sciences, 2024. **467**: p. 123325. https://doi.org/https://doi.org/10.1016/j.jns.2024.123325
141. Omar SH and Preddy J, *Advantages and Pitfalls in Fluid Biomarkers for Diagnosis of Alzheimer's Disease.* J Pers Med, 2020. **10**(3). https://doi.org/10.3390/jpm10030063
142. Bittner T, *What Are the Remaining Challenges before Blood-Based Biomarkers for Alzheimer's Disease Can Be Used in Clinical Practice?* The Journal of Prevention of Alzheimer's Disease, 2022. **9**(4): p. 567-568. https://doi.org/10.14283/jpad.2022.89
143. Francavilla B, Velletrani G, Fiorelli D, Omer GL, Passali FM, Nuccetelli M, and Di Girolamo S, *Olfactory cleft brushing: A minimally invasive tool for biomarker analysis in rhinology.* American Journal of Otolaryngology, 2025. **46**(1): p. 104589. https://doi.org/https://doi.org/10.1016/j.amjoto.2024.104589
144. Lavoie J, Gassó Astorga P, Segal-Gavish H, Wu YC, Chung Y, Cascella NG, Sawa A, and Ishizuka K, *The Olfactory Neural Epithelium As a Tool in Neuroscience.* Trends Mol Med, 2017. **23**(2): p. 100-103. https://doi.org/10.1016/j.molmed.2016.12.010
145. Santillán-Morales V, Rodriguez-Espinosa N, Muñoz-Estrada J, Alarcón-Elizalde S, Acebes Á and Benítez-King G, *Biomarkers in Alzheimer's Disease: Are Olfactory Neuronal Precursors Useful for Antemortem Biomarker Research?* Brain Sciences, 2024. **14**(1): p. 46.
146. Brozzetti L, Sacchetto L, Cecchini MP, Avesani A, Perra D , Bongianni M, Portioli C, Scupoli M, Ghetti B, Monaco S, Buffelli M, and Zanusso G, *Neurodegeneration-Associated Proteins in Human Olfactory Neurons Collected by Nasal Brushing.* Frontiers in Neuroscience, 2020. **14**(145).
147. Jafek BW, Murrow B, Michaels R, Restrepo D and Linschoten M, *Biopsies of Human Olfactory Epithelium.* Chemical Senses, 2002. **27**(7): p. 623-628. https://doi.org/10.1093/chemse/27.7.623
148. Arnold SE, Lee EB, Moberg PJ, Stutzbach L, Kazi H, Han LY, Lee VM, and Trojanowski JQ, *Olfactory epithelium amyloid-beta and paired helical*

filament-tau pathology in Alzheimer disease. Ann Neurol, 2010. **67**(4): p. 462-9. https://doi.org/10.1002/ana.21910

149. Riquelme A, Valdés-Tovar M, Ugalde O, Maya-Ampudia V, Fernández M, Mendoza-Durán L, Rodríguez-Cárdenas L, and Benítez-King G, *Potential Use of Exfoliated and Cultured Olfactory Neuronal Precursors for In Vivo Alzheimer's Disease Diagnosis: A Pilot Study.* Cellular and Molecular Neurobiology, 2020. **40**(1): p. 87-98. https://doi.org/10.1007/s10571-019-00718-z
150. Jankowsky JL and Zheng H, *Practical considerations for choosing a mouse model of Alzheimer's disease.* Mol Neurodegener, 2017. **12**(1): p. 89. https://doi.org/10.1186/s13024-017-0231-7
151. Holmes BB, Furman JL, Mahan TE, Yamasaki TR, Mirbaha H, Eades WC, Belaygorod L, Cairns NJ, Holtzman DM, and Diamond MI, *Proteopathic tau seeding predicts tauopathy in vivo.* Proceedings of the National Academy of Sciences, 2014. **111**(41): p. E4376-E4385. https://doi.org/doi:10.1073/pnas.1411649111
152. Iba M, Guo JL, McBride JD, Zhang B, Trojanowski JQ and Lee VM, *Synthetic tau fibrils mediate transmission of neurofibrillary tangles in a transgenic mouse model of Alzheimer's-like tauopathy.* J Neurosci, 2013. **33**(3): p. 1024-37. https://doi.org/10.1523/jneurosci.2642-12.2013
153. Yoshiyama Y, Higuchi M, Zhang B, Huang SM, Iwata N, Saido TC, Maeda J, Suhara T, Trojanowski JQ, and Lee VMY, *Synapse loss and microglial activation precede tangles in a P301S tauopathy mouse model.* Neuron, 2007. **53**(3): p. 337-351. https://doi.org/10.1016/j.neuron.2007.01.010
154. Ahmad F, Mein H, Jing Y, Zhang H and Liu P, *Behavioural Functions and Cerebral Blood Flow in a P301S Tauopathy Mouse Model: A Time-Course Study.* Int J Mol Sci, 2021. **22**(18). https://doi.org/10.3390/ijms22189727
155. Sun Y, Guo Y, Feng X, Jia M, Ai N, Dong Y, Zheng Y, Fu L, Yu B, Zhang H, Wu J, Yu X, Wu H, and Kong W, *The behavioural and neuropathologic sexual dimorphism and absence of MIP-3α in tau P301S mouse model of Alzheimer's disease.* Journal of Neuroinflammation, 2020. **17**(1): p. 72. https://doi.org/10.1186/s12974-020-01749-w
156. Cao Q, Kumar M, Frazier A, Williams JB, Zhao S and Yan Z, *Longitudinal characterization of behavioral, morphological and transcriptomic changes in a tauopathy mouse model.* Aging 2023. **15**: p. 11697-11719. https://doi.org/https://doi.org/10.18632/aging.205057
157. Takeuchi H, Iba M, Inoue H, Higuchi M, Takao K, Tsukita K, Karatsu Y, Iwamoto Y, Miyakawa T, Suhara T, Trojanowski JQ, Lee VM, and Takahashi R, *P301S mutant human tau transgenic mice manifest early symptoms of human tauopathies with dementia and altered sensorimotor gating.* PLoS One, 2011. **6**(6): p. e21050. https://doi.org/10.1371/journal.pone.0021050

158. Greenberg SG, Davies P, Schein JD and Binder LI, *Hydrofluoric acid-treated tau PHF proteins display the same biochemical properties as normal tau.* J Biol Chem, 1992. **267**(1): p. 564-9.
159. Lundström JN, Boesveldt S and Albrecht J, *Central Processing of the Chemical Senses: an Overview.* ACS Chem Neurosci, 2011. **2**(1): p. 5-16. https://doi.org/10.1021/cn1000843
160. Amani M, Lauterborn JC, Le AA, Cox BM, Wang W, Quintanilla J, Cox CD, Gall CM, and Lynch G, *Rapid Aging in the Perforant Path Projections to the Rodent Dentate Gyrus.* J Neurosci, 2021. **41**(10): p. 2301-2312. https://doi.org/10.1523/jneurosci.2376-20.2021
161. McBride K, Slotnick B and Margolis FL, *Does intranasal application of zinc sulfate produce anosmia in the mouse? An olfactometric and anatomical study.* Chem Senses, 2003. **28**(8): p. 659-70. https://doi.org/10.1093/chemse/bjg053
162. Matulionis DH, *Ultrastructural study of mouse olfactory epithelium following destruction by ZnSO4 and its subsequent regeneration.* Am J Anat, 1975. **142**(1): p. 67-89. https://doi.org/10.1002/aja.1001420106
163. Narvaes RF and Furini CRG, *Role of Wnt signaling in synaptic plasticity and memory.* Neurobiology of Learning and Memory, 2022. **187**: p. 107558. https://doi.org/https://doi.org/10.1016/j.nlm.2021.107558
164. You JE, Kim EJ, Kim HW, Kim JS, Kim K and Kim PH, *Exploring the Role of Guanylate-Binding Protein-2 in Activated Microglia-Mediated Neuroinflammation and Neuronal Damage.* Biomedicines, 2024. **12**(5). https://doi.org/10.3390/biomedicines12051130
165. Gillet LC, Navarro P, Tate S, Röst H, Selevsek N, Reiter L, Bonner R, and Aebersold R, *Targeted Data Extraction of the MS/MS Spectra Generated by Data-independent Acquisition: A New Concept for Consistent and Accurate Proteome Analysis*.* Molecular & Cellular Proteomics, 2012. **11**(6): p. O111.016717. https://doi.org/https://doi.org/10.1074/mcp.O111.016717
166. Kovács T, Cairns NJ and Lantos PL, *Olfactory centres in Alzheimer's disease: olfactory bulb is involved in early Braak's stages.* NeuroReport, 2001. **12**(2): p. 285-288.
167. Ohm TG and Braak H, *Olfactory bulb changes in Alzheimer's disease.* Acta Neuropathologica, 1987. **73**(4): p. 365-369. https://doi.org/10.1007/BF00688261
168. Martel G, Simon A, Nocera S, Kalainathan S, Pidoux L, Blum D, Leclère-Turbant S, Diaz J, Geny D, Moyse E, Videau C, Buée L, Epelbaum J, and Viollet C, *Aging, but not tau pathology, impacts olfactory performances and somatostatin systems in THY-Tau22 mice.* Neurobiol Aging, 2015. **36**(2): p. 1013-28. https://doi.org/10.1016/j.neurobiolaging.2014.10.033

169. Ramirez DMO, Whitesell JD, Bhagwat N, Thomas TL, Ajay AD, Nawaby A, Delatour B, Bay S, LaFaye P, Knox JE, Harris JA, Meeks JP, and Diamond MI, *Endogenous pathology in tauopathy mice progresses via brain networks.* bioRxiv, 2023. https://doi.org/10.1101/2023.05.23.541792
170. Chapuis J, Cohen Y, He X, Zhang Z, Jin S, Xu F, and Wilson DA, *Lateral entorhinal modulation of piriform cortical activity and fine odor discrimination.* J Neurosci, 2013. **33**(33): p. 13449-59. https://doi.org/10.1523/jneurosci.1387-13.2013
171. Zhou G, Lane G, Cooper SL, Kahnt T and Zelano C, *Characterizing functional pathways of the human olfactory system.* Elife, 2019. **8**. https://doi.org/10.7554/eLife.47177
172. Fujishiro H, Tsuboi Y, Lin WL, Uchikado H and Dickson DW, *Co-localization of tau and alpha-synuclein in the olfactory bulb in Alzheimer's disease with amygdala Lewy bodies.* Acta Neuropathologica, 2008. **116**(1): p. 17-24. https://doi.org/10.1007/s00401-008-0383-1
173. Ubeda-Bañon I, Saiz-Sanchez D, Flores-Cuadrado A, Rioja-Corroto E, Gonzalez-Rodriguez M, Villar-Conde S, Astillero-Lopez V, Cabello-de la Rosa JP, Gallardo-Alcañiz MJ, Vaamonde-Gamo J, Relea-Calatayud F, Gonzalez-Lopez L, Mohedano-Moriano A, Rabano A, and Martinez-Marcos A, *The human olfactory system in two proteinopathies: Alzheimer's and Parkinson's diseases.* Transl Neurodegener, 2020. **9**(1): p. 22. https://doi.org/10.1186/s40035-020-00200-7
174. Rey NL, Wesson DW and Brundin P, *The olfactory bulb as the entry site for prion-like propagation in neurodegenerative diseases.* Neurobiology of Disease, 2018. **109**: p. 226-248. https://doi.org/https://doi.org/10.1016/j.nbd.2016.12.013
175. Diez I, Ortiz-Terán L, Ng TSC, Albers MW, Marshall G, Orwig W, Kim C, Bueichekú E, Montal V, Olofsson J, Vannini P, El Fahkri G, Sperling R, Johnson K, Jacobs HIL, and Sepulcre J, *Tau propagation in the brain olfactory circuits is associated with smell perception changes in aging.* Nature Communications, 2024. **15**(1): p. 4809. https://doi.org/10.1038/s41467-024-48462-3
176. Harding JW, Getchell TV and Margolis FL, *Denervation of the primary olfactory pathway in mice. V. Long-term effect of intranasal ZnSO4 irrigation on behavior, biochemistry and morphology.* Brain Res, 1978. **140**(2): p. 271-85. https://doi.org/10.1016/0006-8993(78)90460-2
177. Laska M, *Human and Animal Olfactory Capabilities Compared*. 2017. p. 675-689.
178. Lee SH, Bae E, Park SJ and Lee S, *Microglia-driven inflammation induces progressive tauopathies and synucleinopathies.* Experimental & Molecular

Medicine, 2025. **57**(5): p. 1017-1031. https://doi.org/10.1038/s12276-025-01450-z

179. Maphis N, Xu G, Kokiko-Cochran ON, Jiang S, Cardona A, Ransohoff RM, Lamb BT, and Bhaskar K, *Reactive microglia drive tau pathology and contribute to the spreading of pathological tau in the brain.* Brain, 2015. **138**(6): p. 1738-1755. https://doi.org/10.1093/brain/awv081
180. Chen Y and Yu Y, *Tau and neuroinflammation in Alzheimer's disease: interplay mechanisms and clinical translation.* Journal of Neuroinflammation, 2023. **20**(1): p. 165. https://doi.org/10.1186/s12974-023-02853-3
181. Kinney JW, Bemiller SM, Murtishaw AS, Leisgang AM, Salazar AM and Lamb BT, *Inflammation as a central mechanism in Alzheimer's disease.* Alzheimer's & Dementia: Translational Research & Clinical Interventions, 2018. **4**(1): p. 575-590. https://doi.org/https://doi.org/10.1016/j.trci.2018.06.014
182. Ising C, Venegas C, Zhang S, Scheiblich H, Schmidt SV, Vieira-Saecker A, Schwartz S, Albasset S, McManus RM, Tejera D, Griep A, Santarelli F, Brosseron F, Opitz S, Stunden J, Merten M, Kayed R, Golenbock DT, Blum D, Latz E, Buée L, and Heneka MT, *NLRP3 inflammasome activation drives tau pathology.* Nature, 2019. **575**(7784): p. 669-673. https://doi.org/10.1038/s41586-019-1769-z
183. Kirkby M, Enosi Tuipulotu D, Feng S, Lo Pilato J and Man SM, *Guanylate-binding proteins: mechanisms of pattern recognition and antimicrobial functions.* Trends in Biochemical Sciences, 2023. **48**(10): p. 883-893. https://doi.org/10.1016/j.tibs.2023.07.002
184. Ngo CC and Man SM, *Mechanisms and functions of guanylate-binding proteins and related interferon-inducible GTPases: Roles in intracellular lysis of pathogens.* Cell Microbiol, 2017. **19**(12). https://doi.org/10.1111/cmi.12791
185. Stancu I, Cremers N, Vanrusselt H, Couturier J, Vanoosthuyse A, Kessels S, Lodder C, Brône B, Huaux F, Octave J, Terwel D, and Dewachter I, *Aggregated Tau activates NLRP3–ASC inflammasome exacerbating exogenously seeded and non-exogenously seeded Tau pathology in vivo.* Acta Neuropathologica, 2019. **137**(4): p. 599-617. https://doi.org/10.1007/s00401-018-01957-y
186. Xu W, Huang Y and Zhou R, *NLRP3 inflammasome in neuroinflammation and central nervous system diseases.* Cellular & Molecular Immunology, 2025. **22**(4): p. 341-355. https://doi.org/10.1038/s41423-025-01275-w
187. LaFever BJ and Imamura F, *Effects of nasal inflammation on the olfactory bulb.* J Neuroinflammation, 2022. **19**(1): p. 294. https://doi.org/10.1186/s12974-022-02657-x

188. Alves RL, Gonçalves A, Voytyuk I and Harrison DC, *Behaviour profile characterization of PS19 and rTg4510 tauopathy mouse models: A systematic review and a meta-analysis.* Experimental Neurology, 2025. **389**: p. 115234. https://doi.org/https://doi.org/10.1016/j.expneurol.2025.115234

189. Gallyas F, *Silver staining of Alzheimer's neurofibrillary changes by means of physical development.* Acta Morphol Acad Sci Hung, 1971. **19**(1): p. 1-8.

Appendix I

Appendices

Supplementary Information: An Early Olfactory Transcriptomic Signature of Tauopathy: Gbp2b Emerges as a Candidate Biomarker of Tau-Driven Neuroinflammation

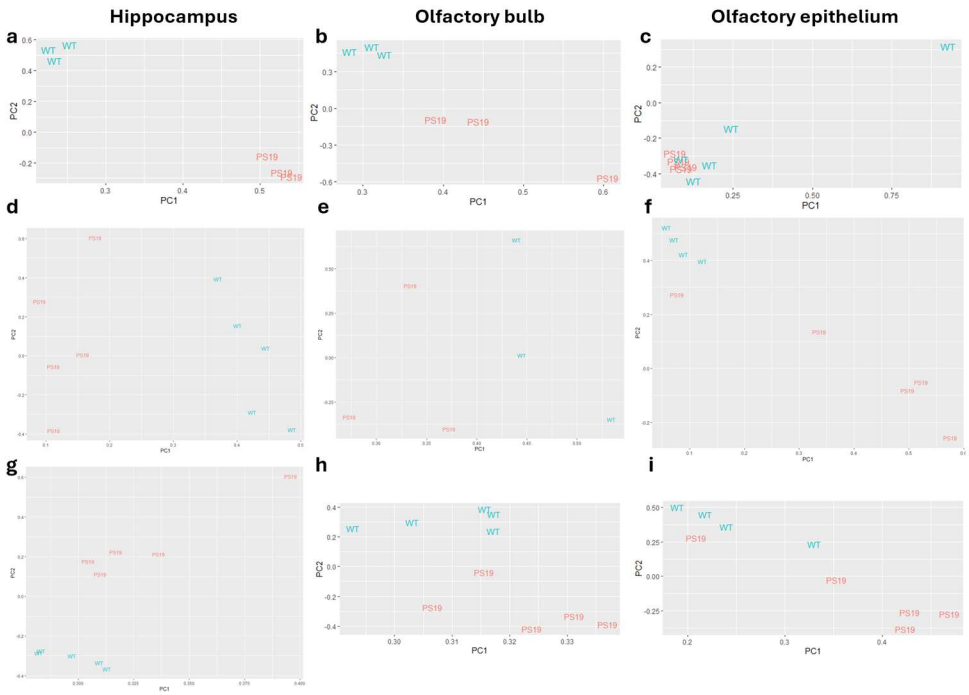

Fig. S1 PCA of normalized gene expression in hippocampus (a, d, g), OB (b, e, h), and OE (c, f, i) from PS19 and WT mice at 3 (a-c), 6 (d-f), and 9 (g-i) months. Each point represents a sample, colored by genotype (PS19 in pink, WT in blue). The first two principal components (PC1 and PC2) are shown.

Appendix I

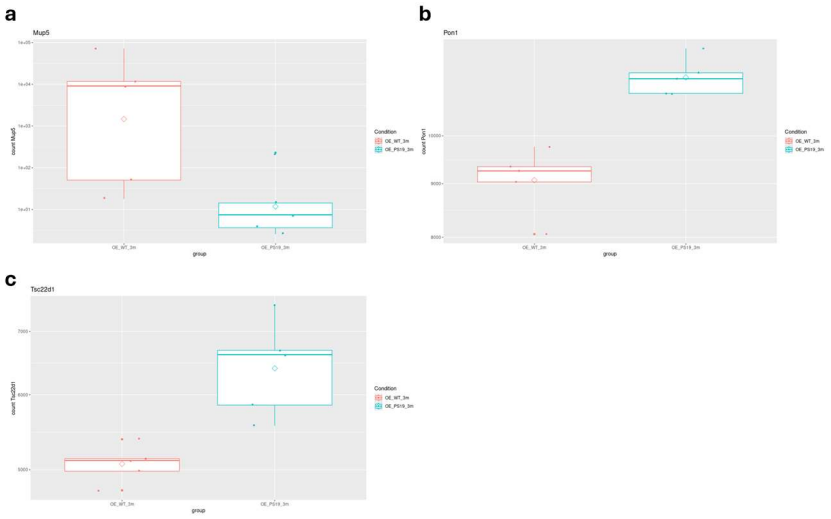

Fig. S2 Expression levels of *Mup5 (a), Pon1 (b)*, and *Tsc22d1 (c)* in the OE of WT and PS19 mice. Boxplots show normalized expression counts for three genes—*Mup5, Pon1,* and *Tsc22d1*—in two experimental groups: OE_WT_3m (red) and OE_Ps19_3m (cyan). Each plot displays the distribution of gene expression levels across biological replicates. Boxes represent the interquartile range (IQR), with horizontal lines indicating the median and diamonds showing the mean. Whiskers extend to 1.5 times the IQR, and individual data points are overlaid to illustrate sample variation.

Appendix II

Academic *Curriculum Vitae*

1. Personal Information

Name: Dourte Marion

Nationality: Belgian

Date of birth: 06.10.1998

2. Education

PhD in biomedical and pharmaceutical sciences 2021-2025

University of Louvain, Institute of Neuroscience, Aging and Dementia (Pr. Pascal Kienlen-Campard)

Funding by ARC (Towards the development of new, non-invasive diagnostic tools for neurodegenerative pathologies, November 2020)

Biomedical Sciences in Preclinical Drug Development MA 2019-2021

University of Namur

Magna cum laude

Biomedical sciences BA 2016-2019

University of Namur

Cum laude

Appendix II

3. Professional Experience

PhD researcher in biomedical and pharmaceutical sciences 2021-2025

UCLouvain, IoNS, CEMO, AGAD – Pr. Pascal Kienlen-Campard

Project: The Nose as a Neurological Frontline: Unraveling Tauopathy through the Olfactory Gateway

European graduate school of neuroscience (EURON) representative for UCLouvain 2022-2025

Professional internship (4 months) 2021

UCLouvain, IoNS, CEMO, AGAD – Pr. Pascal Kienlen-Campard, Dr. Emilien Boyer

Project: Aβ oligomers production using cell transfection and infection, in the frame of Alzheimer's disease

Master thesis (10 months) 2020-2021

UNamur, Namur Research Institute for Life Sciences, Laboratoire Neurodégénérescence et Régénération – Pr. Charles Nicaise, Lindsay Sprimont

Project: Inhibition of System Xc- in microglia using pharmacological inhibitors and RNA interference

Appendix II

4. Scientific Publications

As stated in the results section, the observations reported in this thesis are part of two main research articles:

1. **Dourte M** *et al.,* 2025 (Appendix **III**)

Reference: Dourte M, Paître E, Bouchoucha M, Boyer E, Tomé SO, Doeraene E, Huart C, Leroy K, Thal DR, Decottignies A, Hanseeuw B, Suelves N, Kienlen-Campard P. The olfactory epithelium: a critical gateway for pathological tau propagation and a target for mitigating tauopathy in the central nervous system. Acta Neuropathol. 2025 Jun 19;149(1):64. doi: 10.1007/s00401-025-02902-6. PMID: 40536690; PMCID: PMC12179005.

2. **Dourte M***, Ayeh B* *et al*., 2025

Reference: Dourte M*, Bouloki A*, Dieu M, Magomadov M, Paître E, Suelves N, Renard P, Kienlen-Campard P. An Early Olfactory Transcriptomic Signature of Tauopathy: Gbp2b Emerges as a Candidate Biomarker of Tau-Driven Neuroinflammation. BioRxiv 2025.07.01.662324; doi: https://doi-org/10.1101/2025.07.01.662324.

Besides, participation in other projects has led to the following publication inside the research team:

3. Boyer E, Deltenre L, **Dourte M** *et al*., 2024

Reference: Boyer E, Deltenre L, Dourte M, Colmant L, Paître E, Sleegers K, Suelves N, Hanseeuw B, Kienlen-Campard P. Comparison of plasma soluble and extracellular vesicles-associated biomarkers in Alzheimer's disease patients and cognitively normal individuals. Alzheimers Res Ther. 2024 Jun

28;16(1):141. doi: 10.1186/s13195-024-01508-6. PMID: 38943196; PMCID: PMC11212434.

5. Scientific Communications

- EURON PhD Days 2023 – **Poster** - "Outbreak of tauopathy in the olfactory system of PS19 mice: an early marker for Alzheimer's disease diagnosis"
- IONS Young Researchers Day 2023 – **Poster** - "Outbreak of tauopathy in the olfactory system of PS19 mice: an early marker for Alzheimer's disease diagnosis"
- Belgian Society for Neuroscience meeting 2023 – **Poster** - "Outbreak of tauopathy in the olfactory system of PS19 mice: an early marker for Alzheimer's disease diagnosis"
- AAIC 2023 – Amsterdam – **Poster** - "Outbreak of tauopathy in the olfactory system of PS19 mice: an early marker for Alzheimer's disease diagnosis"
- EURON PhD Days 2024 – **Oral Presentation** – "Early onset of tau pathology in the olfactory system of PS19 mice: A pathway for the progression of tauopathy in the central nervous system"
- CEMO Seminar – **Oral Presentation** – "Early onset of tau pathology in the olfactory system of PS19 mice: A pathway for the progression of tauopathy in the central nervous system"
- IONS Young Researchers Day 2024 – **Oral Presentation** – "Early onset of tau pathology in the olfactory system of PS19 mice: A pathway for the progression of tauopathy in the central nervous system", *Best presentation award*
- FENS 2024 – Vienna – **Poster** – "Early onset of tau pathology in the olfactory system of PS19 mice: A pathway for the progression of tauopathy in the central nervous system"
- URBC Seminar (UNamur) – **Oral Presentation** – "Early onset of tau pathology in the olfactory system of PS19 mice: A pathway for the progression of tauopathy in the central nervous system"

Appendix II

- EURON PhD Days 2025 – **Poster** – “Early onset of tau pathology in the olfactory system of PS19 mice: A pathway for the progression of tauopathy in the central nervous system”
- Tau Global Conference 2025 – London – **Poster** – “Early onset of tau pathology in the olfactory system of PS19 mice: A pathway for the progression of tauopathy in the central nervous system”
- ALZAD meeting 2025 – **Oral Presentation** – “The Olfactory Epithelium: A Critical Gateway for Pathological Tau Propagation and a Target for Mitigating Tauopathy in the Central Nervous System”
- Brains United 2025 – **Oral Presentation** – “Unraveling Tauopathy through the Olfactory Gateway”

Appendix III

Acta Neuropathologica (2025) 149:64
https://doi.org/10.1007/s00401-025-02902-6

ORIGINAL PAPER

The olfactory epithelium: a critical gateway for pathological tau propagation and a target for mitigating tauopathy in the central nervous system

Marion Dourte[1] · Esther Paître[1] · Mongia Bouchoucha[1] · Emilien Boyer[1] · Sandra O. Tomé[2] · Emilie Doeraene[3] · Caroline Huart[4,5] · Karelle Leroy[3] · Dietmar Rudolf Thal[2,6] · Anabelle Decottignies[7] · Bernard Hanseeuw[8,9] · Nuria Suelves[1] · Pascal Kienlen-Campard[1]

Received: 5 March 2025 / Revised: 26 May 2025 / Accepted: 27 May 2025
© The Author(s) 2025

Abstract
Olfactory impairment is a recognized early indicator of neurodegenerative diseases (NDs), such as Alzheimer's disease (AD). Intracellular aggregates of hyperphosphorylated tau protein, referred to as neurofibrillary tangles (NFTs), are a hallmark of AD. NFTs are found in the olfactory bulb (OB) and entorhinal cortex (EC), both crucial for processing olfactory information. We explored the hypothesis that typical tau lesions could appear early and progress along olfactory regions to reach connected areas critically affected in AD (e.g., EC and hippocampal formation). To that end, we used transgenic PS19 mice expressing mutated human tau protein (1N4R isoform, P301S mutation). They recapitulate major phenotypes of AD, such as accumulation of NFTs, synaptic dysfunction, cognitive impairment, and neuronal loss. The presence of pathological hyperphosphorylated human tau protein (pTau) was monitored in olfactory regions: olfactory epithelium (OE), OB, piriform cortex (PC), and in connected regions of the hippocampal formation (hippocampus and EC). pTau was detected in the OE's middle stratum and in the OB's olfactory nerve layer (ONL) at 1.5 months. At 6 months of age, tau accumulations were found in the PC and EC, along with the CA3 region and dentate gyrus of the hippocampus. We found that olfactory function remained unaffected in PS19 mice, despite the presence of tau pathology in key regions of the olfactory system. Targeted treatments ($ZnSO_4$ and AAVs) were applied at the OE level to assess the impact on tau pathology in the CNS. Complete stripping of the OE by intranasal administration of $ZnSO_4$ led to a significant reduction in pretangle-like tau pathology within the PC, amygdala, and EC of 6-month-old PS19 mice. Finally, we observed in human *postmortem* samples that pTau signal was present in the olfactory regions (OE and OB) of patients at early Braak stages (I/II). Based on these observations, we propose that pTau could appear, due to aging or environmental agents, in the OE and subsequently spread in a prion-like manner to the hippocampal formation along neuroanatomical connections. These findings also indicate the interest of the OE as a target for intervention aimed at mitigating the progression of tauopathy in the CNS.

Keywords Tau pathology · Olfactory system · Tau spreading · Olfaction

Abbreviations

AAVs	Adeno-associated viruses
ABs	Axon bundles
AD	Alzheimer's disease
CNS	Central nervous system
DG	Dentate gyrus
EC	Entorhinal cortex
EPL	External plexiform layer
FTLD	Frontotemporal lobe degeneration
GCL	Granular cell layer
IPL	Internal plexiform layer
MAPT	Microtubule-associated protein tau
MCI	Mild cognitive impairment
MCL	Mitral cell layer
NDs	Neurodegenerative diseases
NFTs	Neurofibrillary tangles
OB	Olfactory bulb
OC	Olfactory cortex
OE	Olfactory epithelium
OI	Olfactory impairment
OMP	Olfactory mature protein
ONL	Olfactory nerve layer
OS	Olfactory system

Extended author information available on the last page of the article

Published online: 19 June 2025

Appendix III

OSNs	Olfactory sensory neurons
PC	Piriform cortex
PHF	Paired helical filaments
RE	Respiratory epithelium
WT	Wild type

Introduction

Olfactory function deteriorates with age, likely due to a combination of peripheral and central alterations. One contributing factor is the gradual replacement of the olfactory epithelium (OE)—which resides in the nasal cavities and houses olfactory sensory neurons (OSNs)—by respiratory epithelium [14, 35]. Olfactory dysfunction is a common and early symptom of many neurodegenerative diseases (NDs), including Parkinson's disease (PD), Alzheimer's disease (AD), and frontotemporal lobe degeneration (FTLD) [7, 35]. FTLD and AD are primary and secondary tauopathies—characterized by abnormal tau protein aggregation and deposition in the brain [49]. Whereas primary tauopathies are defined by tau accumulation as the main histopathological hallmark, in secondary tauopathies, another partner is necessary to drive the neurodegeneration, like Aβ in AD [22].

Tau is predominantly found in neuronal axons associated with microtubules. It is known to play a crucial role in microtubule dynamics and stabilization to preserve the integrity of the cell's cytoskeleton [29]. In NDs, tau hyperphosphorylation impairs its ability to associate with microtubules. Hyperphosphorylated tau proteins form the core of neurofibrillary tangles (NFTs), which are pathological hallmarks of various NDs, including AD [28]. The gradual deposition of hyperphosphorylated tau aggregates within specific areas is instrumental to AD pathology. The distribution pattern of tau lesions progresses according to a sequence known as Braak staging [11, 12]. In Braak stages I/II, NFTs are confined mainly to the (trans-)entorhinal region in the temporal lobe. Stages II/III involve limbic regions such as the hippocampal formation and parahippocampal areas, and extensive neocortical involvement is observed in the later stages IV–VI [11, 12].

Several studies have demonstrated that approximately 90% of AD patients suffer from olfactory dysfunction in the early stages of the disease, characterized by decreased odor discrimination and identification, increased olfactory threshold, and olfactory memory loss [5, 8, 74]. Olfactory dysfunction is thus considered a prodromal symptom of AD, preceding cognitive impairment [41, 60, 71]. In addition, *postmortem* analysis of olfactory regions in AD patients showed the presence of tau pathology in the olfactory bulb (OB), anterior nucleus, and piriform cortex (PC) [58, 71]. Olfactory dysfunction and the accumulation of tau pathology in the OB progressively worsen with the severity of Alzheimer's disease and directly correlate with Braak stage progression [7, 8, 65]. Importantly, tau pathology is observed in the olfactory system in all definite AD cases—diagnosis confirmed by neuropathological evidence—and in more than 1/3 of elderly individuals with or without mild cognitive impairment associated with Braak stage II [6].

Since the olfactory system is highly conserved across species [66, 74], mouse models are relevant tools to investigate how impairment of the olfactory system could relate to typical features of human NDs. PS19 mice, also known as Tau P301S mice, were first described as a transgenic tauopathy mouse model by Yoshiyama et al. [72]. They express mutant human microtubule-associated protein tau (MAPT) under the control of the mouse prion protein promoter (*Prnp*). The transgene encodes the 1N4R isoform harboring the disease-associated P301S mutation [72]. Progressive accumulation of NFTs has been observed in the neocortex, amygdala, hippocampus, brainstem, and spinal cord of PS19 mice from 6 months of age. Neurodegeneration starts around 9 months, particularly in the hippocampus [72]. Behavioral abnormalities recapitulating the neurological deficits observed in human tauopathies with dementia were measured in these mice using numerous tests, including the open-field test, elevated plus maze test, hot-plate test, Y-maze test, Barnes maze test, Morris water maze test, and contextual fear conditioning test [1, 61, 63]. Previous studies also showed that PS19 mice exhibited progressive neuronal cell loss in the OB and PC, along with increased latency in finding buried food [74].

The OE is the main olfactory receptor structure, and forms the olfactory system along with other regions, such as the OB, PC, amygdala, and EC. Located in the nasal cavity, the OE consists of three different cell types: OSNs, supporting cells, and basal stem cells [9, 57]. The stem cells are divided into globose basal cells (GBCs), which serve as active progenitors for OSN regeneration throughout life [9, 14, 64], and horizontal basal cells (HBCs), which function as reserve stem cells [9, 57]. The somas of the OSNs are located at an intermediate depth within the OE, while their axons converge to form the axon bundles (AB). These bundles cross the cribriform plate and constitute the olfactory nerve that reaches the outer layer of the OB [14]. The respiratory epithelium, which lacks neurons, is present in the nasal cavities along with the OE. Human olfactory mucosa biopsy showed that aging leads to the replacement of the OE by respiratory epithelium [14].

In mammals, the OB structure is characterized by six cell layers, arranged from the periphery to the center: the olfactory nerve layer (ONL), the glomerular layer (GL), the external plexiform layer (EPL), the mitral cell layer (MCL), the internal plexiform layer (IPL), and the granular cell layer (GCL) [59]. The ONL contains the projections of OSNs, which form synapses with glomerular cells (mitral cells, tufted cells, and

Appendix III

periglomerular cells) in the GL. The mitral and tufted cells, which are the main output neurons of the OB, are involved in the transmission of olfactory information to other regions of the central nervous system (CNS) including the PC [59]. The PC is part of the olfactory cortex and is known to play a critical role in odor encoding and memory [74]. Projections of the OB reach the amygdala via the PC or directly to specific amygdala subregions via monosynaptic projections [47]. Other projections from the OB also reach the EC which is involved in both olfactory learning and memory [74]. The EC sends projections to the dentate gyrus and the CA3 region of the hippocampus, via the perforant path, which originates from layer II of the EC. Neurons from the dentate gyrus (DG) also project to the CA3 region via mossy fibers. Finally, neurons from the CA3 region project to the CA1 region via Schaffer collaterals [62]. This suggests that the progression of pathological forms of tau along the olfactory system could contribute to the appearance of lesions in regions particularly affected by tauopathy in AD (e.g., EC) at the earliest stages.

In this study, we used the PS19 model to monitor the progression of tau pathology across key regions of the olfactory and central nervous systems, including the OE, OB, PC, EC, and hippocampus. We examined the spread of tau pathology within these regions and evaluated its impact on olfactory function. Our findings revealed a distinct pattern of tau propagation in the olfactory system, with aberrant tau phosphorylation first detected in the OE, OB, and EC at 1.5 months. This pathology later appeared in the PC at 3 months and typical NFT-like tau accumulations were observed in both the PC and the EC from 6 months onward. These finding parallels tau pathology observed in the olfactory system of patients with AD [7, 8]. We then investigated whether zinc sulfate ($ZnSO_4$) intranasal treatment, aimed at removing accumulated pathological tau in the OE, could mitigate tau pathology in vulnerable regions of the CNS. Irrigation of the olfactory organ with $ZnSO_4$ triggers the degeneration of OSNs, although the tissue regenerates within a month [34, 45]. Mice repeatedly treated with intranasal irrigation of $ZnSO_4$ at 1.5, 2.5, and 4 months showed a significant decrease in NFT-like tau accumulations in the PC, EC, and amygdala at 6 months. This striking observation indicates that the accumulation of pathological tau in the OE could play a causal role in the progression of tau pathology observed in regions of the CNS involved in the processing of olfactory information, and particularly the EC and amygdala, which are affected in the early/intermediate stages of AD [12, 17, 52].

Materials and methods

Animals

PS19 mice were obtained from the Jackson Laboratory (B6; C3-Tg(Prnp-MAPT*P301S)PS19Vle/J; Strain #008169) and maintained on a C57BL/6 genetic background. Wild-type (WT) and heterozygous PS19 mice were crossed to obtain WT and heterozygous PS19 mice at 1.5, 3, 6, and 9 months of age. The genotype was determined by PCR analysis of ear/tail DNA. The animals were housed in ventilated cages, maintained on a 12-h light/dark cycle, and provided *ad libitum* access to food and water. All the mice were individually identified by ear tagging and their general health was closely monitored. All experiments involving mice were conducted with prior approval from the ethical committee at UCLouvain (2021/UCL/MD/018).

Tissue harvesting

All the mice were sacrificed by cervical dislocation. The cranium was opened, and the brain was cut sagittally in half. Next, the two OBs and the two hippocampi were collected. The mouse snout was then recovered and cut along the midsagittal plane between the two nasal cavities. The OE was recovered from these cavities, distinguishable by its characteristic yellow color. The harvested tissues were snap-frozen by immersion in isopentane maintained at freezing temperature and then stored at − 80 °C until use.

Sample preparation for immunostaining

Decalcification

For immunostaining experiments, decalcification was needed to preserve the OE structure because of its localization within the nasal cavity. The skin, eyes, and lower jaw were removed from the mouse head. The head was directly rinsed in phosphate-buffered saline (PBS) and subsequently fixed with modified Davidson's fixative (mDF) (37% formalin, ethanol, glacial acetic acid, and water) for 4 days under agitation at room temperature (RT). The heads were rinsed for 24 h in PBS and transferred to OsteoRAL R (RAL Diagnostics, #320715-2500), a commercial decalcifier, for 5 days under agitation at RT. After decalcification, the mouse heads were embedded in paraffin. The decalcification method allowed us to obtain coronal sections spanning from the OE to the hippocampus/EC for each mouse.

Paraffin sections

Paraffin-embedded sections were obtained via a microtome. Coronal sections of 5 µm and 10 µm thickness were placed on Superfrost slides for IF and IHC, respectively. The coronal brain sections were collected according to standard stereotaxic coordinates relative to Bregma, as defined in the *Mouse Brain Atlas* by Paxinos and Franklin. Sections ranging from approximately Bregma − 1.82 to − 2.18 mm were used to analyze the hippocampal formation, Bregma

Appendix III

− 1.94 mm to analyze the PC and Bregma − 3.08 mm for the EC.

Immunohistochemistry, histological staining, and immunofluorescence

For immunohistochemistry, paraffin-embedded sections of 10 µm were immersed in different solutions as follows: 2×5 min in toluene, 2×2 min in absolute isopropanol, and 30 min in 0.3% H_2O_2 in methanol. The slides were finally placed in distilled water. Then, 1X Tris-buffered saline (TBS) was placed on each paraffin section for 10 min. This washing step was repeated two times.

Then, the sections were blocked with 10% normal goat serum (NGS) diluted in TBS for 1 h at room temperature. Primary antibodies of interest were prepared in 1% NGS (Supplementary Table s1), placed on each section, and left overnight at RT. The negative control was incubated with 1% NGS only.

The next day, the sections were rinsed three times for 10 min with TBS 1X. The secondary antibodies were diluted with TBS 1X and put on the corresponding sections for 30 min at room temperature. This step was followed by three TBS rinses. Stabilized Elite ABC reagent (Vector Laboratories, #PK-7100) was added to each section for 30 min. After another washing step, ImmPACT® DAB EqV Substrate (Vector Laboratories, #VEC.SK-4103-100) was prepared. Equivalent amounts of reagent 1 and reagent 2 were mixed and incubated on each section. The reaction was stopped after 3 min by transferring the slides into distilled water. The sections were dehydrated by immersion in different solutions as follows: 2 min in 70% isopropanol, 2 min in 90% isopropanol, 2×2 min in absolute isopropanol and 3×2 min in toluene. The sections were mounted with DPX mounting medium (Sigma-Aldrich, #1.00579.0500) and left to dry overnight at room temperature. The images were captured via an Axioskop 40 microscope (Zeiss).

Paraffin-embedded sections of 10 µm were stained with the Gallyas silver-staining method to identify NFTs (Alzheimer and Other Tauopathies Research Group, ULB Neuroscience, Karelle Leroy)[27]. The images were captured via an Axioskop 40 microscope (Zeiss).

For immunofluorescence, 5 µm paraffin sections were dewaxed by immersion in different solutions as described below: 3×5 min in toluene, 3 min in absolute isopropanol, 3 min in 100% ethanol, 3 min in 90% ethanol, 3 min in 70% ethanol, 2 min in distilled water, and a final rinse in 1X PBS. Heat-induced antigen retrieval was performed using 10 mM sodium citrate buffer at pH 6.0. The sections were placed in a tank filled with antigen retrieval solution and heated for 3×5 min in a microwave, maintaining the temperature around 96 °C. The solution was left to cool for 20 min, followed by rinsing with PBS.

For the permeabilization step, the sections were immersed in 0.3% Triton X-100 in PBS for 30 min at room temperature. The blocking solution was prepared with PBS-Triton, normal goat serum (NGS), and bovine serum albumin (BSA) to reach 0.3% PBS-Triton, 3% NGS, and 5% BSA. This solution was added to each section for 1 h at room temperature. The primary antibodies were prepared in blocking solution (Antibodies Table S1), added to the corresponding sections, and left overnight at 4 °C.

The next day, 3×5 min rinses with PBS-Triton 0.1% were performed, followed by 1-h incubation at room temperature with the secondary antibodies prepared in in 0.1% Triton X-100 in PBS (Antibodies Table S1). The sections were rinsed twice in 0.1% Triton X-100 in PBS for 5 min, followed by a final rinse in 1X PBS. The sections were mounted with Mowiol (Merck, #475904-100GM-M) and left to dry overnight. The images were acquired via an EVOS™ FL Auto fluorescence or confocal microscope.

All immunostainings were performed in PS19 males, as sexual dimorphism has been described in this model, with males exhibiting an earlier onset of the pathology [61]. Additionally, all representative images shown for each region were taken from the same mouse at each time point.

Behavioral tests

All behavioral tests were approved beforehand by the ethical committee (2021/UCL/MD/018) and conducted in collaboration with the behavioral analysis platform (BEAP, UCLouvain) following validated protocols. A dedicated cohort of mice (males and females) was used to perform olfactory function measurements at 3, 6, and 9 months. One week before the required time point, the mice were acclimatized on the behavioral analysis platform. Each mouse performed the olfactory discrimination test followed by the buried food test at each time point. Between the analyses, the mice were kept in quarantine and monitored closely. At 9 months, after the last test, the mice were sacrificed by cervical dislocation, and the tissues of interest were harvested.

Olfactory discrimination test

Test animals were placed in a clean plastic cage with a fresh layer of bedding covered by a removable Plexiglas lid with a 1.25 cm central hole for odorant exposure. After a 5-min adaptation period, a dry disposable applicator with a cotton tip was placed at a depth of 2.5 cm through the hole in the cage lid. After each minute, the applicator was removed and immediately replaced with a new applicator. After the sixth

Appendix III

minute, an applicator with a cotton tip saturated with an odorant solution was positioned through the hole and again replaced every minute by a fresh applicator containing the same odor. After the 12th minute, an applicator with a tip saturated with a different odorant was inserted and replaced six times at 1-min intervals. The two odors used were geraniol and lime. The number of times the animal headed toward each applicator introduced into the cage was recorded via a camera throughout the experiment and was counted by an experimenter blinded to the experimental conditions.

Food-seeking test

The mice were deprived of food for 16 h with access to water *ad libitum*. The test mice were introduced into a clean cage covered with a 3 cm-thick layer of bedding, under which a 1.0-g food pellet had been buried. The time elapsed between the animal's introduction into the cage and the moment it retrieved the food with its front paws was measured in seconds, with a maximum of 300 s. From then on, a result equivalent to 300 s indicates that the mouse did not find the food.

Intranasal $ZnSO_4$ irrigation

At 1.5 months, the mice received an intranasal application of either 0.17 M (5%) zinc sulfate ($ZnSO_4$) or vehicle solution (PBS). Awake mice were held on their backs by one experimenter, while a second experimenter administered 25 µL of either PBS or $ZnSO_4$ solution, dropwise to the right nostril with a few seconds between each drop. After an hour to allow the mice to recover, the same procedure was repeated for the left nostril. The mice were then monitored for the next hour for any breathing discomfort. Since the OE regenerates over time [45], the mice were treated three times: at 1.5, 2.5, and 4 months. The mice were finally sacrificed at 6 months by cervical dislocation and samples were retrieved. For the evaluation of olfactory functions following $ZnSO_4$ treatment, the treatment was performed only once at 3 months, and olfactory tests were conducted 24 h after the treatment.

NFT-like tau accumulations quantification

For each region of interest, the numbers of NFT-like tau accumulations visualized with anti-pTau immunostaining were counted in an equivalent area corresponding to the sum of five delimited areas placed in that same region (Fig. S11). The number of NFT-like tau accumulations per mm^2 in the vehicle and $ZnSO_4$-treated conditions was compared and analyzed via statistical tests.

Intranasal hTau-P301S AAVs irrigation

Adeno-associated viruses (AAVs) serotype 8 harboring the human tau sequence with the P301S mutation as well as an EGFP sequence (hereafter referred to as hTau-P301S AAVs) were designed and produced by VectorBuilder (Vector ID #VB240323-1105jux). At 1.5 months, the mice received an intranasal application of either hTau-P301S AAVs prepared in PBS or vehicle solution (PBS). The total dose for each AAV treatment was 1×10^{11} genome copies (GC), administered over two consecutive days. Awake mice were held on their backs by one experimenter, while a second experimenter administered 20 µL of either PBS or AAV solution (2.5×10^{10} GC/nostril/day), dropwise to the right nostril with a few seconds between each drop. After allowing the mice to recover for an hour, the same procedure was repeated for the left nostril. The mice were then monitored for the next hour for any breathing discomfort. Since the OE regenerates over time [45], the mice were treated twice: at 1.5 and 2.5 months. The mice were finally sacrificed at 4 months by cervical dislocation and samples were retrieved.

AT8 signal quantification

A consistent threshold was established to distinguish AT8-positive signal from background noise. This threshold was uniformly applied across a defined region equivalent in size to the sum of five delineated areas positioned within the same anatomical zone. The results presented in Fig. 9e represent the percentage of this total area that is positive for AT8 staining in the vehicle and AAVs-treated conditions. The results were compared and analyzed via statistical tests.

Postmortem human tissues

OBs were collected from four different Braak stage I or II patients and the OE was retrieved from 1 Braak stage II patient (Table S2). The autopsies were performed in UCLouvain (Belgium) in accordance with the applicable laws. Informed consent was obtained following local legislation. The recruitment protocols for the collection of human samples were approved by the ethical committees of UCLouvain (2020/02JUL/355). After collection, the tissues were immediately placed in 10% formalin for 48 h. The tissues were subsequently embedded in paraffin and cut to obtain 5 and 10 µm paraffin sections. Neuropathological evaluation was conducted for each patient at KU Leuven (Leuven Brain Institute, Dietmar Thal), and the patients were classified based on the Braak stage (I or II in this study). Neuropathological analysis of these brains was approved by the UZ/KU-Leuven ethical committee (S-64363).

Appendix III

Statistical analyses

GraphPad Prism software version 10 (GraphPad Software, Inc., La Jolla, CA, USA) was used for statistical analysis. All the data were tested for normality using the Shapiro–Wilk test. Parametric Student's *t* tests or nonparametric Mann–Whitney tests were used to evaluate the level of significance between two groups. When more than two groups were compared, parametric one-way or two-way ANOVA with the indicated post hoc tests or nonparametric Kruskal–Wallis were used. The data are expressed as the mean ± SEM. and P values < 0.05 were considered significant (*$P < 0.05$, **$P < 0.01$, ***$P < 0.001$). The number of mice used in each group of experiment is indicated by "n = ".

Results

Tau pathology in the olfactory system and associated CNS regions in PS19 mice

The presence of hyperphosphorylated tau protein (pTau) was evidenced using the AT8 antibody (pTau (Ser202, Thr205)) in coronal sections of the OE from WT and PS19 mice. To that end, a specific protocol of decalcification has been set up to preserve the integrity of the OE. AT8 immunoreactivity was observed only in PS19 mice and was localized to the OE middle stratum and to the axon bundles (ABs), located in the lamina propria underlying the OE (Fig. 1a-d). The AT8 signal in the OE was assessed and compared at different ages: 1.5, 3, 6, and 9 months (Fig. 1a-d). AT8 immunoreactivity was detected as soon as 1.5 months (Fig. 1a, a'), increased progressively up to 6 months (Fig. 1c, c'), and decreased at 9 months, especially in the middle stratum (Fig. 1d, d'). This region did not exhibit any significant bilateral asymmetry in tau pathology. Based on morphology, no NFT-like tau accumulations were observed in this region for up to 9 months. A closer examination of the nasal cavity showed no pTau signal in the RE of PS19 mice (Fig. 1e). No pTau signal was detected in the OE or ABs of 6-month-old WT mice (Fig. 1f), indicating that the AT8 signal is specific to PS19 mice and related to the expression of pathological human tau. The results were confirmed independently by Western Blotting (Fig. S1) using the PHF-1 antibody. This antibody is generated against paired helical filaments isolated from the brains of AD patients, that recognizes tau phosphorylated at Ser396 and Ser404. It binds to tau filaments and is a recognized standard to evidence the pathological conformations found in NFTs [30, 50]. Immunostaining with the PHF-1 antibody and a human tau (hTau)-specific antibody showed similar results to those obtained with the AT8 antibody in PS19 mice (Fig. S2).

Additional staining with a total tau antibody, detecting both endogenous murine tau protein and human tau protein, confirmed the presence of endogenous tau in the OE of WT mice (Fig. S2). RT-qPCR experiments indicated that the expression of endogenous tau transcripts was stable from 3 to 9 months in the OE of WT mice (Fig. S3). Since tau aggregation does not naturally occur in WT mice, overexpression of human tau with aggregation-prone mutations is required to induce tau pathology in animal models. Together, these observations indicate (i) that tau is endogenously expressed in the mouse OE, (ii) that the specific AT8-positive signal observed in the OE of PS19 mice is not an artifact simply related to ectopic expression of the human tau transgene in in OE of PS19 mice.

Colocalization analyses were carried out via immunofluorescence to confirm the cellular localization of the pTau signal in the OE of PS19 mice. The following antibodies were used: total tau antibody (TTau), olfactory marker protein (OMP) antibody (specific to mature OSNs and their neurites), and AT8 antibody (Fig. 2a–c). Colocalization was observed between the OMP signal and both TTau and AT8 signals in the cellular bodies and neurites of the OSNs, as well as in the ABs of the PS19 mice at 3 months (Fig. 2d, e). OMP and AT8 were also specifically colocalized in the superficial layer where dendritic knobs of OSNs are located (Fig. 2e). This result confirmed that pTau is found not only in mature OSNs of the OE but also in ABs within the lamina propria (Fig. 2e).

Since OSN axons extend through the cribriform plate of the ethmoid bone to reach the OB, where they form its outermost layer (ONL) [14], we next investigated the AT8 staining profile in the OB of PS19 mice. The AT8 signal was specifically present in the ONL of the OB as early as 1.5 months in PS19 mice (Fig. 3a–d). In addition, AT8 immunoreactivity was also detected in the MCL. In some 9-month-old mice, a stronger pTau signal appeared in the central region (e.g., GCL) of the OB (Fig. 3d). Similarly to the OE, no notable bilateral differences in tau pathology were observed in this region. Here also, no AT8 signal was observed in the OB of WT mice (Fig. 3f).

Accumulation of hyperphosphorylated tau in the OB of PS19 mice was confirmed by Western blotting of soluble protein extracts using the AT8 antibody (Fig. S4). The experiments were repeated and quantified using the PHF-1 antibody (Fig. S5). A band around 60 kDa was observed exclusively in PS19 mice, both in males and females, as early as 3 months of age. No positive signal for PHF-1 or AT8 was observed in WT mice at any age (Fig. S5a–c). Western blot quantification revealed no significant differences in pTau expression between males and females in the OB at 3, 6, and 9 months (Fig. S5a–c). Finally, the PHF-1 signal was quite stable over time in PS19 males, suggesting that pTau, although already present at 3 months, did

Appendix III

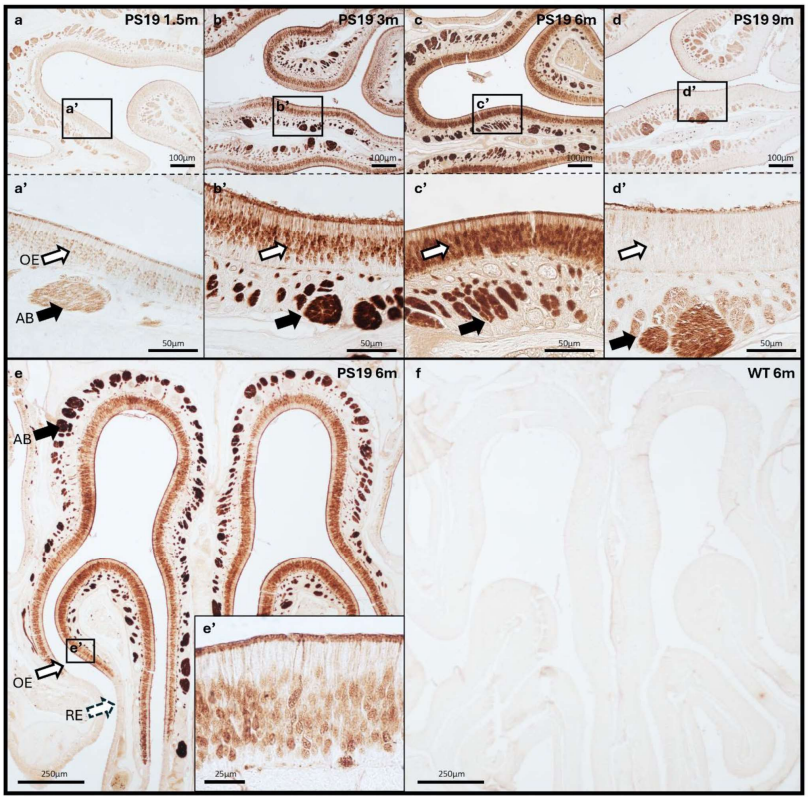

Fig. 1 pTau expression in the OE of PS19 mice. The OE from 1.5-month (**a**, a'), 3-month (**b**, b'), 6-month (**c**, c', **e**), 9-month-old PS19 mice (**d**, d'), and 6-month-old WT mice (**f**) were fixed and stained with the **AT8** antibody (pTau (Ser202.Thr205)). pTau recognized by the **AT8** antibody is found in the middle stratum of the OE (white arrows) and in the ABs (black arrows) as soon as 1.5 months in PS19 mice (**a**, a'). The signal increases up to 6 months (**c**, c', **e**) and appears to decrease at 9 months (**d**, d'). No signal is detected in WT mice (**f**). All the mice used were **males**. The immunostainings shown are representative of n = 4 mice per time point. High magnification of the OE (white arrows) is shown in the inset (e'). ABs: axon bundles, OE: olfactory epithelium, RE: respiratory epithelium

not further accumulate in the OB (Fig. S5d). The presence of human tau in the OBs of PS19 mice was confirmed by immunostaining with the Tau-13 antibody, as well as endogenous tau expression in the OBs of WT mice using a total tau antibody (Fig. S2). Endogenous tau expression in the OBs of WT mice was also confirmed by RT-qPCR (Fig. S6).

Immunofluorescence analyses of the OB in 3-month-old PS19 mice (Fig. 4a–c) revealed colocalization between TTau and OMP, indicating tau protein expression in both the ONL and the GL (Fig. 4d). Additionally, strong colocalization between OMP and AT8 was observed in the ONL, providing evidence of pTau accumulation in the outermost layer of the

Appendix III

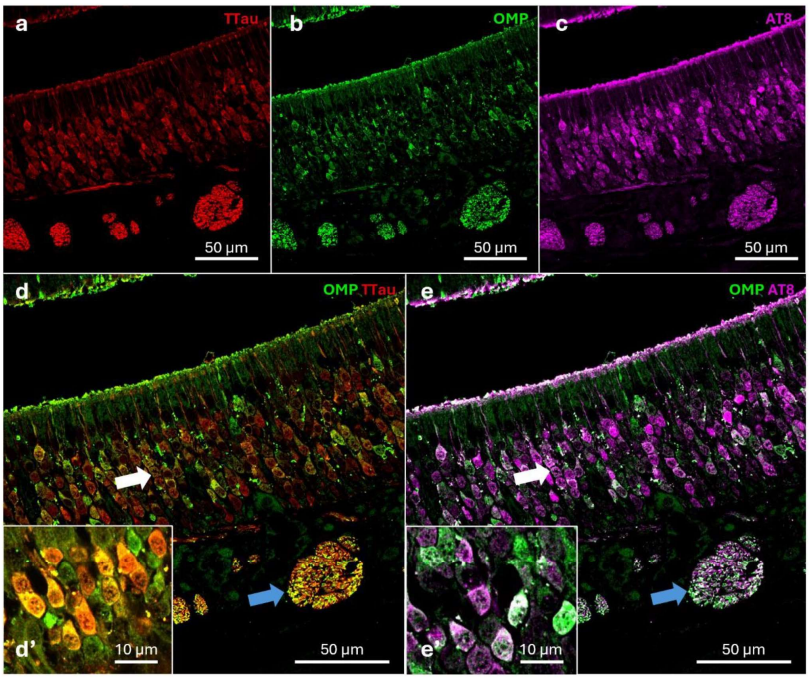

Fig. 2 pTau expression in the OSNs and ABs of PS19 mice. Paraffin sections immunostained for total tau (**TTau**, red) (**a**, **d**), olfactory marker protein (**OMP,** green) (**b**, **d**, **e**), and pTau (**AT8,** purple) (**c**, **e**) show colocalization between **TTau-OMP** (yellow) (**d**) and **AT8-OMP** (white) (**e**) indicating tau hyperphosphorylation in the OSNs (white arrows) and in the ABs (blue arrows) of PS19 mice at 3 months. High magnifications are shown in the insets (d', e'). OSNs: olfactory sensory neurons, ABs: axon bundles

OB in PS19 mice (Fig. 4e). Some AT8 signal, which did not colocalize with OMP, was also observed in the inner layers of the OB (Fig. 4c).

Next, we explored tau pathology in CNS regions of PS19 mice that are connected to the OB and involved in the processing of olfactory information along with olfactory memory: the PC, the EC, and the hippocampus. All these CNS regions are connected by neuroanatomical pathways [43]. Efferent projections from the OB reach both the PC and EC, and the perforant path wires the EC to hippocampal subregions [3]. In the PC, faint pTau immunoreactivity (AT8), indicative of the first step of abnormal tau modification [4], appeared in the neuronal cell bodies at 3 months (Fig. 5b, b'). By 6 months, the first perikaryal NFT-like tau accumulations were observed, with an accumulation of pTau in both the cell bodies and neurites of neurons within the PC pyramidal layer (Fig. 5c, c'). These tau accumulations progressively increased up to 9 months and eventually spread throughout the entire PC (Fig. 5d, d'). 9-month-old WT mice showed no AT8-positive accumulations in the PC (Fig. 5e). In the EC, AT8 immunoreactivity appeared in the neuronal cell bodies as early as 1.5 months and increased over time (Fig. 5f–i). Perikaryal NFT-like tau accumulations were detectable at 6 months, with signal present in both the cell bodies and neurites in the lateral part of the EC (Fig. 5h, h'). Tau lesions gradually accumulated up to 9 months and spread to the whole EC (Fig. 5i, i'). The accumulation pattern of tau pathology was similar to that observed in the PC,

Appendix III

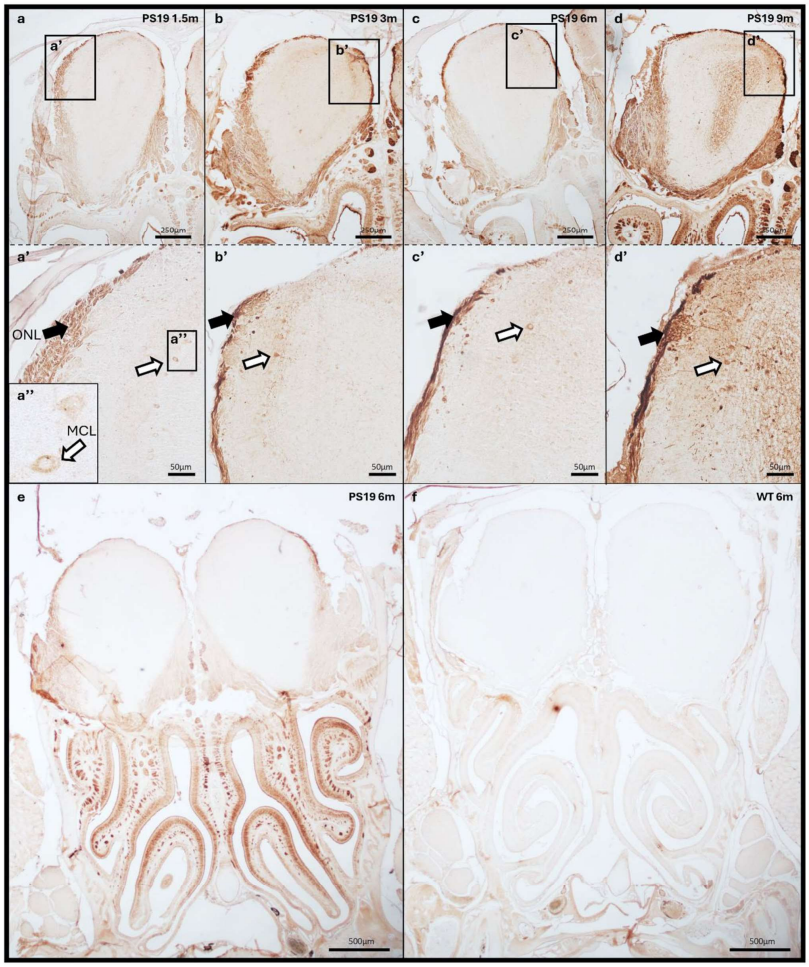

Fig. 3 pTau expression in the OB of PS19 mice. The OB from 1.5-month (**a**, a'), 3-month (**b**, b'), 6-month (**c**, c', **e**), 9-month-old PS19 mice (**d**, d'), and 6-month-old WT mice (**f**) were immunohistochemically stained with **AT8** (**a**–**d**, a'–d'). pTau recognized by the **AT8** antibody is found in the external layer of the OB (black arrows) and in the MCL (white arrows) from 1.5 months (**a**–**d**, a'–d'). The pTau signal seems stable over time (a'–d'). No signal is detected in WT mice (**f**). All the mice used for immunostainings were **males**. The immunostainings shown are representative of n = 4 mice per time point. High magnification of the MCL (white arrows) is shown in the inset (a''). ONL: olfactory nerve layer, MCL: mitral cells layer

Appendix III

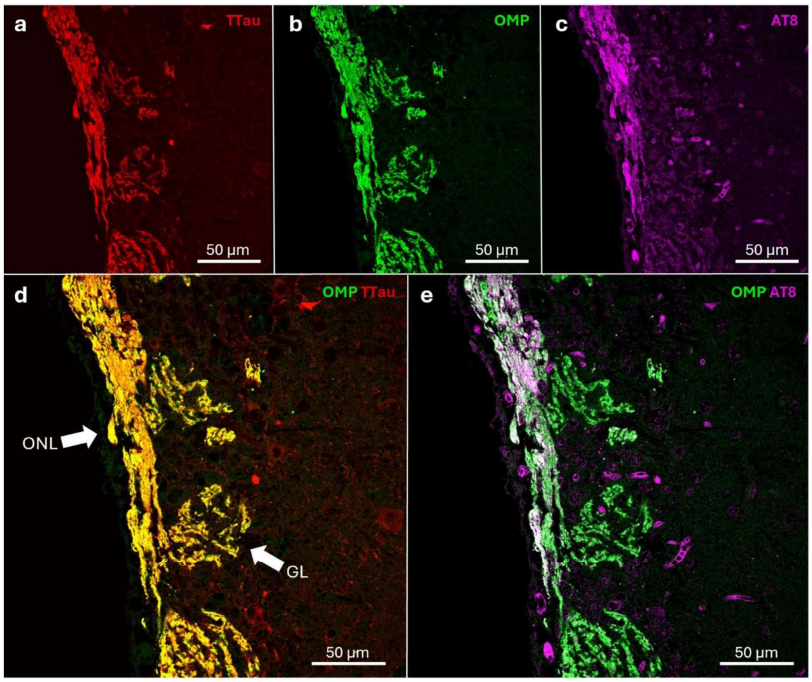

Fig. 4 pTau expression in the ONL of PS19 mice. Paraffin sections immunostained for total tau (**a**, **d**) (**TTau**, red), **OMP** (**b**, **d**, **e**) (green), and **AT8** (**c**, **e**) (purple) show colocalization between **TTau-OMP** (yellow) (**d**) and **AT8-OMP** (white) (**e**) indicating tau protein expression both in ONL and GL as well as pTau expression in the ONL and inner layers of the OB from 3-month-old PS19 mice. ONL: olfactory nerve layer, GL: glomerular layer

although with an earlier onset. In WT mice, AT8 signal was not detected until 9 months of age (Fig. 5j).

In the hippocampus, AT8 immunoreactivity was faintly detected in the CA3 subregion at 3 months (Fig. 6b). By 6 months, pTau (AT8) was clearly present in the CA3 region and in the dentate gyrus (DG) (Fig. 6c), with an increased signal at 9 months (Fig. 6d). In the CA3 region, pTau was found in the CA3 mossy fibers and in the stratum pyramidale (Sp). In the DG, pTau was located primarily in the granular cell layer (Fig. 6e). No AT8 signal was detected in the hippocampus of WT mice (Fig. 6f).

pTau expression in soluble hippocampal extracts was confirmed by Western blotting with the AT8 antibody (Fig. S7). Equivalent results were obtained and quantified using the PHF-1 antibody. pTau was detected as a band around 60 kDa and was present only in PS19 mice, as soon as 3 months of age in both males and females. No positive signal for PHF-1 or AT8 was observed in the WT mice regardless of the aging stage (Fig. S8a–c). At the same age, the average pTau levels were significantly greater in males than in females. Although the difference was already significant at 3 months, it was more pronounced at 9 months (Fig. S8a-c). Western blot analysis finally revealed a significant increase in the pTau signal between 3 and 9 months in PS19 males, consistent with the staining results, suggesting that pTau accumulation in the hippocampus occurs in a time-dependent manner (Fig. S8d).

Appendix III

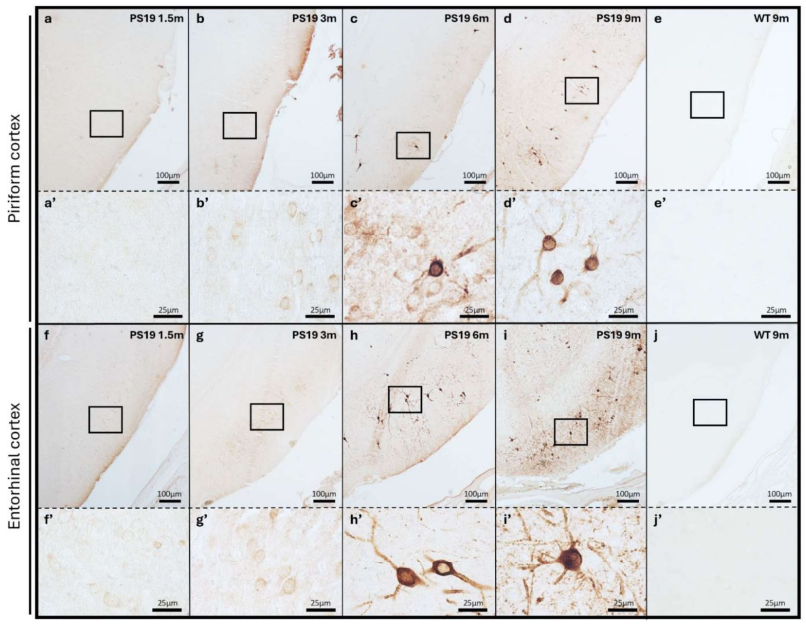

Fig. 5 pTau expression in the PC and EC of PS19 mice. The PC (Bregma − 1.94 mm) from 1.5-month (**a**, a'), 3-month (**b**, b'), 6-month (**c**, c'), 9-month-old PS19 mice (**d**, d'), and 9-month-old WT mice (**e**, e') were immunohistochemically stained with **AT8** (**a**–**e**). pTau recognized by the **AT8** antibody is found in the PC as soon as 3 months (**b**, b') with an accumulation up to 9 months (**b**–**d**, b'–d'). The first NFT-like tau accumulations appear at 6 months (**c**, c'). There is no **AT8** signal in the PC of WT mice (**e**, e'). The EC (Bregma − 3.08 mm) from 1.5-month (**f**, f'), 3-month (**g**, g'), 6-month (**h**, h'), 9-month-old PS19 mice (**i**, i'), and 9-month-old WT mice (**j**, j') were immunohistochemically stained with **AT8** (**f**–**j**). pTau recognized by the **AT8** antibody is found in the EC as soon as 1.5 months (**f**, f') with an accumulation up to 9 months (**f**–**i**, f'–i'). PS19 mice develop NFT-like tau accumulations in this region at 6 months (**h**, h'). No **AT8** signal is detected in the EC of WT mice (**j**, j'). All the mice used were **males**. The immunostainings shown are representative of n = 4 mice per time point. Insets were taken from the PC area (a'–e') and in the lateral EC (f'–j')

To distinguish AT8-positive NFT-like tau accumulations from mature filamentous tau aggregates referred to as mature NFTs, Gallyas silver staining was performed in all previously studied regions and time points. No NFTs were observed in the OE (Fig. 7a–d) and OB (Fig. 7f–i) of PS19 mice. In the PC and EC, Gallyas-positive NFTs were detected only at 9 months of age in PS19 mice (Fig. 7n, s), and were very sparse compared to the AT8 signal observed previously (Fig. 5). In the hippocampus of PS19 mice, no NFTs were observed at any age (Fig. 7u–x). As a control, no NFTs were detected by silver staining in any region of interest in WT mice (Fig. 7e, j, o, t, y).

These results clarify some aspects of the temporal and spatial staging of tau pathology in PS19 mice by distinguishing pTau (i.e., recognized by AT8 or PHF-1 antibodies), perikaryal NFT-like tau accumulations or pretangles (AT8-positive) and mature NFTs evidenced by Gallyas staining. Strikingly, pathological pTau accumulated very early (from 1.5 months of age) in the OE without the formation of typical NFTs, as shown by the Gallyas staining. A similar profile (pTau staining without NFTs) was observed in the OBs. pTau immunoreactivity was found in the EC and OE from 1.5 months on and in the hippocampus from 6 months. NFT-like tau accumulations appeared later, from 6 months in the PC and EC, and

Appendix III

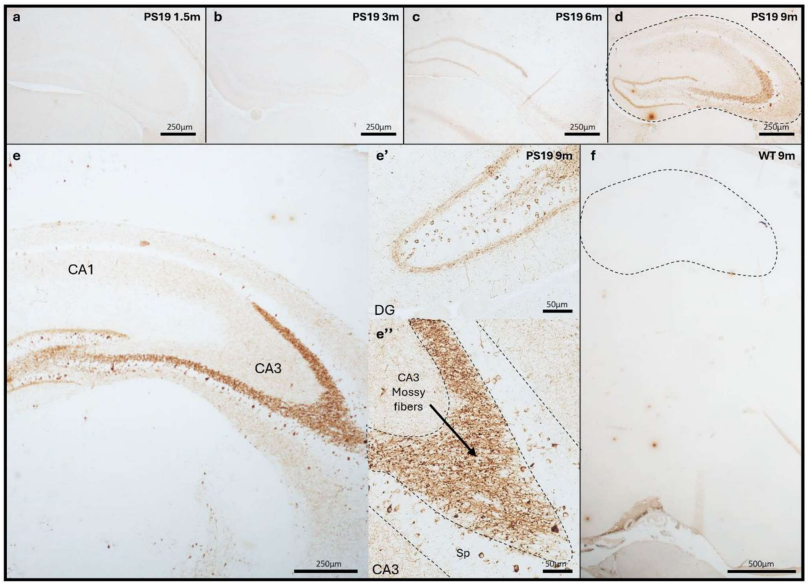

Fig. 6 pTau expression in the hippocampus of PS19 mice. The hippocampus (Bregma − 1.82 to − 2.18 mm) from 1.5-month (**a**), 3-month (**b**), 6-month (**c**), 9-month-old PS19 mice (**d**, **e**), and 9-month-old WT mice (**f**) were immunohistochemically stained with **AT8** (**a**–**f**). pTau recognized by the **AT8** antibody is found in specific hippocampal subregions like the CA3 (e'') and DG (e') as soon as 6 months with an increased signal at 9 months (**c**–**e**). No **AT8** signal is found in the hippocampus of WT mice (**f**). All the mice used for immunostainings were **males**. The immunostainings shown are representative of n = 4 mice per time point. DG: Dentate gyrus, CA: Cornu Ammonis, Sp: Stratum pyramidale

at 9 months in the hippocampus (Sp). While only a few NFTs (Gallyas-positive) were present in the PC and EC at 9 months. Taken together, our extensive analysis of the accumulation of pTau in connected olfactory regions gives a solid support to the hypothesis that tau pathology progresses along the olfactory system to reach regions of the temporal lobe that are particularly vulnerable in AD (e.g., EC and hippocampus).

Olfactory function in PS19 mice

The impact of tau lesions in the olfactory system on olfactory function was assessed in PS19 mice using two specific olfactory tests: the olfactory discrimination test and the food-seeking test. The first test evaluated odor discrimination, whereas the food-seeking test measured odor threshold in mice. As a proof of concept, control and $ZnSO_4$-treated mice were first evaluated, since intranasal irrigation with $ZnSO_4$ induces OE stripping and transient anosmia [46].

In the olfactory discrimination test, the curve for the number of sniffing events in non-treated (control mice) showed two peaks at 6 and 12 min (Fig. S9a). The first peak corresponded to the presentation of the geraniol odor, which induced a greater number of head movements toward the cotton swab in the control mice. Following this peak, the mice exhibited fewer head movements as they became accustomed to the odor. A second peak was observed after 12 min, when the second odor, lime, was presented. Both peaks were absent in the mice that received intranasal $ZnSO_4$ administration (Fig. S9a). Similarly, during the food-seeking test, none of the $ZnSO_4$-treated mice were able to locate buried food before the end of the test (300 s) (Fig. S9a').

Appendix III

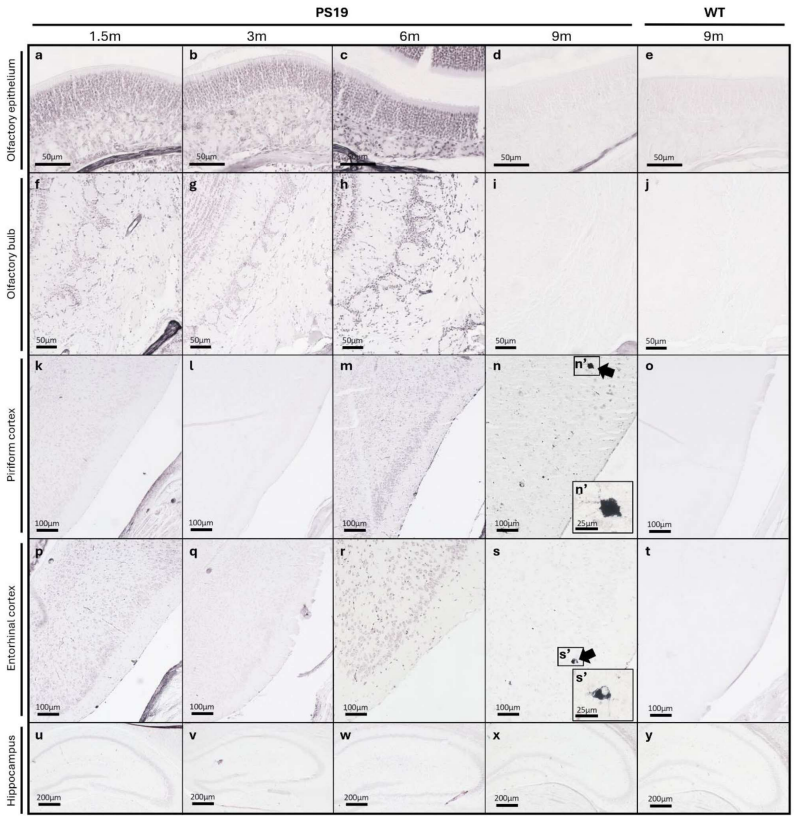

Fig. 7 Gallyas staining in the OE, OB, PC, EC, and hippocampus of PS19 mice. The OE (**a**–**e**), OB (**f**–**j**), PC (**k**–**o**), EC (**p**–**t**), and hippocampus (**u**–**y**) of PS19 mice at 1.5, 3, 6, and 9 months, as well as 9-month-old WT mice were stained with Gallyas silver staining to highlight NFT inclusions. A few Gallyas-positive inclusions (black arrows) are only observed in the PC (n) and EC (s) from 9 months PS19 mice. No NFTs are detected in the OE, OB, or hippocampus at any time point, nor in the PC or EC before 9 months. No signal is detected in WT mice (**e**, **j**, **o**, **t**, **y**). High magnifications of the Gallyas-positive aggregates (black arrows) are shown in the inset (n') and (s'). All the mice used for Gallyas silver staining were **males.** The Gallyas stainings shown are representative of n = 3 mice per time point

The same tests were conducted in WT and PS19 mice at 3, 6, and 9 months (Fig. 8a–f) to evaluate the impact of tau pathology in the OE and associated CNS regions on olfactory function. In the olfactory discrimination test, both WT and PS19 mice showed two peaks corresponding to the introduction of each new odor. Each peak was followed by reduced reactions due to habituation to the odor (Fig. 8a–f). All mice appeared to react more strongly,

Appendix III

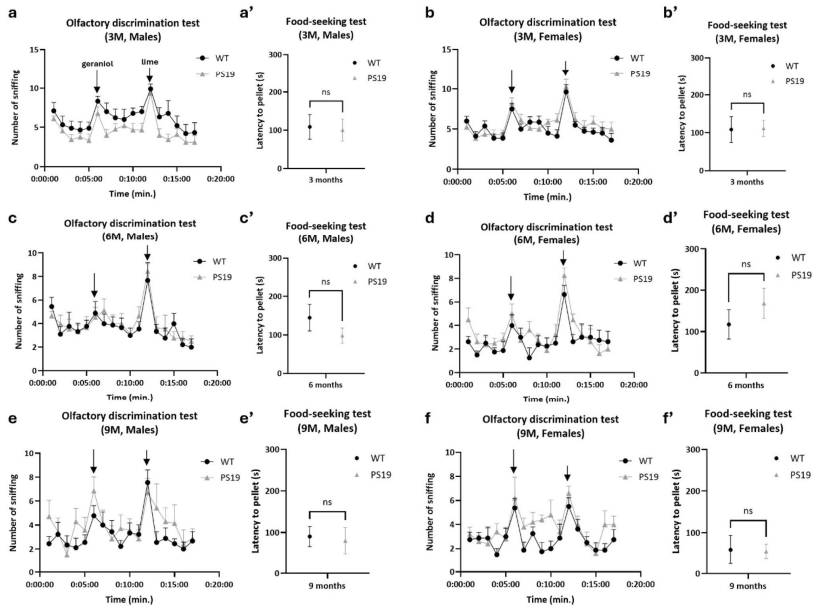

Fig. 8 Olfactory function assessment in PS19 mice. The olfactory discrimination (**a**–**f**) and food-seeking tests (a'–f') show no significant effect of genotype (PS19) on olfaction at either 3, 6, or 9 months, both in males and females (**a**–**f**, a'–f'). For PS19 males; n = 9 (3 months), n = 9 (6 months), and n = 7 (9 months). For WT males; n − 9 (3 months), n − 9 (6 months), and n − 9 (9 months). For PS19 females; n = 8 (3 months), n = 8 (6 months), and n = 5 (9 months). For WT females; n = 8 (3 months), n = 8 (6 months), and n = 8 (9 months). Data were analyzed using two-way ANOVA with Šídák's multiple comparisons test (olfactory discrimination test) or using independent *t* test (food-seeking test)

with a greater number of head movements, when presented with the second odor of lime. The superposition of curves indicates that all the mice, independently of their genotype and age, have similar olfactory capacities and that PS19 mice do not perform worse as they age. Statistical analyses revealed a significant impact of time as the mice responded to odor changes. However, no significant effect of genotype on olfactory capacities was observed at 3, 6, and 9 months in both males and females (Fig. 8a–f). The results from the olfactory discrimination test suggested that the odor discrimination abilities of PS19 mice are not impaired by the presence of tau pathology in the OE. In the food-seeking test, there was no significant difference between WT and PS19 mice in the latency to find the pellet. This observation was consistent at 3, 6, and 9 months in both males and females. Compared to WT mice, PS19 mice did not exhibit an impaired ability to find the food (Fig. 8a'–f'). Together, these data indicate that despite progression of tau pathology along the olfactory regions with age, PS19 mice did not show a significant impairment in odor discrimination or detection threshold (sensitivity). Of note, another parameter (odor identification) difficult to address in mice was not evaluated here.

Modulation of tau pathology in the CNS via intranasal interventions

Given the staged progression of tauopathy in olfactory regions and its early manifestation in the OE, we administered localized treatments to the OE to either mitigate tau pathology or exacerbate its spread to the CNS.

Appendix III

First, we examined the impact of targeted removal of the source of pathological tau present in the OE on tau pathology progression in the CNS. Our approach was designed to specifically remove the pTau accumulation in the OE using $ZnSO_4$ nasal irrigation, known to strip the OE and ONL (OB), and cause transient anosmia [32, 45], which can later regenerate (OE) and recover (anosmia). The impact on tauopathy progression was assessed in regions with varying degrees of connectivity to the OB, such as the PC, EC, and amygdala. PS19 mice were intranasally administered either $ZnSO_4$ or phosphate-buffered saline (PBS, control). To ensure that the accumulation of tau in the OE was prevented for a sufficiently long period, nasal irrigation with $ZnSO_4$ was performed repeatedly at 1.5, 2.5, and 4 months prior to analysis of tauopathy at 6 months.

In vehicle-treated PS19 mice, the structure of the OE remained intact, with strong AT8-positive tau immunoreactivity in OSNs and ABs. However, following intranasal $ZnSO_4$ administration, the OE was completely stripped, and the AT8 signal was almost absent at 6 months (Fig. 9a). In the OB of PBS-treated mice, all six layers were present and structurally preserved, with AT8-positive signal characteristic of PS19 mice. After $ZnSO_4$ treatment, the AT8 signal in the ONL was no longer detectable (Fig. 9a). The efficient stripping of the OE and the ONL after $ZnSO_4$ treatment was further confirmed by Masson's trichrome blue staining (Fig. S10a–d). Tau pathology was next examined in regions receiving direct inputs from the OB, such as the PC, EC, and amygdala. At 6 months, vehicle-treated PS19 mice exhibited NFT-like tau accumulations in these regions. However, following $ZnSO_4$ treatment of PS19 mice, no NFT-like tau accumulations were detectable in the PC, and only a few remained in the EC and amygdala at 6 months compared to control PS19 mice (Fig. 9a). Quantification of the number of NFT-like tau accumulations per mm^2 in the PC, EC, and amygdala (Fig. S11) further confirmed a massive reduction of pTau signal associated with tau pathology in the PC, EC, and amygdala following intranasal $ZnSO_4$ administration (Fig. 9b). No overt morphological alterations were found in these regions after staining with Masson's trichrome blue (Fig. S10e–j), indicating that $ZnSO_4$ treatment of the OE did not result in loss of density of the connected olfactory regions. In other terms, removing the source of pTau present in the OE sharply reduces tau pathology in the connected regions of the temporal lobe and limbic system.

To further validate the hypothesis that tau pathology spreads from olfactory regions, we aimed to determine whether increasing pathology at the OE level could accelerate the progression of tau pathology in the CNS. To this end, we performed intranasal administrations of AAVs encoding the P301S-mutated human tau protein (referred to as hTau-P301S AAV). The efficacy of AAV infection was first validated by the presence of GFP, which is co-expressed from the same vector. One week after the infection, a GFP-positive (green) signal was detected exclusively in the OE of AAV-treated mice, but not in PBS-treated controls (Fig. 9c), confirming successful transduction.

Subsequently, we assessed tau pathology using the AT8 antibody. We focused our analysis on the PC, a region directly connected to the OB and one of the first affected areas in tauopathies. At the end of the treatment, when the mice were 4 months old, we observed that the intranasal delivery of hTau-P301S AAV increased AT8 immunoreactivity in the PC of AAV-treated mice compared to controls (Fig. 9d, e). Although the difference did not reach statistical significance—likely due to variability in transduction efficiency—the pattern was consistent: all control mice displayed similar baseline levels of pathology, whereas all AAV-treated mice exhibited more advanced tau pathology, with severity likely varying in relation to the efficacy of AAV delivery (Fig. 9d, e).

Overall, our data indicate that early accumulation of pTau in the OE can be instrumental to the progression of tau pathology that eventually reaches the EC and the hippocampal formation.

Pathological pTau protein in the human olfactory system

Finally, we investigated whether a similar pattern of tau pathology was observed in OE and OB collected from patients at early Braak stages I and II (patients 1–4, Table S2). In the OE collected from patient 4 (Braak stage II), pTau immunoreactivity (PHF-1 Ser396, Ser404) was detected and colocalizing with the OMP signal, indicating the presence of pTau in OSNs (Fig. 10b). PHF-1 signal was also detected in the ABs present within the OE structure and revealed by the OMP antibody (Fig. 10c–e). Still, PHF-1 and OMP signals are not fully overlapping. PHF-1 signal is mostly around the nuclei, while the OMP stains all the axonal fibers present in the ABs (Fig. 10f'). Interestingly, while colocalization was observed between OMP and PHF-1 within the ABs (Fig. 10f), AT8 signal was detected neither in the ABs (Fig. 10g) nor in the OSNs.

In the OB of Braak stage I/II patients, PHF-1 and OMP colocalization was consistently detected in the ONL, and to a lesser extent, in the GL (Fig. 11a–d, d'). Some PHF-1 pTau signal was additionally found in the inner layers of the OB (Fig. 11a–d, d''). No colocalization was observed between OMP and AT8 in the ONL (Fig. 11e–h, h'), but similarly to PHF-1, neuropil threads highlighted by the AT8 antibody were observed in the inner layers of the OB from Braak stage I and II patients (Fig. 11e–h, h''). All OB included in the study were Gallyas-negative, highlighting the absence of mature NFTs at this stage (Braak stage I/II) of the pathology

Appendix III

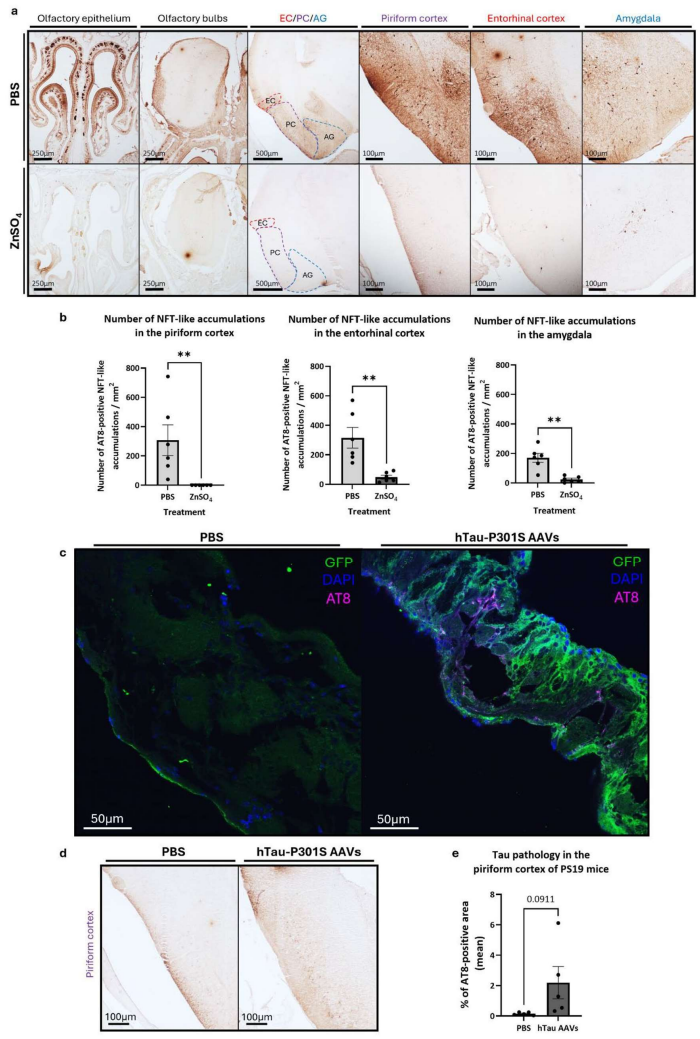

Appendix III

◂**Fig. 9** Modulation of tau pathology in the CNS via intranasal interventions. Sections of the OE, OB, PC, EC, and amygdala from 6-month-old PS19 males were fixed and stained with the **AT8** antibody. After intranasal $ZnSO_4$ irrigation, the OE and ONL from the OB are stripped, no more pTau signal is found in these regions (**a**). Quantification of the number of NFT-like tau accumulations/mm^2 was performed in the PC, EC, and amygdala. In the PC, there are no NFT-like tau accumulations compared to the PBS-treated mice. In the EC and amygdala, there is a significant decrease in NFT-like accumulations compared to the control condition. $^{**}P < 0.01$ (Mann–Whitney test, n = 6 mice/group) (**b**). OE sections immunostained for **GFP** (green), **AT8** (purple), and DAPI showed efficient transduction following intranasal AAVs administration (**c**). In the PC, AT8 immunoreactivity appeared increased in AAV-treated mice compared to PBS controls (**d**). Quantification of the AT8-positive area in the PC showed a trend toward increased pTau signal following nasal delivery of hTau-P301S AAVs (Mann–Whitney, n = 5 mice per group) (**e**). ONL: olfactory nerve layer, AG: amygdala

(data not shown). These results underscore the early appearance of pathological tau markers in the sensory regions of the human olfactory system in agreement with observations in the PS19 mouse model.

Discussion

The OE forms a direct appendix of the CNS. In fact, OSNs are the only neurons connected to the CNS being in direct contact with the external environment [60], lacking the protection of the blood–brain barrier [10]. These unique anatomical characteristics make the OE highly vulnerable to harming environmental conditions and a possible starting point for the spread of pathologies through its connections to various regions of the olfactory and central nervous systems. It also sheds light on the importance of studying this region from both diagnostic and therapeutic perspectives. Regarding tauopathies, the presence of pTau immunoreactivity in the OE of AD patients has been reported [5, 58, 60, 66]. NFTs are also present in the OB of AD patient early in AD progression [37, 48] and are correlated to bulb size reduction [44]. Tau pathology could thus appear early in the sensory part of the olfactory system (OE), due to neurotoxic compounds present in the environment or to the gradual loss of its ability to regenerate. Considering that tau spreading along neuronal connections is now well documented [53], one can imagine that pathological forms cross the cribriform plate to penetrate the CNS and spread through the olfactory tract to regions known to be affected in AD (EC, amygdala, hippocampus). Here, we provide the first evidence of the staging of tau pathology across the olfactory system, and, more importantly, that preventing the accumulation of pathological tau in the OE reduces NFT-like tau accumulations in the PC, EC, and amygdala.

Prion-like spreading of tauopathy within the olfactory system

Our study revealed the presence of hyperphosphorylated tau protein in the OSNs of the OE as early as 1.5 months in PS19 mice. The signal increased up to 6 months, and decreased at 9 months, which could be explained by the reduction in the number of OSNs with aging [23]. Neurogenesis occurs in the OE throughout life, but aging and exposure to pathogens contribute to a reduction in this regenerative capacity [16, 51]. Strong positive signal was observed in the superficial layer where the dendritic knobs of OSNs are located. This signal appears to persist over time—unlike in OSNs—suggesting that pTau could be secreted and become trapped in the mucus of this layer, where it may not be efficiently cleared. pTau immunoreactivity was also detected in ABs, suggesting that the signal appears early in OSNs and spreads following their axonal projections to accumulate within ABs. These nerve fibers then reach the OB following efferent projections and constitute its most external layer, the ONL. Immunohistochemical analyses showed strong pTau signal in the ONL but also in the MCL. Mitral cells in the MCL are neurons that receive afferences from OSNs within the olfactory glomeruli and project to various regions in the brain, notably the PC or EC that are part of the olfactory cortex. The OC allows the integration of olfactory information [10, 59]. pTau was also detected in these two cortical regions: as early as 3 months in the PC—which receives direct inputs from the OB—and 1.5 months in the lateral EC—receiving direct inputs from the PC [13]. Finally, the last region investigated was the hippocampus due to its connections with the EC layers II and III, which project to specific hippocampal subregions. Neurons from EC layer II project to the DG via the perforant path, initiating the trisynaptic circuit: from the DG to CA3 through mossy fibers, and from CA3 to CA1 via Schaffer collaterals. In parallel, neurons from EC layer III project directly to CA1 [69]. pTau immunoreactivity was observed in these hippocampal subregions, especially in the molecular layer of the DG where the axons coming from the medial EC terminate [33]. The presence of tau pathology in PS19 mice was demonstrated in all areas of interest, from the OE to the hippocampus, and its time-dependent spread seemed to follow neuroanatomical pathways, such as the perforant path, consistent with the previous findings in the CNS regions of PS19 mice [53]. It was suggested that tau pathology may spread along neuroanatomically connected pathways. For instance, injection of brain extracts from PS19 mice into the brains of transgenic animals expressing human tau animals induced the assembly of WT human tau into filaments and the spread of pathology from the injection site to neighboring brain regions [15]. This type of neuron-to-neuron progression is found in many cerebral proteinopathies, which share similar cellular and

Appendix III

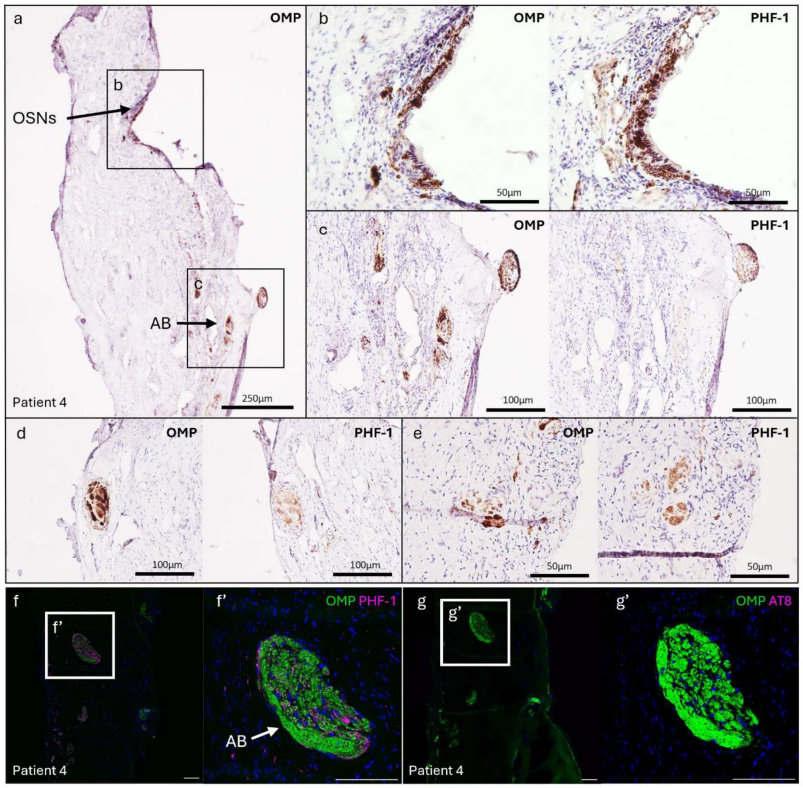

Fig. 10 pTau expression in human OE. The OE was obtained from a Braak stage II patient (patient 4). The sections were immunohistochemically stained with **PHF-1** or with **OMP** (**a**–**e**). **PHF-1** signal is observed in the **OMP**-positive OSNs (**b**) and ABs (**c**–**e**) of the OE. Paraffin sections immunostained for **OMP** (green) and **PHF-1** (purple) show colocalization between **OMP-PHF-1** (white) in the AB (**f**, f'). PHF-1 signal is also observed inside the tissue (**f**). Paraffin sections immunostained for **OMP** (green) and **AT8** (purple) show no colocalization between **OMP-AT8** (**g**, g'). No signal is detected in the negative controls without primary antibodies. Scale bar: 100 µm. OSNs: olfactory sensory neurons, ABs: axon bundles

molecular patterns of pathological protein propagation [22]. Termed "prion-like" propagation, this process implies that the tau protein can actively propagate trans-synaptically and that misfolded tau can affect tau folding in healthy surrounding neurons through a seeding mechanism [22]. Owing to its direct connection with the OE and other CNS regions, the OB is often regarded as a hub for the spread of misfolded proteins or as an entry point for pathogens [60, 73, 75]. Our results suggest that pTau appears early in OSNs from the OE of PS19 mice and likely spreads following the olfactory pathway to the OB, without maturation of tau seeds into mature NFTs in these regions, as shown by the Gallyas staining. pTau then appears in the olfactory cortex (PC and EC) and further in the hippocampal regions (essentially CA3 and

Appendix III

DG) which are projection regions of neurons from layer II (and possibly layer VI) of the EC. Of note, Gallyas-positive inclusions are readily present only in PC and EC 9 months, indicating that NFTs are a late manifestation of tau pathology that do not appear in all brain regions where pathological tau (e.g., AT8-positive) is available. This crucial point should be further investigated to define what pathological forms of tau are responsible for its transsynaptic spreading. Evidence from studies in the retina suggests that the induction of fibrillar aggregates is essential to induce pTau spreading in the brain [68]. Additionally, it is imperative to elucidate how pTau contributes to the formation of typical paired helicoidal filaments (PHFs) in more specific subregions.

Given the anatomical proximity between the OB and limbic regions, and considering the olfactory deficits in AD patients, it has previously been suggested that tau pathology spreads from olfactory circuits to limbic structures including the amygdala, as well as the piriform and entorhinal cortices [2, 56]. This route of propagation may exacerbate an already existing tauopathy within the CNS, making the OE a promising target region for early treatment intervention. The expression pattern of tau pathology observed in the olfactory system of PS19 mice might resemble that found in AD patients where tau-immunoreactive fibers have been reported in the ONL [36], and tau-containing neurites were present in the OE [5, 36]. We showed here pTau staining (PHF-1) in the ONL—formed by the axons of olfactory neurons—from Braak stage I/II patients, as well as in OSNs and ABs within the OE. PHF-1 has been reported to detect phosphorylated tau in axons and the neuropil, preceding pretangle formation, while AT8 stains pretangles and is considered an early marker of tau pathology [4]. In our observations, PHF-1 staining was detected in the OE and in the ONL of the OB but also evidenced neuropil threads in the inner layers of the OB, whereas AT8 staining was restricted to these inner layers of the bulbs. This suggests that hyperphosphorylated tau may be present in the OE at early Braak stages without converting over time to aggregate, possibly due regenerative capacity of the OE that continuously produces newborn OSNs. Still, these pTau forms detected by PHF-1 in the OSNs could be heading for the ONL, which is formed by the axons of the OSNs. Consistent with our data, hyperphosphorylated tau then accumulates within the inner layers of the OB to form pretangles evidenced by both AT8 and PHF-1 staining. These results and the underlying scenario of pTau progression are consistent with the other studies showing phosphorylated tau evidenced by AT8 or PHF-1 staining in the OB of AD patients [25, 58].

This strongly suggests that tau pathology may develop early in these regions. These findings extend beyond the transgenic mouse model, indicating the relevance of our observations to human pathology. While there is an ongoing debate regarding whether tau pathology in the olfactory system arises earlier, simultaneously, or subsequently than in the EC, our results suggest that the olfactory system may be a site of early tau pathology development in NDs [36, 67]. Importantly, the direction of the progression of tau pathology in the olfactory system is matter of different hypothesis. On the one hand, different studies postulate that the olfactory system serves as an entry point for pathogens or as an access point for environmental aggressions, which can trigger pathological changes that would then spread throughout the brain via anterograde olfactory pathways [16, 21, 54, 60] Our data illustrate this hypothesis but are not at odds with the one supporting Tau pathology appears early in the brain, particularly in the EC, and then spreads to the olfactory system using the retrograde olfactory circuit [18].

Olfactory dysfunction: a prodromal sign of dementia

Olfactory deficits have been observed and associated with NDs, including AD, since 1974 [18, 70]. Olfactory dysfunction is present not only in the early stages of AD but also in MCI patients [60] and is now recognized as a prodromal sign of dementia [10] and as a tool to predict MCI-to-AD conversion [38].

Since then, behavioral studies aimed at evaluating olfactory function have been conducted to characterize mouse models of these pathologies. In our study, the results of the food-seeking and olfactory discrimination tests did not show any significant difference between the PS19 and age-matched control mice. PS19 mice did not take longer to find the buried food and reacted in the same way as the control mice did when presented with two different odors, contrary to what had been previously demonstrated [41]. These results could be explained by the fact that the term "olfactory deficits/dysfunction/impairment" encompasses several functions, such as a decline in odor threshold, odor identification, odor discrimination, and odor memory that cannot be measured by the same tests [10]. In addition, differentiating olfactory deficits caused by physiological aging from those associated with NDs presents a challenge [23]. During normal aging, the OE, which contains OSNs, is gradually replaced by respiratory epithelium. This is accompanied by ossification and closure of the foramina in the cribriform plate. Together, these changes can disrupt the transduction of olfactory information from the OE to the OB and the olfactory cortex [10, 60] and lead to an increase in odor threshold, which relies solely on the integrity of the OE and OSN transduction [10, 35]. In contrast, olfactory memory relies on hippocampal integrity, whereas odor identification/discrimination relies on the integrity of central olfactory structures [23, 36]. In AD patients, it has been shown that odor identification is particularly

Appendix III

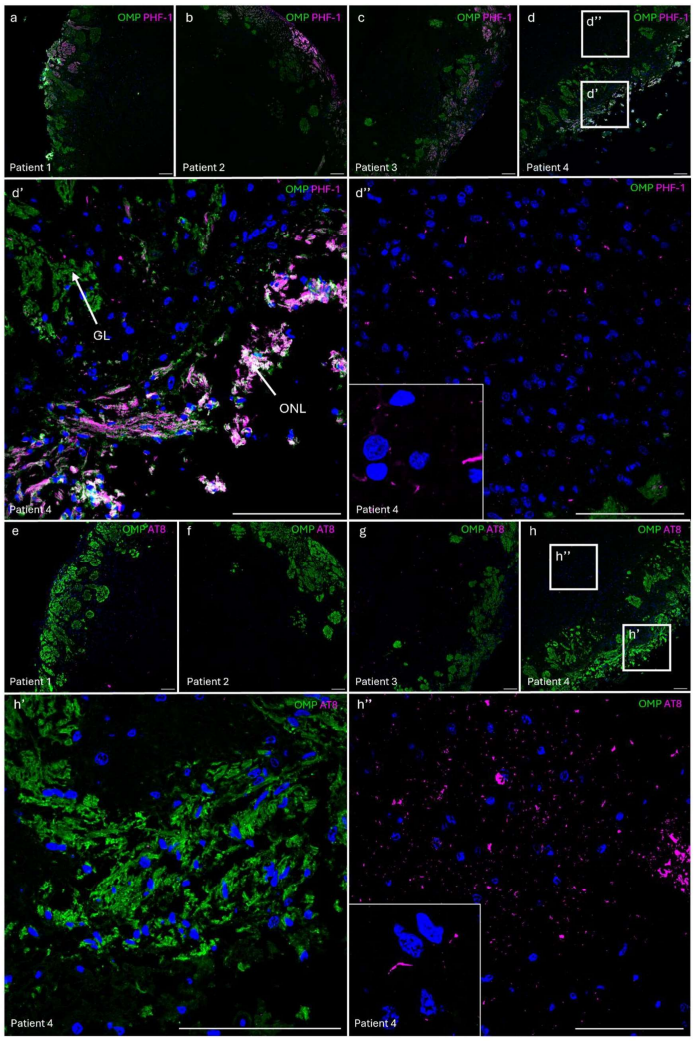

Appendix III

◂**Fig. 11** pTau expression in human OB. The OB were obtained either from patients 1 and 2 (Braak stage I) (**a**, **b**, **e**, **f**) or from patients 3 and 4 (Braak stage II) (**c**, **d**, **g**, **h**). Paraffin sections immunostained for **OMP** (green) and **PHF-1** (purple) show colocalization between **OMP-PHF-1** (white) in the ONL of all patients (**a**–**d**, d'). **PHF-1** signal is also found in the inner layers of the OB (**a**–**d**, d''). Paraffin sections immunostained for **OMP** (green) and **AT8** (purple) show no colocalization between **OMP-AT8** (**e**–**h**, h'). AT8 signal is only found in the inner layers of the OB, similarly to **PHF-1** (**e**–**h**, h''). No signal is detected in the negative controls without primary antibodies. Scale bar: 100 µm. ONL: Olfactory nerve layer, GL: Glomerular layer

impaired [10, 38, 60, 70]. This impairment reflects a cognitive deficit rather than a direct impairment of olfactory perception [24, 36, 38], since higher cognitive skills, such as verbal and semantic skills, are required [23]. Some odor identification tests have already been proposed, in which certain odors can differentiate AD patients from individuals with normal aging [60]. Our findings show that following intranasal $ZnSO_4$ irrigation, which disrupts the peripheral olfactory system [32], mice are no longer able to find buried food, suggesting an increased odor threshold. Additionally, they are no longer able to differentiate between odors, indicating that their discrimination abilities could be impaired. The effectiveness of the tests conducted cannot, therefore, be questioned. These tests primarily evaluate peripheral damage at the level of the OE (odor threshold). It is thus possible that PS19 mice do not present strong peripheral impairment despite the presence of tau pathology in the OE. They might retain their ability to smell odors because of the lack of fibrillar tau (NFTs) in this region. However, the presence of lesions in the primary olfactory cortex (OB, PC, and EC) might compromise olfactory discrimination and identification [10], two functions that are truly challenging to evaluate in mice. Consistent with our hypothesis, in Tg2576 mice—an amyloid mouse model—odor memory is impaired, while odor perception is spared, suggesting that the underlying mechanisms might be different [10]. In addition, it is known that, compared with mice, humans have a poorly developed sense of smell [40]. In rodents, the OE covers 50% of the nasal cavities, while it covers only 3–5% of these cavities in humans. Consequently, olfactory neuronal loss has a greater impact on odor perception in humans than in rodents [20]. Mice rely heavily on their olfactory function for survival, and given their significant olfactory capabilities, we hypothesize that the pTau pathological pattern detected in the olfactory regions might not be sufficient to induce olfactory dysfunction detectable by the two tests conducted.

Targeting the OE mitigates tau pathology in the CNS

To establish a causal link demonstrating that the OE serves as a gateway for pathology and worsens pre-existing conditions in the CNS of PS19 mice, we directly targeted the OE and assessed its impact on the tau pathology progression in the CNS. Intranasal $ZnSO_4$ irrigation was used to specifically strip the OSNs in the OE and ONL in the OB [32, 39], providing a model to study the downstream effects on the CNS. Repeated intranasal irrigation with $ZnSO_4$ in PS19 mice resulted in near-complete stripping of the OE and ONL. Additionally, NFT-like tau accumulations were absent in the PC and only a few residual lesions were present in the EC and amygdala, compared to vehicle-treated controls. This suggests that modulating tau pathology in the olfactory system delays its progression in interconnected CNS regions. Given that all these regions receive input from the OB, our findings reinforce the hypothesis that the olfactory pathway—particularly the OE—serves as an early site for pathology development and as a potential entry point for the spread of pathology to the PC and EC. Our "prion-like" propagation hypothesis was further strengthened by the results obtained following intranasal administration of AAVs encoding the P301S-mutated human tau protein, which lead to increased tau pathology in the PC of PS19 mice.

These findings highlight the potential of intranasal drug delivery to target NDs via the olfactory pathway, offering a way to reduce the side effects associated with systemic administration [36]. Research in mouse models has demonstrated that nasal tau immunotherapy can clear intracellular tau pathology and improve cognitive function in aged tauopathy mice [26]. In humans, the intranasal route has also been explored in multiple studies as a promising therapeutic strategy for various NDs [19, 31, 42].

Limitations of this study

In this study, the limitations of using PS19 mice, a transgenic model with random transgene insertion and artificial overexpression driven by the mouse prion protein promoter, must be taken into account when interpreting the results [55]. It is also important to emphasize that this is exclusively a tauopathy model, with no amyloid pathology present. As a result, we were unable to study the impact of co-existing amyloid pathology on the appearance and progression of tau pathology in the olfactory and central nervous systems, which would be of interest but particularly challenging to carry out. We focused on tauopathy rather than on amyloid pathology for its closer correlation to neurodegeneration. To partially address this limitation and give indication about the relevance of our results, we incorporated results obtained from human

Appendix III

samples with a *postmortem* diagnosis of early Braak stage pathology.

Conclusions

Our study highlights that pTau appears early in the OE of PS19 mice and subsequently spreads to the CNS following neuroanatomical pathways, like the olfactory and perforant pathways. Despite the presence of tau lesions in regions of the olfactory system, the olfactory threshold of PS19 mice was not significantly impaired. By specifically targeting olfactory neurons in the OE, we were able to either mitigate or increase tau pathology in CNS regions that share direct connections with the OB. We additionally confirmed the appearance of pTau signal in the olfactory regions of Braak stage I/II patients. Overall, our findings support the spread of tau pathology according to anatomical neuronal connectivity, highlight the therapeutic potential of the OE region in tauopathies, and suggest its likely contribution to the progression of pathology in the CNS.

Supplementary Information The online version contains supplementary material available at https://doi.org/10.1007/s00401-025-02902-6.

Acknowledgements We thank Olivier Schakman for conducting behavioral studies in mice. We thank Yasmine Salman, Benoît Lengelé and Catherine Behets for collecting and handling the human samples. We thank Marc de Bournonville and Olivier Van Kerk for their technical support. We finally thank the team of Peter Davies, who kindly provided the PHF-1 antibody.

Author contributions Conceptualization: MD, PKC; Methodology: MD, EP, EB, CH, MB, ED; Formal analysis and investigation: MD; Writing – original draft preparation: MD; Writing – review and editing: MD, EB, NS, SOT, KL, ED, DRT, BH, PKC; Funding: AD, CH, BH, PKC; Supervision: PKC. All authors read and approved the final manuscript.

Funding NS is funded by a Chargé de Recherche postdoctoral fellowship from the F.R.S.-FNRS. This work was supported by grants from the SAO-FRA Alzheimer Research Foundation (SAO-FRA 2018/0025), UCLouvain Action de Recherche Concertée (Toward the development of new, non-invasive diagnostic tools for neurodegenerative pathologies), Fondation Louvain, Queen Elisabeth Medical Foundation (FMRE AlzHex), F.R.S.-FNRS (FNRS J.0106.22) to PKC, and SAO-FRA Alzheimer Research Foundation (SAO-FRA 2020/0028) to NS. Fonds Wetenschappelijk Onderzoek Vlaanderen (FWO: G065721N, G024925N (DRT)). FWO (1225725N) (SOT).

Data availability All datasets generated and analyzed during this study are included in this published article and its supplementary material.

Declarations

Conflicts of interest DRT and SOT received consultant honoraria from Muna Therapeutics. DRT collaborated with Novartis Pharma AG (Switzerland), and GE Healthcare (UK). The other authors have no competing interests to declare that are relevant to the content of this article.

Ethical approval All animal procedures were conducted in accordance with institutional and European guidelines and approved by the UCLouvain Ethical Committee for Animal Welfare (2021/UCL/MD/018). Human *postmortem* brain tissue was collected in accordance with the applicable legislation in Belgium. The recruitment protocols for the collection of human brains were approved by the ethical committee (2020/02JUL/355).

Open Access This article is licensed under a Creative Commons Attribution-NonCommercial-NoDerivatives 4.0 International License, which permits any non-commercial use, sharing, distribution and reproduction in any medium or format, as long as you give appropriate credit to the original author(s) and the source, provide a link to the Creative Commons licence, and indicate if you modified the licensed material. You do not have permission under this licence to share adapted material derived from this article or parts of it. The images or other third party material in this article are included in the article's Creative Commons licence, unless indicated otherwise in a credit line to the material. If material is not included in the article's Creative Commons licence and your intended use is not permitted by statutory regulation or exceeds the permitted use, you will need to obtain permission directly from the copyright holder. To view a copy of this licence, visit http://creativecommons.org/licenses/by-nc-nd/4.0/.

References

1. Ahmad F, Mein H, Jing Y, Zhang H, Liu P (2021) Behavioural functions and cerebral blood flow in a P301S Tauopathy mouse model: a time-course study. Int J Mol Sci. https://doi.org/10.3390/ijms22189727
2. Ahnaou A, Rodriguez-Manrique D, Biermans R, Embrechts S, Manyakov NV, Drinkenburg WH (2020) Functional alterations in the olfactory neuronal circuit occur before hippocampal plasticity deficits in the P301S mouse model of tauopathy: implications for early diagnosis and translational research in Alzheimer's disease. Int J Mol Sci. https://doi.org/10.3390/ijms21155431
3. Amani M, Lauterborn JC, Le AA, Cox BM, Wang W, Quintanilla J et al (2021) Rapid aging in the Perforant path projections to the rodent dentate gyrus. J Neurosci 41(10):2301–2312. https://doi.org/10.1523/jneurosci.2376-20.2021
4. Aragão Gomes L, Uytterhoeven V, Lopez-Sanmartin D, Tomé SO, Tousseyn T, Vandenberghe R et al (2021) Maturation of neuronal AD-tau pathology involves site-specific phosphorylation of cytoplasmic and synaptic tau preceding conformational change and fibril formation. Acta Neuropathol 141(2):173–192. https://doi.org/10.1007/s00401-020-02251-6
5. Arnold SE, Smutzer GS, Trojanowski JQ, Moberg PJ (1998) Cellular and molecular neuropathology of the olfactory epithelium and central olfactory pathways in Alzheimer's disease and schizophrenia. Ann N Y Acad Sci 855:762–775. https://doi.org/10.1111/j.1749-6632.1998.tb10656.x
6. Attems J, Jellinger KA (2006) Olfactory tau pathology in Alzheimer disease and mild cognitive impairment. Clin Neuropathol 25(6):265–271
7. Attems J, Lintner F, Jellinger KA (2005) Olfactory involvement in aging and Alzheimer's disease: an autopsy study. J Alzheimers Dis 7(2):149–157. https://doi.org/10.3233/jad-2005-7208
8. Attems J, Walker L, Jellinger KA (2014) Olfactory bulb involvement in neurodegenerative diseases. Acta Neuropathol 127:459–475. https://doi.org/10.1007/s00401-014-1261-7
9. Barrios AW, Núñez G, Sánchez QP, Salazar I (2014) Anatomy, histochemistry, and immunohistochemistry of the olfactory

Appendix III

subsystems in mice. Front Neuroanat. https://doi.org/10.3389/fnana.2014.00063
10. Bathini P, Brai E, Auber LA (2019) Olfactory dysfunction in the pathophysiological continuum of dementia. Ageing Res Rev 55:100956. https://doi.org/10.1016/j.arr.2019.100956
11. Braak H, Alafuzoff I, Arzberger T, Kretzschmar H, Del Tredici K (2006) Staging of Alzheimer disease-associated neurofibrillary pathology using paraffin sections and immunocytochemistry. Acta Neuropathol 112(4):389–404. https://doi.org/10.1007/s00401-006-0127-z
12. Braak H, Braak E (1991) Neuropathological stageing of Alzheimer-related changes. Acta Neuropathol 82(4):239–259. https://doi.org/10.1007/BF00308809
13. Chapuis J, Cohen Y, He X, Zhang Z, Jin S, Xu F et al (2013) Lateral entorhinal modulation of piriform cortical activity and fine odor discrimination. J Neurosci 33(33):13449–13459. https://doi.org/10.1523/jneurosci.1387-13.2013
14. Chen CR, Kachramanoglou C, Li D, Andrews P, Choi D (2014) Anatomy and cellular constituents of the human olfactory mucosa: a review. J Neurol Surg B Skull Base 75(5):293–300. https://doi.org/10.1055/s-0033-1361837
15. Clavaguera F, Bolmont T, Crowther RA, Abramowski D, Frank S, Probst A et al (2009) Transmission and spreading of tauopathy in transgenic mouse brain. Nat Cell Biol 11(7):909–913. https://doi.org/10.1038/ncb1901
16. Dan X, Wechter N, Gray S, Mohanty JG, Croteau DL, Bohr VA (2021) Olfactory dysfunction in aging and neurodegenerative diseases. Ageing Res Rev 70:101416. https://doi.org/10.1016/j.arr.2021.101416
17. DeTure MA, Dickson DW (2019) The neuropathological diagnosis of Alzheimer's disease. Mol Neurodegener 14(1):32. https://doi.org/10.1186/s13024-019-0333-5
18. Diez I, Ortiz-Terán L, Ng TSC, Albers MW, Marshall G et al (2024) Tau propagation in the brain olfactory circuits is associated with smell perception changes in aging. Nat Commun 15(1):4809. https://doi.org/10.1038/s41467-024-48462-3
19. Djupesland PG, Messina JC, Mahmoud RA (2014) The nasal approach to delivering treatment for brain diseases: an anatomic, physiologic, and delivery technology overview. Ther Deliv 5(6):709–733. https://doi.org/10.4155/tde.14.41
20. Dorman DC (2010) 13.15—Olfactory system. In: McQueen CA (ed) Comprehensive toxicology (Second Edition). Elsevier, Oxford, pp 263–276
21. Doty RL (2017) Olfactory dysfunction in neurodegenerative diseases: is there a common pathological substrate? Lancet Neurol 16(6):478–488. https://doi.org/10.1016/S1474-4422(17)30123-0
22. Dujardin S, Hyman BT (2019) Tau prion-like propagation: state of the art and current challenges. Adv Exp Med Biol 1184:305–325. https://doi.org/10.1007/978-981-32-9358-8_23
23. Fatuzzo I, Niccolini GF, Zoccali F, Cavalcanti L, Bellizzi MG, Riccardi G et al (2023) Neurons, nose, and neurodegenerative diseases: olfactory function and cognitive impairment. Int J Mol Sci. https://doi.org/10.3390/ijms24032117
24. Franco R, Garrigós C, Lillo J (2024) The olfactory trail of neurodegenerative diseases. Cells. https://doi.org/10.3390/cells13070615
25. Fujishiro H, Tsuboi Y, Lin WL, Uchikado H, Dickson DW (2008) Co-localization of tau and alpha-synuclein in the olfactory bulb in Alzheimer's disease with amygdala Lewy bodies. Acta Neuropathol 116(1):17–24. https://doi.org/10.1007/s00401-008-0383-1
26. Gaikwad S, Puangmalai N, Sonawane M, Montalbano M, Price R, Iyer MS et al (2024) Nasal tau immunotherapy clears intracellular tau pathology and improves cognitive functions in aged tauopathy mice. Sci Transl Med 16(754):eadj5958. https://doi.org/10.1126/scitranslmed.adj5958
27. Gallyas F (1971) Silver staining of Alzheimer's neurofibrillary changes by means of physical development. Acta Morphol Acad Sci Hung 19(1):1–8
28. Gao YL, Wang N, Sun FR, Cao XP, Zhang W, Yu JT (2018) Tau in neurodegenerative disease. Ann Transl Med 6(10):175
29. Gayatri D (2023) Handbook of clinical neurology. In: Chapter 12—The tauopathies Vol 196
30. Greenberg SG, Davies P, Schein JD, Binder LI (1992) Hydrofluoric acid-treated tau PHF proteins display the same biochemical properties as normal tau. J Biol Chem 267(1):564–569
31. Guo H, Wang G, Zhai Z, Huang J, Huang Z, Zhou Y et al (2024) Rivastigmine nasal spray for the treatment of Alzheimer's disease: olfactory deposition and brain delivery. Int J Pharmaceut 652:123809. https://doi.org/10.1016/j.ijpharm.2024.123809
32. Harding JW, Getchell TV, Margolis FL (1978) Denervation of the primary olfactory pathway in mice. V. Long-term effect of intranasal $ZnSO_4$ irrigation on behavior, biochemistry and morphology. Brain Res 140(2):271–285. https://doi.org/10.1016/0006-8993(78)90460-2
33. Hildebrandt-Einfeldt L, Yap K, Paul MH, Stoffer C, Zahn N, Drakew A et al (2021) Crossed entorhino-dentate projections form and terminate with correct layer-specificity in organotypic slice cultures of the mouse hippocampus. Front Neuroanat 15:637036. https://doi.org/10.3389/fnana.2021.637036
34. Keller M, Douhard Q, Baum MJ, Bakker J (2006) Destruction of the main olfactory epithelium reduces female sexual behavior and olfactory investigation in female mice. Chem Senses 31(4):315–323. https://doi.org/10.1093/chemse/bjj035
35. Kondo K, Kikuta S, Ueha R, Suzukawa K, Yamasoba T (2020) Age-related olfactory dysfunction: epidemiology, pathophysiology, and clinical management. Front Aging Neurosci 12:208. https://doi.org/10.3389/fnagi.2020.00208
36. Kovács T (2013) The olfactory system in Alzheimer's disease: pathology, pathophysiology and pathway for therapy. Transl Neurosci 4(1):34–45. https://doi.org/10.2478/s13380-013-0108-3
37. Kovács T, Cairns NJ, Lantos PL (2001) Olfactory centres in Alzheimer's disease: olfactory bulb is involved in early Braak's stages. NeuroReport 12(2):285–288
38. Lad M, Sedley W, Griffiths TD (2024) Sensory loss and risk of dementia. Neuroscientist 30(2):247–259. https://doi.org/10.1177/10738584221126090
39. LaFever BJ, Imamura F (2022) Effects of nasal inflammation on the olfactory bulb. J Neuroinflammation 19(1):294. https://doi.org/10.1186/s12974-022-02657-x
40. Laska M (2017) Human and animal olfactory capabilities compared. pp 675–689
41. Li S, Li W, Wu X, Li J, Yang J, Tu C et al (2019) Olfactory deficit is associated with mitral cell dysfunction in the olfactory bulb of P301S tau transgenic mice. Brain Res Bull 1(148):34–45. https://doi.org/10.1016/j.brainresbull.2019.03.006
42. Lofts A, Abu-Hijleh F, Rigg N, Mishra RK, Hoare T (2022) Using the intranasal route to administer drugs to treat neurological and psychiatric illnesses: rationale, successes, and future needs. CNS Drugs 36(7):739–770. https://doi.org/10.1007/s40263-022-00930-4
43. Lundström JN, Boesveldt S, Albrecht J (2011) Central processing of the chemical senses: an overview. ACS Chem Neurosci 2(1):5–16. https://doi.org/10.1021/cn1000843
44. Martel G, Simon A, Nocera S, Kalainathan S, Pidoux L, Blum D et al (2015) Aging, but not tau pathology, impacts olfactory performances and somatostatin systems in THY-Tau22 mice. Neurobiol Aging 36(2):1013–1028. https://doi.org/10.1016/j.neurobiolaging.2014.10.033
45. Matulionis DH (1975) Ultrastructural study of mouse olfactory epithelium following destruction by $ZnSO_4$ and its subsequent

Appendix III

regeneration. Am J Anat 142(1):67–89. https://doi.org/10.1002/aja.1001420106
46. McBride K, Slotnick B, Margolis FL (2003) Does intranasal application of zinc sulfate produce anosmia in the mouse? An olfactometric and anatomical study. Chem Senses 28(8):659–670. https://doi.org/10.1093/chemse/bjg053
47. Noto T, Zhou G, Yang Q, Lane G, Zelano C (2021) Human primary olfactory amygdala subregions form distinct functional networks, suggesting distinct olfactory functions. Front Syst Neurosci. https://doi.org/10.3389/fnsys.2021.752320
48. Ohm TG, Braak H (1987) Olfactory bulb changes in Alzheimer's disease. Acta Neuropathol 73(4):365–369. https://doi.org/10.1007/BF00688261
49. Orr ME, Sullivan AC, Frost B (2017) A brief overview of tauopathy: causes, consequences, and therapeutic strategies. Trends Pharmacol Sci 38(7):637–648. https://doi.org/10.1016/j.tips.2017.03.011
50. Otvos L Jr, Feiner L, Lang E, Szendrei GI, Goedert M, Lee VM (1994) Monoclonal antibody PHF-1 recognizes tau protein phosphorylated at serine residues 396 and 404. J Neurosci Res 39(6):669–673. https://doi.org/10.1002/jnr.490390607
51. Parvand M, Rankin CH (2020) Is there a shared etiology of olfactory impairments in normal aging and neurodegenerative disease? J Alzheimers Dis 73(1):1–21. https://doi.org/10.3233/jad-190636
52. Poulin SP, Dautoff R, Morris JC, Barrett LF, Dickerson BC (2011) Amygdala atrophy is prominent in early Alzheimer's disease and relates to symptom severity. Psychiatry Res 194(1):7–13. https://doi.org/10.1016/j.pscychresns.2011.06.014
53. Ramirez DMO, Whitesell JD, Bhagwat N, Thomas TL, Ajay AD, Nawaby A et al (2023) Endogenous pathology in tauopathy mice progresses via brain networks. bioRxiv. https://doi.org/10.1101/2023.05.23.541792
54. Rey NL, Wesson DW, Brundin P (2018) The olfactory bulb as the entry site for prion-like propagation in neurodegenerative diseases. Neurobiol Dis 109:226–248. https://doi.org/10.1016/j.nbd.2016.12.013
55. Sahara N, Yanai R (2023) Limitations of human tau-expressing mouse models and novel approaches of mouse modeling for tauopathy. Front Neurosci. https://doi.org/10.3389/fnins.2023.1149761
56. Samudra N, Lane-Donovan C, VandeVrede L, Boxer AL (2023) Tau pathology in neurodegenerative disease: disease mechanisms and therapeutic avenues. J Clin Invest. https://doi.org/10.1172/jci168553
57. Schröder H, Moser N, Huggenberger S (2020) Neuroanatomy of the Mouse. Springer, Cham
58. Shimizu S, Tojima I, Nakamura K, Kouzaki H, Kanesaka T, Ogawa N et al (2022) A Histochemical analysis of neurofibrillary tangles in olfactory epithelium, a study based on an autopsy case of juvenile Alzheimer's disease. Acta Histochem Cytochem 55(3):93–98. https://doi.org/10.1267/ahc.22-00048
59. Smith TD, Bhatnagar KP (2019) Anatomy of the olfactory system. Handb Clin Neurol 164:17–28. https://doi.org/10.1016/b978-0-444-63855-7.00002-2
60. Son G, Jahanshahi A, Yoo SJ, Boonstra JT, Hopkins DA, Steinbusch HWM et al (2021) Olfactory neuropathology in Alzheimer's disease: a sign of ongoing neurodegeneration. BMB Rep 54(6):295–304. https://doi.org/10.5483/BMBRep.2021.54.6.055
61. Sun Y, Guo Y, Feng X, Jia M, Ai N, Dong Y et al (2020) The behavioural and neuropathologic sexual dimorphism and absence of MIP-3α in tau P301S mouse model of Alzheimer's disease. J Neuroinflamm 17(1):72. https://doi.org/10.1186/s12974-020-01749-w
62. Takehara-Nishiuchi K (2014) Entorhinal cortex and consolidated memory. Neurosci Res 84:27–33. https://doi.org/10.1016/j.neures.2014.02.012
63. Takeuchi H, Iba M, Inoue H, Higuchi M, Takao K, Tsukita K et al (2011) P301S mutant human tau transgenic mice manifest early symptoms of human tauopathies with dementia and altered sensorimotor gating. PLoS ONE 6(6):e21050. https://doi.org/10.1371/journal.pone.0021050
64. Talamo BR, Feng WH, Perez-Cruet M, Adelman L, Kosik K, Lee MY et al (1991) Pathologic changes in olfactory neurons in Alzheimer's disease. Ann N Y Acad Sci 640:1–7. https://doi.org/10.1111/j.1749-6632.1991.tb00182.x
65. Tsuboi Y, Wszolek ZK, Graff-Radford NR, Cookson N, Dickson DW (2003) Tau pathology in the olfactory bulb correlates with Braak stage, Lewy body pathology and apolipoprotein epsilon4. Neuropathol Appl Neurobiol 29(5):503–510. https://doi.org/10.1046/j.1365-2990.2003.00453.x
66. Tzeng WY, Figarella K, Garaschuk O (2021) Olfactory impairment in men and mice related to aging and amyloid-induced pathology. Pflügers Arch Eur J Physiol 473(5):805–821. https://doi.org/10.1007/s00424-021-02527-0
67. Ubeda-Bañon I, Saiz-Sanchez D, Flores-Cuadrado A, Rioja-Corroto E, Gonzalez-Rodriguez M, Villar-Conde S et al (2020) The human olfactory system in two proteinopathies Alzheimer's and Parkinson's diseases. Transl Neurodegener 9(1):22. https://doi.org/10.1186/s40035-020-00200-7
68. Walkiewicz G, Ronisz A, Ospitalieri S, Tsaka G, Tomé SO, Vandenberghe R et al (2024) pTau pathology in the retina of TAU58 mice: association with ganglion cell degeneration and implications on seeding and propagation of pTau from human brain lysates. Acta Neuropathol Commun 12(1):194. https://doi.org/10.1186/s40478-024-01907-8
69. Witter MP, Naber PA, van Haeften T, Machielsen WCM, Rombouts S, Barkhof F et al (2000) Cortico-hippocampal communication by way of parallel parahippocampal-subicular pathways. Hippocampus 10(4):398–410
70. Yan Y, Aierken A, Wang C, Song D, Ni J, Wang Z et al (2022) A potential biomarker of preclinical Alzheimer's disease: the olfactory dysfunction and its pathogenesis-based neural circuitry impairments. Neurosci Biobehav Rev 132:857–869. https://doi.org/10.1016/j.neubiorev.2021.11.009
71. Yang S, Kuan WL, Spillantini MG (2016) Progressive tauopathy in P301S tau transgenic mice is associated with a functional deficit of the olfactory system. Eur J Neurosci 44(6):2396–2403. https://doi.org/10.1111/ejn.13333
72. Yoshiyama Y, Higuchi M, Zhang B, Huang SM, Iwata N, Saido TC et al (2007) Synapse loss and microglial activation precede tangles in a P301S tauopathy mouse model. Neuron 53(3):337–351. https://doi.org/10.1016/j.neuron.2007.01.010
73. Yu H, Wang F, Jia D, Bi S, Gong J, Wu JJ et al (2024) Pathological features and molecular signatures of early olfactory dysfunction in 3xTg-AD model mice. CNS Neurosci Ther 30(2):e14632. https://doi.org/10.1111/cns.14632
74. Zhang J, Zhao Z, Sun S, Li J, Wang Y, Dong J et al (2022) Olfactory evaluation in Alzheimer's disease model mice. Brain Sci. https://doi.org/10.3390/brainsci12050607
75. Zhou X, Kumar P, Bhuyan DJ, Jensen SO, Roberts TL, Münch GW (2023) Neuroinflammation in Alzheimer's disease: a potential role of nose-picking in pathogen entry via the olfactory system? Biomolecules. https://doi.org/10.3390/biom13111568

Publisher's Note Springer Nature remains neutral with regard to jurisdictional claims in published maps and institutional affiliations.

Appendix III

Authors and Affiliations

Marion Dourte[1] · Esther Paître[1] · Mongia Bouchoucha[1] · Emilien Boyer[1] · Sandra O. Tomé[2] · Emilie Doeraene[3] · Caroline Huart[4,5] · Karelle Leroy[3] · Dietmar Rudolf Thal[2,6] · Anabelle Decottignies[7] · Bernard Hanseeuw[8,9] · Nuria Suelves[1] · Pascal Kienlen-Campard[1]

✉ Pascal Kienlen-Campard
pascal.kienlen-campard@uclouvain.be

[1] Aging and Dementia Group, Cellular and Molecular Division (CEMO), Institute of Neuroscience (IoNS), UCLouvain, Brussels, Belgium

[2] Laboratory for Neuropathology, Department of Imaging and Pathology, Leuven Brain Institute (LBI), KU Leuven, Leuven, Belgium

[3] Alzheimer and Other Tauopathies Research Group, ULB Neuroscience Institute (UNI), ULB Center for Diabetes Research (UCDR), Faculty of Medicine, Université Libre de Bruxelles, Brussels, Belgium

[4] OlfactIoNS Group, Institute of Neuroscience (IoNS), UCLouvain, Brussels, Belgium

[5] Department of Otorhinolaryngology, Head and Neck Surgery, Cliniques Universitaires Saint-Luc, Brussels, Belgium

[6] Department of Pathology, University Hospital Leuven, Leuven, Belgium

[7] Genetic and Epigenetic Alterations of Genomes Unit, de Duve Institute, UCLouvain, Brussels, Belgium

[8] Louvain Aging Lab, Institute of Neuroscience (IoNS), UCLouvain, Brussels, Belgium

[9] Neurology Department, Cliniques Universitaires Saint-Luc, Brussels, Belgium